



SCMS SCHOOL OF ENGINEERING & TECHNOLOGY

PUBLICATION DETAILS 2023

SI No:	Name	First Author	Second Author	Third Author	Fourth Author	INDEXING
1	Chaithanya Nidhin	PEC2301				SCI
2	Dr. Varun Menon		PCS2308	PCS2302,PCS2304, PCS2305,PCS2311, PCS2313,PCS2314	PCS2301,PCS2303, PCS2307,PCS2312, PCS2318,PCS2319, PCS2320	SCI
			PCS2315			SCI
3	Neethu Krishna	PCS2306			PCS2316,PCS2317	SCOPUS
4	Asha S	PCS2307				SCI
5	Dr. Arshey	PCS2310				UGC CARE
6	Susmi Jacob	PCS2314				SCI
7	Reshma K V			PCS2317		UGC CARE
8	Dony				PCS2317	UGC CARE
9	Dr Raghav G R	PME2302 PME2303				SCI
10	Dr. Nisha L	PCE2301				SCOPUS
11	Dr. Manoj kumar B	PAU2301				SCOPUS
12	Dr. Rag L				PME2301	SCI
13	Beena Puthilath	PEE2301				SCOPUS
14	Dr. Santhosh	PBSH2301				UGC CARE
15	Dr. Geethu R		PBSH2301			UGC CARE
16	Dr. Nithya Mohan	PBSH2302				UGC CARE
17	Surya	PBSH2303				UGC CARE
18	Divya M S	PBSH2304,PBSH2305				UGC CARE
Total Publication for the calender year 2023						30




 PRINCIPAL
 SCMS SCHOOL OF ENGINEERING & TECHNOLOGY
 VIDYANAGAR, PALLISSERY, KARUKUTTY
 ERNAKULAM, KERALA-689 576



Solvothermal synthesis of WS₂ rectangular nanoplates and their application in photothermal therapy

M. V. Santhosh^{1,2,*} , R. Geethu¹, and K. S. Devaky²

¹Department of Basic Science and Humanities, SCMS School of Engineering and Technology, Karukutty, Kerala, India

²School of Chemical Sciences, Mahatma Gandhi University, Kottayam, Kerala, India

Received: 16 September 2022

Accepted: 26 December 2022

© The Author(s), under exclusive licence to Springer Science+Business Media, LLC, part of Springer Nature 2023

ABSTRACT

Refined WS₂ rectangular nanoplates were synthesized employing solvothermal method. X-ray diffraction results confirmed the crystalline nature of the sample without undesirable phases. Scanning electron microscopy (SEM) and transmission electron microscopy analyses show that the powder consists of rectangular nanoplates having thickness below ~ 100 nm. UV–Vis–NIR studies show absorption around near infra-red (NIR) region signifying its application as a photothermal agent in photothermal therapy. Surface area and porosity of the samples were studied using N₂ adsorption–desorption isotherm and Barrett–Joyner–Halenda pore size distribution curve. Photothermal responses (PTR) of WS₂ nanoplates at different concentrations were studied. It was observed that within 10 min of irradiation (NIR laser of wavelength-808 nm), WS₂ nanoplates with 0.4 mg/mL concentration reach a temperature of 45 °C which is sufficient to kill tumor cells. Photothermal response of WS₂ nanoplate suspension recorded after one day exhibited very small diminution in photothermal performance. Dynamic light scattering (DLS) and absorption studies were employed for explaining the photothermal response of WS₂ nanoplates. Stability of WS₂ nanoplate suspension at different pH values were studied by measuring zeta potential and the suspension exhibited good stability in the pH range 4–10. WS₂ nanoplate suspensions exhibited reasonably good reproducibility and hence consistency in PTR, which were investigated by noting polydispersity index, zeta potential, and drawing PTR curves at different trials. Finally, the capability of simple and fast DLS technique to measure the lateral size of WS₂ nanosheets in the suspension, correlating with SEM analysis was exploited.

Address correspondence to E-mail: santhoshvmurali@gmail.com

1 Introduction

Transition metal dichalcogenides (TMDs) such as molybdenum disulfide (MoS_2) and tungsten disulfide (WS_2) have recently attracted enormous interest due to their fascinating physicochemical properties arising from altering its no of layers, 2D nanostructure, and preparation conditions [1, 2]. Due to these unique characteristics, they have wide applications in catalysis, lithium ion batteries, hydrogen evolution, optoelectronics, biomedical applications, and many others [3, 4]. Among the various TMDs, WS_2 -2D structures have drawn particular attention with layered structure formed by unit S-W-S atomic tri-layers stacked together via van der Waals interactions. They have favorable structural, optical, electronic, chemical, and thermal properties that enable them to stand as an apt candidate for variety of applications [5, 6]. WS_2 nanoplates can be synthesized using various methods such as solvothermal methods, thermal evaporation of WO_3 and S powder, thermal decomposition of $(\text{NH}_4)_2\text{WS}_4$, solid phase reaction, reaction under autogenic pressure at elevated temperature (RAPET), sulfuration of WO_3 etc. [7–12]. But most of these methods are complex and encountering the issues of refinement level, uniformity in the prepared samples.

Photothermal therapy (PTT) is an emerging physical tumor therapy modality that can be employed as an alternative or supplement to conventional cancer treatments such as surgery, radiation therapy, and chemotherapy. In PTT, near-infrared (NIR) light-absorbing agents (photothermal agent) in tumor tissue absorb and transduce near infrared light into heat that results in thermal ablation of solid tumor. NIR (808 nm in particular) laser employed in PTT can penetrate skin and tissues to a reasonable depth without damaging the healthy tissues. Compared to current cancer treating protocols PTT is gentle, less invasive, and inexpensive technique that offers highly localized and specific tumor treatment with high therapeutic efficiency and mitigated side effects [13–16]. The effectiveness of PTT lies in the development of highly efficient photo-absorber that is biocompatible and easily prepared. There have been extensive researches on various types of photothermal agents (PTA). One among them is carbon-based materials which include carbon nano-tubes, graphene, and conductive polymers. But the downsides such as toxicity, photobleaching, and inadequate

photothermal conversion efficiency have declined their clinical translation potentials. Noble metal nanostructures including Pd-based nanosheets and Au nanostructures have also been explored. However, the poor biocompatibility and low photothermal stability have hindered their wide spread application potentials. The last type is 2D TMDs including WS_2 and MoS_2 nanosheets [15, 16]. TMD nanostructures are excellent candidates for photothermal agent in PTT due to their absorption of tissue penetrating NIR light, high specific surface area, biocompatibility, and photostability [13–16]. Superior interest in tungsten based 2D nanostructures lies in the fact that it could be function as an ideal multifunctional nano-platform for bio-imaging, drug delivery, and PTT. Strong X-ray attenuation ability of tungsten, sheet like structure with a high surface area, and broad NIR absorption of WS_2 validates the aforesaid applications [14].

Present paper reports, for the first time: solvothermal synthesis, systematic study, and exploitation of highly refined rectangular WS_2 nanoplates as photothermal agent for PTT. Stability and reproducibility related study of PTA suspension are very essential for consistent photothermal response. As far as the authors are aware, there are not much attempts in this regard. To address this issue, we have employed simple, fast, and straightforward dynamic light scattering (DLS) measurements for the first time to investigate stability and reproducibility of WS_2 nanoplate suspension. Moreover, since photothermal studies are conducted on WS_2 aqueous suspension, in situ characterization techniques like DLS are more useful. It will be inaccurate and tedious to analyze nanoplate dimension and behavior in powdered form for PTT studies due to nanoplate aggregation [17–19]. Stability of the suspension with aging was studied by monitoring average hydrodynamic size and zeta potential. As the stability of photothermal agent in various pH environments have paramount importance when utilized them for clinical trials, zeta potential measurements were effectively used to study this facet. The extent of reproducibility, a crucial factor that determines consistency in photothermal response was investigated by monitoring polydispersity index and zeta potential of WS_2 nanoplate suspension prepared in different trials. Usually atomic force microscopy (AFM) or transmission electron microscopy (TEM) or scanning electron microscopy (SEM) techniques has to be

employed to study the extent of homogeneity of PTA suspension prepared in different trials, which is tedious and can be inaccurate due to nanoplate aggregation in powdered form. To address this issue, attempts were made to obtain lateral size of nanosheets from particle size distribution of simple DLS measurements.

2 Experimental

2.1 Materials and methods

For the preparation of WS₂ nanoplates, 0.8 mmol ammonium tungstate hydrate [(NH₄)₆H₂W₁₂O₄₀·xH₂O] and 25 mmol of sublimed sulfur powder were dissolved in 35 mL of *N*-methyl-2-pyrrolidone (NMP). The mixture was vigorously shaken to form a homogeneous solution. Then the solution was transferred to a 50 mL Teflon-lined stainless steel autoclave and placed in a high temperature furnace. Solvothermal reaction was carried out at 230 °C for 24 h. The precipitate formed was collected by centrifuging followed by washing with distilled water and ethanol. The black powder was finally dried to form WS₂ powder.

2.2 Characterization

X-Ray diffraction studies were conducted using PANalytical X'pert PRO high resolution X-ray diffractometer (HRXRD) with CuK α ($\lambda = 1.5418$ Å) radiation. Size and shape of nanosheets in powdered form were analyzed using scanning electron microscopy (SEM) on a JEOL, JSM-840 system. Elemental analysis of the prepared powder was done using Energy Dispersive X-ray (EDAX) analysis in SEM. High-resolution transmission electron microscopy (HRTEM) images of the prepared samples were taken using JEOL-JEM 3010 instrument. Optical absorbance spectra of the samples were recorded using JASCO V-570 model UV-Vis-NIR spectrophotometer. Surface area and porosity analysis of the sample were accomplished using a high performance gas and vapor adsorption instrument (BELSORP-max, Bel Japan). Dynamic light scattering (DLS) experiments were performed on WS₂ nanosheet suspension using SZ-100 nanoparticle analyzer (Horiba Scientific).

2.3 Photothermal study

For photothermal experiments, WS₂ nanosheets suspension taken in plastic tube (10 × 10 × 20 mm³) was irradiated with NIR laser having wavelength of 808 nm and spot size of 0.75 cm². Power density and laser to sample distance were fixed as 1.5 W/cm² and 10 cm, respectively. The temperature of the suspension was recorded using a digital thermometer (accuracy 0.1 °C).

3 Results and discussion

XRD graph of the prepared sample (Fig. 1) revealed various diffraction peaks, implying the existence of different planes matching with highly crystalline hexagonal structure of WS₂ (JCPDS card no. 87-2417). The peaks at ~15.24°, 33.40°, and 58.55° are corresponding to (002), (101), and (110) planes of WS₂ [3]. Absence of any other remarkable peaks in XRD pattern designates highly refined WS₂ nanoplates without oxides and sulfides impurities.

The morphology and nanostructure of the prepared samples were analyzed by SEM and TEM. SEM analysis (Fig. 2) indicates the presence of large number of regular nanoplates having rectangular shape with length of about 300–600 nm, width of about 200–300 nm and thickness below 100 nm. The chemical compositions of these nanoplates were unveiled by EDAX as shown in Fig. 3a. The peaks of W and S elements are detected in the spectrum. Small

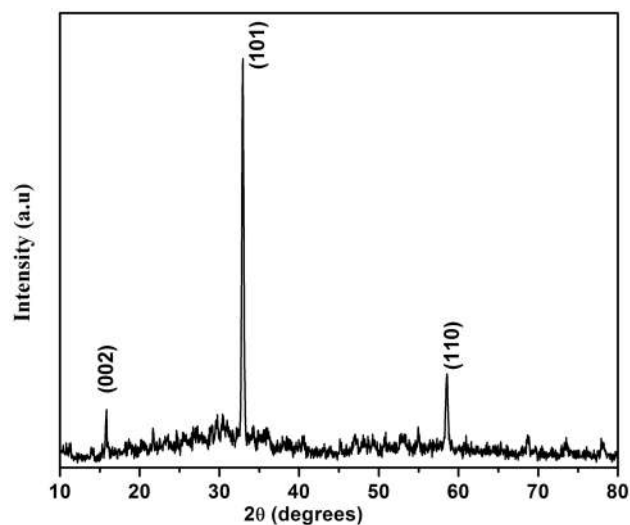


Fig. 1 XRD pattern of WS₂ powder

Fig. 2 SEM images of different regions of the sample

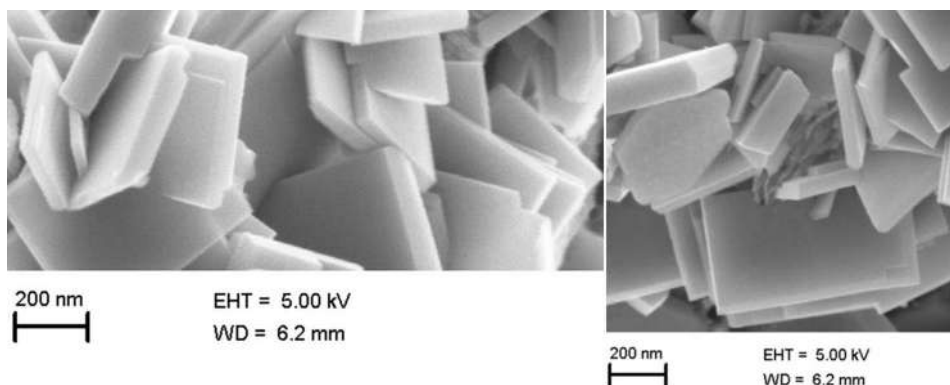
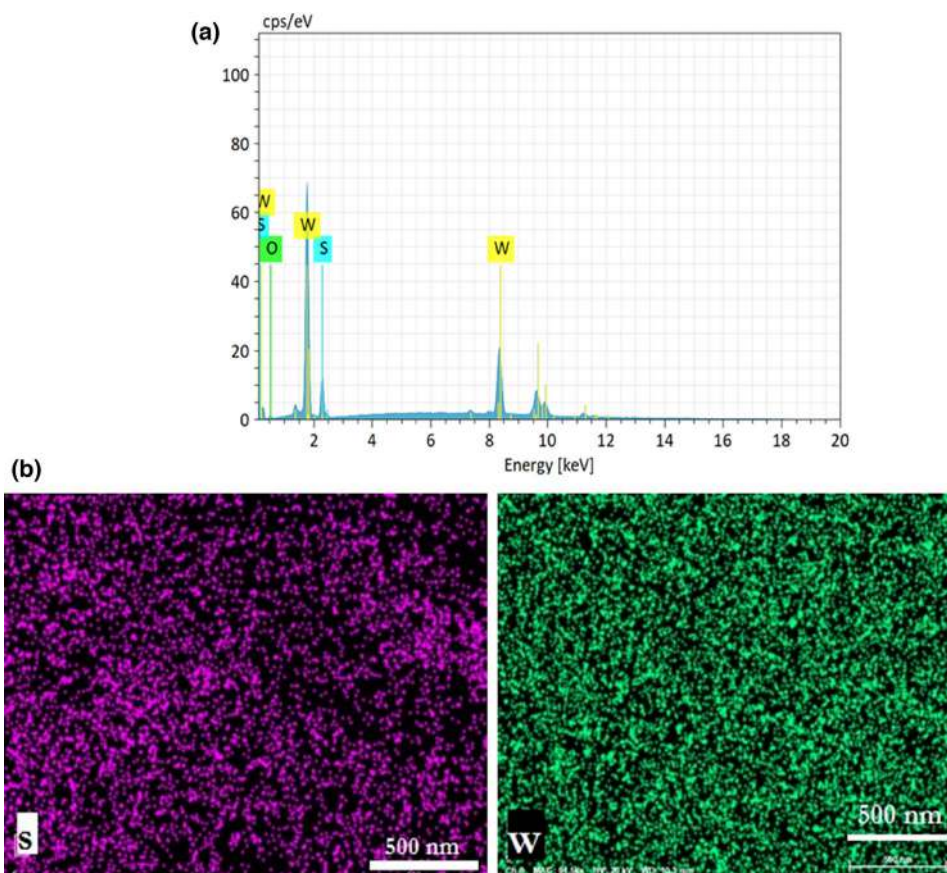


Fig. 3 **a** EDAX spectrum
b elemental mappings of WS₂ nanoplates



traces of oxygen was also identified, which can affect the refinement level of the sample as XRD analyses does not give any clue regarding oxide phases in the sample. The elemental mapping (Fig. 3b) revealed the homogeneous distribution of W and S elements in the whole sample. To further disclose the morphology and nanostructure of the synthesized material, TEM measurements were performed (Fig. 4). It can be inferred from TEM images that the powder consists of rectangular shaped nanoplates. TEM images

are in good agreement with the morphology as presented in the SEM pictures.

The UV–Vis–NIR absorption spectrum of WS₂ nanoplates (Fig. 5) exhibited excellent absorption in the NIR region up to 925 nm. Band gap of the sample was estimated to be 1.37 eV. Due to such strong optical absorption in the NIR region, prepared samples can be excellent aspirant for NIR laser (808 nm) induced PTT [3, 15]. It was also observed a slight decrease in absorbance when the nanoplate suspension was kept for 1 day, caused by possible nanoplate aggregation

Fig. 4 TEM images of the sample

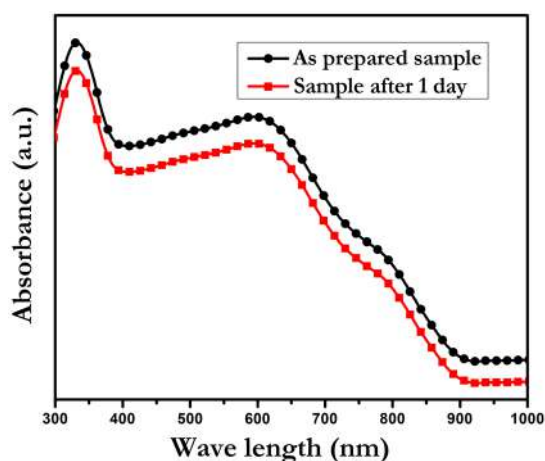
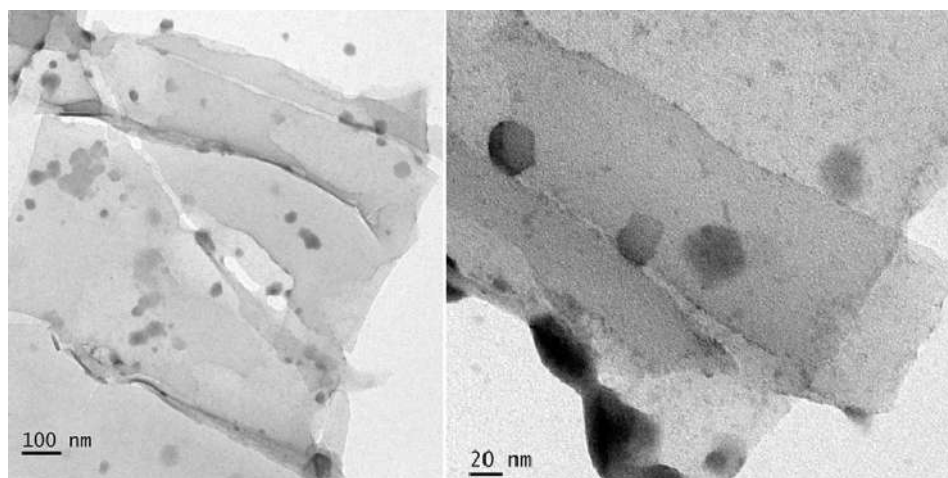


Fig. 5 UV–Vis–NIR spectra of aqueous WS₂ nanoplate dispersion

over time [15]. Porosity and surface area of WS₂ nanoplates are key factors that affect the extent of NIR light absorption and subsequent heat generation. To study the sample in this aspect, N₂ adsorption–desorption isotherm and Barrett–Joyner–Halenda (BJH) pore size distribution curve were plotted at 77 K (Fig. 6). Sample shows type IV isotherm, characteristic of a mesoporous material. The Brunauer–Emmett–Teller (BET) equation was employed to estimate the specific surface area (2.51 m²/g) of the sample. Since there are not much works related to BET analysis of WS₂ nanoplates of same kind as reported in the present work, specific surface area of the sample can be compared with reported values of WS₂ nanoplates (4 m²/g) by Pol et al, WS₂ nanosheets (0.5816 m²/g) by Khataee et al and Dai et al (5.419 m²/g) [11, 20–22]. Pore volume and mean pore diameter for WS₂ nanoplates evaluated using BJH method are

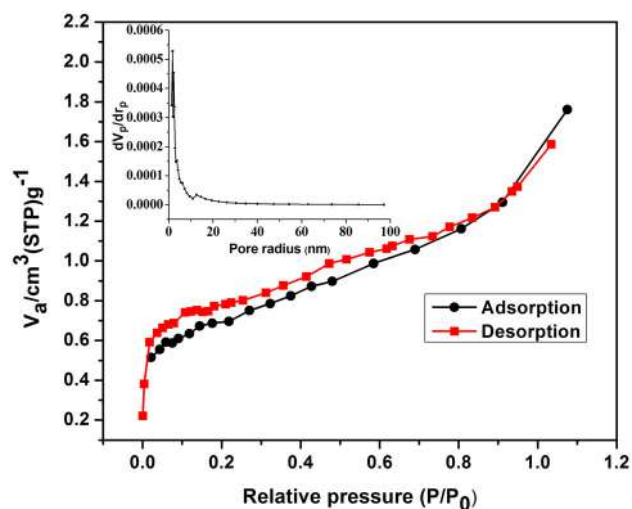


Fig. 6 Nitrogen adsorption–desorption isotherm of WS₂ nanoplates. The BJH pore size distribution curve is shown as inset

0.0023 cm³/g and 3.73 nm, respectively. Surface area and porosity measurements designate reasonably good values that can ensure satisfactory photothermal effect of the prepared WS₂ nanoplate suspension [20, 21].

Photothermal conversion capabilities of the WS₂ nanoplates were studied by irradiating its aqueous solution with 808 nm laser (1.5 Wcm⁻²). Light to heat conversion mechanism of WS₂ nanoplates relies on multiphonon relaxation of excited states. Synthesized nanoplates have a broad NIR absorption band. Following to the irradiation with 808 nm laser, excited PTT agent undergoes nonradiative vibrational relaxation by collision with surrounding molecules. This process heats up the water molecules [23, 24]. Trials were conducted by varying the concentration of WS₂

nanosheets in the range 0.05–0.6 mg/mL. Photothermal response of pure water was also monitored and observed no significant temperature change because water has almost no absorption at 808 nm. Photothermal heating curves of pure water and WS₂ nanoplates at different concentrations are shown in Fig. 7. The rate of increase in the temperature is positively correlated with the concentration of WS₂ nanoplates under laser irradiation. This is because; high concentration of WS₂ nanoplates improves its NIR photon absorption capability resulting in better heat conversion efficiency. After initial rapid increase, the heating rate was lowered due to faster heat loss at higher temperatures [15]. For practical PTT application, it is desirable to get good photothermal conversion for smaller concentration of PTT agent and irradiation time. Present studies show that for a concentration of 0.4 mg/mL, temperature of the suspension reaches around 45°C within 10 min of laser irradiation. Most of the tumor cells can be killed in this temperature range [3, 25]. Photothermal stability of nanoplates at 0.4 mg/mL was studied by recording temperature of the suspension for 5 cycles of laser irradiation. Each cycle takes 25 min in which 15 min for laser irradiation and 10 min for returning the temperature of suspension to initial value. Nanoplate suspension exhibited excellent photothermal stability by displaying temperature $51 \pm 1.2^\circ\text{C}$ for 15 min of laser irradiation in each cycle.

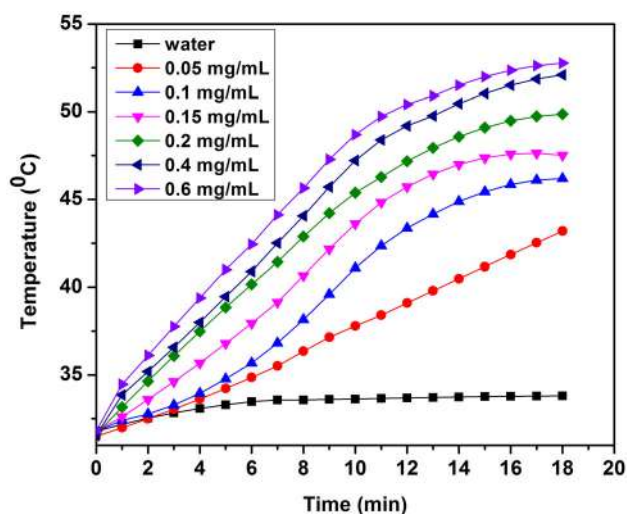


Fig. 7 Photothermal heating curves of pure water and WS₂ nanoplate suspension with different concentrations under 808 nm laser irradiation having power density of 1.5 Wcm^{-2}

Charge and size distribution profile of nanoplate suspension in water is crucial to elucidate their photothermal effect and stability. For comprehensive analysis in this concern, DLS measurements were performed on 0.4 mg/mL nanoplate suspension. Visibly, these nanoplates are highly hydrophilic and readily dispersed in water. DLS data revealed that the average hydrodynamic sizes of the WS₂ nanoplates are 215 nm and the suspension is uniform with no large agglomerates (Fig. 8a). The nanoplate suspension obtained has an obvious Tyndall effect, designating the presence of freestanding and homogeneous distribution of nanoplates making them excellent candidate for PTT agent [26]. Zeta potential is a key physicochemical parameter that impacts the stability of nano suspensions. Stable suspensions must have extremely positive or negative zeta potential values (with magnitude) that ensure larger repulsive forces [27, 28]. Average zeta potential for WS₂ nanoplates in water is -37 mV , which indicates high colloidal stability of the suspension (Fig. 8b).

Photothermal performance of WS₂ nanoplate suspension with aging was also monitored (Fig. 9a). Photothermal performance of the sample was found to decrease by a small extend when kept for one day. The result is expected as we observed that there is a slight decrease in NIR photon absorption for suspensions kept for one day (Fig. 5). DLS results also disclose that the average hydrodynamic size of these nanoplates have not varied significantly even after one day, denoting stable dispersion without particle aggregation (Fig. 9b). All these results point towards the excellent stability of nanoplate suspension [15].

Stability of photothermal agent at environments having different pH values are of great importance while dealing with their practical applications. Value of zeta potential, which indicates dispersion stability, was monitored for WS₂ nanoplate suspension at different pH values. The pH of the suspension was adjusted by adding 0.01 M NaOH solution. It was observed that zeta potential value increases as the value of pH increases (Fig. 9c). WS₂ nanoplate suspension have negative zeta potential (-37 mV) at pH value of 4. If more alkali (NaOH) is added to this suspension, the nanoplates tend to acquire more negative charge. That's why zeta potential increases with pH value. Shalom et al also observed similar variation in zeta potential with pH for WS₂ nanoplatelets [29]. In general WS₂ nanoplate suspension is stable in the pH range 4–10 [30, 31].

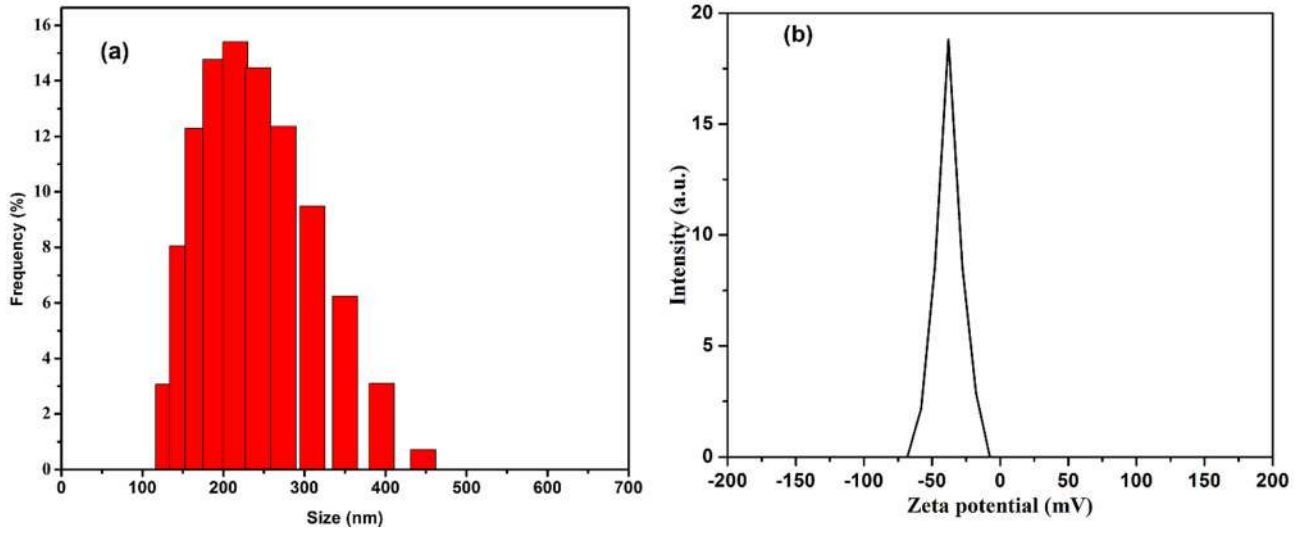


Fig. 8 a The size distribution and b zeta potential of WS₂ nanoplates measured by DLS

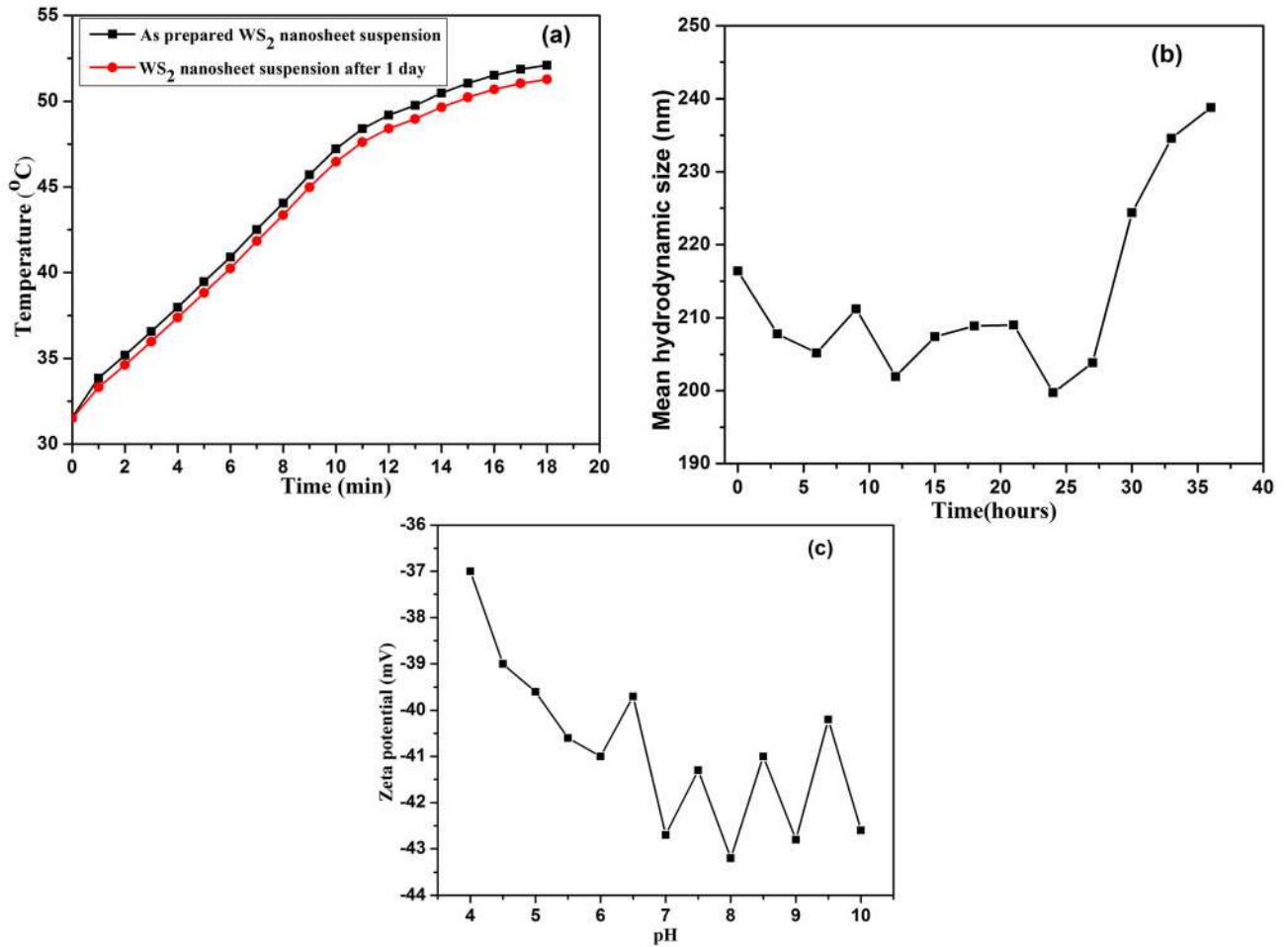


Fig. 9 a Photothermal conversion curves of WS₂ nanoplate and b aggregation stability of WS₂ nanoplate suspension studied over time c variation in zeta potential of WS₂ nanoplate suspension with pH

Preparations of reproducible suspension of nanostructures are the basic requirement in photothermal therapy related experiments. Reproducibility of a suspension is mainly governed by size distribution, shape, and surface charge of their particles. DLS studies were employed to investigate the reproducibility of WS₂ nanoplate suspension prepared at different times (maintaining same concentration of 0.4 mg/mL) by monitoring polydispersity index and mean zeta potential (Fig. 10). For 5 trials, zeta potential values were in the range $-(37 \pm 4)$ mV and polydispersity index values in the range 0.76 ± 0.37 . For each trial, photothermal heating curves were drawn and temperature after 10 min of NIR laser irradiation was found to be in the range 46.9 ± 1.9 °C. Range of zeta potential and polydispersity index was within the range for good colloidal stability [27, 32–34]. As a result, the measured temperature of WS₂ nanoplate suspension is almost consistent in all the trials.

In order to check the extent of homogeneity of the WS₂ suspensions prepared in different trials, DLS and SEM measurements were taken in each trial. It was observed that for each trial, there is a clear correlation between the peak of the particle size distribution as obtained by the DLS study and the nanosheet length (L) as measured by SEM (Fig. 11). The values can be correlated to some extent using the equation

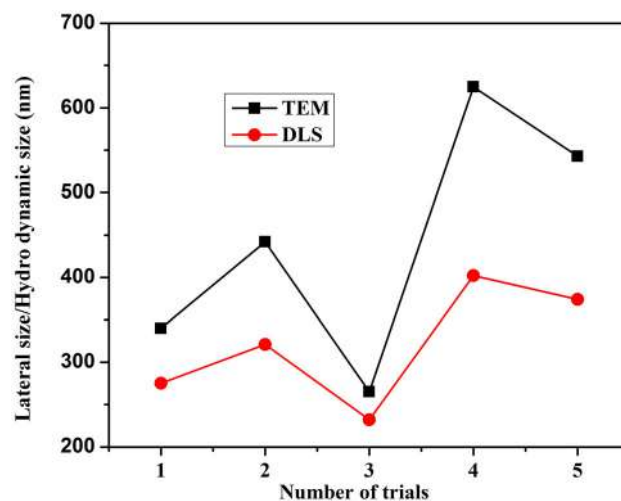


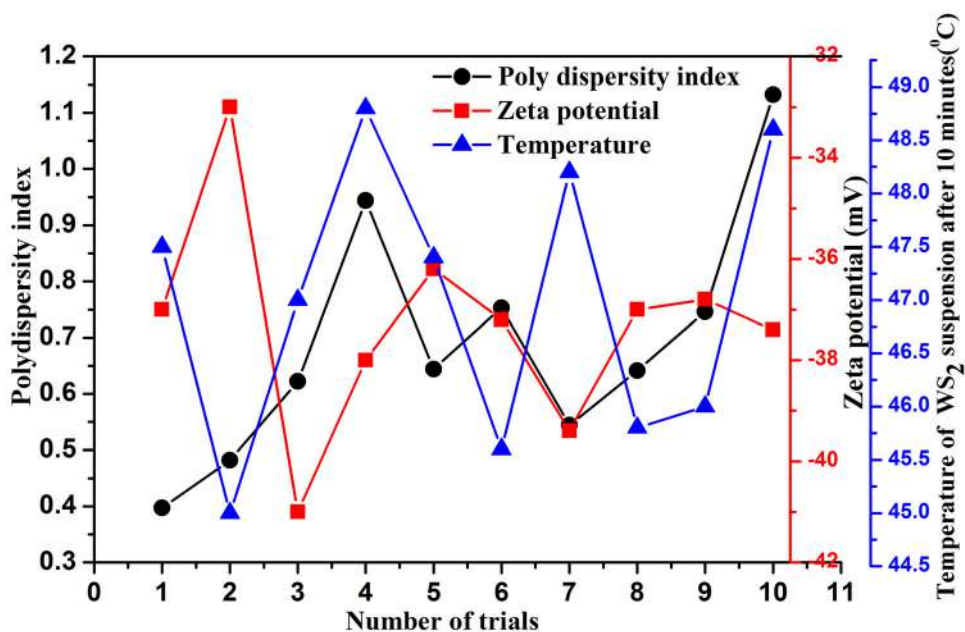
Fig. 11 Comparison of lateral size and hydrodynamic size of WS₂ nano plates for different trials obtained from SEM and DLS measurements

$$L = (0.07 \pm 0.03)d^{1.5 \pm 0.15}$$

where d is hydrodynamic radius obtained from DLS measurements [17, 35].

Generally atomic force microscopy or transmission electron microscopy was used for measuring length of nanosheets or nanoplates. These methods are tedious and can be inaccurate due to nanosheet aggregation during deposition from the dispersion. But DLS is a simple, straightforward, and fast in situ method that uses equipment which is commonly available. From the above observations it is clear that

Fig. 10 Variations in polydispersity index, zeta potential, and temperature (after 10 min of NIR laser irradiation) for WS₂ nanoplate suspension for different trials



if the DLS data is calibrated once using SEM data, DLS data can provide information about the length of the suspended nanoplates.

4 Conclusion

Highly refined rectangular shaped WS₂ nanoplates were prepared through solvothermal method and characterized using XRD, SEM, TEM, N₂ adsorption–desorption isotherm, and BET analysis. UV–Vis–NIR absorption spectrum of the samples shows remarkable absorption in NIR region and hence used as photothermal agent for photothermal therapy. Even for a concentration of 0.4 mg/mL, the temperature of WS₂ suspension reaches around 45 °C within 10 min of laser irradiation, which is enough to destroy many cancer cells. WS₂ suspension also showed excellent photothermal stability and reproducibility which are essential in photothermal therapy. Attempts were done to study the photothermal performance of WS₂ nanoplate suspension by monitoring size and charge distribution using DLS method. Average sizes of the WS₂ plates are 215 nm without large agglomerates and average zeta potential is -37 mV, indicating high colloidal stability. Photothermal performance of WS₂ suspension does have small depreciation even the suspension kept for one day. Small decrease in absorption as indicated in UV–Vis–NIR absorption studies and no drastic variation in hydrodynamic radius support above results. Zeta potential of the suspension increase as pH of the medium increases, indicating excellent stability of prepared suspension at different pH environments. Finally, attempts were performed for correlating peak of the particle size distribution as obtained by the DLS study and the nanoplate length as measured by SEM and it revealed satisfactory correlation between the two.

Acknowledgements

One of the author (SMV) acknowledges the financial support from UGC, India, for providing fellowship under “Dr. D S Kothari Post-Doctoral fellowship scheme.” We thank CSIF, University of Calicut, Kerala, for taking BET analysis. The Authors are also thankful to Prof M. K. Jayaraj, Department of Physics, Cochin University of Science And Technology,

Kerala, India, for providing facilities and having discussions.

Author contributions

All authors contributed to the overall preparation of the manuscript. The preparation of samples, data collection, interpretation, and the first drafting of the manuscript was performed by MVS. The draft was thoroughly checked and valuable comments were given by RG and KSD.

Funding

Funding was provided by University Grants Commission.

Data availability

The datasets generated during and/or analyzed during the current study are available from the corresponding author on reasonable request.

Declarations

Conflict of interest The authors declare that they have no known competing financial interests or personal relationships that could have appeared to influence the work reported in this paper.

References

1. X. Zhang, S.Y. Teng, A.C.M. Loy, B.S. How, W.D. Leong, X. Tao, *Nanomaterials* **10**, 1012 (2020)
2. Y. Wang, K. Huang and Xu Wu, *Biosens. Bioelectron.*, 2017, 97, 305–316.
3. H. Yan, J. Li, D. Liu, X. Jing, D. Wang, L. Meng, *CrytEngComm* **20**, 2324 (2018)
4. G. Huang, H. Liu, S. Wang, X. Yang, B. Liu, H. Chena, M. Xu, *J. Mater. Chem. A* **3**, 24128 (2015)
5. L. Zhou, S. Yan, Z. Lin, Y. Shi, *Mater. Chem. Phys.* **171**, 16–21 (2016)
6. Q. Liu, X. Li, Z. Xiao, Y. Zhou, H. Chen, A. Khalil, T. Xiang, J. Xu, W. Chu, X. Wu, J. Yang, C. Wang, Y. Xiong, C. Jin, P.M. Ajayan, L. Song, *Adv. Mater.* **27**, 4837–4844 (2015)
7. X. Shang, J. Chi, S. Lu, J. Gou, B. Dong, X. Li, Y. Liu, K. Yan, Y. Chai, C. Liu, *Appl. Surf. Sci.* **392**, 708–714 (2017)

8. J. Qian, Z. Peng, P. Wang, X. Fu, A.C.S. Appl, Mater Interfaces **8**(26), 16876–16884 (2016)
9. Y. Sang, Z. Zhao, M. Zhao, P. Hao, Y. Leng, H. Liu, Adv. Mater. **27**, 363–369 (2015)
10. X. Zhang, J. Wang, H. Xu, H. Tan, X. Ye, Nanomaterials **9**, 840 (2019)
11. V.G. Pol, S.V. Pol, A. Gedanken, Cryst. Growth Des. **8**, 1126–1132 (2008)
12. M. Liu, A. Geng, J. Yan, Int. J. Hydrog. Energy **45**, 2909–2916 (2020)
13. L. Cheng, J. Liu, X. Gu, H. Gong, X. Shi, T. Liu, C. Wang, X. Wang, G. Liu, H. Xing, W. Bu, B. Sun, Z. Liu, Adv. Mater. **26**, 1886–1893 (2014)
14. Y. Yong, L. Zhou, Z. Gu, L. Yan, G. Tian, X. Zheng, X. Liu, X. Zhang, J. Shi, W. Cong, W. Yin, Y. Zhao, Nanoscale **6**, 10394 (2014)
15. Q. Liu, C. Sun, Q. He, A. Khalil, T. Xiang, D. Liu, Y. Zhou, J. Wang, L. Song, Nano Res. **8**, 3982–3991 (2015)
16. S. Wang, J. Zhao, H. Yang, C. Wu, F. Hu, H. Chang, G. Li, D. Ma, D. Zou, M. Huang, Acta Biomater. **58**, 442–454 (2017)
17. M. Lotya, A. Rakovich, J.F. Donegan, J.N. Coleman, Nanotechnology **24**, 265703 (2013)
18. V. Uskoković, J. Dispers. Sci. Technol. **33**, 1762–1786 (2012)
19. P.M. Carvalho, M.R. Felício, N.C. Santos, S. Gonçalves, M.M. Domingues, Front Chem. **6**, 237 (2018)
20. A. Khataee, P. Eghbali, M.H. Irani-Nezhad, A. Hassani, Ultrason. Sonochem. **48**, 329–339 (2018)
21. K. Hu, J. Zhou, Z. Yi, C. Ye, H. Dong, K. Yan, Appl. Surf. Sci. **465**, 351–356 (2019)
22. Y. Dai, L. Wei, M. Chen, J. Wang, J. Ren, Q. Wang, Y. Wu, Y. Wang, X. Cheng, X. Yan, J. Nanosci. Nanotechnol. **18**, 3165–3170 (2018)
23. H.S. Han, K.Y. Choi, Biomedicines. **9**, 305 (2021)
24. A. Pasciak, R. Marin, L. Abiven, A. Pilch-Wróbel, M. Misiaik, W. Xu, K. Prorok, O. Bezkravnyy, Ł. Marciniak, C. Chanéac, F. Gazeau, R. Bazzi, S. Roux, B. Viana, V. Lehto, D. Jaque, A. Bednarkiewicz, A.C.S. Appl, Mater. Interfaces. **14**, 33555–33566 (2022)
25. K.M. Mayle, K.R. Dern, V.K. Wong, S. Sung, K. Ding, A.R. Rodriguez, Z. Taylor, Z.H. Zhou, W.S. Grundfest, T.J. Deming, D.T. Kamei, SLAS Technol. **22**, 18–25 (2017)
26. Y. Liu, J. Xiong, S. Luo, R. Liang, N. Qin, S. Liang, L. Wu, Chem. Commun. **51**, 15125–15128 (2015)
27. S.N.A. Shah, S. Shahabuddin, M.F.M. Sabri, M.F.M. Salleh, S.M. Said, K.M. Khedher, N. Sridewi, Nanomaterials **10**, 1340 (2020)
28. W. Liao, L. Zhang, Y. Zhong, Y. Shen, C. Li, N. An, Onco Targets Ther. **11**, 1949–1960 (2018)
29. H. Shalom, T. Bendikov, Y. Feldman, N. Lachman, A. Zak, R. Tenne, Chem. Phys. Lett. **761**, 138052 (2020)
30. R. Bhandavat, L. David, G. Singh, J. Phys. Chem. Lett. **3**, 1523–1530 (2012)
31. D. Mosconi, G. Giovannini, N. Maccaferri, M. Serri, S. Agnoli, D. Garoli, Materials **12**, 3286 (2019)
32. M. Ciancone, K. Mebrouk, N. Bellec, C.L. Goff-Gaillard, Y. Arlot-Bonnemains, B.T. Benvegnu, M. Fourmigué, F. Camerela, S. Cammas-Marion, J. Mater. Chem. B **6**, 1744–1753 (2018)
33. J. Amaro-Gahete, A. Benítez, R. Otero, D. Esquivel, C. Jiménez-Sanchidrián, J. Morales, Á. Caballero, F.J. Romero-Salguero, Nanomaterials **9**, 152 (2019)
34. D. Maziukiewicz, B.F. Grzeskowiak, E. Coy, S. Jurga, R. Mrówczyński, Biomimetics **4**, 3 (2019)
35. Y. Yue, Y. Kan, H. Choi, A. Clearfield, H. Liang, Appl. Phys. Lett. **107**, 253103 (2015)

Publisher's Note Springer Nature remains neutral with regard to jurisdictional claims in published maps and institutional affiliations.

Springer Nature or its licensor (e.g. a society or other partner) holds exclusive rights to this article under a publishing agreement with the author(s) or other rightsholder(s); author self-archiving of the accepted manuscript version of this article is solely governed by the terms of such publishing agreement and applicable law.

Structural Tuning Effect to Enhance the Nonlinear Optical Response of Salen Type Compounds

Nithya Mohan^{1, 2}, Sreejith S. S.^{3, a)}, Mohanan P.V.¹, and M. R. Prathapachandra Kurup¹

¹Department of Applied Chemistry, Cochin University of Science and Technology, Kochi, Kerala, India.

²SCMS School of Engineering & Technology (SSET), Vidya Nagar, Palissery, Karukutty, Kerala, India

³Department of Chemical Oceanography, School of Marine Sciences, Cochin University of Science and Technology, Kochi, Kerala, India.

^{a)} Corresponding author: sssreejith@cusat.ac.in

Abstract. Third order nonlinear optical properties of salen Schiff base complexes (1-4) functionalized with different electron donor acceptor groups (DA groups) were investigated in solution state via Z-Scan technique with Nd:YAG laser source. Among the two different complexes (Ni(II) and Cu(II)), having same DA ligands; the one with Cu(II) centre shows highest response. Also, the ligand having extended π -conjugation exhibit highest third order NLO activity. Electron donating substituent present in the imine spacer also affects the nonlinear response of the compound and also indicates that nonlinear optical (NLO) response of an inorganic material can be fine-tuned by the proper selection of central metal atom as well as the organic counterpart.

INTRODUCTION

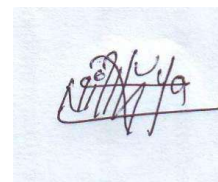
The materials with large macroscopic nonlinearities have great interdisciplinary interest as the design and synthesis of these materials are hot topic in the research field in modern chemistry, physics and material science.¹⁻³ The multifaceted application of NLO materials include signal processing, bioimaging, optical switching etc. From the early time itself different organic molecules and polymers were reported as NLO active materials and later on the inorganic chemists explored this field employing metal complexes. Among the various NLO active materials, inorganic complexes draw great attention since one can make use of the advantages of both inorganic and organic moieties. The metal atom present in these complexes can impart structural rigidity and can alter the properties of organic ligands so as to tune for better NLO responses.^{4, 5} Among the various transition metal complexes, complexes of Schiff bases possess relatively large hyper polarizabilities due to the delocalization of π electrons which make them good NLO molecules.^{6, 7}

In short, successful synthesis of nonlinear optical materials can be developed for commercial device -applications like optical limiters, optical switching, optical phase conjugation etc.^{8, 9} As far as salen-type Schiff bases and their complexes are concerned this field is still in its infancy since third order nonlinear property study and reports on these ligand systems and their complexes are very rare to find in the literature.

MATERIALS AND METHODS

General Information

All reagents and solvents used for the syntheses and studies were of analytical grade and used without further purification.



Syntheses

We have synthesized five different nickel complexes using bicompartamental salen Schiff base ligands via [2+1] condensation reaction (Figure 1).¹⁰ All the complexes reported are synthesized by adopting one pot method. The aldehyde and diamines were mixed in 1:2 molar ratios for about 2 hours in acetonitrile solvent. Once the ligand formation is confirmed, the metal salt was added to the same reaction mixture in 1:1 ratio for complexation.

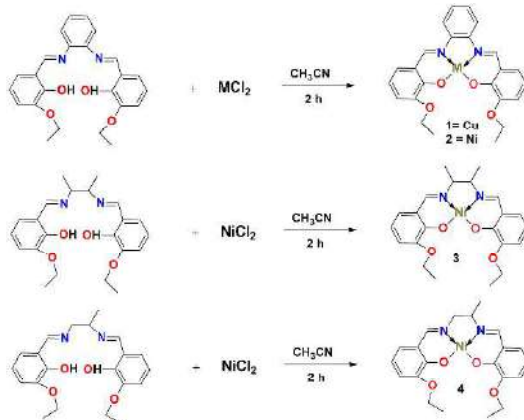


FIGURE 1. Synthetic route for the formation of salen compounds (1-4).

Physical Measurements

Elemental analyses (C, H and N) were performed in Vario EL III CHNS elemental analyser. IR spectra of the compounds were recorded on a JASCO FT-IR-5300 Spectrometer and electronic absorption spectra of the compounds were taken on a Thermo scientific Evolution 220 spectrophotometer. ¹H NMR spectra of the ligands and compounds were recorded in Bruker AVANCE II 500 NMR Spectrometer using CDCl₃ as solvent. The Z-scan measurements were done with a Q switched Nd:YAG laser (Quanta-Ray INDI-40) of 7 ns pulse width and 10 Hz repetition rate operating at 532 nm wavelength as the excitation source and the energy of reference and transmitted beam energy were measured from RjP-735, Laser Probe, USA. The ratiometric measurements of energy were done using Rj-7620, Laser Probe Corp., USA. Single-crystal analyses were performed on a Bruker SMART APEX diffractometer, equipped with a graphite crystal incident-beam monochromator, and a fine focus sealed tube with Mo K α ($\lambda = 0.71073$ Å) as the X-ray source.

RESULTS AND DISCUSSIONS

Characterization Of Compounds 1 to 4

Compound **1 (CuL1)**: Yield (79.3%); FTIR/cm⁻¹ (KBr) 3504 (–OH_{assy}), 3481 (–OH_{sy}) 2942 (CH_{st}), 1614 (C=N), 1473 (Ar C=C), 1352 (C–O_{phenolic}), 1242 (C–O_{ethoxy}). Anal.calc. for C, 59.56; H, 5.00; N, 5.79; Found C, 60.18; H, 5.17; N, 5.52.

Compound **2 (NiL1)**: Yield (74.2%); FTIR/cm⁻¹ (KBr) 3557 (–OH_{assy}), 3507 (–OH_{sy}) 2945 (CH_{st}), 1618 (C=N), 1468 (Ar C=C), 1364 (C–O_{phenolic}), 1241 (C–O_{ethoxy}), Anal.calc. for C₂₄ H₂₄ N₂ Ni O₅: C, 60.16; H, 5.05; N, 5.85; Found: C, 60.24; H, 4.97; N, 6.12.

Compound **3 (NiL2)**: Yield (76.4%); FT IR/cm⁻¹ (KBr) 3566 (–OH_{assy}), 3514 (–OH_{sy}) 2928 (CH_{st}), 1621 (C=N), 1463 (Ar C=C), 1389 (C–O_{phenolic}), 1241 (C–O_{ethoxy}), Anal. calc. for C₂₂ H₂₈ Ni N₂O₄: C, 57.55; H, 6.15; N, 6.10; Found: C, 57.22; H, 5.82; N, 6.44.

Compound **4 (NiL3)**: Yield (76.8%); FT IR/cm⁻¹ (KBr) 3452 (–OH_{st}), 2947 (CH_{st}), 1623 (C=N), 1451 (Ar C=C), 1327 (C–O_{phenolic}), 122 (C–O_{ethoxy}), Anal.calc. for C₂₁H₂₄Ni N₂O₄: C, 59.05; H, 5.66 ;N, 6.56. Found C, 59.02 ;H, 5.68; N, 6.57%.

Nonlinear Optical Properties

It is reported that in a given set of salen-type Schiff base metal compounds with different central metal ions, Cu(II) and Ni(II) compounds show the most nonlinear absorption.¹¹⁻¹⁴ So compounds containing Cu(II) and Ni(II) metal ions were selected for the study. As far as the ligand systems are concerned, H₂L¹ was the first choice since it represents the system with o-phenylenediamine as the diamine group. This in turn results in the maximum π -conjugation and therefore strong delocalization of π -electrons, a criterion to enhance NLO activity.¹⁵ Moreover, it contains both electrons that are free to move within the extended π -systems of the ligands and the additional energy levels introduced by the presence of the metal. The second ligand system chosen was H₂L² which contains donor methyl carbon groups attached to the two carbons intervening the two nitrogen atoms of the diimine spacer group. These donor groups can pump electrons to the system which again assists in the NLO activity. For the measurements, liquid samples of concentration 1×10^{-5} mol/L were prepared in DMSO.

Here, we have synthesized four different Ni(II)/Cu(II) complexes having different spacer groups in order to study the nonlinear optical behavior and also the effect of substituent in their nonlinear behavior. The samples were prepared in DMSO solution having 10^{-5} M concentration and the Z scan curve of all the four compounds show a decrease in transmittance with the increase of intensity which evidences \textbackslash RSA (Fig. 2). The obtained results can be fitted, TPA coefficient β and two photon cross section were determined (Table 1). A blank experiment with the solvent was also conducted and confirm that the solvent has no significant effect on NLO activity of the synthesized compounds.

TABLE 1. Calculated values of two photon absorption coefficients (β) and imaginary part of third order susceptibility ($\text{Im } \chi^{(3)}$) of compounds (1 to 4) at 532 nm.

Compounds	Two photon		$\text{Im } \chi^{(3)}$ (10^{-6} esu)
	absorption coefficient (β) (10^{-10} m/W)	Two photon cross section (σ) (GM)	
1	4.62	2864	19.86
2	2.58	1599	11.08
3	1.64	1016	7.28
4	1.28	793	5.46

Substituents Effect on NLO Responses

In order to find the structural effect on NLO activity of salen Ni(II)/Cu(II) compounds, We have measured two photon absorption coefficient (β) and third order nonlinear susceptibility ($\text{Im } \chi^{(3)}$) by open aperture z-scan technique. Only those materials having high value of susceptibility are suitable for nonlinear optics. On comparing the same spacer groups, compounds having extended π conjugation exhibits highest NLO response. Among the four compounds, 1 and 2 bearing o-phenylene imine groups have the highest value of two photon absorption coefficients (β). Comparing 3 and 4, compound 3 shows highest NLO response due to the presence of one additional +I group present which pumps electrons to the central metal atom. Also, It can be concluded that among the tested compounds, compounds having the same ligand system, always Cu(II) compound shows the highest NLO absorption which is in agreement with the reported literature.¹² Jahn-Teller distortion of d⁹ Cu(II) metal ion can be credited to this phenomenon where by the magnitude of splitting of electronic energy levels are higher than other first row transition metals. This results in the easy transfer of electrons between ligand system and the metal.¹⁶ This reveals the fact that, besides changing the electronic structure of the ligand system, the NLO response can be fine-tuned by using a metal centre of appropriate choice which can't be achieved in organic counterparts.

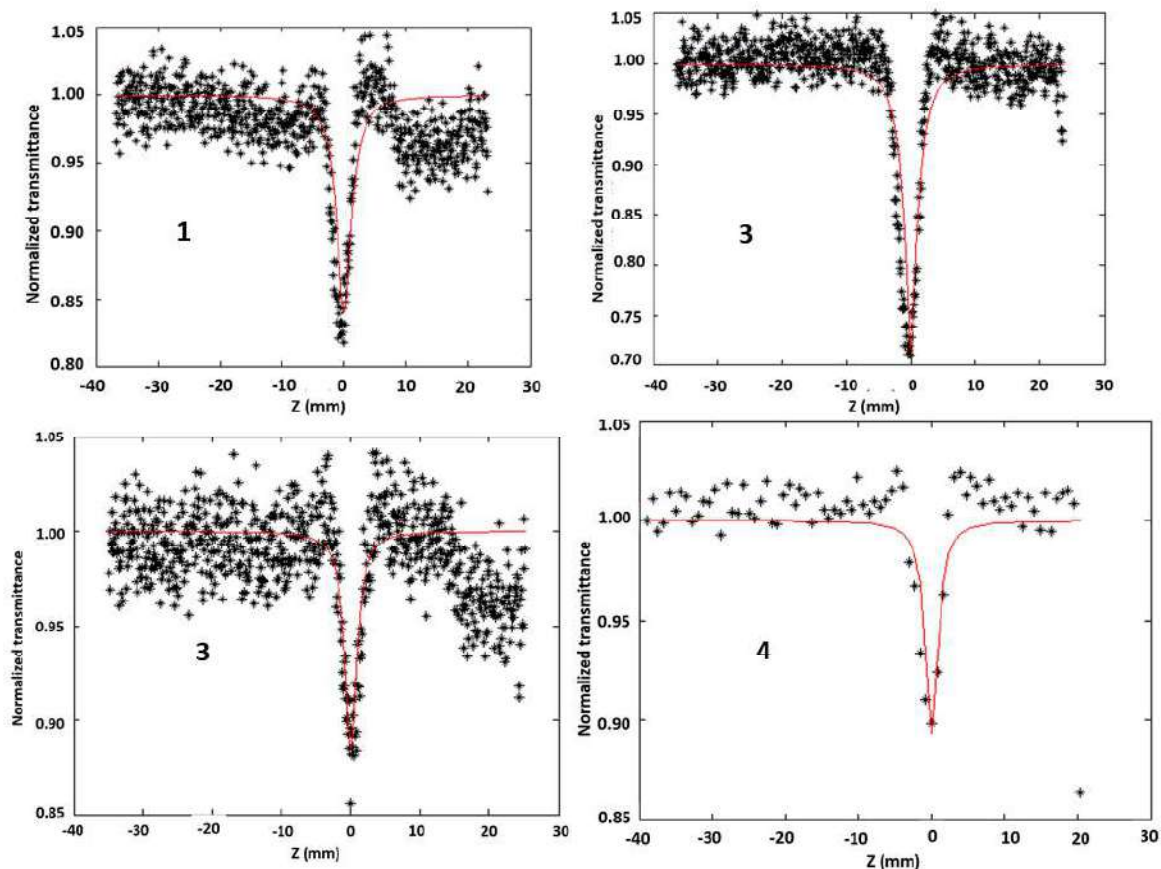


FIGURE 2. Open aperture Z- scan trace of compounds 1 to 4.

(Red line is the theoretical fit to the experimental data)

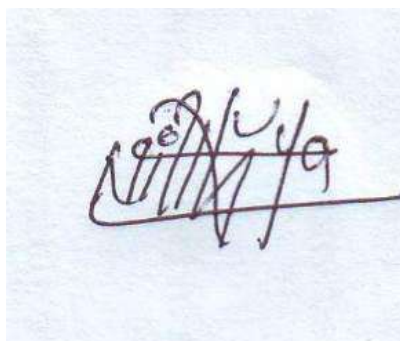
CONCLUSION

In this work, we report four salen Ni(II)/Cu(II) complexes with excellent non-linear optical activity. Third order nonlinear optical (NLO) activity of the complexes were probed using laser pulses of wavelength 532 nm by employing open aperture Z-scan technique. Compound 1 and 2 belonging to the salophen family (o-phenylene diimine spacer group) exhibited the highest activity followed by 3 which has an 1,2-diimino propane spacer group. Among the salophen compounds, one with Cu(II) at the centre exhibits highest activity over the other. These observations reveal that proper tuning of delocalization by introducing different substituent at the organic ligand moiety and the metal center will enhance the optical nonlinearity.

REFERENCES


1. M.-Y. Ran, Z. Ma, X.-T. Wu, H. Lin and Q.-L. Zhu, *Inorganic Chemistry Frontiers* **8** (22), 4838-4845 (2021).
2. G. Lingamallu, S. G. Palivela, G. Reddy and S. Prasanthkumar, *Physical Chemistry Chemical Physics* (2021).
3. Z. Xing, W. Wu, Y. Miao, Y. Tang, Y. Zhou, L. Zheng, Y. Fu, Z. Song and Y. Peng, *Organic Chemistry Frontiers* **8** (8), 1867-1889 (2021).
4. J. A. McCleverty, *Comprehensive coordination chemistry II*. (Amsterdam: Elsevier, 2003).
5. N. Mohan, S. SS, V. Kuttippurath, C. Keloth and M. P. Kurup, *Applied Organometallic Chemistry* **33** (5), e4900 (2019).
6. H. Ünver, A. Karakas and A. Elmali, *Journal of molecular structure* **702** (1-3), 49-54 (2004).

7. A. Karakaş, A. Elmali, H. Ünver and I. Svoboda, *Spectrochimica Acta Part A: Molecular and Biomolecular Spectroscopy* **61** (13-14), 2979-2987 (2005).
8. N. J. Long, *Angewandte Chemie International Edition in English* **34** (1), 21-38 (1995).
9. S. Shi, *Contemporary physics* **35** (1), 21-36 (1994).
10. N. Mohan, S. SS, P. S. Begum and M. P. Kurup, *Applied Organometallic Chemistry* **33** (9), e5064 (2019).
11. N. Novoa, T. Roisnel, P. Hamon, S. Kahlal, C. Manzur, H. M. Ngo, I. Ledoux-Rak, J.-Y. Saillard, D. Carrillo and J.-R. Hamon, *Dalton Transactions* **44** (41), 18019-18037 (2015).
12. J. Tedim, S. Patrício, R. Bessada, R. Morais, C. Sousa, M. B. Marques and C. Freire, (WILEY-VCH Verlag Weinheim, 2006).
13. A. Trujillo, M. Fuentealba, D. Carrillo, C. Manzur, I. Ledoux-Rak, J.-R. Hamon and J.-Y. Saillard, *Inorganic chemistry* **49** (6), 2750-2764 (2010).
14. J. P. Costes, J. F. Lamere, C. Lepetit, P. G. Lacroix, F. Dahan and K. Nakatani, *Inorganic chemistry* **44** (6), 1973-1982 (2005).
15. D. M. Roundhill and J. P. Fackler Jr, *Optoelectronic properties of inorganic compounds*. (Springer Science & Business Media, 2013).
16. J. M. Floyd, G. M. Gray, A. G. V. Spivey, C. M. Lawson, T. M. Pritchett, M. J. Ferry, R. C. Hoffman and A. G. Mott, *Inorganica chimica acta* **358** (13), 3773-3785 (2005).



RESEARCH ARTICLE | SEPTEMBER 22 2023

Fuzzy Z+ transforms: An overview and applications in nondestructive testing

Surya Kattazhath Appukuttan; Reshma Raveendranath 

 Check for updates

AIP Conf. Proc. 2856, 040023 (2023)

<https://doi.org/10.1063/5.0165990>


View
Online


Export
Citation

CrossMark

Articles You May Be Interested In

A functional integral formalism for quantum spin systems

J. Math. Phys. (July 2008)

Modes selection in polymer mixtures undergoing phase separation by photochemical reactions

Chaos (June 1999)

Spreading of a surfactant monolayer on a thin liquid film: Onset and evolution of digitated structures

Chaos (March 1999)

500 kHz or 8.5 GHz?
And all the ranges in between.

Lock-in Amplifiers for your periodic signal measurements



Find out more

 Zurich
Instruments

Fuzzy Z+ Transforms: An Overview And Applications In Nondestructive Testing

Surya Kattazhath Appukuttan^{1,a)} and Reshma Raveendranath^{2,b)}

^{1,2} SCMS School of Engineering and Technology, Karukutty, Kerala, India.

Corresponding author ^{b)} reshmar@scmsgroup.org

^{a)} suryaka@scmsgroup.org

Abstract. This work puts forth the fuzzy Z+ Transform concept.. A simple definition is provided. Some Examples are used to study related properties.. Using this properties difference equations of fuzzy is solved.

Keywords : Fuzzy valued functions , Fuzzy number ,Fuzzy set, Z+ Transform of Fuzzy , Inverse Z+ Transform on Fuzzy

INTRODUCTION

Different types of transforms of classical mechanics like Laplace and Fourier are an effective tool for solving differential equations and analysing continuous signals. They work by converting a space of regular functions into a space of special functions that makes computing significantly simpler.

Z+ Transform is considered as the Laplace transform of a sampled signal. It is a valuable tool for the analysis of discrete functions and for the solution of linear constant coefficient difference equation.

Zadeh was the one who initially came up with fuzzy sets (1965)¹ . Dubois and Prade(1980)² made use of extension principle in their works.This idea of fuzzy set was applied to various fields of mathematics including application of fuzzy set to transforms.Further works on Fuzzy transform was carried out by I.Perfilieva in her paper ³ (2006).Fuzzy Laplace Transform and its use in solving Fuzzy differential equation was studied by TofighAllahviranloo and M.Barkhordani Ahmadi(2010)⁴ .

I've attempted to define a novel paradigm for the analysis of discrete fuzzy functions in this work. Some of its properties studied and some basic formulas developed.

The structure of the paper is given below .

The fundamental definitions of fuzzy number, Extension principle and the definition of addition and fuzzy number scalar multiplication is listed in Section 2 . The Fuzzy Z+ Transform and its fundamental characteristics are defined examined in Section 3.. In Section 4 inverse Fuzzy Z+ Transform is defined and In Section 5 Solution of Fuzzy difference equation using Fuzzy Z+ Transform are investigated.

PRELIMINARIES

The basic definition of fuzzy number as given by Song and Wu (2000) in his paper ⁵ is as given below. Here R

Let the fuzzy number be $\mu:R \rightarrow [0,1]$ in which μ is a fuzzy set of real line R

- (1) There exist $x \in R$ such that $\mu(x) = 1$ where μ is normal
- (2) $\mu\lambda x + (1-\lambda)y \geq \min\{\mu(x), \mu(y)\} \quad \forall x,y \in R, \lambda$ belongs to the interval $[0,1]$ such that μ is convex .
- (3) μ is upper semi continuous.
- (4) Support of μ , $supp\mu = \{x \in R / \mu(x) > 0\}$ is bounded in R.

Let $E = \{\mu / \mu: R \rightarrow [0,1]\}$ such that E has been taken as collection of all fuzzy numbers on real numbers .

Let A_1, A_2, \dots, A_n be n fuzzy numbers on X_1, X_2, \dots, X_n and $X = X_1 \times X_2 \times \dots \times X_n$ is a Cartesian product of universe . f maps from X to Y, where $y = f(x_1, x_2, \dots, x_n)$. We can define fuzzy set in Y using the extension principle as :X

$B = \{(y, \mu(y)) / y = f(x_1, x_2, \dots, x_n), (x_1, x_2, \dots, x_n) \in X\}$, where

$$\mu_B(y) = \begin{cases} \text{supremum of } \min\{\mu_{A_1}(x_1), \mu_{A_2}(x_2), \dots, \mu_{A_n}(x_n)\} & \text{if } f^{-1}(y) \neq \emptyset \\ 0 & \text{if otherwise} \end{cases}$$

where f^{-1} is the inverse of f .

Now we consider the special case when $n=1$

Let X be the universe and A be a fuzzy number in X . f maps from X to Y , the universal set, that is $f: X \rightarrow Y$ where $y = f(x)$.

Then we can define fuzzy set in Y using the extension principle as :

$$B = \{(y, \mu_B(y)) / y = f(x), x \in X\}$$

$$\mu_B(y) = \begin{cases} \text{supremum of } \mu_A(x) & \text{if } f^{-1}(y) \neq \emptyset \\ 0 & \text{if otherwise} \end{cases}$$

Define operation of addition on E as

$$(u \oplus v) = \sup_{y \in R} \min\{u(y), v(x - y)\}, x \in R \quad (1)$$

The fuzzy number defined with the scalar multiplication is given as

$$(k \otimes u)(x) = \begin{cases} ku(x), & k > 0 \\ \tilde{0}, & k = 0 \end{cases} \quad (2)$$

where $\tilde{0} \in E$.

FUZZY Z^+ TRANSFORM

Let $f(n)$ be a discrete fuzzy valued function defined for all values of n . Then fuzzy Z^+ Transform of $f(n)$ is given as

$$F(x) = Z^+(f(m)) = \sum_{m=1}^{\infty} f(m) \otimes x^{-m}, \text{ for all integers } x > 0 \quad (3)$$

This fuzzy Z^+ Transform exist for all x such that equation (3) converges and $F(x) \in [0, 1]$

The set of values of x for which the sum (3) converges and belong to $[0, 1]$ is called the Region of convergence (ROC) of the fuzzy Z^+ Transform. For a given $f(m)$ there exist one and only one fuzzy Z^+ Transform and its associated ROC.

Similarly for a given fuzzy Z^+ Transform there exist one and only one discrete fuzzy function for which the summation (3) converges.

Theorem 1

Take $g(m)$ and $f(m)$ as fuzzy discrete valued functions and K_1, K_2 are constants then

$$Z^+[(K_1 \otimes f(m)) \oplus (K_2 \otimes g(m))] = (K_1 \otimes Z^+(f(m))) \oplus (K_2 \otimes Z^+(g(m))) \quad (4)$$

Proof:

$$\begin{aligned}
& Z^+[(K_1 \otimes f(m)) \oplus (K_2 \otimes g(m))] \\
&= \sum_{m=1}^{\infty} [(K_1 \otimes f(m)) \oplus (K_2 \otimes g(m))] \otimes x^{-m} \\
&= \sum_{m=1}^{\infty} K_1 \otimes f(m) \otimes x^{-m} \oplus \sum_{m=1}^{\infty} K_2 \otimes g(m) \otimes x^{-m} \\
&= (K_1 \otimes Z^+(f(m))) \oplus (K_2 \otimes Z^+(g(m)))
\end{aligned}$$

This shows that Z^+ transform is linear.

Theorem 2

$$Z^+(a^n) = \frac{a}{x-a} \tag{5}$$

$$\text{ROC} = \begin{cases} x > a : 0 \leq a \leq 0.5, a = 1, \\ x > a + 1 : 0.5 < a \leq 1, \end{cases}$$

Proof :

$$\begin{aligned}
Z^+(f(n)) &= \sum_{n=1}^{\infty} f(n) \otimes x^{-n} \\
Z^+(a^n) &= \sum_{n=1}^{\infty} a^n \otimes x^{-n} \\
&= a^1 \otimes x^{-1} + a^2 \otimes x^{-2} + a^3 \otimes x^{-3} + \dots \dots \dots \\
&= \frac{a}{x} + \frac{a^2}{x^2} + \frac{a^3}{x^3} + \dots \dots \dots
\end{aligned}$$

It is an infinite geometric series with common ratio $r = a/x$, $\text{Sum} = \frac{a/x}{1-a/x} = a/(a-x)$

converges if $\left| \frac{a}{x} \right| < 1 \Rightarrow |x| > a$ which implies $x > a$

If $0 \leq a \leq 0.5$ and $a = 1$, then ROC is $x > a$

If $0.5 < a \leq 1$, then ROC is $x > a + 1$

Example

$$Z^+(\delta\{n\}) = 0 \text{ where } \delta(n) = \begin{cases} 1, n = 0 \\ 0, n \neq 0 \end{cases} \tag{6}$$

Proof:

$$\begin{aligned}
Z^+(\delta\{n\}) &= \sum_{n=1}^{\infty} \delta\{n\} \otimes x^{-n} \\
&= \delta\{1\} \otimes x^{-1} + \delta\{2\} \otimes x^{-2} + \dots \\
&= 0 \otimes \frac{1}{x} + 0 \otimes \frac{1}{x^2} + \dots \dots \\
&= 0, \text{ region of convergence is the integer } x > 0
\end{aligned}$$

Example

$$Z^+([u(m)]) = \frac{1}{x-1} \text{ where } u\{m\} = \begin{cases} 1, m \geq 0 \\ 0, m < 0 \end{cases} \tag{7}$$

Proof:

By definition

$$\begin{aligned} Z^+\{(f(m))\} &= \sum_{m=1}^{\infty} (f(m)) \otimes x^{-m} \\ Z^+\{(u(m))\} &= \sum_{m=1}^{\infty} (u(m)) \otimes x^{-m} \\ &= 1 \otimes \frac{1}{x^1} + 1 \otimes \frac{1}{x^2} + 1 \otimes \frac{1}{x^3} + \dots \dots \dots \\ &= \frac{1}{x^1} + \frac{1}{x^2} + \frac{1}{x^3} + \dots \dots \dots \\ &= \frac{\frac{1}{x}}{1-\frac{1}{x}} = \frac{1}{x-1}, \text{ ROC is } x > 1 \end{aligned}$$

Theorem 3

$$Z^+[(f(m) u(m))] = Z^+(f(m)) \tag{8}$$

Proof :

$$\begin{aligned} Z^+[(f(m) u(m))] &= \sum_{m=1}^{\infty} [f(m)] [u(m)] \otimes x^{-m} \\ &= \sum_{m=1}^{\infty} [f(m)] (1) \otimes x^{-m} \\ &= \sum_{m=1}^{\infty} [f(m)] \otimes x^{-m} = Z^+(f(m)) \end{aligned}$$

Theorem 4

Take $f(m)$ as a fuzzy discrete valued function defined where $f[m] = 0$ for $m \leq 0$

Let $f(m - k)$ be the discrete function obtained by shifting $f(m)$ to the right by the positive integer k . Then

$$Z^+(f[m - k]) = x^{-k} F(x) \text{ where } Z^+(f(m)) = F(x) \tag{9}$$

Proof :

$$\begin{aligned} Z^+(f[m - k]) &= Z^+(f[m - k]u[m - k]) \\ &= \sum_{n=1}^{\infty} (f[m - k])(u[m - k]) \otimes x^{-m} \\ &= \sum_{n=k}^{\infty} (f[m - k]) \otimes (x^{-m}) \end{aligned}$$

Take $t = n-k$

$$\begin{aligned} &= \sum_{m=1}^{\infty} f(t) \otimes x^{-[m-k]} \\ &= \sum_{m=1}^{\infty} f[m] \otimes x^{-m} x^{-k} \\ &= [x^{-k}] [F(x)] \end{aligned}$$

Theorem 5

Take $f[m]$ to be fuzzy discrete valued function as $f[m]$ defined such that $f[m] = 0$ for $m \leq 0$. Let $f[m + k]$ be the function obtained by shifting $f(m)$ to the left by the integer k .

$$Z^+(f[m + k]) = x^k \left[F(x) - \frac{f(1)}{x} - \frac{f(2)}{x^2} - \dots \dots \dots - \frac{f(k)}{x^k} \right] \text{ where } F(x) = Z^+(f(m)) \tag{10}$$

Proof :-

$$\begin{aligned} Z^+(f(m+k)) &= \sum_{n=1}^{\infty} f\{m+k\} \otimes x^{-m} \\ &= x^k \sum_{n=1}^{\infty} f[m+k] \otimes x^{-m-k} \end{aligned}$$

Put $m+k = t$

$$\begin{aligned} &= x^k \sum_{m-k=1}^{\infty} [f[m] \otimes [x^{-m}]] \\ &= x^k \sum_{m=1+k}^{\infty} [f[m] \otimes x^{-m}] \\ &= x^k [\sum_{m=1}^{\infty} f[m] \otimes x^{-m} - \sum_{m=1}^k f[m] \otimes x^{-m}] \\ &= x^k [F(x) - (f(1)x^{-1} + f(2)x^{-2} + \dots + f(k)x^{-k})] \\ &= x^k \left[F(x) - \frac{f(1)}{x^1} - \frac{f(2)}{x^2} - \dots - \frac{f(x)}{x^k} \right] \end{aligned}$$

INVERSE FUZZY Z^+ TRANSFORM

Let $\{f(n)\}$ or $f(n)$ be a discrete fuzzy valued function defined for all values of n such that

$Z^+(f(n)) = F(x)$, for all integers $x > 0$. Then Inverse Fuzzy Z^+ Transform is given by $Z^{+^{-1}}(F(x)) = f(n)$.

NON-DESTRUCTIVE TESTING WITH THE FUZZY Z^+ TRANSFORM

⁷ Non-destructive testing is becoming an increasingly significant aspect of structural and material testing since it allows for the detection of physical qualities, internal anomalies such as cracks, and structural weakness that are not visible to the naked eye. Infrared testing, radiographic testing, guided wave testing, vibration analysis, and other procedures are routinely utilised. The majority of these tests are employed primarily in the construction business, and in most situations, the detection system can discover cracks and physical imperfections before a structure or product fails.

When compared to other traditional methods, image processing provides a greater benefit and accuracy in crack detection⁶. The crack detecting procedure's difficulty is solely determined on the image size.

The following is the procedure for fracture identification using image processing:

- (1) First, use a high-definition camera or other sources which make use of infrared testing or radiographic testing to capture structure image which when exposed to the crack detection method.
- (2) After the picture acquisition, the images collected are preprocessed, with various approaches, make the image processing process more productive and efficient.
- (3) To process the processed picture sample, certain approaches are used in image processing.
- (4) The end outcome of the processed image make the detection of fracture efficient.
- (5) Crack feature extraction helps in detecting cracks which are separated based on the direction of propagation, its width and depth

The difficulty of the crack detection procedure is entirely dependent on the image size.

A morphological technique for processing picture data is the Fuzzy Z^+ Transform. To use this tool, the collected photographs are processed and turned into discrete function. Using the fundamental formula, we can convert the gathered sample, which is represented as a discrete function, into a fuzzy valued image. This mathematical morphological technique reduces noise and interruptions by fuzzifying the sample to locate a crack-like structure in a noisy environment. The clarity and precision of the produced image are significantly increased with the help of the Fuzzy Z^+ Transform.

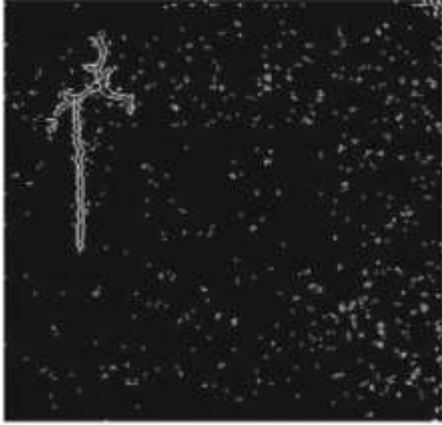


Figure 1



Figure 2

Figure 1 represents the picture data of the crack which is processed and made apt for image processing.

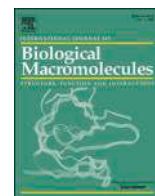
Figure 2 represents the processed image with less noise or disturbance.

CONCLUSION

Fuzzy Z^+ Transform forms a tool for the analysis of many fuzzy discrete functions. Along with its inverse it provides solution to initial valued fuzzy difference equation. It can also be used in many engineering problems involving image compression.

REFERENCES

1. Lotfi A. Zadeh. "Fuzzy sets. " [Information and control](#). 8(3), pp.338-353, (1965).
2. Didier Dubois and Henri Prade. "Fuzzy sets and systems: Theory and applications. " *Mathematics in science and engg.* vol 144(1980) pp.36-67.
3. I.Perfilieva . "Fuzzy transforms: Theory and applications. " [Fuzzy sets and systems](#). vol 157,issue 8, (16 April 2006), pp. 993-1023.
4. Tofigh Allahviranloo and M. Barkhordari Ahmadi. "Fuzzy Laplace transforms." [Soft Computing](#) (2010) 14:235-243.
5. Dubios D, Prade H. "Towards Fuzzy Differential calculus." [Fuzzy set systems](#) 8 (1982):1-7, 105-116, 225-233.
6. Arun Mohan and Sumathi Poobal "Crack Detection using image Processing:A Critical Review And Analysis". [Alexandria Engineering Journal](#) .Volume 57, Issue 2, June 2018, Pages 787-798
7. Christiane Maierhofer, Hans-Wolf Reinhardt and Gerd Dobmann "Non destructive Evaluation Of reinforced Concrete Structures-Volume 2".



Reuse of used paper egg carton boxes as a source to produce hybrid AgNPs-carboxyl nanocellulose through bio-synthesis and its application in active food packaging

G.R. Raghav^a, K.J. Nagarajan^{b,*}, M. Palaninatharaja^b, M. Karthic^c, R. Ashok kumar^d, M.A. Ganesh^b

^a Department of Mechanical Engineering, SCMS School of Engineering & Technology Karukutty, Cochin, Kerala, India

^b Department of Mechatronics Engineering, Thiagarajar College of Engineering, Madurai-625015, Tamil Nadu, India

^c Department of Mechanical Engineering, Thiagarajar College of Engineering, Madurai-625015, Tamil Nadu, India

^d Department of Mechanical Engineering, SRM Madurai College for Engineering and Technology, Pottapalayam-630612, Tamil Nadu, India

ARTICLE INFO

Keywords:

Urban solid waste
Bio-acid hydrolysis
In-situ generation process
AgNPs nanocellulose
Antibacterial properties

ABSTRACT

The proper disposal of disposable synthetic plastic food packaging materials presents a significant challenge for both the environment and the solid waste management community. To address this issue, an antibacterial-based high-strength bio-composite serves as the optimal alternative to conventional packaging materials. This study aims to produce a hybrid material of AgNPs-carboxyl cellulose nanocrystals (AgNPs-CCNCs), obtained from used egg carton boxes (UECBs), through bio acid hydrolysis and an in-situ generation process. Furthermore, AgNPs-carboxyl cellulose nanofibers (AgNPs-CCNFs) will be synthesized through a combination of bio acid hydrolysis and ball milling, followed by an additional in-situ generation step. The AgNPs-carboxyl nanocellulose (AgNPs-CCNCs, and AgNPs-CCNFs) exhibited excellent crystallinity index, morphology, thermal, and antibacterial properties. The morphological analysis was performed by electron microscopy, and the results showed the uniform distribution and spherical form of AgNPs appearing over the carboxyl nanocellulose through the in-situ generation process, which was confirmed through XRD analysis. The study further explores the impact of AgNPs-carboxyl nanocellulose on the mechanical, chemical, antibacterial, and thermal properties of the PVA matrix. The results demonstrate that the bio-nanocomposite film offers opportunities for utilization in active packaging applications.

1. Introduction

As people's schedules become more hectic, the demand for fresh, ready-to-cook, or ready-made food has increased in recent years, resulting in considerable advancements in active packaging within the food packaging business [1,2]. Incorporating nanofillers into bio-based, sustainable polymer matrices has been proven in several research studies to result in strong thermal, mechanical, and gas barrier properties as well as antibacterial activity, making them potentially helpful for food packaging applications. Biodegradable polymers not only fulfill this purpose, but they also help to minimize reliance on synthetic polymers, which pose a considerable environmental risk. Several naturally derived polymers, such as agar, polylactic acid (PLA), starch,

chitosan, cellulose, and proteins, are available and commonly employed as biomaterials in food packaging applications [3]. Among all biopolymers, cellulose is the most prevalent biodegradable polymer, with high thermal stability, biocompatibility, renewability, good mechanical strength, and low density. The use of cellulose in nanoscale dimensions as a reinforcement enhances the mechanical, thermal, and barrier qualities of the packaging material [4]. Nevertheless, because cellulose does not have antibacterial characteristics, it is regarded as having a significant drawback for usage as a reinforcing material in food packaging applications. To address this limitation, researchers have explored the use of silver nanoparticles (AgNPs), which are well-known for their antibacterial properties and ability to exhibit antifungal and antiviral activities even in trace amounts [5].

* Corresponding author.

E-mail addresses: raghavmechknce@gmail.com (G.R. Raghav), kjnmech@tce.edu, designnagarajan@gmail.com (K.J. Nagarajan), pnatharaja@tce.edu (M. Palaninatharaja), karthicmanokar@gmail.com (M. Karthic), ashok.hail@gmail.com (R.A. kumar), ganeshma2015@tce.edu (M.A. Ganesh).

<https://doi.org/10.1016/j.ijbiomac.2023.126119>

Received 16 June 2023; Received in revised form 21 July 2023; Accepted 1 August 2023

Available online 3 August 2023

0141-8130/© 2023 Elsevier B.V. All rights reserved.

Two primary methods are used to create hybrid metal nanoparticle and nanocellulose-reinforced polymer composites: 1) Blending pre-prepared metal nanoparticles and nanocellulose into a compatible polymer matrix, and 2) Utilizing in-situ chemical techniques to synthesize and embed metal nanoparticles onto the surface of nanocellulose, which can then be used as reinforcement in a polymer matrix [6].

The in-situ chemical technique offers several advantages over other methods, including reduced agglomeration, easier processing, shorter processing time, and the ability to generate metal nanoparticles on nanocellulose in a single step [7]. However, the use of a reducing agent is necessary for this process to produce stable AgNPs on nanocellulose. Commonly employed reducing agents like NaBH_4 , ascorbic acid, or hydrazine have been associated with human toxicity, rendering them unsuitable for biomedical and food packaging applications where residual agents may remain in the system [8,9].

To overcome this drawback, the research attitude among the researchers points towards exploring the alternatives for the toxic natured reducing agents such as natural polymers such as gelatin, keratin, starch, and carbohydrates like glucose, fructose, lactose, and sucrose to facilitate the conversion of the silver ions (Ag^+) into silver atoms (Ag^0), leading to the formation of AgNPs. These alternatives possess advantageous characteristics, including non-toxicity, cost-effectiveness, easy availability, energy efficiency, safety, and environmental friendliness. By utilizing these agents, processing hybrid AgNPs-nanocellulose composites can minimize the risk of environmental hazards [10].

Glucose ($\text{C}_6\text{H}_{12}\text{O}_6$) is a widely utilized food-grade compound among various types of bio-based reducing agents. It serves as a safe and cost-effective green-reducing agent to produce AgNPs [11]. Glucose, a monosaccharide with the molecular formula $\text{C}_6\text{H}_{12}\text{O}_6$, is derived from natural sources such as plants and fruits. It consists of a hexose structure, featuring a six-carbon chain with hydroxyl (-OH) groups attached to each carbon atom. When compared to other bio-reducing agents, glucose offers advantages such as control over nanoparticle size, affordability, biocompatibility, and stability of the metal particles on the nanocellulose. These characteristics make it a promising choice for a wide range of applications including catalysis, electronics, biomedicine, and environmental remediation [12,13]. In recent research, glucose ($\text{C}_6\text{H}_{12}\text{O}_6$) has been employed as a reducing agent under alkaline conditions for rapid and complete reaction. Sodium hydroxide (NaOH) acts as an accelerator in reducing solution-dispersed silver nanoparticles [14]. In addition, the hydroxyl groups found in nanocellulose carry numerous negative charges when in water. Furthermore, the presence of functional groups like carboxylic, sulfate, or amine groups in nanocellulose can facilitate the coordination of Ag^+ ions with the nanocellulose surface. These interactions promote the binding of Ag^+ ions and enhance their deposition onto the nanocellulose, aiding in the formation and stabilization of silver nanoparticles [15,16].

In India, there is an abundance of cellulose-rich plant fibers available in the form of agricultural, commercial, and domestic waste that remains unexplored. Consequently, in the latest trends, material science researchers and academicians are placing more emphasis on using waste products to produce nanocellulose and applying it to a range of applications, including engineering, cosmetic, medical, and food applications [17]. The use of paper egg carton boxes for packaging eggs is prevalent in the Indian state of Tamil Nadu. However, like numerous other packaging materials, improper disposal of these boxes can cause solid waste accumulation and the release of greenhouse gases in landfills. To address this issue, the Tamil Nadu Pollution Control Board has introduced various measures to promote waste reduction, recycling, and appropriate disposal of packaging materials, including paper egg carton boxes. In this scenario, there is a requirement to convert used egg carton boxes (UECBs) into useful forms without causing harm to the environment and potentially even generating economic benefits. These boxes can be effectively utilized to produce a value-added AgNPs - carboxylic nanocellulose for food packaging applications with the appropriate

sustainable technology.

Furthermore, there is no previous documentation of producing the hybrid AgNPs -carboxyl nanocellulose through a bio acid hydrolysis and in-situ generation process from UECBs. This aspect significantly contributes to the research's novelty and establishes a sustainable approach to developing eco-friendly antibacterial nanocomposites for active food packaging applications.

Following that, this research work has two main goals:

1. To synthesize hybrid AgNPs-carboxyl nanocellulose from UECBs using the bio acid hydrolysis and in-situ generation method. It will be characterized by standard chemical methods, X-ray photoelectron spectroscopy (XPS), X-ray diffraction (XRD), Fourier transform infrared spectroscopy (FT-IR), conductometric titration, field emission scanning electron microscopy (FE-SEM), high-resolution transmission electron microscopy (HR-TEM), antibacterial tests, and thermogravimetric analysis (TGA).
2. To investigate the potential of the synthesized AgNPs-carboxyl nanocellulose as a reinforcing component in PVA matrices for biodegradable polymer composites. This investigation will include mechanical, barrier, antibacterial, and TGA analyses.

2. Materials and methods

2.1. Materials

The damaged used paper egg carton boxes were collected from an egg wholesale distributor in Madurai City, Tamil Nadu, India. The chemicals used, such as acetic acid (CH_3COOH), formic acid (CH_2O_2), hydrogen peroxide (H_2O_2), cyanamide (NH_2CN), hydrochloric acid (HCl), citric acid ($\text{C}_6\text{H}_8\text{O}_7$), ethanol ($\text{C}_2\text{H}_5\text{OH}$), sodium hydroxide (NaOH), Polyvinyl alcohol (98 % hydrolyzed), glycerine, and silver nitrate (AgNO_3), were purchased from Sigma-Aldrich located in Bengaluru, Karnataka, India.

2.2. Hydra pulping process

The dried UECBs were sliced into pieces measuring 1–1.5 cm, as shown in Fig. 1c and loaded into a pulp disintegrator. The water to UECBs ratio was maintained at 200:2 (g:g). The disintegrator operated at a speed of 1500 rpm for 15 min at a temperature of 27 °C during the hydra pulping process (Fig. 1a). The resulting UECBs pulp was filtered through a square wire mesh measuring 0.3 cm × 0.3 cm and then dried in an oven at 80 °C for 120 min. The yield of UECBs pulp from UECBs was determined to be 95.5 %.

2.3. Cellulose extraction

Cellulose was extracted from UECBs pulp through a two-stage acidic organosolv treatment, followed by a hydrogen peroxide bleaching process activated by cyanamide. The organosolv treatment involved using a solution of $\text{CH}_2\text{O}_2/\text{CH}_3\text{COOH}/\text{H}_2\text{O}$ (30/60/10, v/v/v) with a liquor-to-pulp ratio of 20:1 (ml/g) at 85 °C for 4 h. To enhance the efficiency of the process, 0.1 % HCl was added as a catalyst. The resulting residue was filtered using Whatman filter paper, and the filtered material was washed sequentially with ethanol and distilled water. It was then dried in an oven at 68 °C for 16 h. The obtained residue underwent cyanamide-activated hydrogen peroxide bleaching using a mixture of 1.8 % H_2O_2 and 0.18 % NH_2CN (residue: extractant, 1:30, g/ml) at 50 °C and pH 10.0 for a duration of 4 h. The pure white isolated α -cellulose (Fig. 1a) obtained from the process was filtered, washed with water and ethanol, and subsequently dried in an oven at 60 °C for a day.

2.4. Isolation of CCNCs

The isolation of carboxyl cellulose nanocrystals (CCNCs) involved

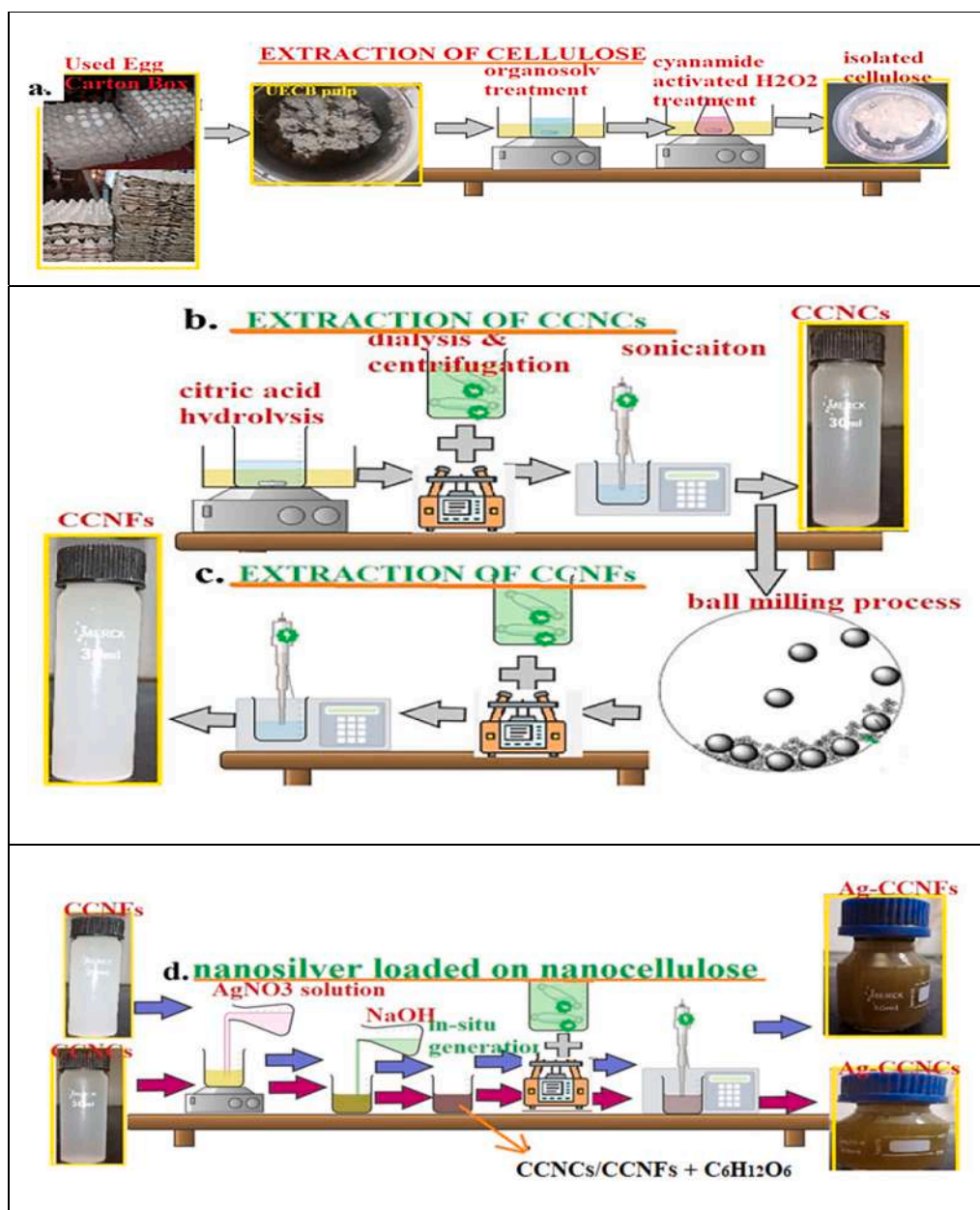


Fig. 1. a–c Systematic diagram of extraction methods of CCNCs and CCNFs from UECBs, d. in-situ generation process.

using isolated α -cellulose as the primary material and subjecting it to citric acid hydrolysis. The process consisted of stirring a citric acid solution (76 wt%) with a high-speed mechanical stirrer at a speed of 1500 rpm and a constant temperature of 100 °C for 4 h, with an isolated α -cellulose to liquor ratio of 1:50 (g/g). Once hydrolyzed, the suspension was filtered over a polypropylene support filter membrane, and the recovered cellulose solids were dissolved in distilled water. The cellulose solids were washed by centrifugation at a constant temperature of 15 °C, and the excess citric acid was removed through a series of washes. The resulting CCNCs suspension was dialyzed until it reached a pH value of around 5–5.6, and subsequently sonicated under an ice bath for 25 min with 950 W at a frequency of 25 kHz to fragment the α -cellulose into nano-dimensions in a homogeneously dispersed suspension. Finally, the CCNCs were isolated by separating the precipitate (α -cellulose residue) from the supernatant (containing CCNCs) via centrifugation. The final CCNCs suspension was then dried in an oven set to maintain a constant temperature of 102 °C for 48 h. The yield of CCNCs obtained from the dried isolated α -cellulose was found to be 45 wt%. A systematic diagram

of the extraction process of CCNCs from UECBs pulp is shown in Fig. 1.

2.5. Isolation of CCNFs

The α -cellulose residue obtained after filtration (Fig. 1(c)) was dried in a hot air oven at 90 °C for approximately 24 h. The dried residue had a measured pH value of around 2.2, indicating the presence of acid concentration. To extract carboxyl cellulose nanofibrils (CCNFs), a planetary ball mill (XQM-0.4A) was used. The mill was equipped with a sintered corundum container and zirconia balls measuring 0.6 mm in diameter. The milling process was carried out for 120 min with a ball-to- α -cellulose residue ratio of 60:1. Wet conditions were maintained using deionized water at a rotation speed of 850 rpm and a room temperature of 27 °C. After the milling process, the resulting nanocellulose slurry was collected and subjected to centrifugation at 8000 rpm for 10 min. This centrifugation step was repeated five times using a bench-top refrigerated centrifuge. The resulting suspension was then dialyzed in deionized water for 5 days to achieve a stable pH value of 6–6.5. Subsequently, the

CCNFs were sonicated for 10 min and dried in a hot air oven at 102 °C for approximately 48 h.

2.6. In-situ generation of silver-loaded nanocellulose

The experiment began with the dissolution of 170 mg of silver nitrate (AgNO₃) in 10 ml of deionized water (DIW) and 400 mg of sodium hydroxide in 10 ml of DIW. The solutions were placed in a dark environment at room temperature. Next, the silver nitrate solution was added to 50 ml of CCNCs/CCNFs (15 mg/ml) in a water bath set at 80 °C. While continuously stirring, the sodium hydroxide solution was gradually added drop by drop to the mixture until the pH reached 8. Over a span of 4 h, 2000 mg of glucose was gradually introduced into the solution. Afterward, the solution underwent sequential centrifugation using absolute ethanol and DIW. Subsequently, dialysis against distilled water was performed to eliminate any remaining Ag⁺ ions, followed by a 30-min sonication process. These steps were conducted to remove residual contaminants and ensure the purity of the solution. The resulting AgNPs-CCNCs and AgNPs-CCNFs are illustrated in Fig. 1d.

2.7. Preparation of PVA composite films

To begin, predetermined dried AgNPs-CCNCs (6, 12, and 18 wt% based on PVA weight) were diluted in 200 ml of distilled water and vigorously stirred at a speed of 2000 rpm for 20 min. The resulting suspension was then sonicated for 10 min to ensure uniform dispersion of AgNPs-CCNCs in the water. Subsequently, 10 g of PVA was added to the suspension and continuously stirred for 180 min at a speed of 1700 rpm, maintaining a constant temperature of 85 °C. After the mixture was cooled, any bubbles present were removed using an ultrasonic oscillator. Additionally, 25.2 % of glycerine, relative to the mass of PVA, was added as a plasticizer to the suspension. The mixed solution was then poured into a non-stick stainless steel disc mold and dried until a constant weight was achieved at room temperature. The pristine PVA film did not exhibit any color change. However, upon incorporating AgNPs-CCNCs into the PVA films, a noticeable reddish-brown color change occurred, as depicted in the provided Fig. 5i. The same procedure was applied to prepare the AgNPs-CCNFs reinforced PVA composite with loadings of 6 wt%, 12 wt%, and 18 wt% and no color change was observed in the pristine PVA film.

2.8. Characterization techniques

The chemical composition of extracted UECBs pulp, isolated cellulose after Organosolv treatment, and isolated α-cellulose after Cyanamide-activated H₂O₂ treatment were analyzed using the standard methods established by the Technical Association of the Pulp and Paper Associations (TAPPI) for different components: T 203 cm-99 for α-cellulose and T 222 om-06 for lignin. The holocellulose content was determined following the method described by Wise et al. [18,19]. To obtain the hemicellulose fraction, the difference between the holocellulose and α-cellulose content was calculated. The chemical contents of α-cellulose, hemicellulose, and lignin were determined based on three samples, and the reported values are the averages of these measurements. The moisture content in isolated α-cellulose and UECB pulp was determined using a Sartorius MA45 moisture analyzer [20].

XPS analysis was conducted to determine the chemical composition of isolated α-cellulose, AgNPs-CCNCs, and AgNPs-CCNFs. To perform the analysis, a small amount of the sample was mounted on double-sided adhesive tape and placed in a PHI5000 VersaProbe spectrometer manufactured by ULVAC-PHI in Japan. The spectrometer utilized a hemispherical energy analyzer and a monochromatic Al/K source (1486.6 eV). The acquired spectra were analyzed using XPSPEAK41 software.

X-ray diffraction (XRD) was conducted to study the ultrastructure of UECBs pulp, isolated α-cellulose, AgNPs-CCNCs, and AgNPs-CCNFs. The XRD spectra were obtained using a PANalytical X-pert pro-MRD

diffractometer equipped with Cu-Kα radiation (wavelength of 0.154 nm). The diffraction angle ranged from 0 to 80°, and the scanning resolution was set at 0.9/min. The measurements were performed at a temperature of 22 °C. Eq. (1) is used to calculate the CrI (cellulose Crystallinity Index) of the sample specimens [3].

$$CrI = \frac{I_{200} - I_{am}}{I_{200}} \times 100 \quad (1)$$

Eq. (2) is used to calculate the crystalline size (CrS) of the sample specimens [3].

$$CrS = \frac{K\lambda}{(\beta \cos\theta)} \times 100 \quad (2)$$

where, I₂₀₀ indicates the intensity of the peak with maximum height (2, 0, 0) that indicates crystalline cellulose fraction and I_{am} indicates the intensity of the peak with minimum height that gives an amorphous fraction, β is the peak's full-width at half-maximum (deconvolution), k is the Scherrer constant (0.84), λ is X-ray wavelength (0.154 nm), and θ is the Bragg angle.

The AgNPs-CCNCs and AgNPs-CCNFs were immersed in a 100 ml solution of water and ethanol (50/50 v/v) and subjected to shaking for 24 h. The total silver (Ag) content was then determined using an inductively coupled plasma optical emission spectrometer (PerkinElmer Optima7300 DV ICP-OE) after acidification with a 10 % nitric acid solution.

The FT-IR transmittance spectra of UECBs pulp, isolated α-cellulose, AgNPs-CCNCs, AgNPs-CCNFs, and composite film samples were acquired using a Shimadzu spectrometer (FT-IR-8400S, Japan). The measurements covered the wave number range of 400–4000 cm⁻¹ with a scan rate of 32 scans per minute. A resolution of 0.6 cm⁻¹ was used, and the measurements were carried out under ambient conditions. Before the analysis, a mixture of 0.002 g of finely powdered samples and 0.2 g of potassium bromide was prepared.

The carboxyl content of CCNCs and CCNFs was performed using the conductometric titration process, following a previously reported procedure [3].

The surface morphology of isolated α-cellulose and PVA composite film samples was observed using a Thermo company HITACHI S4800 field emission scanning electron microscope (FE-SEM). Before the examination, the samples were coated with gold sputtering. The morphology of CCNCs, CCNFs, AgNPs-CCNCs, and AgNPs-CCNFs suspensions was examined using a high-resolution transmission electron microscope (JEM-2010F) operating at 200 kV. A drop of nanosuspension (0.1 wt%) was placed on a carbon grid and air-dried at room temperature (25 °C). The size distribution of nanoparticles was measured from the HR-TEM images using Imaging-J software, with 100 counts taken for each sample.

Electronic absorption spectra analysis was conducted on the AgNPs dispersions over the nanocellulose surface using an OCEAN OPTICS spectrophotometer model USB 4000 in absorbance mode. A quartz cuvette with a path length of 10 mm was employed for this analysis. To ensure the proper concentration, the samples were diluted with Milli-Q water in a ratio of 2:1 (v/v) of water to the sample.

To assess the antimicrobial properties, the disc diffusion method was employed to test the effectiveness against *Enterococcus faecalis* (ATCC 29212) as Gram-positive bacteria, as well as *E. coli* (ATCC 25922) as Gram-negative bacteria. The methodology followed the agar plate disc diffusion technique, as outlined by Barry et al. [21]. Initially, the bacteria were cultured in a flask containing 9000 μL of LB medium and incubated at 35 °C with oscillation at 250 rpm for 18 h. Subsequently, 100 μL of each bacterial culture suspension, with a concentration of 106 CFU/ml, was evenly spread onto agar plates. Isolated α-cellulose, AgNPs-CCNCs, AgNPs-CCNFs samples, circular pristine PVA film, and nanocomposite films, measuring 5 mm in diameter, underwent sterilization in an autoclave at 120 °C for 20 min and were then placed directly

in contact with the bacterial agar gel. After incubating for 24 h at 55 °C, the samples were visually examined to detect any bacterial growth in the vicinity of the AgNPs-CCNCs, AgNPs-CCNFs, and composite films.

The TGA spectra of UECBs pulp, isolated α -cellulose, AgNPs-CCNCs, AgNPs-CCNFs, and composite film samples were obtained using a Jupiter thermal analyzer, specifically the STA 449 F3 model. The measurements were conducted in a temperature range of 27 °C to 750 °C with a heating rate of 0.1 °C/s. The experiments were carried out under a nitrogen atmosphere with a flow rate of 0.3 ml/s.

The % yield (g/g) of the UECBs pulp, isolated α -cellulose, and AgNPs-CCNCs was calculated by using Eq. (3):

$$\% \text{Yield} = \left[\frac{\text{dry weight of output material}}{\text{dry weight of input material (predecessor)}} \right] \quad (3)$$

The thickness of each pristine PVA and composite film was assessed using a digital micrometer (Mitutoyo, Japan) with a sensitivity of 0.001 mm. Measurements were taken at five random positions for every film. The average value of these measurements was utilized for the subsequent mechanical testing.

To evaluate the tensile strength, Young's modulus, and elongation at the break of both pristine PVA films and PVA composite films, an ASTM-D882 tensile testing machine with a 100 N load cell (10 × 100 mm) was utilized. The specimens for testing were meticulously cut using sharp scissors. The test was conducted under standard room temperature conditions, with a crosshead speed of 0.9 mm/s and a specimen grip length of 3 cm.

To assess the transparency of pristine PVA films and PVA composite films, transmittance measurements were performed using a UV-VIS spectrophotometer. The transmittance was measured within the wavelength range of 200 to 800 nm.

The packaging (visually) ability of the prepared composite films was evaluated using a Canon EOS 1500D DSLR camera. In this experiment, five fresh tomatoes were washed and dried to remove any dust particles. One tomato was stored without any packaging, while the other four were packed using PVA films reinforced with 12 wt% AgNPs-CCNCs and 12 wt% AgNPs-CCNFs. The storage temperature for all the tomatoes was maintained at 25 ± 2 °C. Throughout the storage period, the decay levels of both the packed and unpacked tomatoes were consistently recorded in the form of photographs.

To determine the moisture retention ability (MRA) of the prepared films, the measurements were performed according to the ASTM D570-98 standard. The films were tested before and after undergoing a drying process in an oven set at a temperature of 105 °C for a period of 24 h. The weight of the film samples was subsequently calculated using Eq. (4) to obtain the MRA percentage

$$\text{MRA} = \left[\frac{(\text{Wet Weight} - \text{Dry Weight})}{\text{Dry Weight}} \right] \quad (4)$$

3. Result and discussion

3.1. Characterization of AgNPs-CCNCs and AgNPs-CCNFs

3.1.1. Chemical analysis

The chemical compositions of the UECBs pulp and isolated α -cellulose are shown in Table 1. The results show that the UECBs pulp contains

40.2 wt% α -cellulose, 18.8 wt% hemicellulose, 28.9 wt% lignin, and 12.1 wt% moisture.

After the organosolv treatment, the lignin, hemicellulose, and moisture contents of the pulp are illustrated in Table 1. In plant-based lignocellulosic fibers, the lignin binds the α -cellulose fibrils together, while the hemicellulose acts as a compatibilizer between the α -cellulose and lignin [3]. During the organosolv treatment, formic acid acts as a proton donor, leading to the hydrolysis of hemicellulose and lignin. Acetic acid, on the other hand, serves as a solvent for the aromatic structure of lignin and the amorphous structure of hemicelluloses. Water plays a role in the dissociation of organic acids and contributes to hemicellulose hydrolysis [22].

The organosolv treatment involves the acid hydrolysis of a portion of the original hemicelluloses, which increases the accessibility of the cell wall by creating macropores. Consequently, this results in enhanced delignification under acidic conditions. By the end of the process, the lignin content decreases from 28.9 wt% to 15.9 wt% and the hemicellulose content decreases from 18.8 wt% to 8.5 wt%.

Furthermore, in the case of organosolv treatment, the residual lignin composition closely resembles that of the native lignin due to the nature of depolymerization reactions involved in lignin breakdown. As a result, the residues are generally susceptible to bleaching. In addition, the organosolv-treated UECBs pulp undergoes chlorine-free cyanamide-activated hydrogen peroxide treatment to remove the remaining lignin and hemicellulose content from the pulp. During the treatment, there is a notable degradation of residual lignin. This treatment involves a direct attack on the α -aryl ether bonds between lignin and hemicellulose while also reacting with lignin molecules until they are dissolved in the solution. Simultaneously, the remaining amount of hemicellulose is partially dissolved along with the lignin content [53]. Following this treatment, the hemicellulose content is reduced to 4.8 wt% and the bleaching process degrades 3.2 wt% of the lignin. Finally, the isolated α -cellulose yield from the dried UECBs pulp is determined to be 42.0 wt%.

Following the chemical treatment, the moisture content of the isolated cellulose underwent a decrease from 12.1 wt% to 7.2 wt%. This reduction in moisture content typically results in a decrease in the hydrophilic nature of the fibers and enhances their moisture resistance properties. Additionally, in this study, the reduction in lignin and hemicellulose contents led to an increase in both holocellulose and α -cellulose contents. Specifically, the holocellulose content increased from 59.0 wt% to 89.6 wt% and the α -cellulose content increased from 40.2 wt% to 84.8 wt%. These outcomes indicate an increase in the crystalline degree of cellulose.

The analysis of the chemical composition indicates that the pulp derived from UECBs contains a significant amount of crystalline cellulose. As a result, this raw material holds promise for extracting cellulose as well as producing AgNPs-CCNCs and AgNPs-CCNFs, making it particularly valuable due to its abundant availability as discarded municipal solid waste products.

3.1.2. XPS, XRD, and ICP-OES analysis

The XPS spectrum of isolated α -cellulose, AgNPs-CCNCs, and AgNPs-CCNFs are shown in Fig. 2 (a–c), providing significant information about the chemical state and composition of AgNPs on nanocellulose.

The spectrum, which is depicted in Fig. 2a, shows the binding energy spectra of C1s peaks (288 eV) and O1s peaks (528 eV) for the isolated

Table 1
Chemical compositions of the UECBs pulp and isolated α -cellulose.

S.No	Fiber type	Extraction process	Holo-cellulose (α -Cellulose ⁺ Hemicellulose) (wt%)	α -Cellulose	Hemicellulose	Lignin	Moisture
1.	UECBs pulp	Hydra pulping	59.0	40.2	18.8	28.9	12.1
2.	isolated α -cellulose	Organosolv treatment	76.2	67.7	8.5	15.9	7.9
		Cyanamide-activated H2O2 treatment	89.6	84.8	4.8	3.2	7.2

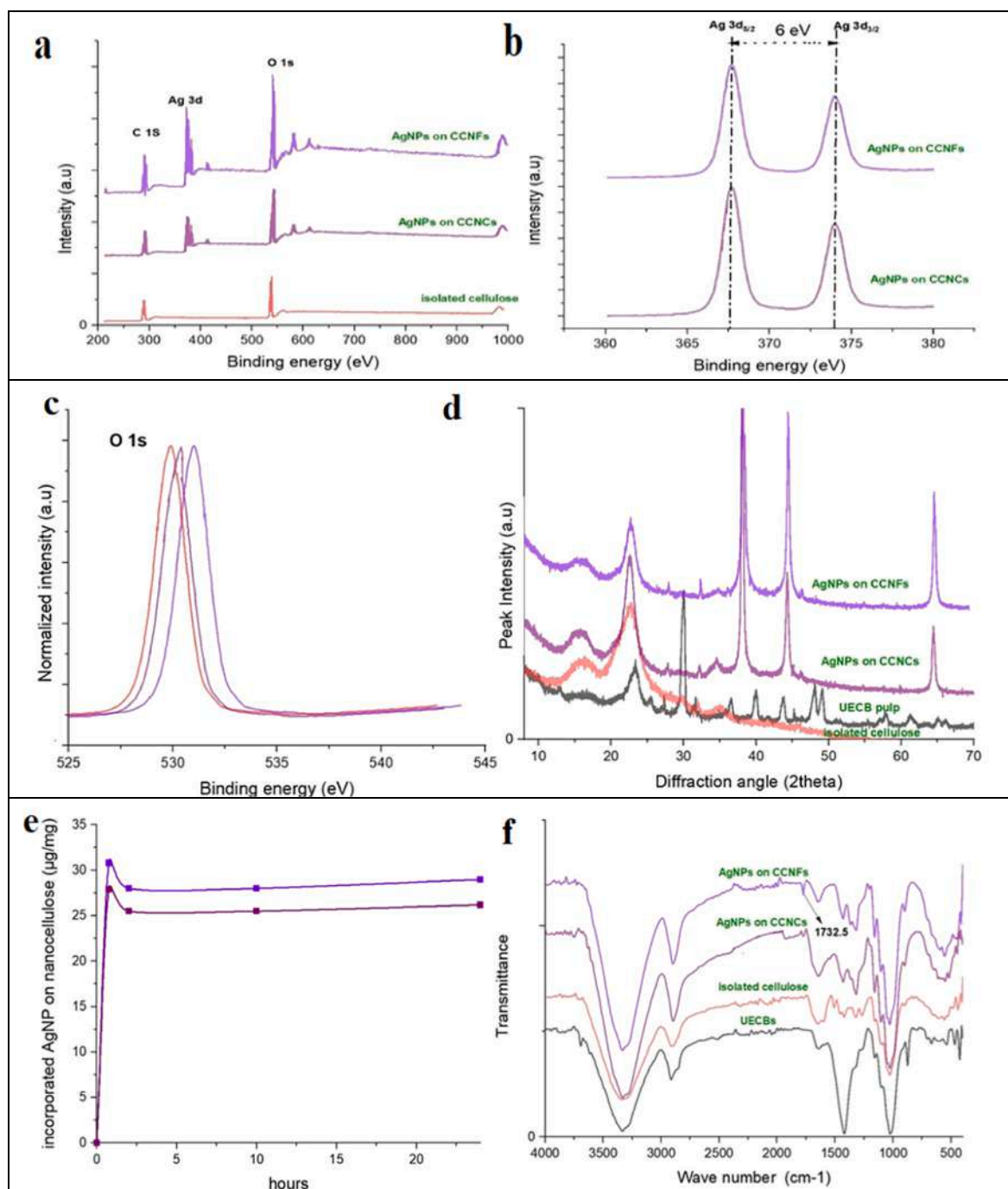


Fig. 2. a–c XPS spectra, d. XRD spectra of the UECBs, isolated α -cellulose and AgNPs-carboxyl nanocellulose, e. quantification of adsorbed AgNPs on AgNPs-carboxyl nanocellulose, f. FT-IR spectra of UECBs, isolated α -cellulose and AgNPs-carboxyl nanocellulose.

α -cellulose, demonstrating distinctive peaks connected with the cellulosic components. Additionally, the isolated α -cellulose contained no Ag peaks [23].

Following the in-situ generation, two distinct peaks emerged at 367.9 eV and 373.9 eV, representing the binding energies of Ag 3d_{5/2} and Ag 3d_{3/2}, respectively. The high-resolution scanning for Ag 3d for both AgNPs-CCNCs and AgNPs-CCNFs revealed that the two components at 367.9 eV for Ag 3d_{5/2} and 373.9 eV for Ag 3d_{3/2} with typical Ag metal separation energy of 6 eV [42] (Fig. 2b).

The O 1s spectra of isolated α -cellulose, AgNPs-CCNCs, and AgNPs-CCNFs showed no discernible differences as shown in Fig. 2c. However, there was a positive shift in the spectra due to the binding energy of O1s

in AgNPs embedded on nanocellulose. This change reveals that, by a coordination model, AgNPs are evenly spread over the surface of the nanocellulose, further supporting the transformation of Ag⁺ into Ag nanometal. These results give substantial evidence that nanocellulose has been successfully loaded with stable zero-valence AgNPs [24,25].

The XRD pattern of UECBs pulp in Fig. 2d reveals the presence of two distinct peaks at approximately 15.1° (1 1 0) and 22.4° (2 0 0), which are typical peaks associated with cellulosic materials. Upon isolation of α -cellulose materials, the peak intensity around $2\theta = 22.4^\circ$ exhibits a narrow and sharp profile, with a significant increase compared to the peaks observed in UECBs pulp. Additionally, a broad Cellulose I peak is observed at approximately 15.1° (1 1 0) and 16.5° (1–10) in Fig. 2d. The

calculated CrI (Eq. (1)) value for the isolated α -cellulose (77.2 %) is higher than that of the UECBs pulp (45.3 %). This increase in CrI can be attributed to the removal of hemicellulose and lignin through the organosolv and cyanamide-activated hydrogen peroxide treatment process.

The presence of sharp and narrow intensity diffraction peaks at $2\theta = 16.5^\circ$, 22.4° , and 34.6° in AgNPs-CCNCs and AgNPs-CCNFs suggests that the nanocellulose has a higher crystalline nature when compared to isolated α -cellulose as shown in Fig. 2d. The estimated CrI values for AgNPs-CCNCs (87.5 %) and AgNPs-CCNFs (84.3 %) are higher than the isolated α -cellulose (77.2 %). This indicates that the nanocellulose's high crystallinity is crucial for enhancing the mechanical properties (strength, and stiffness) when used as fillers in reinforced biopolymer composites for applications in medical, engineering, and food packaging [26].

As a result of this process, additional diffraction peaks of metallic Ag are observed at $2\theta = 38.1^\circ$, 44.2° , and 64.5° , corresponding to (1 1 1), (2 0 0), and (2 2 0) planes of the face-centered cubic (FCC) structure in AgNPs-CCNCs and AgNPs-CCNFs as shown in Fig. 2d. These new peaks confirm the presence of metallic Ag in nanocellulose [27]. Furthermore, the narrow and sharp diffraction peaks of the Ag suggest a small size of Ag crystallites, estimated (Eq. (2)) to be approximately 13 nm for both AgNPs-CCNCs and AgNPs-CCNFs.

According to inductively coupled plasma-optical emission spectrometry, it was confirmed that the adsorption of AgNPs-CCNCs and AgNPs-CCNFs was measured at 28.9 and 30.5 $\mu\text{g}/\text{mg}$ respectively. Fig. 2 (e) indicates that the silver ions remained unchanged and did not convert to metallic silver after a 45-min in-situ generation process. Based on our speculation, the formation of AgNPs is primarily influenced by the amount of silver absorbed by the carboxyl nanocellulose. The plots illustrate that there was no significant increase in silver adsorption observed after 2 h. These results strongly support the notion that the in-situ generation process effectively promotes the formation of AgNPs on the surface of carboxyl nanocellulose.

3.1.3. FT-IR analysis and estimation of carboxyl groups

The FTIR transmittance spectra of the UECBs pulp, isolated α -cellulose, AgNPs-CCNCs, and AgNPs-CCNFs are presented in Fig. 2(f). The wide vibration band in the 3250–3500 cm^{-1} range corresponds to the OH stretching vibration of hydroxyl groups found in UECBs pulp and extracted samples [28]. The stretching vibrations of CH and CH_2 are assigned to a relatively strong band at 1420 cm^{-1} and smaller bands in the 2790–2890 cm^{-1} range, respectively [29]. In the UECBs pulp spectrum, the bands at 1470 cm^{-1} are attributed to the C=C stretching from aromatic hydrocarbons of lignin. These peaks appear to decrease after applying chemical treatments, as shown in Fig. 2(f). The main characteristic bands of the cellulose skeleton are observed around 1045 cm^{-1} , 1105 cm^{-1} , and 1175 cm^{-1} , corresponding to C–O stretching, ring asymmetric stretching, and C–O–C asymmetric stretching, respectively. These bands remain mostly unchanged but become sharp after isolating α -cellulose, AgNPs-CCNCs, and AgNPs-CCNFs. This is likely due to an increase in the crystallinity degree of cellulose. The peak intensity at 894 cm^{-1} has significantly increased for α -cellulose, AgNPs-CCNCs, and AgNPs-CCNFs. The peak corresponds to the distinctive glycosidic C1-H deformation coupled with ring vibration and OH bending. This peak is indicative of β -glycosidic linkages connecting glucose units within cellulose crystals [30]. The sharp peak at 1732 cm^{-1} in the spectra of AgNPs-CCNCs, and AgNPs-CCNFs indicates the esterification reaction and the interaction between cellulose's hydroxyl groups and carboxylic acids (COOH) [31]. The peak at 1732 cm^{-1} observed in AgNPs-CCNCs is slightly lower compared to that of AgNPs-CCNFs due to a lesser quantity of carboxylic groups present on the surface. The initial carboxylic group values for CCNCs and CCNFs before the in-situ generation process are 0.76 mmol/g and 0.85 mmol/g, respectively. These values are comparable to those reported for other types of CCNCs, such as commercially used microcrystalline cellulose (1.39 ± 0.1 mmol/g), banana peduncle

(0.91 mmol/g), bleached bagasse pulp (0.60 mmol/g), disposal cups (UDPCs) (0.72 mmol/g), and bleached sugarcane bagasse (0.65 mmol/g) [3,31].

The presence of carboxylic groups in nanocellulose is advantageous as it facilitates the coordination of Ag^+ ions to the surface of nanocellulose. Carboxylic groups can act as binding sites for the Ag^+ ions, promoting their attachment and enhancing the interaction between silver ions and nanocellulose [32,33]. This coordination phenomenon is beneficial for applications involving AgNPs-CCNCs and AgNPs-CCNFs, as it contributes to their antibacterial and electrical properties. These advantageous properties make them well-suited for a wide range of industries such as biomedical, food packaging, catalysis, electronics, and sensors.

The FT-IR transmittance spectra of isolated α -cellulose AgNPs-CCNCs, and AgNPs-CCNFs exhibit similar visible peaks, confirming the presence of metallic nanosilver in the nanocellulose rather than potential metalorganic compounds. Based on the results obtained from FT-IR studies, it can be concluded that the in-situ generation method used to embed Ag-NPs on the surfaces of CCNCs and CCNFs did not cause any significant alterations to the fundamental structure of cellulose. Various studies have documented similar trends in different approaches to embedding AgNPs onto nanocellulose samples.

3.1.4. Morphology analysis

The FE-SEM image (Fig. 3 (a)) reveals the presence of separated individual cellulosic fibers with a rough surface and cylindrical shape, confirming the successful extraction of α -cellulose from UECBs pulp using organosolv and cyanamide-activated hydrogen peroxide treatment. The chemical treatment process resulted in a noticeable transformation of the brownish color of UECBs pulp (Fig. 1a) to a completely milky white color, indicating the removal of hemicellulose and lignin from UECBs pulp. Furthermore, the isolated α -cellulose exhibited an average diameter of approximately $20 \pm 3 \mu\text{m}$ (Fig. 3a).

The morphology of the obtained CCNCs and AgNPs-CCNCs are investigated through HR-TEM as shown in Fig. 3 (b–d). The HR-TEM image (Fig. 3(b–d)) reveals that CCNCs hydrolyzed with citric acid exhibit needle-like cellulose crystal shapes. During the citric acid interaction with the amorphous regions of α -cellulose bundles, releasing cellulose nanocrystals longitudinally. Simultaneously, carboxylic groups are introduced onto the cellulose surface through citric acid hydrolysis, promoting the coordination of Ag^+ ions during in-situ generation. After the in-situ generation process, the obtained AgNPs-CCNCs with different magnifications are shown in Fig. 3 (c & d). The measured dimensions of the cellulose crystals were 550 ± 20 nm in width and 17 ± 6 nm in length. The cellulose nanocrystal surface shows uniformly distributed spherical AgNPs with an average diameter of 8 ± 2 nm (Fig. 3 (c & d)). This can be attributed to the bonding between the nanosilver crystal nucleus and the O atom in cellulose crystals throughout the reaction process. The elongated chains extending in all directions effectively prevent AgNPs agglomeration, ensuring even adsorption of silver atoms on the nucleation surface and resulting in spherical AgNPs [8].

Fig. 3(e) presents the magnified FE-SEM image of α -cellulose residue, which serves as the input material for ball milling, after the isolation of CCNCs. However, the citric acid hydrolyzed α -cellulose residue appears as short microfibrils with a rough surface. Analysis of the micrographs from Fig. 3 (e) indicates that the diameter range of the α -cellulose residue measures approximately $8 \pm 2 \mu\text{m}$, which is smaller than the diameter of isolated α -cellulose ($20 \pm 3 \mu\text{m}$). The morphology of the α -cellulose residue demonstrates a reduction in depolymerization during acid pre-hydrolysis (citric acid hydrolysis), which consequently helps in minimizing the energy input during the production of mechanical fibrillation of cellulose nanofibers [34].

The morphology of the obtained CCNFs and AgNPs-CCNFs was examined using HR-TEM at different magnifications, as depicted in Fig. 3(f–h). Notably, the HR-TEM image demonstrates that CCNFs and AgNPs-CCNFs possess a web-like structure. This distinctive structure is

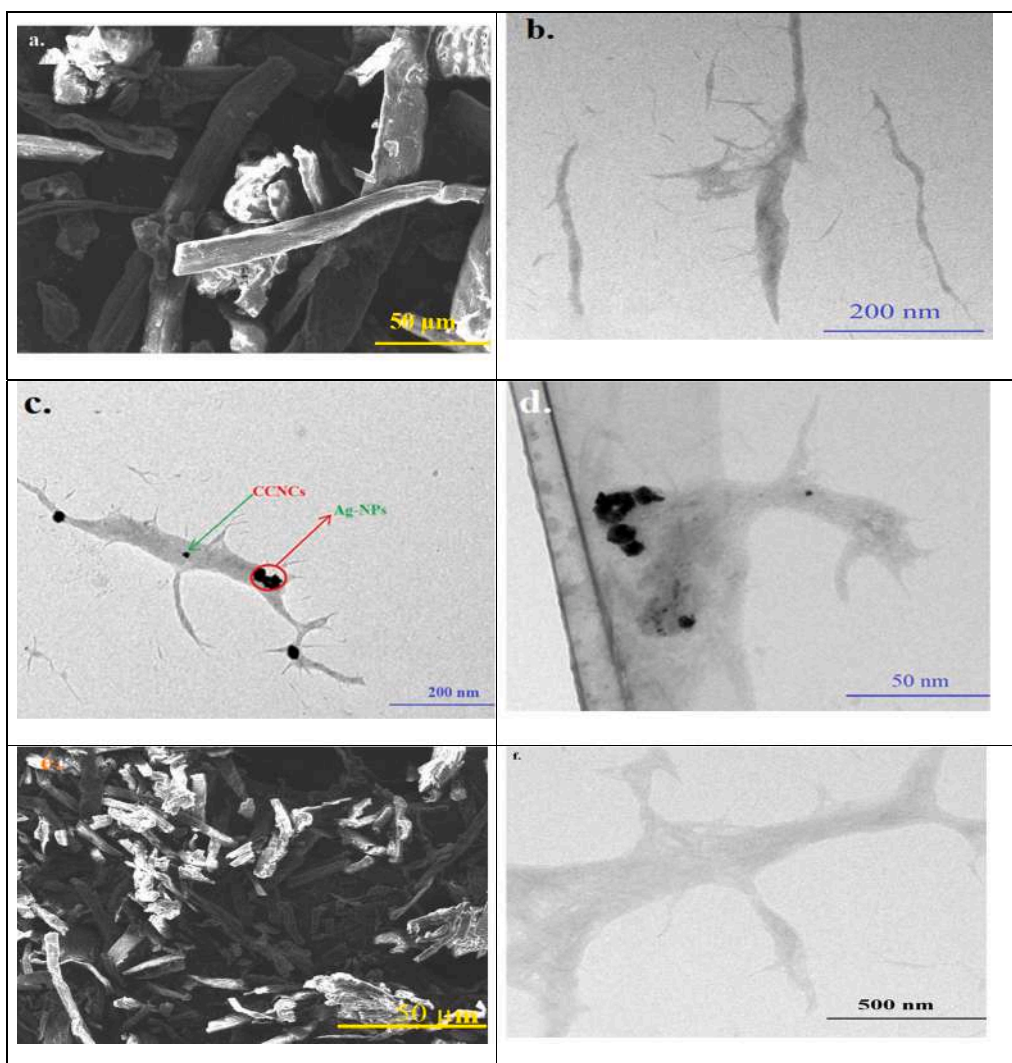


Fig. 3. a. isolated α -cellulose, b. CCNCs, c & d. different magnification of AgNPs-CCNCs, e. citric acid hydrolyzed cellulose residue, f. CCNFs, g & h. different magnification of AgNPs-CCNFs, i. UV-vis spectra of isolated cellulose and AgNPs-carboxyl nanocellulose.

formed during the ball milling process, where friction between the balls and drum walls generates intense shear forces. Consequently, carboxyl cellulose nanofibers are extracted longitudinally from the α -cellulose residue [35]. The presence of CCNFs in the web-like structure is evident, with separated fibrils exhibiting micron-scale lengths and a width of 45 ± 10 nm. After the in-situ generation, uniformly distributed spherical AgNPs with a diameter of 9.5 ± 4 nm are observed on the surface of the cellulose nanofibers following the in-situ generation process (Fig. 3 (g & h)). This phenomenon can be attributed to the interaction between the nano argent crystal nucleus and the O atom in the nanocellulose during the entire in-situ generation process.

The observation of absorption peaks through UV-spectral analysis makes it a valuable method for confirming the presence of silver nanoparticles (AgNPs) on nanocellulose. In Fig. 3 (i), the isolated cellulose spectrum shows no visible range band, while the AgNPs-CCNCs and AgNPs-CCNFs samples exhibit a prominent absorption peak between 310 and 500 nm, with a peak around 405–415 nm, which corresponds to the typical plasmon resonance band of AgNPs [8]. This peak and its specific location indicate the successful reduction of Ag^+ ions in the silver nitrate solution to AgNPs. Moreover, the absorption peak suggests the presence of numerous spherical or nearly spherical AgNPs in the solutions. Comparing the AgNPs-CCNCs with the AgNPs-CCNFs, the

latter shows a higher absorbance peak, suggesting an increased presence of AgNPs on the CCNFs surfaces.

The comprehensive HR-TEM analysis of AgNPs-CCNCs and AgNPs-CCNFs is crucial for understanding their structural characteristics and unlocking their potential uses as nano reinforcements in various industries such as medical, electronics, and food packaging.

3.1.5. Antibacterial activity

The antibacterial activity of AgNPs-CCNCs and AgNPs-CCNFs was evaluated using the disc-diffusion method against *E. faecali* (Gram+) and *E. coli* (Gram-) bacteria (Fig. 4 (a&b)). Interestingly, isolated α -cellulose displayed no antibacterial activity, which was expected considering cellulose's known susceptibility to bacterial attack.

In contrast, AgNPs-CCNCs and AgNPs-CCNFs exhibited notable antibacterial activity, as evidenced by the formation of inhibition zones against both *E. faecali* and *E. coli*. This can be attributed to the interaction between the AgNPs and the bacteria's outer membrane, leading to structural changes, cell death, and the generation of reactive oxygen species that catalyze bacterial destruction [36].

Comparing AgNPs-CCNCs and AgNPs-CCNFs, it was observed that AgNPs-CCNFs showed larger inhibition zones against both *E. faecali* and *E. coli*. This can be attributed to the lower concentration of antibacterial

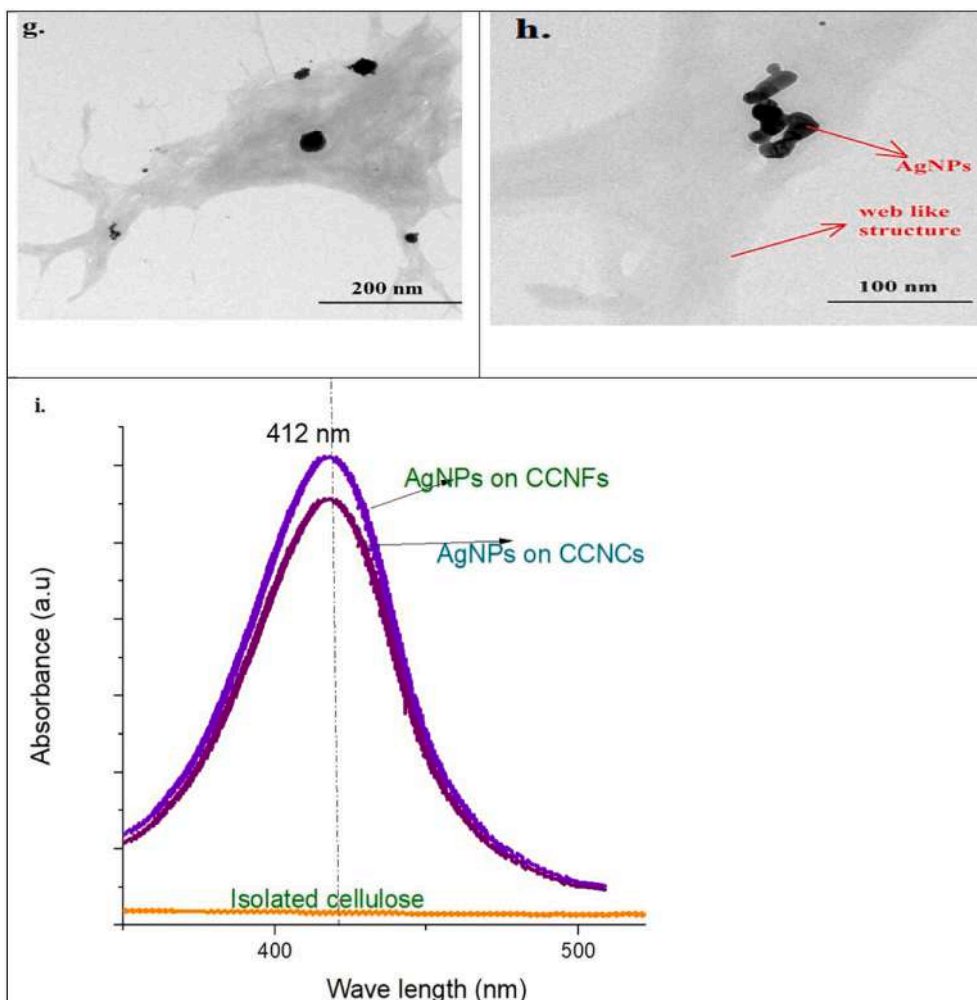


Fig. 3. (continued).

AgNPs on CCNCs surface, resulting in reduced direct contact with bacteria and decreased release of silver into the surrounding environment. The clear zone diameters for AgNPs-CCNCs were 8.2 mm (*E. faecali*) and 10.4 mm (*E. coli*), while for AgNPs-CCNFs, they were 9.1 mm (*E. faecali*) and 11.5 mm (*E. coli*). The higher antibacterial activity against Gram+ bacteria compared to Gram- bacteria may be attributed to differences in their structural and chemical compositions, particularly in their cell membranes.

The test results revealed that both AgNPs-CCNCs and AgNPs-CCNFs possess substantial antibacterial properties. This finding indicates that these materials hold promise for diverse applications in sectors like healthcare, food packaging, and other industries where effective control of bacterial growth is crucial.

3.1.6. TGA analysis

Thermogravimetric analysis was performed to examine the thermal stability and thermal degradation behavior of UECBs pulp, isolated α -cellulose, AgNPs-CCNCs, and AgNPs-CCNFs samples. The TGA and DTG curves of these samples are presented in Fig. 4 (c & d), and the onset temperature (T_{onset}) and maximum degradation temperature (T_{max}) values obtained from the curves are summarized in Table 2. The results indicate that all samples exhibit initial stage weight loss of about 5 to 7 % at temperatures below 100 °C, which can be attributed to the evaporation of moisture present on the surface and/or within the cellulosic fibers [37].

The UECBs pulp exhibited an T_{onset} of 321 °C and a corresponding maximum degradation temperature (T_{max}) of 347 °C, indicating the

decomposition of organic compounds such as α -cellulose, hemicellulose, and lignin present in the pulp [38,39].

Significantly, the isolated α -cellulose sample exhibits a T_{onset} of 334 °C and T_{max} of 357 °C, which are 15 °C and 10 °C higher, respectively, than the corresponding values observed for the UECBs pulp sample. This suggests that non-cellulosic compounds were removed during the organosolv and cyanamide-activated hydrogen peroxide treatment.

Consequently, the TGA curve of the isolated α -cellulose exhibited a broad weight loss range (76 %) that occurred within the temperature range of 340 °C to 357 °C during the second stage of thermal degradation. This indicates the removal of non-cellulosic components and an increase in the degree of α -cellulose crystallinity, resulting in enhanced thermal resistance. The degradation of α -cellulose generally involves cleavage of the glucose units, as well as processes such as dehydration, decarboxylation, depolymerization, oxidation, and decomposition of glycosyl units [40]. These findings align with the XRD results (Fig. 2 (d)), which demonstrate sharper cellulosic peaks in the isolated α -cellulose, indicating the absence of non-cellulosic regions.

In Fig. 4 (d), it can be observed that the AgNPs-CCNCs and AgNPs-CCNFs samples exhibit lower T_{onset} and T_{max} values compared to isolated α -cellulose and UECBs pulp. During the second stage of thermal degradation, both AgNPs-CCNCs and AgNPs-CCNFs experience a significant weight loss of approximately 50 wt% to 60 wt% within the temperature range of 280 °C to 332 °C and 290 °C to 334 °C, respectively.

Notably, AgNPs-CCNCs demonstrate the lowest onset temperature

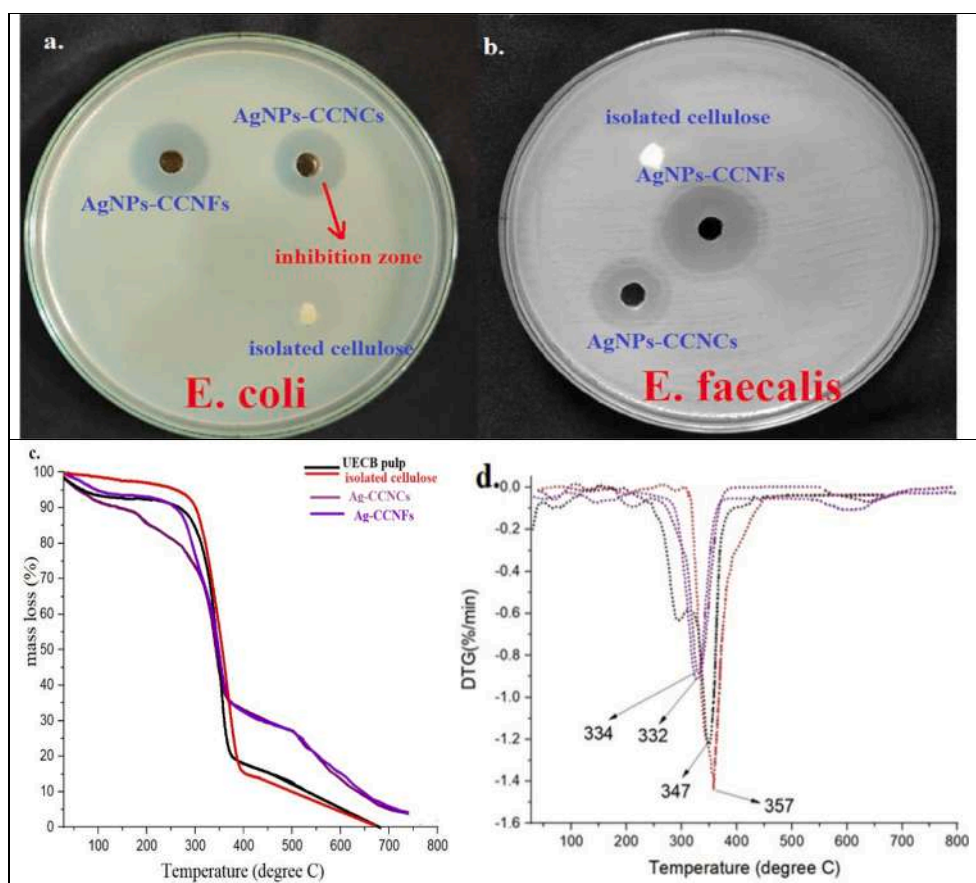


Fig. 4. a & b antibacterial test on isolated cellulose, AgNPs-CCNCs and AgNPs-CCNFs, c. TGA, d. DTG curve of UECB pulp, isolated α -cellulose and AgNPs- carboxyl nanocellulose.

Table 2

Characterization of the UECBs pulp, isolated α -cellulose, AgNPs-CCNCs, and AgNPs-CCNFs.

S. No	Fiber nature	Physical properties		Chemical properties		Thermal properties		Morphology			Antibacterial activity	
		Crystallinity index (%)	AgNPs crystalline size (nm)	Carboxyl content (mmol/g)	Adsorption of AgNPs ($\mu\text{g}/\text{mg}$)	T onset ($^{\circ}\text{C}$)	T degradation ($^{\circ}\text{C}$)	Width (nm)	Length (nm)	Size of AgNPs (nm)	Inhibition zone of <i>E. coli</i> (mm)	Inhibition zone of <i>E. faecali</i> (mm)
1.	UECBs pulp	45.3	–	–	–	321	347	–	–	–	–	–
2.	Isolated α -cellulose	77.2	–	–	–	334	357	20,000 \pm 3000	–	–	0	0
3.	AgNPs-CCNCs	87.5	13	0.76	28.9	272	332	17 \pm 6	550 \pm 20	8 \pm 2	8.3	10.5
4.	AgNPs-CCNFs	84.3	13	0.85	30.5	285	334	45 \pm 10	–	9.5 \pm 4	9	11.5

(272 $^{\circ}\text{C}$) and thermal degradation temperature (332 $^{\circ}\text{C}$) when compared to AgNPs-CCNFs, as shown in the Table 2. This can be attributed to the disruption of the crystalline structure, low aspect ratio and the presence of carboxylic groups on the surface of AgNPs-CCNCs, which negatively impact their thermal stability [41]. Additionally, the nanoscale dimensions of AgNPs-CCNCs result in a larger surface area exposed to heat, further contributing to reduced thermal stability [3].

During the final (third) stage of thermal degradation, it can be observed that isolated α -cellulose and UECBs pulp leave behind negligible char residue. In contrast, AgNPs-CCNCs and AgNPs-CCNFs show a char residue of approximately 2 % and 2.5 %, respectively, when exposed to a temperature of 750 $^{\circ}\text{C}$. It is speculated that these remaining residues after the pyrolysis process consist of AgNPs. Similar characteristics are found in the literature previously reported [16].

Based on the obtained results, the AgNPs-CCNCs and AgNPs-CCNFs demonstrate potential for utilization as reinforcements in bio-thermo and bio-thermosetting polymers, particularly in applications where the operating temperature remains below 270 $^{\circ}\text{C}$.

3.2. Characterization of composite films

3.2.1. Mechanical properties

The mechanical properties of food packaging films play a crucial role in assessing their strength and durability. These properties are essential for providing protection, durability, and stability to the packaged food product, as well as enabling the film to withstand handling and transportation.

Table 3 presents the tensile strength (MPa), Young's modulus (GPa),

Table 3

Characterization of the composite PVA films.

S. No	Film nature	Mechanical properties				Moisture retention capability (%)	Transmittance (%)	Antibacterial activity	
		Tensile strength (MPa)	Elongation at break (%)	Young's modulus (GPa)	Thickness (μm)			Inhibition zone of <i>E. coli</i> (mm)	Inhibition zone of <i>E. faecali</i> (mm)
1.	Pristine PVA	29 ± 1	80 ± 2	6.8 ± 0.1	40.2 ± 1	85.6	95	0	0
2.	PVA + 6 wt% AgNPs-CCNCs	45 ± 2	11 ± 0.8	41.2 ± 0.2	42.2 ± 1.5	90.5	90.8	10.2	10.5
3.	PVA + 12 wt% AgNPs-CCNCs	56 ± 2	5 ± 0.5	46 ± 0.4	45.7 ± 2	93.5	80.2	12.2	12.5
4.	PVA + 18 wt% AgNPs-CCNCs	52 ± 1.4	7 ± 1.0	45 ± 0.3	48.3 ± 2	94.9	72.5	14.1	14.4
5.	PVA + 6 wt% AgNPs-CCNFs	46 ± 1.5	16 ± 1.2	42.5 ± 0.2	43.2 ± 1	90.8	86.7	7.2	7.5
6.	PVA + 12 wt% AgNPs-CCNFs	64 ± 1.2	10 ± 1.8	47 ± 0.1	46.4 ± 2	93.8	79.6	12.4	12.5
7.	PVA + 18 wt% AgNPs-CCNFs	51 ± 1.7	12 ± 0.9	45 ± 0.4	49.5 ± 2	94.9	69.5	14.3	14.5

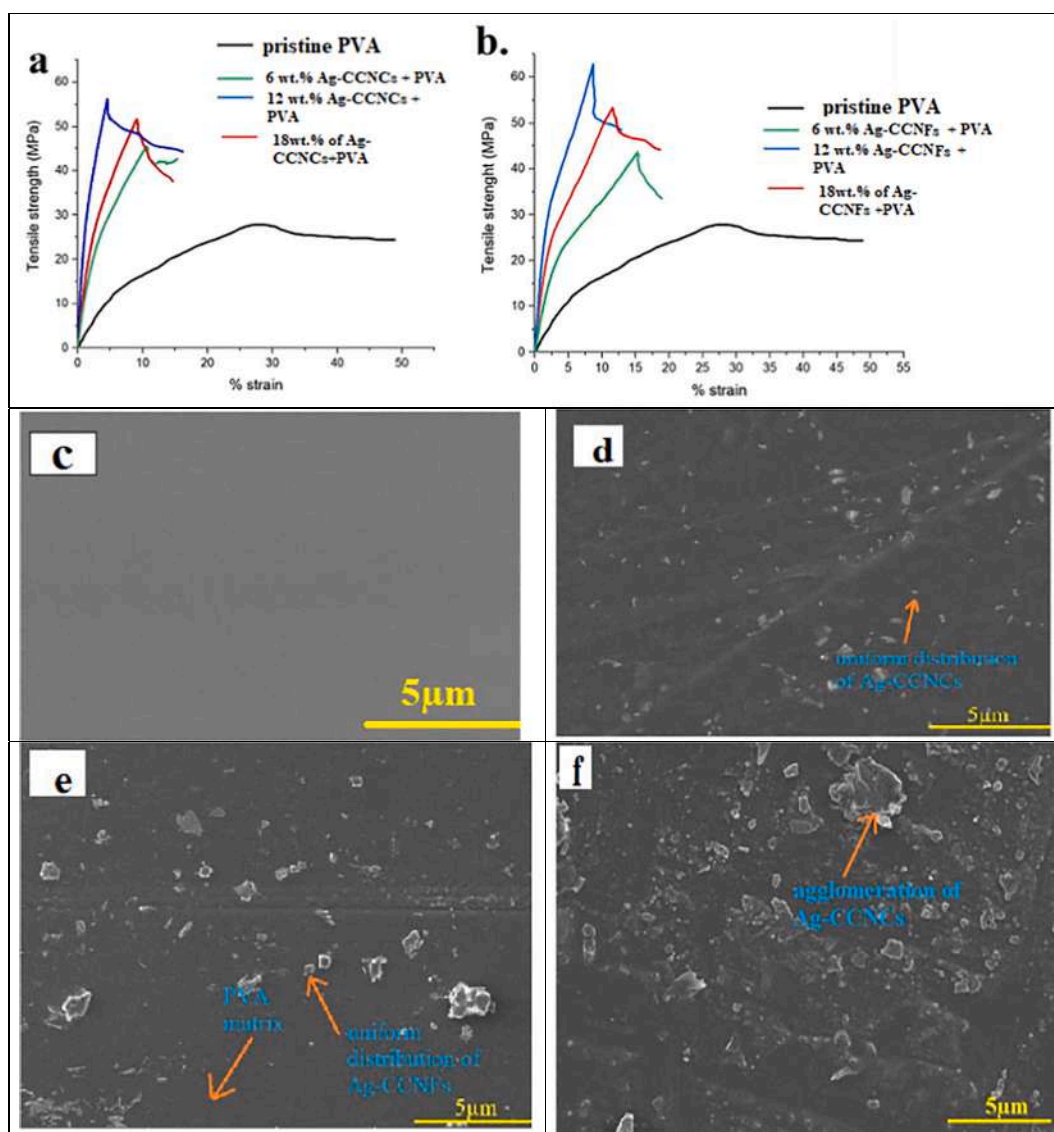


Fig. 5. a. stress- strain curve of composite films, FE-SEM image of c. pristine PVA, d. 12 wt% AgNPs-CCNCs loading PVA, e. 12 wt% AgNPs-CCNFs loading PVA, f. 18 wt% AgNPs-CCNCs loading PVA, g. 18 wt% AgNPs-CCNFs loading PVA, h. transmittance curve of PVA and composites, i. appearance of the PVA and composite films in front of printed paper.

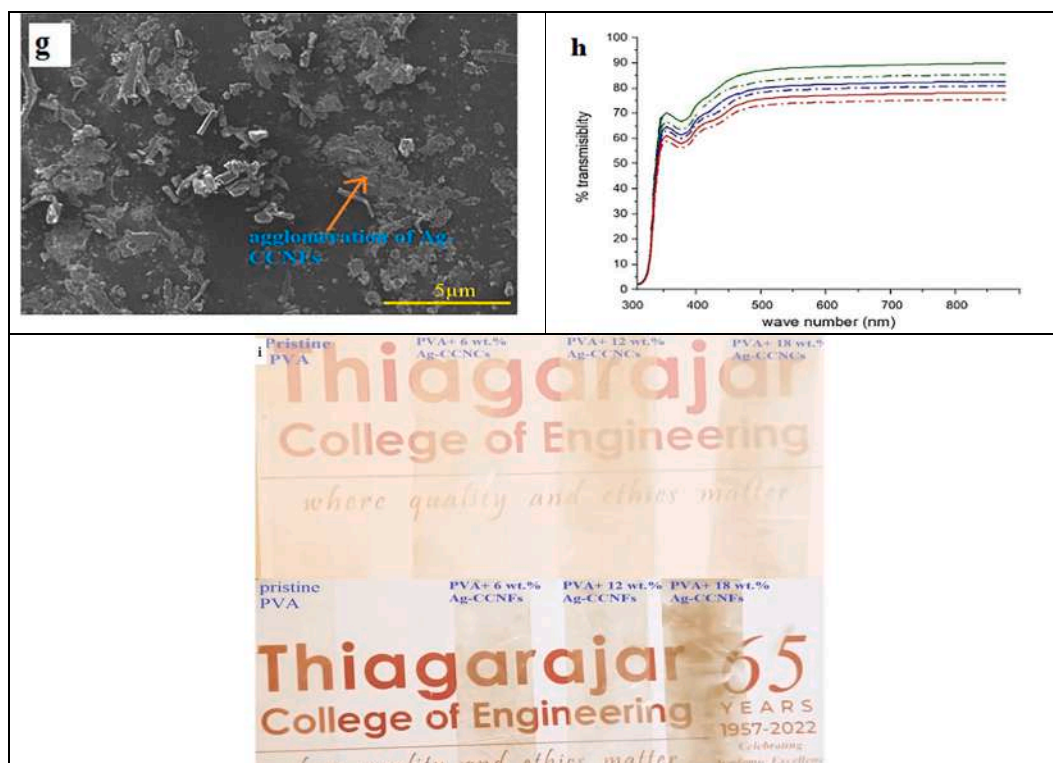


Fig. 5. (continued).

percentage of elongation at the break, and thickness (μm) for pristine PVA and different composite PVA film samples with varying weight percentages of AgNPs-nano cellulose loading. Notably, the inclusion of solid, crystalline AgNPs-nano cellulose content into the PVA matrix resulted in a substantial increase in the thickness of the composite films compared to the pristine PVA film [58].

The maximum tensile strength, young's modulus, and % of elongation at break of pristine PVA film are measured at 29 ± 1 MPa, 6.8 ± 0.1 GPa, and 80 ± 2 % respectively. With the incorporation of AgNPs-CCNCs/AgNPs-CCNFs into the PVA matrix, the tensile strength and young's modulus of the PVA film increase.

The maximum tensile strength of AgNPs-CCNCs loaded PVA films at 6 wt% is measured at 45 ± 2 MPa, while the maximum tensile strength of AgNPs-CCNFs loaded PVA films at 6 wt% is 46 ± 1.5 MPa. Consequently, the young's modulus is increased by 83 % and 84.6 % respectively, in comparison to pristine PVA film.

In Fig. 5 (a & b), the Stress-Strain curves of pristine PVA, PVA with different wt% of AgNPs-CCNCs loading, and PVA with different wt% of AgNPs-CCNFs loading samples are depicted. The graph illustrates that PVA films with AgNPs-CCNFs loading exhibit higher mechanical strength compared to PVA films with AgNPs-CCNCs loading for the same wt% of reinforcement in the PVA matrix. This can be attributed to the higher aspect ratio and improved mechanical properties, such as higher tensile strength and modulus, typically offered by AgNPs-CCNFs compared to AgNPs-CCNCs [43,44]. Therefore, AgNPs-CCNFs reinforced PVA films generally demonstrate superior tensile strength.

However, the incorporation of AgNPs-CCNCs/AgNPs-CCNFs in the PVA matrix enhances the tensile strength and Young's modulus while reducing the elongation at break (Fig. 5 (a & b)). This is due to the increased stiffness of the composite film, which restricts the mobility of the PVA molecular chains. Consequently, the elongation at break (%) of the composite film is significantly reduced, as shown in Table 3.

For the PVA composite films loaded with 12 wt% AgNPs-CCNCs, the optimum maximum tensile strength was found to be 56 ± 2 MPa. Similarly, for the PVA composite films loaded with 12 wt% AgNPs-

CCNFs, the optimum maximum tensile strength was at 64 ± 1.2 MPa. This improvement can be attributed to the uniform dispersion of nanofillers within the PVA matrix, as well as the enhanced crystallinity and hydrophobic properties of the nanocellulose, which facilitate an intermolecular force transfer between the nanocellulose and PVA matrix [45].

Moreover, a higher proportion of AgNPs- carboxyl nanocellulose (18 wt%) resulted in a decline in the tensile strength, although it remained superior to that of the original PVA film, as indicated in Table 3. Excessive nanocellulose content caused agglomeration, weakening the interaction with the PVA matrix, and consequently diminishing the mechanical properties of the films [46].

The tensile strength of the prepared 12 wt% AgNPs-CCNCs reinforced PVA composite film and the 12 wt% AgNPs-CCNFs composite film is superior to that of other filler-reinforced PVA composites, including WO_3 nanorods/PVA (30.5 MPa), PVA/CCNCs (52.5 ± 2.5 MPa), TiO_2 /PVA (31.3 MPa), AgNPs into PVA/NC (30.5 MPa), and peel/PVA (18 MPa). Additionally, the tensile strength of the AgNPs-CCNFs composite is comparable to that of trimethylammonium chloride cellulose/PVA composite films (65.56 MPa) [3,54–57].

The results indicate that the prepared PVA film reinforced with 12 wt % AgNPs-carboxyl nanocellulose exhibits excellent mechanical properties, making it a suitable material for food packaging purposes.

3.2.2. Surface morphology and transparency of the composite films

Morphological tests were conducted on pristine PVA films as well as PVA films loaded with different concentrations of AgNPs-CCNCs and AgNPs-CCNFs. The tests were performed using FE-SEM, and the corresponding images are presented in Fig. 5 (c–g). The initial examination of pristine PVA film (Fig. 5 (c)) revealed a smooth surface. However, upon the addition of fillers to the PVA matrix, the surface morphology of the films transformed into a rough texture (Fig. 5 (d–g)). This roughness can be attributed to the formation of hydrogen bonds between the carboxyl and hydroxyl groups of AgNPs-nanocellulose and the hydroxyl groups of PVA [47].

Furthermore, the incorporation of 12 wt% AgNPs-CCNCs led to notable changes in the microstructure, as depicted in Fig. 5 (d). The enhanced dispersion of AgNPs-CCNCs within the PVA matrix resulted in a stronger interaction and adhesion between the fillers and the PVA matrix. This denser structure contributed to the improved tensile properties of the bio-nanocomposite films and is confirmed in the previous Section 3.2.1 [48]. Similar characteristics were observed in the case of 12 wt% AgNPs-CCNFs loaded PVA matrix, as depicted in Fig. 5 (e).

However, when the AgNPs-CCNCs content was increased to 18 wt%, more agglomeration and non-uniform distribution of the AgNPs-CCNCs were observed, as shown in Fig. 5(f). This agglomeration, where the AgNPs-CCNCs were surrounded by an insufficient amount of PVA resin, can adversely affect the strength of the composite films. Similar characteristics were observed in the case of 18 wt% AgNPs-CCNFs loaded PVA matrix, as depicted in Fig. 5(g). The FE-SEM analysis has provided insights that support the measured mechanical properties of the bio-nanocomposite films due to the incorporation of AgNPs-carboxyl nanocellulose.

Fig. 5 (h) depicts the light transmittance of composite PVA films at visible light wavelengths. Specifically, the pristine PVA film exhibits a light transmittance of 95 % at a wavelength of 500 nm [3]. In contrast, the transmittance of AgNPs-CCNCs loaded PVA films at 6 wt% is 90.8 % at the same wavelength, while the transmittance of 6 wt% AgNPs-CCNFs

loaded PVA films is 86.7 %. The transmittance decreases as the levels of AgNPs-CCNCs and AgNPs-CCNFs in PVA increase. This decrease can be attributed to the introduction of AgNPs-carboxyl nanocellulose, which disrupts the transmission of light through the films. The respective optimal loadings of AgNPs-CCNCs and AgNPs-CCNFs in PVA films for a wavelength of 500 nm are 80.2 % and 79.4 %, each comprising 12 wt%. This serves as evidence for the absence of AgNPs-carboxyl nanocellulose agglomeration in the PVA matrix and highlights the remarkable compatibility between AgNPs-carboxyl nanocellulose and PVA. Consequently, translucent, and structured biocomposite films are achieved. At 18 wt% loading of AgNPs-CCNCs in PVA and AgNPs-CCNFs in PVA, the transmittance is significantly reduced to 72.5 % and 69.5 % respectively. However, this decrease in transmittance can be attributed to the increased aggregation of the AgNPs-carboxyl nanocellulose filler as its concentration reaches 18 wt%. Consequently, the reinforcement capability is diminished due to the formation of clusters and microvoids in the interfacial regions of the PVA matrix.

Fig. 5 (i) displays the visual appearance of both pristine PVA films and composite films when placed in front of printed paper. The observations align with previous studies that have indicated a decrease in the transparency of biopolymer films upon the addition of AgNPs-carboxyl nanocellulose [49].

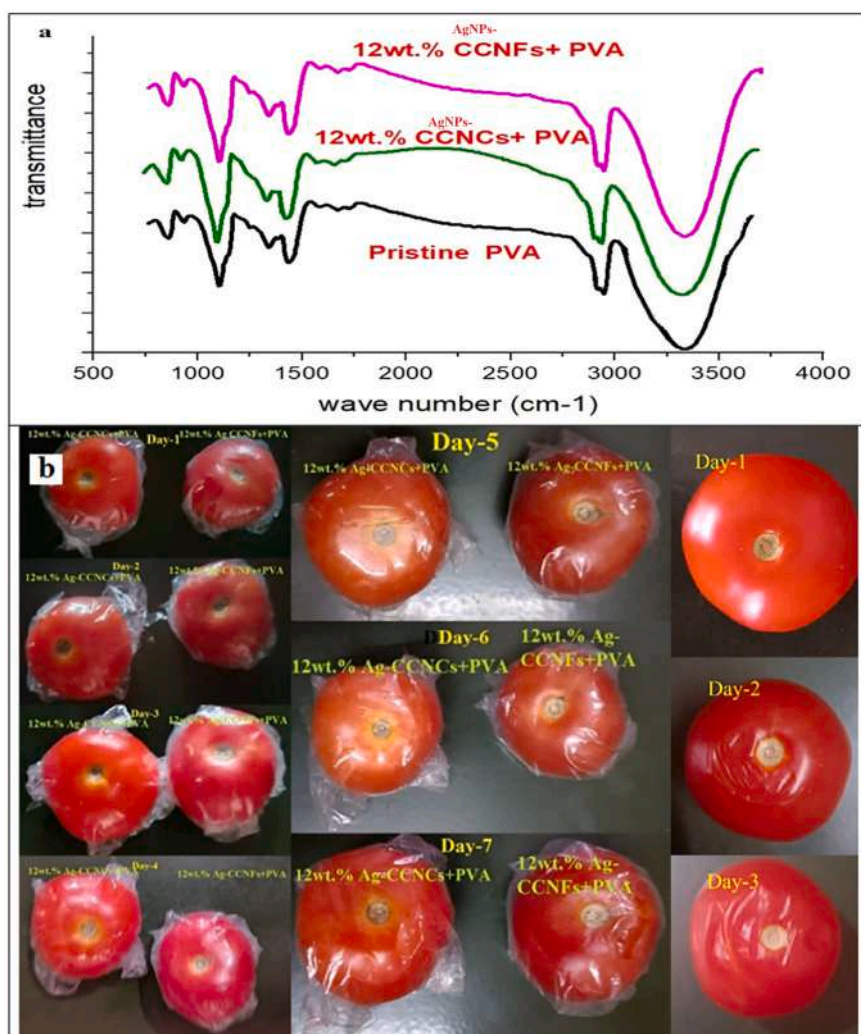


Fig. 6. a. FT-IR image of pristine PVA and 12wt.% AgNPs-carboxyl nanocellulose composite films, b. Images of changes in the external appearance of composite film packed and unpacked tomatoes for various storage times.

3.2.3. FT-IR analysis

The FT-IR transmittance spectra of the pristine PVA, PVA composite films loaded with 12 wt% of AgNPs-CCNCs, and PVA composite films loaded with 12 wt% of AgNPs-CCNFs are shown in Fig. 6a. The presence of similar spectra confirms that there was no chemical reaction during composite preparation. The broad stretched peak occurring at 3040–3660 cm^{-1} indicates the presence of hydroxyl (OH) groups, demonstrating the hydrophilic characteristics of PVA and its affinity for water [45]. However, the composite films with AgNPs-CCNCs and AgNPs-CCNFs exhibit shorter bands compared to pristine PVA, indicating a decrease in the availability of free O–H groups due to the presence of nanocellulose content in PVA. These groups are essential for

maintaining hydration by penetrating the nanocellulose structure. The peaks at 1085 cm^{-1} , 1732 cm^{-1} , 2852 cm^{-1} , and 2930 cm^{-1} correspond to C–O stretching, C=O stretching, symmetric and asymmetric stretching from an alkyl group, and C–H stretching, respectively [50]. The short peak at 1641 cm^{-1} in pristine PVA is attributed to the deformation vibration of absorbed water molecules [51]. The intensity of this peak increases with the addition of AgNPs-CCNCs and AgNPs-CCNFs in PVA, indicating good compatibility between PVA and AgNPs-carboxyl nanocellulose, resulting in favorable packaging applications. The results indicate that incorporating AgNPs-carboxyl nanocellulose into PVA composites has no impact on the chemical properties of PVA, aligning with the research conducted by Sarwar et al. [45], who

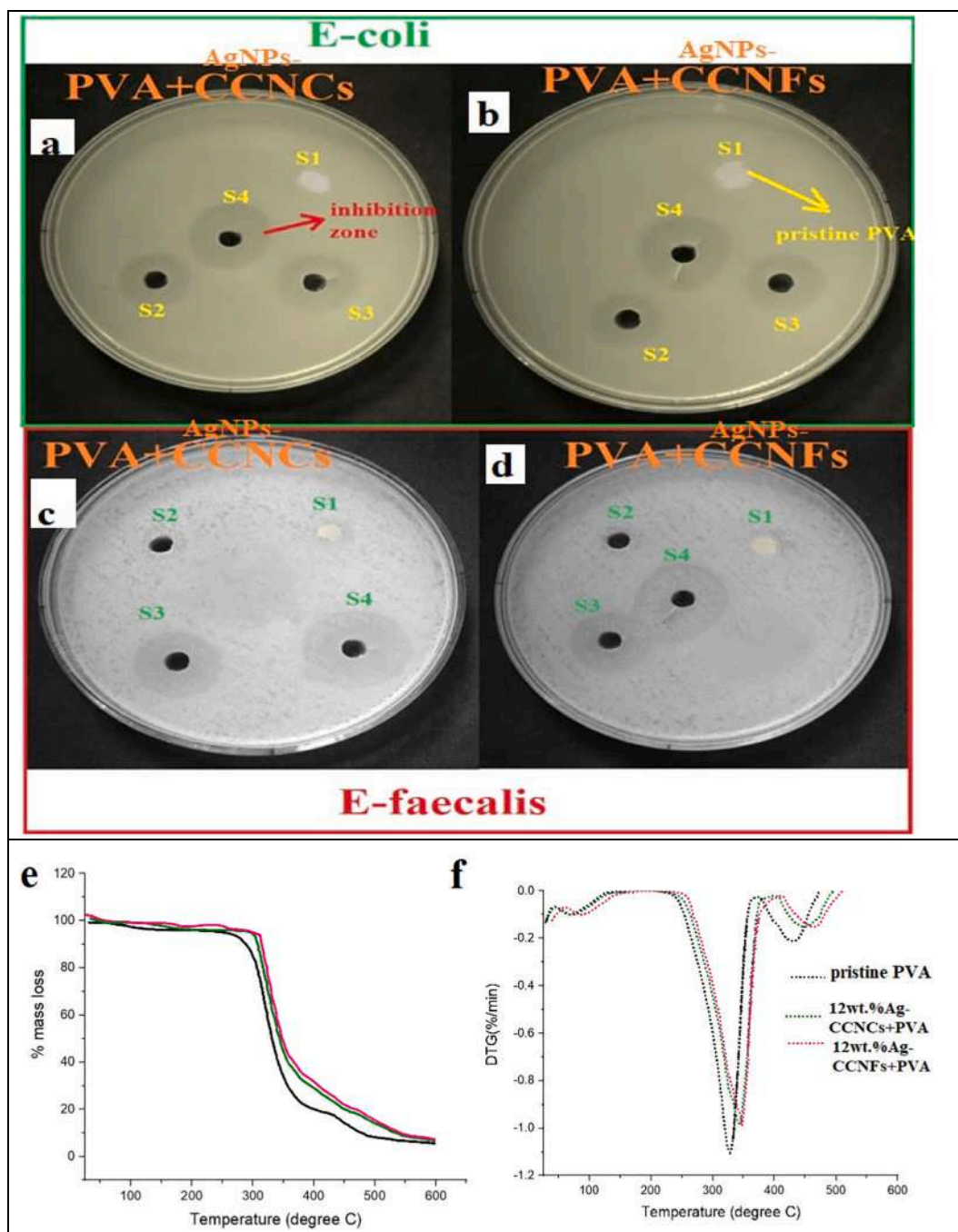


Fig. 7. a. antibacterial (*E. coli*) test on AgNPs-CCNCs/PVA, b. antibacterial (*E. coli*) test on AgNPs-CCNFs/PVA, c. antibacterial (*E. faecalis*) test on AgNPs-CCNCs/PVA, d. antibacterial (*E. faecalis*) test on AgNPs-CCNFs/PVA (s1-pristine PVA, s2-6wt% of AgNPs-nanocellulose + PVA, s3-12wt% of AgNPs nanocellulose + PVA, s4-18wt% of AgNPs-nanocellulose + PVA), e & f TGA and DTG curve of the pristine PVA and composite PVA film.

effectively produced PVA/nanocellulose/Ag nanocomposite films.

3.2.4. Packaging and moisture retention ability

Tomatoes play a vital role in Indian cuisine, being used in curries, and chutneys, and as a foundation for various dishes. To maintain their freshness, refrigeration or proper packaging is essential as it helps in preserving them. One of the common causes of tomato spoilage is the fungus *Colletotrichum coccodes*, which leads to a condition known as anthracnose. Over time, the unpacked or non-refrigerated tomatoes develop dark reddish circular soft spots and textures on their skins, as shown in Fig. 6(b).

However, Fig. 6 (b) demonstrates that when tomatoes are packed with PVA film loaded with 12 wt% AgNPs-CCNCs and PVA film loaded with 12 wt% AgNPs-CCNFs, which possess antimicrobial properties, they remain disease-free. Consequently, these films effectively prevent microbial spoilage, extending the tomato's shelf life for over a week.

The moisture retention ability (MRA) of food packaging films is essential to maintain the freshness and quality of packaged food products. The excellent MRA of the films can be attributed to their hydrophilic nature. The water-holding capacity within the composite films is facilitated by the presence of free O—H groups. Table 3 illustrates the MRA of the developed PVA composite films, demonstrating a positive correlation between the AgNPs-carboxyl nanocellulose content and the percentage of moisture retained. As previously mentioned, (Section 3.2.3), an increase in the AgNPs-carboxyl nanocellulose content leads to a decrease in the availability of free O—H groups. These groups play a vital role in maintaining hydration by penetrating the AgNPs-carboxyl nanocellulose structure. Both AgNPs-CCNCs loaded PVA composite films and AgNPs-CCNFs loaded PVA composite films exhibit a notable MRA within the range of 78–95 %, which falls within the standard MRA range specified by ITC Limited, India [50]. On the other hand, the pristine PVA film exhibits the lowest MRA, while the composite films with varying AgNPs-carboxyl nanocellulose contents display a high MRA, showing no significant difference. Other authors have previously reported similar characteristics [50,54–57].

3.2.5. Antibacterial properties of the films

The study examined the antibacterial properties of different types of films: pristine PVA, AgNPs-CCNCs loaded PVA composite films, and AgNPs-CCNFs loaded PVA composite films against *E. faecali* and *E. coli* bacteria. The antibacterial test lasted for 24 h, and the resulting zones of inhibition were captured in photographs (Fig. 7 (a–d)). Table 3 illustrates how the film characteristics influence the antimicrobial activity, as indicated by the diameter of the inhibition zone. Analysis of Fig. 7 (a–d) reveals that the pristine PVA film did not exhibit any antibacterial activity, whereas the AgNPs-CCNCs loaded PVA films and AgNPs-CCNFs loaded PVA films displayed distinct inhibitory zones against both *E. faecali* and *E. coli*. A similar observation was made in the case of AgNPs/CNCs reinforced PVA and CNCs reinforced PVA nanocomposites [45,50].

Compared to all other prepared PVA composite films, the findings demonstrate that the inclusion of 12 wt% of AgNPs-CCNCs in PVA films, as well as 12 wt% of AgNPs-CCNFs in PVA films exhibit superior characteristics in inhibiting bacterial growth. Therefore, these films are considered good materials for food packaging applications.

3.2.6. TGA studies

To study the effect of 12 wt% of AgNPs-CCNCs and 12 wt% of AgNPs-CCNFs on the thermal stability of the PVA matrix using TGA and DTG as shown in Fig. 7 (c & d).

The initial onset temperature (T_{onset}) of the pristine PVA was determined to be 290 °C. This can be attributed to the degradation of PVA caused by dehydration and the formation of volatile by-products [52]. However, the PVA composite films containing 12 wt% of AgNPs-CCNCs and 12 wt% of AgNPs-CCNFs exhibited lower T_{onset} values of 320 °C and 325 °C, respectively. This indicates that the thermal stability of the PVA

composite films surpasses that of the pristine PVA, likely due to the degradation of the PVA matrix and the pyrolysis of AgNPs-carboxyl nanocellulose [3].

Upon incorporating 12 wt% of AgNPs-CCNCs in PVA and 12 wt% of AgNPs-CCNFs in PVA, the DTG curve's onset temperature shows a slight shift towards the higher temperatures, as depicted in Fig. 7(d). Additionally, the degradation temperature of the composite film exhibits a slight increase from 335 °C to 342 °C for 12 wt% of AgNPs-CCNCs in PVA and from 335 °C to 345 °C for 12 wt% of AgNPs-CCNFs in PVA, respectively. This behavior can be attributed to the strong interactions between the hydroxyl groups of polyvinyl alcohol molecules and the carboxyl groups of AgNPs-nanocellulose. This study demonstrates that prepared composites with 12 wt% of AgNPs-carboxyl nanocellulose in PVA exhibit favorable thermal properties, suggesting their potential as a viable alternative to traditional polythene bags in society.

4. Conclusions

In this study, AgNPs-CCNCs were successfully isolated from used paper egg carton boxes through a combination of sequential organosolv and cyanamide-activated hydrogen peroxide treatments, citric acid hydrolysis, and an in-situ generation process. The resulting AgNPs-CCNCs display a rod-like structure with AgNPs uniformly dispersed throughout the entire formation.

The α -cellulose residue obtained from citric acid hydrolysis serves as an input material to produce CCNFs using ball milling. Subsequently, this material is utilized in an in-situ generation process to create AgNPs-CCNFs. The obtained AgNPs-CCNFs exhibit a web-like structure with AgNPs homogeneously dispersed throughout the structure. Remarkably, both AgNPs-CCNCs and AgNPs-CCNFs displayed significant antibacterial activity against both Gram-positive and Gram-negative bacteria.

Furthermore, nanocomposite PVA films reinforced with AgNPs-CCNCs and AgNPs-CCNFs were prepared using the solution casting method, and their properties were examined. Specifically, the films containing 12 wt% of AgNPs-CCNCs and 12 wt% of AgNPs-CCNFs displayed favorable mechanical strength, thermal stability, and packaging capabilities. Scanning electron microscopy (SEM) images revealed that the 12 wt% AgNPs-CCNCs reinforced PVA film and 12 wt% AgNPs-CCNFs reinforced PVA film was free from any filler agglomeration, indicating a uniform distribution of the nanoparticles within the PVA matrix.

These films were also found to possess high moisture retention capability, making them ideal for packaging fresh fruits and vegetables with a high respiration rate. Moreover, the films demonstrated strong antimicrobial activity against both Gram-positive and Gram-negative bacteria, enhancing their potential applications in food preservation and safety.

Overall, these findings suggest that the developed AgNPs-nanocellulose biocomposite PVA films have the potential for various packaging applications, making them a promising material in this field.

CRedit authorship contribution statement

G.R. Raghav: Conceptualization, Methodology, Investigation; K.J. Nagarajan & M.Palanimatharaja: Conceptualization, Methodology, Investigation, and Writing - original draft, testing; M. Karthic & M. A. Ganesh: Writing - review & editing. R. Ashok kumar: Writing - Conceptualization, review & editing.

Declaration of competing interest

The authors declare that they have no known competing financial interests or personal relationships that could have appeared to influence the work reported in this paper.

Acknowledgments

The authors are grateful for the support rendered by the Management of Thiagarajar College of Engineering (TCE), Madurai-625015, Tamil Nadu, India. They sincerely thank SITRA (South Indian Textile Research Association) for chemical composition measurements. The Department of advanced research of Madurai Kamaraj University for FE-SEM, and HR-TEM measurements. Physics and Chemistry Department of Alagappa University for the XRD and UV-Vis and FT-IR measurement, and antibacterial activities, Department of Mechanical Engineering (Nanotechnology Laboratory) of TCE for the synthesis of the nano-materials. They sincerely thank TSSCAR- TCE for the tensile testing of the films.

References

- [1] S.M.K. Thiagamani, N. Rajini, S. Siengchin, A.V. Rajulu, N. Hariram, N. Ayrilmis, Influence of silver nanoparticles on the mechanical, thermal, and antimicrobial properties of cellulose-based hybrid nanocomposites, *Compos. Part B* 165 (2019) 516–525.
- [2] Marilena Carbone, Domenica Tommasa Donia, Gianfranco Sabbatella, Riccarda Antiochia, Silver nanoparticles in polymeric matrices for fresh food packaging, *J. King Saud Univ. Sci.* 28 (4) (2016) 273–279.
- [3] K.J. Nagarajan, M.R. Sanjay, G.R. Raghav, Anish Khan, Extraction of cellulose nanocrystals from red banana peduncle agro-waste and application in environmentally friendly biocomposite film, *Polym. Compos.* 43 (8) (2022) 4942–4958.
- [4] Babak Ghanbarzadeh, Seyed Amir Oleyaei, Hadi Almasi, Nanostructured materials utilized in biopolymer-based plastics for food packaging applications, *Crit. Rev. Food Sci. Nutr.* 55 (12) (2015) 1699–1723.
- [5] Pooyan Makvandi, Chen-yu Wang, Ehsan Nazarzadeh Zare, Assunta Borzacchiello, Li-na Niu, Franklin R. Tay, Metal-based nanomaterials in biomedical applications: antimicrobial activity and cytotoxicity aspects, *Adv. Funct. Mater.* 30 (22) (2020) 1910021.
- [6] Madalina Oprea, Denis Mihaela Panaitescu, Nanocellulose hybrids with metal oxides nanoparticles for biomedical applications, *Molecules* 25 (18) (2020) 4045.
- [7] V. Sadanand, N. Rajini, A. Varada Rajulu, B. Satyanarayana, Preparation of cellulose composites with in situ generated copper nanoparticles using leaf extract and their properties, *Carbohydr. Polym.* 150 (2016) 32–39.
- [8] Li Fan, Hui Zhang, Mengxi Gao, Meng Zhang, Pengtao Liu, Xinliang Liu, Cellulose nanocrystals/silver nanoparticles: in-situ preparation and application in PVA films, *Holzforchung* 74 (5) (2020) 523–528.
- [9] Wei Wang, Yu Zhilong, Fouad K. Alsammarraie, Fanbin Kong, Mengshi Lin, Azlin Mustapha, Properties and antimicrobial activity of polyvinyl alcohol-modified bacterial nanocellulose packaging films incorporated with silver nanoparticles, *Food Hydrocoll.* 100 (2020), 105411.
- [10] Sachin M. Meshram, Shital R. Bonde, Indarchand R. Gupta, Aniket K. Gade, Mahendra K. Rai, Green synthesis of silver nanoparticles using white sugar, *IET Nanobiotechnol.* 7 (1) (2013) 28–32.
- [11] S.M. Yakout, A.A. Mostafa, novel green synthesis of silver nanoparticles using soluble starch and its antibacterial activity, *Int. J. Clin. Exp.* 8 (3) (2015) 3538.
- [12] Piming Ma, Long Jiang, Yu Manman, Weifu Dong, Mingqing Chen, Green antibacterial nanocomposites from poly (lactide)/poly (butylene adipate-co-terephthalate)/nanocrystal cellulose-silver nanohybrids, *ACS Sustain. Chem. Eng.* 4 (12) (2016) 6417–6426.
- [13] Shiwen Wang, Jiashu Sun, Lu Yuexiao Jia, Nuoxin Wang Yang, Yunlei Xianyu, Wenwen Chen, Xiaohong Li, Ruitao Cha, Xingyu Jiang, Nanocrystalline cellulose-assisted generation of silver nanoparticles for nonenzymatic glucose detection and antibacterial agent, *Biomacromolecules* 17 (7) (2016) 2472–2478.
- [14] Beatrice Swensson, Monica Ek, Derek G. Gray, In situ preparation of silver nanoparticles in paper by reduction with alkaline glucose solutions, *ACS Omega* 3 (8) (2018) 9449–9452.
- [15] Madhu Kaushik, Audrey Moores, Nanocelluloses as versatile supports for metal nanoparticles and their applications in catalysis, *Green Chem.* 18 (3) (2016) 622–637.
- [16] Amira Errokh, Albert Magnin, Jean-Luc Pataux, Sami Boufi, Hybrid nanocellulose decorated with silver nanoparticles as reinforcing filler with antibacterial properties, *Mater. Sci. Eng. C* 105 (2019), 110044.
- [17] K.J. Nagarajan, N.R. Ramanujam, M.R. Sanjay, Suchart Siengchin, B. Surya Rajan, K. Sathick Basha, P. Madhu, G.R. Raghav, A comprehensive review on cellulose nanocrystals and cellulose nanofibers: pretreatment, preparation, and characterization, *Polym. Compos.* 42 (4) (2021) 1588–1630.
- [18] L.E. Wise, M. Murphy, A.A. D'Addieco, Chlorite holocellulose: its fractionation and bearing on summative wood analysis and studies on the hemicellulose, *Pap. Trade J.* 122 (2) (1946) 35–43.
- [19] K.O. Reddy, C.U. Maheswari, M.S. Dhlamini, B.M. Mothudi, V.P. Kommula, J. Zhang, A.V. Rajulu, Extraction and characterization of cellulose single fibers from native african napier grass, *Carbohydr. Polym.* 188 (2018) 85–91.
- [20] Y. Seki, M. Sarikanat, K. Sever, C. Durmuşkahya, Extraction and properties of *Ferula communis* (chakshir) fibers as novel reinforcement for composites materials, *Compos. Part B* 44 (1) (2013) 517–523.
- [21] Arthur L. Barry, Marie B. Coyle, Clyde Thornsberry, E.H. Gerlach, R.W. Hawkinson, Methods of measuring zones of inhibition with the Bauer-Kirby disk susceptibility test, *J. Clin. Microbiol.* 10 (6) (1979) 885–889.
- [22] X.F. Sun, R.C. Sun, P. Fowler, M.S. Baird, Isolation and characterisation of cellulose obtained by a two-stage treatment with organosolv and cyanamide activated hydrogen peroxide from wheat straw, *Carbohydr. Polym.* 55 (4) (2004) 379–391.
- [23] Zhiguo Zhang, Guihua Yang, Ming He, Letian Qi, Xincai Li, Jiachuan Chen, Synthesis of silver nanoparticles and detection of glucose via chemical reduction with nanocellulose as carrier and stabilizer, *Int. J. Mol. Sci.* 23 (23) (2022) 15345.
- [24] Jun-Gill Kang, Youngku Sohn, Interfacial nature of Ag nanoparticles supported on TiO₂ photocatalysts, *J. Mater. Sci.* 47 (2012) 824–832.
- [25] Jianghu Cui, Hu Chaofan, Yunhua Yang, Wu Yongjian, Lufeng Yang, Yaling Wang, Yingliang Liu, Zhenyou Jiang, Facile fabrication of carbonaceous nanospheres loaded with silver nanoparticles as antibacterial materials, *J. Mater. Chem.* 22 (16) (2012) 8121–8126.
- [26] Subair Naduparambath, T.V. Jinita, V. Shaniba, M.P. Sreejith, Aparna K. Balan, E. Purushothaman, Isolation and characterisation of cellulose nanocrystals from sago seed shells, *Carbohydr. Polym.* 180 (2018) 13–20.
- [27] Kun Peng, Yanan Huang, Na Peng, Chunyu Chang, Antibacterial nanocellulose membranes coated with silver nanoparticles for oil/water emulsions separation, *Carbohydr. Polym.* 278 (2022), 118929.
- [28] K.J. Nagarajan, A.N. Balaji, S. Thanga Kasi Rajan, K. Sathick Basha, Effect of sulfuric acid reaction time on the properties and behavior of cellulose nanocrystals from *Cocos nucifera* var-*Aurantiaca* peduncle's cellulose microfibrils, *Mater. Res. Express* 6 (12) (2019), 125333.
- [29] Mohamed El-Sakhawy, Samir Kamel, Ahmed Salama, Hebat-Allah S. Tohamy, Preparation and infrared study of cellulose based amphiphilic materials, *Cellul. Chem. Technol.* 52 (3–4) (2018) 193–200.
- [30] S.G. Kostyukov, H.B. Matyakubov, Yu Yu Masterova, A. Sh Kozlov, M. K. Pryanichnikova, A.A. Pynenkov, N.A. Khlichina, Determination of lignin, cellulose, and hemicellulose in plant materials by FTIR spectroscopy, *J. Anal. Chem.* 78 (6) (2023) 718–727.
- [31] Yu Cen, Zhouyang Xiang, Tingting Han, Yu Long, Tao Song, Effect of microfluidizing cycles after citric acid hydrolysis on the production yield and aspect ratio of cellulose nanocrystals, *Cellulose* 29 (13) (2022) 7193–7209.
- [32] Olga Sambalova, Kerstin Thorwarth, Norbert Victor Heeb, Davide Bleiner, Yucheng Zhang, Andreas Borgschulte, Alexandra Kroll, Carboxylate functional groups mediate interaction with silver nanoparticles in biofilm matrix, *ACS Omega* 3 (1) (2018) 724–733.
- [33] Ji Un Shin, Jaeyoung Gwon, Sun-Young Lee, Hyuk Sang Yoo, Silver-incorporated nanocellulose fibers for antibacterial hydrogels, *ACS Omega* 3 (11) (2018) 16150–16157.
- [34] Liyuan Zhang, Takuya Tsuzuki, Xungai Wang, Preparation of cellulose nanofiber from softwood pulp by ball milling, *Cellulose* 22 (2015) 1729–1741.
- [35] P. Phanthong, G. Guan, Y. Ma, X. Hao, A. Abudula, Effect of ball milling on the production of nanocellulose using mild acid hydrolysis method, *J. Taiwan Inst. Chem. Eng.* 60 (2016) 617–622.
- [36] Benjamin Le Ouay, Francesco Stellacci, Antibacterial activity of silver nanoparticles: a surface science insight, *Nano Today* 10 (3) (2015) 339–354.
- [37] K.J. Nagarajan, A.N. Balaji, S. Thanga Kasi Rajan, N.R. Ramanujam, Preparation of bio-eco based cellulose nanomaterials from used disposal paper cups through citric acid hydrolysis, *Carbohydr. Polym.* 235 (2020), 115997.
- [38] O.M. Prakash, Malaya Naik, Rajesh Katiyar, Satyanarayan Naik, Deepak Kumar, Deepamala Maji, Anugrah Shukla, Ashween Deepak Nannaware, Alok Kalra, Prasant Kumar Rout, Novel process for isolation of major bio-polymers from *Mentha arvensis* distilled biomass and saccharification of the isolated cellulose to glucose, *Ind. Crop. Prod.* 119 (2018) 1–8.
- [39] N.S. Prasanna, J. Mitra, Isolation and characterization of cellulose nanocrystals from *Cucumis sativus* peels, *Carbohydr. Polym.* 247 (2020), 116706.
- [40] Chérif Ibrahima Khalil Diop, Jean-Michel Lavoie, Isolation of nanocrystalline cellulose: a technological route for valorizing recycled tetra pak aseptic multilayered food packaging wastes, *Waste Biomass Valorization* 8 (2017) 41–56.
- [41] Akira Isogai, Tsuguyuki Saito, Hayaka Fukuzumi, TEMPO-oxidized cellulose nanofibers, *Nanoscale* 3 (1) (2011) 71–85.
- [42] Zahid Hanif, Zeeshan Ahmad Khan, Dongwhi Choi, Moonwoo La, Sung Jea Park, One-pot synthesis of silver nanoparticle deposited cellulose nanocrystals with high colloidal stability for bacterial contaminated water purification, *J. Environ. Chem. Eng.* 9 (4) (2021), 105535.
- [43] Hohyun Lee, Jinhwa You, Hyoung-Joon Jin, Hyo Won Kwak, Chemical and physical reinforcement behavior of dialdehyde nanocellulose in PVA composite film: a comparison of nanofiber and nanocrystal, *Carbohydr. Polym.* 232 (2020), 115771.
- [44] Xuezu Xu, Fei Liu, J.Y. Long Jiang, Darrin Haagensohn Zhu, Dennis P. Wiesenborn, Cellulose nanocrystals vs. cellulose nanofibrils: a comparative study on their microstructures and effects as polymer reinforcing agents, *ACS Appl. Mater. Interfaces* 5 (8) (2013) 2999–3009.
- [45] M.S. Sarwar, M.B.K. Niazi, Z. Jahan, T. Ahmad, A. Hussain, Preparation and characterization of PVA/nanocellulose/Ag nanocomposite films for antimicrobial food packaging, *Carbohydr. Polym.* 184 (2018) 453–464.
- [46] Adriana N. Frone, Denis M. Panaitescu, Dan Donescu, Catalin I. Spataru, Constantin Radovici, Roxana Trasca, Raluca Somoghi, Preparation and characterization of PVA composites with cellulose nanofibers obtained by ultrasonication, *BioResources* 6 (1) (2011) 487–512.
- [47] Qian Li, Jinping Zhou, Lina Zhang, Structure and properties of the nanocomposite films of chitosan reinforced with cellulose whiskers, *J. Polym. Sci. B Polym. Phys.* 47 (11) (2009) 1069–1077.

- [48] Kaiwen Choo, Yern Chee Ching, Cheng Hock Chuah, Sabariah Julai, Nai-Shang Liou, Preparation and characterization of polyvinyl alcohol-chitosan composite films reinforced with cellulose nanofiber, *Materials* 9 (8) (2016) 644.
- [49] Sihang Zhang, Xu Jiangtao, Zhichao Liu, Yingying Huang, Shouxiang Jiang, Rapid and scalable preparation of flexible Ag nanoparticle-decorated nanocellulose SERS sensors by magnetron sputtering for trace detection of toxic materials, *Cellulose* 29 (18) (2022) 9865–9879.
- [50] Manu L. Naik, Ashok M. Sajjan, T.M. Sharanappa Achappa, Yunus Khan, Nagaraj R. Banapurmath, Prakash B. Kalahal, Narasimha H. Ayachit, Nanobacterial cellulose production and its antibacterial activity in biodegradable poly (vinyl alcohol) membranes for food packaging applications, *ACS Omega* 7 (48) (2022) 43559–43573.
- [51] Mohammad Asad, Naheed Saba, Abdullah M. Asiri, M. Jawaid, Eti Indarti, W. D. Wanrosli, Preparation and characterization of nanocomposite films from oil palm pulp nanocellulose/poly (vinyl alcohol) by casting method, *Carbohydr. Polym.* 191 (2018) 103–111.
- [52] M.I. Voronova, O.V. Surov, S.S. Guseinov, V.P. Barannikov, A.G. Zakharov, Thermal stability of polyvinyl alcohol/nanocrystalline cellulose composites, *Carbohydr. Polym.* 130 (2015) 440–447.
- [53] F. Xu, Z.C. Geng, C.F. Liu, J.L. Ren, J.X. Sun, R.C. Sun, Structural characterization of residual lignins isolated with cyanamide-activated hydrogen peroxide from various organosolvs pretreated wheat straw, *J. Appl. Polym. Sci.* 109 (1) (2008) 555–564.
- [54] D. Hu, L. Wang, Physical and antibacterial properties of polyvinyl alcohol films reinforced with quaternized cellulose, *J. Appl. Polym. Sci.* 133 (25) (2016).
- [55] Q. Wang, H. Wang, T. Zhang, Z. Hu, L. Xia, Jiang Li, S., Antibacterial activity of polyvinyl alcohol/WO₃ films assisted by near-infrared light and its application in freshness monitoring, *J. Agric. Food Chem.* 69 (3) (2021) 1068–1078.
- [56] N.E. Kochkina, O.A. Butikova, Effect of fibrous TiO₂ filler on the structural, mechanical, barrier and optical characteristics of biodegradable maize starch/PVA composite films, *Int. J. Biol. Macromol.* 139 (2019) 431–439.
- [57] S. Rathinavel, S.S. Saravanakumar, Development and analysis of silver nano particle influenced PVA/natural particulate hybrid composites with thermo-mechanical properties, *J. Polym. Environ.* 29 (2021) 1894–1907.
- [58] J.P. Reddy, J.W. Rhim, Characterization of bionanocomposite films prepared with agar and paper-mulberry pulp nanocellulose, *Carbohydr. Polym.* 110 (2014) 480–488.

EFFECT OF CELLULOSE NANOFIBERS FROM RED COCONUT PEDUNCLE WASTE AS REINFORCEMENT IN EPOXY COMPOSITE SHEETS

GURUMOORTHY R. RAGHAV,^{*} RAJENDRAN ASHOK KUMAR,^{**}
JAWAHARLAL K. NAGARAJAN,^{***} CHANDRAN VIGNESH,^{***}
FELIZ SAHAYARAJ AROKIASAMY^{****} and EDI SYAFRI^{*****}

^{*}*SCMS School of Engineering and Technology, Ernakulam, Kerala, India*

^{**}*SRM Madurai College for Engineering and Technology, Madurai, Tamilnadu, India*

^{***}*Thiagarajar College of Engineering, Madurai-625015, Tamil Nadu, India*

^{****}*Kalaignarkarunanidhi Institute of Technology, Coimbatore, Tamil Nadu, India*

^{*****}*Politeknikpertanian Negeri Payakumbuh, West Sumatra, Indonesia*

✉ *Corresponding author: G. R. Raghav, raghavmechklnc@gmail.com*

Received May 17, 2023

Organic filler-reinforced thermosetting polymer composites, when contrasted with ferrous, nonferrous, and their respective alloys, offer a broad spectrum of applications. Extensive research has been dedicated to enhancing the intrinsic mechanical and thermal properties of composite materials, with a particular focus on environmentally friendly, recyclable, and biodegradable reinforcements. As a result, the present study involved the preparation of composites by amalgamating cellulose nanofibers (CNFs) sourced from agricultural waste with epoxy to augment the characteristics of polymer composites. The CNFs-reinforced epoxy composites were fabricated via the compression molding process, incorporating filler loadings ranging from 1% to 3% by weight. A comprehensive experimental investigation was conducted on the mechanical properties (tensile, flexural, impact, and hardness) and thermal properties (heat deflection temperature) of these composites. Additionally, scanning electron microscopy was employed to examine the surface characteristics and fractured surfaces of the composites. The results revealed that, among the produced composites, those containing 2 wt% CNFs in the epoxy exhibited superior mechanical properties, outstanding tensile and flexural strengths of 42.8 ± 2 MPa and 106.1 ± 1.6 MPa, respectively, along with an impact strength of 13 ± 2.5 KJ/m² and a hardness rating of 21.2. Notably, these 2 wt% CNFs-reinforced epoxy composites exhibited a 7% increase in the heat deflection temperature, compared to the pristine epoxy resin.

Keywords: red coconut peduncle waste, cellulose nanofibers, mechanical properties, morphology

INTRODUCTION

Increasing environmental concerns have brought into focus the need to minimize the dependence on non-renewable mineral resources for engineered products. Synthetic fibers/fillers are commonly used to reinforce polymer composite structures, typically made of materials such as glass, aramid, and carbon fibers. Moreover, synthetic nanofillers are becoming increasingly important due to their specific properties required in polymer composites. However, despite the widespread use of synthetic fibers/fillers reinforced polymer composite structures in various engineering applications, they have several disadvantages, including high

production costs and significant pollution during production, resulting in potential health hazards.¹ The non-recyclable nature of these synthetic materials poses a significant threat to the environment.²

To address these issues, scientists are shifting their research efforts towards replacing synthetic fibers in composite structures with eco-friendly biodegradable cellulosic fillers at the nanoscale.³ As a result, cellulose nanofibers reinforced biopolymer composites are gaining popularity in various fields, from structural to electronic applications. Cellulose nanofibers (CNFs) in biopolymers are also being used in

structural, automotive, electrical, 3D printing, and electronic industries due to their unique properties, including high tensile modulus, large surface area with a network structure, and their non-toxic and eco-friendly nature.^{4,5}

CNFs can be produced from cellulosic materials, such as plant fibers, agricultural waste, rayon cloths, and waste newspapers.⁶ Cellulose nanofiber (CNF) is a fibrous substance with a diameter ranging from 1 to 100 nm and a length that is 100 times or more the diameter. It is obtained through various mechanical processes, such as ball milling, high-pressure homogenization, steam explosion grinding, micro-fluidization, and cryo-crushing.⁷ CNFs have a web-like structure and contain cellulose, as well as certain amorphous elements. To reduce energy consumption, raw macrocellulosic resources are transformed into pure microcellulosic fibers before CNF extraction.⁸ Among the different mechanical processes, ball milling is a simple and cost-efficient method for producing a large quantity of CNFs from cellulosic macrofibers.⁹

In a study by Saba *et al.*,¹⁰ CNFs from bleached softwood kraft pulp were used to reinforce polymer composites with varying CNFs filler loadings, and it was found that a 0.75 wt% CNFs loading in the epoxy matrix produced the best tensile (26 MPa) and flexural strength (42 MPa). Similarly, Jahanbaani *et al.*¹¹ investigated the mechanical properties of spinning-coated CNFs sheets made from wheat straw and epoxy-reinforced composites, which exhibited good tensile (117 MPa) and impact strength (202 kJ/m²), compared to lignocellulosic wheat straw fiber-reinforced epoxy composites. Pandurangan *et al.*¹² analyzed the effect of CNFs on epoxy composites with varying CNFs loading percentages and found that an epoxy composite containing 5 wt% CNFs had improved tensile strength (46.2 MPa) and thermal properties. Kurita *et al.*⁴ successfully extracted CNFs using a water jet-based mechanical technique, and the epoxy matrix reinforced with 2.25 vol% CNFs exhibited better tensile strength (74 MPa) and flexural strength (120 MPa), compared to other CNFs loading combinations.

The existing literature indicates that cellulose nanofibers (CNFs) obtained from various mechanical processes can enhance the mechanical and thermal properties of polymer composites. In light of this, Nagarajan *et al.*¹³ conducted research

where they successfully isolated CNFs from red coconut peduncle waste using a combination of chemical and ball milling processes. Their efforts resulted in CNFs with favorable physical, thermal, and morphological characteristics. However, it is worth noting that, as of now, there is no published research available on the utilization of CNFs extracted from red coconut peduncle waste as a reinforcement material in epoxy composites.

Recognizing this research gap, the current study aimed to employ CNFs extracted from red coconut peduncle waste as a reinforcement component in epoxy composites, with a specific focus on applications requiring lightweight structural materials. To assess the performance of these epoxy composites, a series of tests were conducted, including tensile, flexural, impact, hardness, heat deflection and dynamic-mechanical analyses. Additionally, field electron-scanning electron microscopy (FE-SEM) was used to examine the morphology of fractured tensile, flexural and impact test specimens. This research seeks to provide valuable insights into the potential of CNFs from red coconut peduncle waste as a sustainable and effective reinforcement for epoxy composites in structural applications.

EXPERIMENTAL

Materials

The extraction of CNFs from red coconut peduncle waste (RCPW) was carried out at the Nanotechnology Laboratory (Mechanical Department) situated at Thiagarajar College of Engineering in Madurai, Tamil Nadu, India. The CNFs used in this study were derived through an extraction process outlined in Figure 1 (a-c) and further detailed in Table 1. The properties of the obtained CNFs are summarized in Table 2. The morphology of these CNFs, derived from RCPW using a combination of chemical and ball milling methods, was examined using transmission electron microscopy (TEM). The sample preparation procedure for TEM analysis has been thoroughly described in a prior study.¹³ As depicted in Figure 1 (d), the TEM images clearly illustrate the extracted CNFs as having a web-like structure, with individual CNFs, measuring around 55 nm to 64 nm in width.

The epoxy used in this research was obtained from Javanthee Traders, situated in Chennai, Tamil Nadu, India. Specifically, it was epoxy LY556, which is the diglycidyl ether of Bisphenol-A, and it exhibited a density ranging from 1.15 to 1.2 g/cm³. Additionally, the hardener employed was HY951, an aliphatic primary amine, with a density of 0.97 g/cm³.

Preparation of composites

The compression moulding method was used to prepare epoxy composites with varied CNFs loadings (1, 2, and 3 wt%). A predetermined amount of CNFs was mixed with epoxy and thoroughly dispersed for 240 minutes using a homogenizer at 10,000 rpm, followed by 10 minutes of sonication to remove air

bubbles from the mixture. The hardener was then added to the mixture in a 10:1 (g/g) stoichiometric ratio (resin: hardener). After that, the mixture was poured into a 30 cm x 20 cm mould. The closed mould was placed in a compression moulding machine and the mixture was cured for a day at a uniaxial compressive pressure of 18 MPa. The prepared composites sheets are shown in Figure 1 (e).

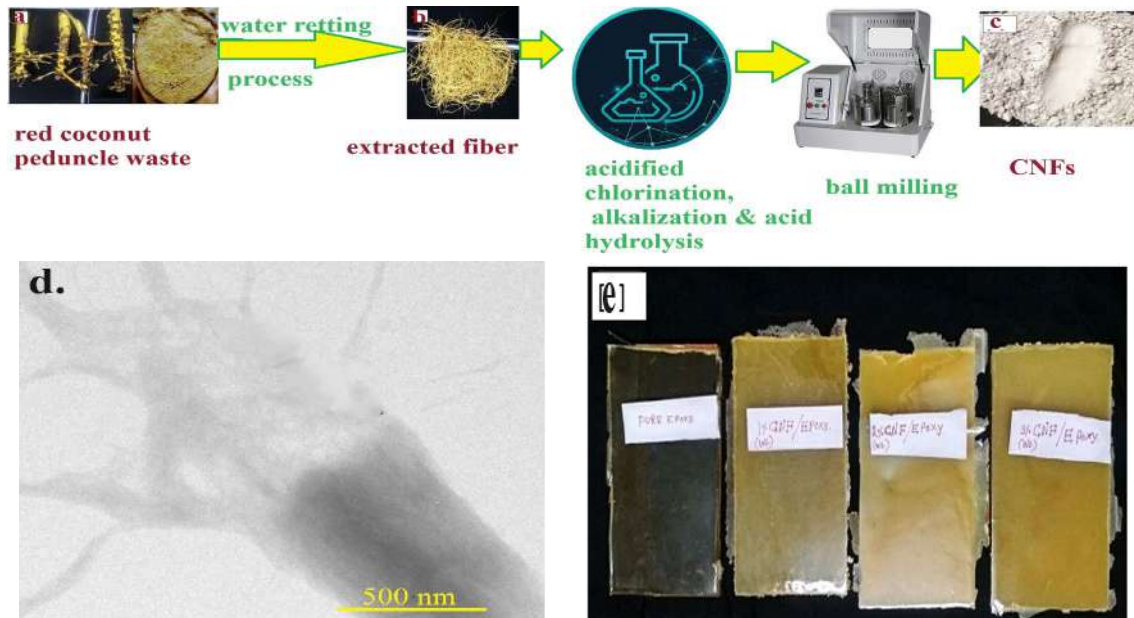


Figure 1: (a-c) extraction process of CNFs, (d) TEM image of CNFs, and (e) prepared composites through compression moulding

Table 1
Chemical treatment and ball milling process, as well as the results of each treatment stage

Stage No.	Chemical treatment	Process specifics	Treatment outcome
Stage I	Toluene-ethanol (2:1, v/v) at 70 °C for 4 h	Waxy contents are dissolved in toluene-ethanol solution	Pure lignocellulosic fibers are obtained
Stage II	0.7 wt% sodium chlorite at 100 °C for 120 min in an acidic solution	Lignin dissolved in acidified chlorination solution	Remaining hemicellulose coupled cellulose is retrieved
	17.5 wt% /v NaOH solution at room temperature (30 °C) for 35 min	In NaOH solution, hemicelluloses are dissolved	Crude α -cellulose is synthesized
Stage III	80% acetic acid and 70% nitric acid (10:1 ratio) at 120 °C for 15 min	α -Cellulose defibrillation	Cellulose microfibril is synthesized
Stage IV	Ball milling process	Cellulose microfibrils are milled for 2 h with 0.6 mm zirconia balls at 850 rpm, at 60:1 ball-to-microfibril ratio	CNFs are obtained

Table 2
Characteristics of CNFs

Type of fiber	Crystallinity index (%)	Crystallite size (nm)	Thermal stability (°C)	Thermal degradation (°C)	Width (nm)	Ref.
CNFs	77.8	6.95	230	325	55-64	13

Mechanical and thermal characterization

Tensile testing was performed using a UTM machine (Tinius Olsen H10KL) with a 10 kN load cell and a 1.0 mm/min crosshead speed. The tensile characteristics of specimens were determined according to the ASTM D638-10 standard, on samples of 165.0 x 10 x 3.0 mm and the test was carried out with a gauge length of 60 mm.¹⁴ The ASTM D790-10 three-point flexural test was performed with the same machine (127 x 13 x 3 mm) with a cross head speed of 2 mm/min.¹⁵ The impact strength of the composite sheets was evaluated using a Tinius Olsen (Model: 104) in accordance with ASTM D 256-10 (65 mm x 13 mm x 3 mm) standard.¹⁶

The hardness of composite sheets was tested using a Barcol Hardness tester (Model: VBH2) in accordance with ASTM 2583.¹⁷ During the test, the specimens' surfaces were polished to remove scratches. The gap between the pin tip and the edge was kept to a minimum of 3 mm.

An HDT-VICAT tester (XRW300A, Chengde Jinhe Instrument Manufacturing Co., Ltd., Chengde, China) was used to conduct the heat deflection test for measuring the deflection temperature of the composite sheets according to the ASTM D648 (60 mm x 12 mm x 3 mm) standard under the pressure of 1.86 MPa. During the test, silicone oil was utilised as a heat transfer medium with no influence on the mechanical qualities of the specimens.¹⁸ The specimens were heated in an oil bath at a rate of 2 °C/min until deflection was achieved.

For each mechanical and thermal characteristic, an average of five specimens were examined for pristine epoxy and various CNFs filler reinforced epoxy composites as a function of filler loading (wt%). The viscoelastic properties of both pristine epoxy and composite specimens were assessed using an ASTM D4065-01-compliant DMA (Dynamic Mechanical Analysis) Q 800 machine. The testing was conducted in the three-point bending mode, utilizing specimens with dimensions of 65 mm length, 10 mm width, and 3 mm thickness. The oscillation frequency during testing was set at 1 Hz. The temperature range explored during the test spanned from 45 °C to 150 °C, with a controlled heating rate of 5 °C per min.

Fractographic analysis of the composite specimens following tensile, flexural, and impact tests was performed using an FE-SEM instrument, specifically the SUPRA 55 VP-4132 model from Carl Zeiss. The instrument operated within a voltage range from 10 to 30 kV. To prepare the samples for analysis, the

fractured regions were initially sectioned into 10 x 10 mm squares. Subsequently, a thin layer of gold coating was applied to these specimens to improve their conductivity for the electron microscopy examination.

RESULTS AND DISCUSSION

Tensile testing

In Figure 2a, the tensile strength, measured in MPa, is plotted against varying percentages of CNFs filler in the epoxy resin. The tensile strength of the pristine epoxy measures 31.2±1.7 MPa. Upon the inclusion of CNFs, the epoxy composite achieves its highest tensile strength with a 2 wt% CNFs content, reaching 42.8±2 MPa, and surpassing the strength of the pure epoxy. As shown in Figure 2a, this marks a significant improvement, of 35.4%, in tensile strength, compared to the pure epoxy resin, indicating improved contact and interaction between the CNFs and the epoxy matrix. This enhanced interaction enables more efficient transmission of the applied tensile load.¹⁹ When evaluating the tensile strength, it was observed that, at a 3 wt% CNFs content in the epoxy matrix, there was a decrease of up to 10.7% in comparison to the optimal CNF loading. This decline can be attributed to the agglomeration of CNFs within the epoxy matrix. The agglomeration phenomenon reduces the ability of the composite sheets to effectively transmit stress, leading to a reduction in tensile strength.⁴

As shown in Figure 2b, the tensile modulus of the composite sheets follows a similar trend to the tensile strength. It increases as the CNFs concentration rises to the optimal level. Specifically, for the 2 wt% CNFs-reinforced composite, the maximum tensile modulus reached 3.62±0.05 GPa. This indicates that the reinforcement exhibits excellent stiffness characteristics and adheres well to the epoxy matrix.

However, the tensile modulus drops significantly when the CNFs content exceeds the optimal limit. This decline can be attributed to the deterioration of adhesive strength between the CNFs and the epoxy matrix. The study highlights significant improvements in properties, such as

tensile strength and tensile modulus, resulting from the incorporation of organic fillers derived from materials like *Cocos nucifera* shell, tamarind seed, *Polyalthia longifolia* seed, and date palm seed into thermosetting plastics.^{17,18,20,21}

Flexural strength tests

In various engineering structural applications, such as pavements, beams and slabs, the

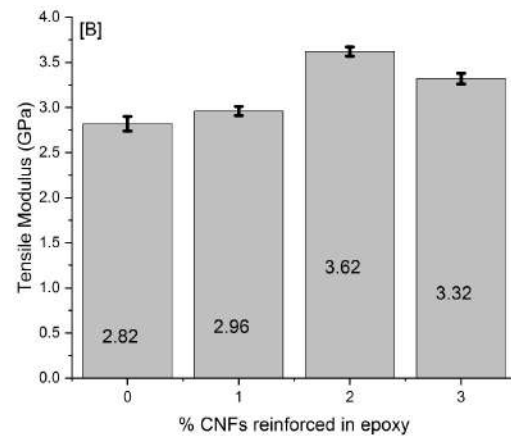
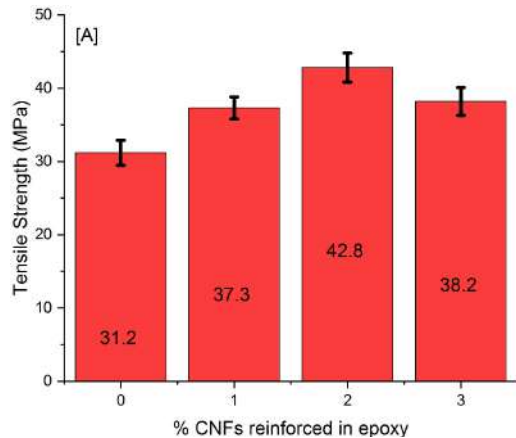


Figure 2: (A) Tensile strength and (B) tensile modulus of composites

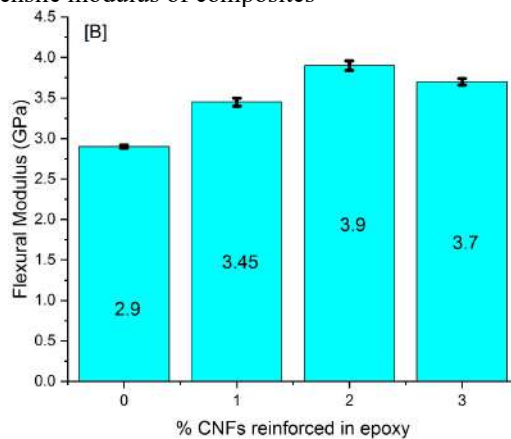
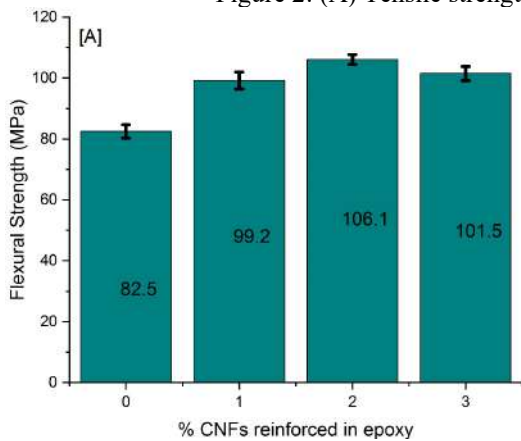


Figure 3: (A) Flexural strength and (B) flexural modulus of composites

The pristine epoxy exhibited a flexural strength of 82.5 ± 2.28 MPa. When CNFs were incorporated, the flexural strength values for 1 wt%, 2 wt%, and 3 wt% CNFs-reinforced epoxy composites were 99.2 ± 2 , 106.1 ± 1.6 , and 101.5 ± 2.3 , respectively. As depicted in the figure, the highest values for flexural strength and flexural modulus were observed at approximately 106.1 ± 1.6 MPa and 3.9 ± 0.06 GPa, respectively. These values represented an improvement of 36.2% and 37.9%, respectively, compared to the pristine epoxy.

The optimal composite containing 2 wt% CNFs was likely achieved due to the uniform distribution of CNFs and their superior

susceptibility to bending is a critical consideration. Hence, the flexural characteristics play a significant role when designing and constructing composites for these purposes. In this study, the addition of up to 2 wt% of CNFs into the epoxy matrix resulted in noticeable increases in both flexural strength (measured in MPa) and flexural modulus (measured in GPa), as illustrated in Figure 3 (a and b).

adhesiveness with the epoxy matrix. Table 3 provides a comparison of the optimal flexural strength of CNFs-reinforced thermosetting composites with that of composites reinforced with other organic fillers. The results indicate that the optimal flexural strength of the CNFs-reinforced composite closely aligns with that of composites reinforced with other organic fillers.

Impact strength testing

Impact strength serves as a crucial measure to evaluate the ability of epoxy and its composite materials to withstand sudden applied loads. Figure 4 presents the results of impact tests

conducted on pristine epoxy and epoxy sheets containing varying weight percentages of CNFs.

It is worth noting that all CNFs-reinforced epoxy composites exhibited higher impact strength when compared to pristine epoxy, which had an impact strength of $9.1 \pm 1 \text{ kJ/m}^2$. Among the CNFs-reinforced epoxy composites, the lowest impact strength, of $11.1 \pm 1.5 \text{ kJ/m}^2$, was recorded in the case of 1 wt% CNFs-reinforced composites, representing a 22% improvement over the impact strength of pristine epoxy.

The highest impact strength value, amounting to $13 \pm 2.5 \text{ kJ/m}^2$, was achieved by the 2 wt% CNFs-reinforced epoxy composites, marking a substantial 39.1% increase over the impact

strength of pristine epoxy. These results indicate that when CNFs were introduced into the epoxy matrix, they exhibited strong accommodation within the matrix, and the nanostructure of the fillers had excellent wettability. Additionally, the matrix displayed robust bonding properties, enabling enhanced stress transmission between the matrix and the filler.²²

However, it is important to note that, beyond the optimal CNFs content, the impact strength decreased rapidly. This reduction can be attributed to decreased absorption capabilities and a subsequent decrease in the bonding between the matrix and CNFs, reaching a notably low level.

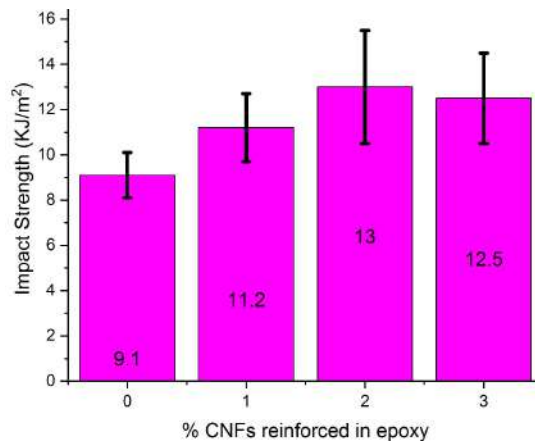


Figure 4: Impact strength of composites

Table 3
Mechanical properties of CNFs reinforced epoxy composite compared with other organic filler reinforced thermosetting composite

Source of organic filler	Matrix	Tensile strength (MPa)	Flexural strength (MPa)	Impact strength (KJ/m ²)	Reference
CNFs from red coconut peduncle	Epoxy	42.8±2	106±1.6	13±2.5	Present study
Wood apple	Epoxy	43.6	78.19	-	Nagaprasad ²⁰ <i>et al.</i> , 2019
Coconut shell	Epoxy	41.3	68.25	-	Karakoti ²³ <i>et al.</i> , 2019
Bio-char	Epoxy	60	-	10	Gnanaraj ¹⁸ <i>et al.</i> , 2021
Coconut shell	Vinyl ester	38.70	105.13	33.04	Stalin ¹⁷ <i>et al.</i> , 2020
Polyalthia longifolia seed	Vinyl ester	32.5	125	31.09	Nagaraj ²¹ <i>et al.</i> , 2019
Date seed	Vinyl ester	40.3	149	17	Nagaprasad ²⁰ <i>et al.</i> , 2019
Tamarind seed	Vinyl ester	34.3	121	14	

Morphology of fractured mechanical testing specimens

Figure 5 (a and b) provides insights into the fractured tensile specimens. In Figure 5a, the fractured specimen exhibits a smooth and glassy outer flat surface (labeled as B), indicating a brittle plastic nature, with extremely poor

resistance to cracking, and a fracture mode characterized by crack propagation during the tensile test of the 1 wt% CNFs-loaded epoxy composite. Fractures are visible in the matrix (labeled as C) of the fractured specimens, as shown in Figure 5a.

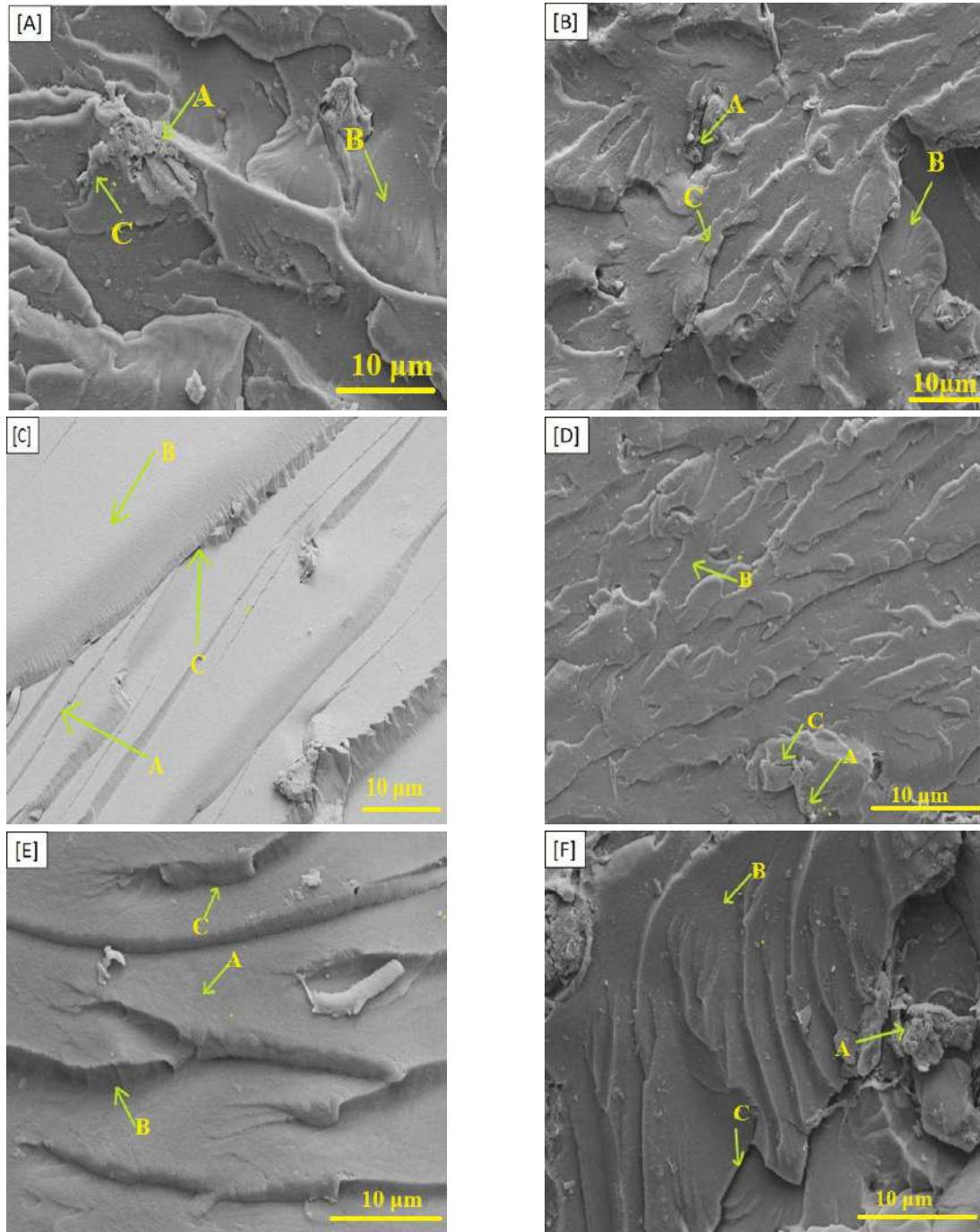


Figure 5: FE-SEM images of (a) tensile fractured specimen (1 wt% CNFs loading), (b) tensile fractured specimen (2 wt% CNFs loading), (c) flexural fractured specimen (1 wt% CNFs loading), (d) flexural fractured specimen (2 wt% CNFs loading), (e) impact fractured specimen (1 wt% CNFs loading), (f) impact fractured specimen (2 wt% CNFs loading)

Table 4
 Characteristics of fractured specimens of 1 wt% and 2 wt% CNFs reinforced epoxy composites

S. no	Fractured specimen	Irregular and jagged pattern (A)	Glassy exterior wavy or stream-like pattern (B)	Matrix fracture (C)
1.	Tensile (1 wt% of CNFs loading in epoxy)	Less	High	High
2.	Tensile (3 wt% of CNFs loading in epoxy)	High	Less	Less
3.	Flexural (1 wt% of CNFs loading in epoxy)	Less	High	High
4.	Flexural (2 wt% of CNFs loading in epoxy)	High	Less	Less
5.	Impact (1 wt% of CNFs loading in epoxy)	Less	High	High
6.	Impact (2 wt% of CNFs loading in epoxy)	High	Less	Less

On the other hand, Figure 5b illustrates a fractured surface featuring a high number of uneven and jagged patterns (labeled as A), along with a limited number of glassy external wavy or stream-like patterns (labeled as B), representing the 2 wt% CNFs-loaded epoxy composite. The presence of uneven and jagged patterns suggests that improved CNF dispersion resulted in good interfacial adhesion characteristics between CNFs and the epoxy matrix, enabling better transmission of tensile stress.

This behavior of improved interfacial adhesion and stress transmission is also observed in the tested specimens during flexural and impact tests, as depicted in Figure 5 (c-f). The characteristics of the fractured specimens for both 1 wt% and 2 wt% CNFs-reinforced epoxy composites are summarized in Table 4.

Heat deflection test (HDT)

The Heat Deflection Temperature (HDT) is a critical parameter that indicates the temperature at which a polymer starts to deform under a specified load. Figure 6 displays the HDT values of pristine epoxy and CNFs-reinforced epoxy composite sheets with varying weight percentages.

The HDT value for pristine epoxy was determined to be 210 ± 4.5 °C. Notably, the HDT values exhibited a rapid increase as different weight percentages of CNFs were introduced into the epoxy matrix. Importantly, when considering filler contents ranging from 1 to 3 wt%, the maximum HDT value was achieved by the 2 wt% CNFs-reinforced epoxy composites, reaching

224.2 ± 3.8 °C. It is evident that the HDT value improved with the inclusion of CNFs content.

These findings underscore the superior thermal properties of CNFs when compared to other natural fillers commonly used in reinforced thermosetting composites. For instance, CNFs-reinforced epoxy composites exhibit significantly higher HDT values than those reinforced with tamarind seed (71 °C), date seed (84 °C), *Polyalthia longifolia* seed (66 °C), and coconut shell (171 °C). This demonstrates the potential of CNFs as a valuable reinforcement material for enhancing the thermal stability of epoxy composites.^{17,18,20,21}

The slight decrease in the HDT value observed in the case of the 3 wt% CNFs reinforced epoxy (219.2 ± 3.1 °C) suggests that the bonding between the CNFs and the epoxy may not be as stable at this higher filler content. However, it is important to note that this decrease in HDT is still within a relatively high temperature range, indicating that the thermal stability of the composite is not significantly compromised. The HDT value remains quite robust, emphasizing the overall effectiveness of CNFs as a reinforcement material for enhancing the thermal properties of the epoxy composite.

Hardness testing

Figure 7 presents the Barcol hardness values of both the pristine epoxy resin and various weight percentages of CNFs-reinforced epoxy composites. The pristine epoxy exhibited a hardness value of 19.67 ± 0.5 . However, when 2 wt% CNFs were added, the hardness value significantly increased to 21.2 ± 1.5 . This

enhancement can be attributed to the even dispersion of CNFs, which results from proper mixing proportions. It leads to strong adhesive bonding between the matrix and the reinforcement, especially when the optimal CNFs content is added.^{23,24}

Remarkably, both the pristine epoxy and the 3 wt% CNFs-reinforced epoxy composite exhibited a hardness value of around 20 ± 1.7 , as depicted in Figure 7. This suggests that the addition of 3 wt%

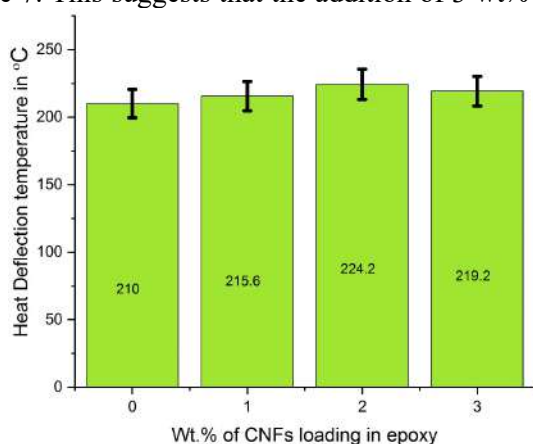


Figure 6: Heat deflection test of composites

Dynamic analysis

Dynamic mechanical analysis was employed to examine the viscoelastic properties of both unmodified epoxy and epoxy composite loaded with an optimal 2 wt% of CNF under dynamic loading conditions. In Figure 8 (a and b), the curves for loss modulus illustrate the differences between pure epoxy and epoxy composites reinforced with CNFs.

At room temperature, the storage modulus for pristine epoxy stands at 1500 MPa, while the epoxy composite with 2 wt% CNF reinforcement reaches 2095 MPa, marking a substantial 39% increase compared to pristine epoxy. However, as depicted in Figure 8a, the storage modulus of both unmodified epoxy and 2 wt% CNF-reinforced composites decline as the temperature rises. This decline is evident in three distinct states: the glassy (solid) state, the transitional state, and the rubbery state (Fig. 8a).

A glassy state was identified within the temperature range from 40 °C to 78 °C for pristine epoxy and from 40 °C to 87 °C for the epoxy composite reinforced with 2 wt% of CNFs. In this state, characterized by limited molecular mobility within the polymer chains, the storage modulus exhibited a continuous and gradual decrease. Notably, the storage modulus of the 2

CNFs resulted in inappropriate bonding because of insufficient matrix material. Additionally, it increased the porosity of the composites, which consequently led to a lower hardness value. This heightened hardness value contributes to improved wear resistance in the composites and renders them suitable for use in dynamic loading conditions.

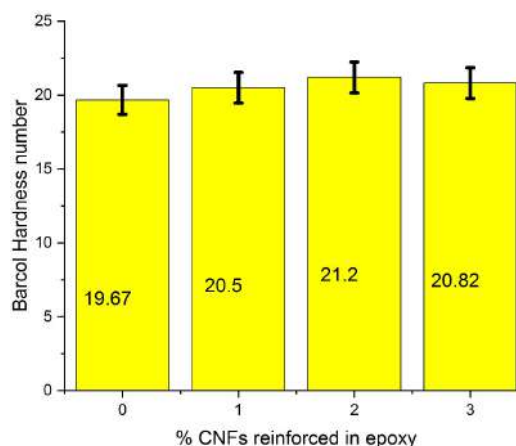


Figure 7: Barcol hardness of composites

wt% CNFs-reinforced composite in the glassy state exceeded that of pure epoxy.

Figure 8a illustrates that the epoxy composite with 2 wt% CNFs displayed a higher storage modulus in the glassy state, below its glass transition temperature (T_g). This enhancement can be attributed to the binding interactions between the nano-fillers and the matrix, a phenomenon discussed above during the analysis of tensile testing results.

The transition state was marked by a sudden decrease in the slope of the storage modulus as the temperature increased, occurring between 84 °C to 112 °C for pristine epoxy and 90 °C to 107 °C for 2 wt% CNFs-reinforced epoxy composites, following the conclusion of the glassy state. During this stage, the specimens underwent plastic deformation, leading to an increase in free volume due to heightened viscosity (segmental mobility) of the epoxy molecules. This resulted in a physically softer epoxy matrix and a reduction in interfacial bonding between the CNFs and the epoxy matrix.²⁵

Towards the end of the transition stage, there were no significant variations in the storage modulus in the rubbery state for both pristine epoxy and the epoxy composite reinforced with 2 wt% CNFs.

As depicted in Figure 8b, the loss modulus values for both pristine epoxy and the optimally loaded (2 wt%) CNFs epoxy composites exhibit an initial increase until reaching the glass transition temperature, followed by a subsequent decrease. Notably, the loss modulus curve for the 2 wt% CNFs-reinforced epoxy composite covers a broader range and exhibits a higher peak, with a maximum loss modulus of 247 MPa, as observed in comparison to the curve for pristine epoxy. Furthermore, this curve shifts towards the right-hand side. This behavior can be attributed to the uniform dispersion of CNFs within the epoxy matrix and the immobilization of matrix segments at the surface of the CNFs. Similar findings have been reported in previous literature concerning polymer composites reinforced with cellulosic fillers.²⁶⁻²⁸

In conclusion, both pristine epoxy and 2 wt% CNFs-reinforced epoxy demonstrate the highest

loss modulus values, indicating increased mechanical energy dissipation. However, beyond the glass transition temperature, the loss modulus values gradually decline with increasing temperature, primarily due to the softening of the matrix material, as illustrated in Figure 8b.

The integral of the tan (δ) curve signifies the degree of molecular mobility within the polymer and consequently, the damping behaviour of both the pristine epoxy and its composite. This damping factor undergoes a significant increase with rising temperature, reaching its peak at the conclusion of the transition state for both pristine epoxy and 2 wt% CNF-reinforced epoxy, as illustrated in Figure 8c. Notably, when compared to pure epoxy, the 2 wt% CNF-reinforced epoxy composite exhibits the lowest damping factor at the end of the transition region due to the constrained movement of polymer chains.

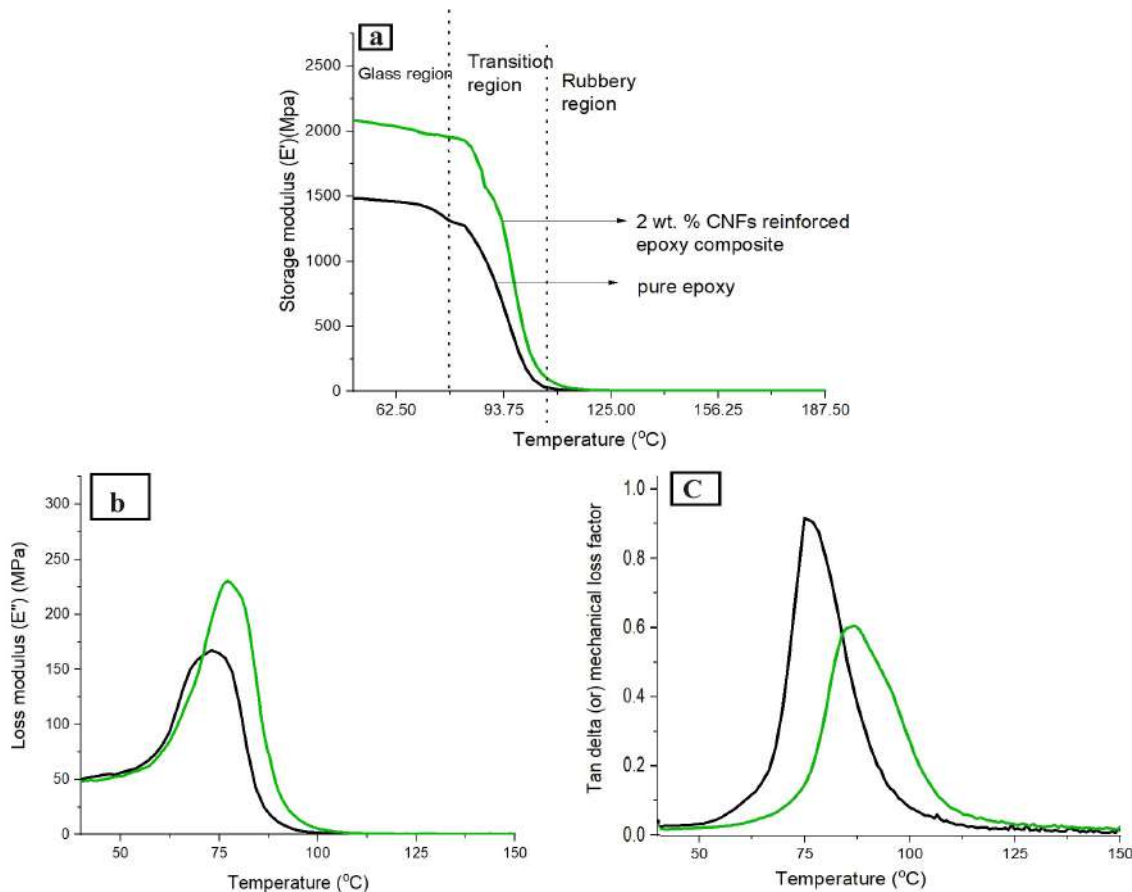


Figure 8: (a) Storage modulus, (b) loss modulus, and (c) tan delta curve of pristine epoxy and 2 wt% CNF reinforced epoxy composite

Moreover, the glass transition temperature (T_g) experiences an elevation in the case of the 2 wt% CNF-reinforced epoxy composite,

surpassing that of pristine epoxy by approximately 13%. This improvement is attributed to the influence of CNFs, coupled with

their uniform dispersion and strong interfacial interaction with the epoxy matrix, which enables the storage of load energy rather than its dissipation, thus augmenting the T_g of the CNF-reinforced epoxy composite. Subsequently, T_g decreases, and the loss modulus curve follows a similar pattern.

CONCLUSION

CNFs were extracted from red coconut peduncle waste and were used as a reinforcing material in the production of epoxy composites. The tensile, flexural, impact, hardness and heat deflection assessments were carried out to analyse the performance of CNFs manufactured epoxy composites, compared to pristine epoxy composite. The results of the study revealed that the 2 wt% CNFs reinforced epoxy composite exhibited the maximum tensile strength and tensile modulus (42.8 ± 2 MPa and 3.62 ± 0.05 GPa, respectively), the highest value of flexural strength and flexural modulus (106.1 ± 1.6 MPa and 3.9 ± 0.06 GPa, respectively), the highest impact strength (13 ± 2.5 kJ/m²) and the maximum HDT value (224.2 °C), along with a hardness value of 21.2. SEM analysis confirmed the better dispersion of CNFs in the epoxy composite with 2 wt% of CNFs loading. DMA analysis showed that the storage modulus and glass transition temperature were enhanced for the 2 wt% CNFs reinforced epoxy composite, when compared to the pristine epoxy.

Based on the research findings presented above, it can be concluded that the incorporation of 2 wt% CNFs in epoxy is considered optimal for a range of industrial structural applications. These applications may include the construction of partition walls, door panels, window frames, and similar structural components. The research suggests that this 2 wt% of CNF reinforcement enhances the mechanical properties and thermal behavior of epoxy composites, making them well-suited for use in these industrial contexts.

REFERENCES

- ¹ P. Narayanasamy, P. Balasundar, S. Senthil, M. R. Sanjay, S. Siengchin *et al.*, *Int. J. Biol. Macromol.*, **150**, 793 (2020), <https://doi.org/10.1016/j.ijbiomac.2020.02.134>
- ² G. R. Raghav, K. J. Nagarajan, M. Palaninatharaja, M. Karthic and M. A. Ganesh, *Int. J. Biol. Macromol.*, **249**, 126119 (2023), <https://doi.org/10.1016/j.ijbiomac.2023.126119>

- ³ A. George, M. R. Sanjay, R. Srisuk, J. Parameswaranpillai and S. A. Siengchin, *Int. J. Biol. Macromol.*, **154**, 329 (2020), <https://doi.org/10.1016/j.ijbiomac.2020.03.120>
- ⁴ H. Kurita, R. Ishigami, C. Wu and F. Narita, *J. Compos. Mater.*, **55**, 455 (2021), <https://doi.org/10.1177/0021998320967430>
- ⁵ E. Syafri, A. Kasim, H. Abral, Sudirman, G. T. Sulungbudi *et al.*, *Int. J. Biol. Macromol.*, **120**, 578 (2018), <https://doi.org/10.1016/j.ijbiomac.2018.08.134>
- ⁶ K. J. Nagarajan, N. R. Ramanujam, M. R. Sanjay, S. Siengchin and B. S. Rajan *et al.*, *Polym. Compos.*, **42**, 1588 (2021), <https://doi.org/10.1002/pc.25929>
- ⁷ A. F. M. Halim, *Indian J. Fibre Text. Res.*, **46**, 287 (2021), <https://doi.org/10.56042/ijftr.v46i3.31971>
- ⁸ P. Phanthong, P. Reubroycharoen, X. Hao, G. Xu, A. Abudula *et al.*, *Carbon. Resour. Convers.*, **1**, 32 (2018), <https://doi.org/10.1016/j.crcon.2018.05.004>
- ⁹ L. Zhang, T. Tsuzuki and X. Wang, *Cellulose*, **22**, 1729 (2015), <https://doi.org/10.1007/s10570-015-0582-6>
- ¹⁰ N. Saba, F. Mohammad, M. Pervaiz, M. Jawaid, O. Y. Alothman *et al.*, *Int. J. Biol. Macromol.*, **97**, 190 (2017), <https://doi.org/10.1016/j.ijbiomac.2017.01.029>
- ¹¹ A. R. Jahanbaani, T. Behzad, S. Borhani and M. H. K. Darvanjooghi, *Fibers Polym.*, **17**, 1438 (2016), <https://doi.org/10.1007/s12221-016-6424-9>
- ¹² M. T. Pandurangan and K. Kanny, *Catalysts*, **10**, 831 (2020), <https://doi.org/10.3390/catal10080831>
- ¹³ K. J. Nagarajan, A. N. Balaji and N. R. Ramanujam, *Carbohydr. Polym.*, **212**, 312 (2019), <https://doi.org/10.1016/j.carbpol.2019.02.063>
- ¹⁴ K. J. Nagarajan, A. N. Balaji, N. R. Ramanujam and S. T. K. Rajan, *Mater. Res. Express.*, **6**, 125310 (2019), <https://doi.org/10.1088/2053-1591/ab54ff>
- ¹⁵ P. V. Reddy, R. V. S. Reddy, P. R. Prasad, D. M. Krishnudu, R. M. Reddy *et al.*, *J. Nat. Fibers*, **19**, 2218 (2020)
- ¹⁶ A. Stalin, S. Mothilal, V. Vignesh, K. J. Nagarajan and T. Karthick, *J. Nat. Fibers*, **19**, 5227 (2022), <https://doi.org/10.1080/15440478.2021.1875366>
- ¹⁷ B. Stalin, N. Nagaprasad, V. Vignesh, M. Ravichandran, N. Rajini *et al.*, *Carbohydr. Polym.*, **248**, 116748 (2020), <https://doi.org/10.1016/j.carbpol.2020.116748>
- ¹⁸ J. D. Gnanaraj, S. Mothilal, V. Vignesh, T. Karthick, S. O. Ismail *et al.*, *J. Polym. Environ.*, **30**, 2142 (2022), <https://doi.org/10.1007/s10924-021-02343-8>
- ¹⁹ B. Wetzal, F. Hauptert and Q. Zhang, *Compos. Sci. Technol.*, **63**, 2055 (2003), [https://doi.org/10.1016/S0266-3538\(03\)00115-5](https://doi.org/10.1016/S0266-3538(03)00115-5)
- ²⁰ N. Nagaprasad, B. Stalin, V. Vignesh, M. Ravichandran, N. Rajini *et al.*, *Polym. Compos.*, **42**, 791 (2021), <https://doi.org/10.1002/pc.25865>
- ²¹ N. Nagaraj, S. Balasubramaniam, V. Venkataraman, R. Manickam, R. Nagarajan *et al.*, *Int. J. Biol. Macromol.*, **147**, 53 (2020), <https://doi.org/10.1016/j.ijbiomac.2019.11.247>

²² V. A. Prabu, R. D. J. Johnson, P. Amuthakkannan and V. Manikandan, *J. Environ. Chem. Eng.*, **5**, 1289 (2017), <https://doi.org/10.1016/j.jece.2017.02.007>

²³ J. Panta, A. N. Rider, J. Wang, C. H. Yang, R. Hugh Stone *et al.*, *Compos. Part B*, **249**, 110401 (2023), <https://doi.org/10.1016/j.compositesb.2022.110401>

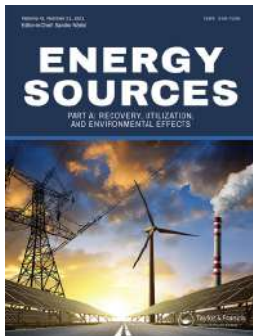
²⁴ M. S. Jamil, I. Ahmad and I. Abdullah, *J. Polym. Res.*, **13**, 315 (2006), <https://doi.org/10.1007/s10965-005-9040-8>

²⁵ S. Thanga Kasi Rajan, K. J. Nagarajan, V. Balasubramani, K. Sathickbasha, M. R. Sanjay *et al.*, *Int. J. Adhes. Adhes.*, **126**, 103492 (2023), <https://doi.org/10.1016/j.ijadhadh.2023.103492>

²⁶ N. Saba, M. T. Paridah, K. Abdan and N. A. Ibrahim, *Constr. Build. Mater.*, **124**, 133 (2016), <https://doi.org/10.1016/j.conbuildmat.2016.07.059>

²⁷ N. Saba, A. Safwan, M. L. Sanyang, F. Mohammad, M. Pervaiz *et al.*, *Int. J. Biol. Macromol.*, **102**, 822 (2017), <https://doi.org/10.1016/j.ijbiomac.2017.04.074>

²⁸ K. J. Nagarajan, A. N. Balaji, K. S. Basha, N. R. Ramanujam and R. A. Kumar, *Int. J. Biol. Macromol.*, **152**, 327 (2020), <https://doi.org/10.1016/j.ijbiomac.2020.02.255>



Analysis of methanol recovery using component specific reaction kinetics in biodiesel synthesis

Christy Thomas Sani, Rupesh S, Chris Ben Xavier & Rag R L

To cite this article: Christy Thomas Sani, Rupesh S, Chris Ben Xavier & Rag R L (2023) Analysis of methanol recovery using component specific reaction kinetics in biodiesel synthesis, Energy Sources, Part A: Recovery, Utilization, and Environmental Effects, 45:2, 5608-5620, DOI: 10.1080/15567036.2023.2209033

To link to this article: <https://doi.org/10.1080/15567036.2023.2209033>



Published online: 09 May 2023.



Submit your article to this journal [↗](#)



View related articles [↗](#)



View Crossmark data [↗](#)



Analysis of methanol recovery using component specific reaction kinetics in biodiesel synthesis

Christy Thomas Sani^a, Rupesh S ^b, Chris Ben Xavier^a, and Rag R L^c

^aDepartment of Chemical Engineering, National Institute of Technology, Calicut, Kerala, India; ^bDepartment of Mechanical Engineering, Biofuel Research Information and Demonstration Centre, PES College of Engineering, Mandya, Karnataka, India; ^cDepartment of Mechanical Engineering, SCMS School of Engineering & Technology, Cochin, India

ABSTRACT

Transesterification is the process of transmutation of fatty acids to alkyl esters (biodiesel) when reacted with alcohols such as methanol, ethanol, etc. The unreacted methanol in the process downstream can be recovered and reused economically by integrating methanol recovery with transesterification, thereby mitigating the environmental and health hazards caused by direct release of the same. The present work deals with the simulation of methanol recovery integrated transesterification of poppy seed oil in ASPEN Plus process simulator. The transesterification process is simulated using a component-specific kinetic model by considering four constituent triglycerides of poppy seed oil, namely, oleic acid, palmitic acid, linoleic acid, and stearic acid. The model is made more comprehensive by incorporating six-step reaction mechanism for each triglyceride to simulate its respective alkyl ester conversion. Recovery of excess methanol is implemented using a distillation-based methanol recovery unit. The prediction accuracy of the model is found to be 3.51% when the model predicted biodiesel yield is compared with the corresponding experimental values. The validated model is used to analyze the effect of methanol-to-oil ratio, reboiler duty, temperature, pressure and reflux ratio on methanol recovery. From the analysis, it is found that a methanol-to-oil ratio of 6:1 and process temperature of 60°C corresponds to maximum biodiesel yield. For the maximum yield condition, a maximum methanol recovery of 0.945 can be attained economically at a reboiler duty of 500 cal/s and reflux ratio 2.

ARTICLE HISTORY

Received 7 November 2022

Revised 27 February 2023

Accepted 25 March 2023

KEYWORDS

Poppy seed oil; biodiesel; methanol recovery; ASPEN Plus

Introduction

Price escalation of depleting fossil fuels and their adverse environmental footprints has spurred research in renewable energy sources such as biodiesel (Tyagi et al. 2010). Biodiesel is defined as an alkyl ester derived from long-chain carboxylic acids of triglycerides present in plant oils, animal fats, or waste cooking oil (Chang and Liu 2010). Transesterification is the transmutation of triglycerides to fatty acid alkyl esters and glycerol when reacted with alcohol in the presence of a catalyst (Borges and Díaz 2012). The selection of a proper triglyceride source or feedstock has a vital role in the process as well as quality, yield, and cost of biodiesel produced. In general, non-edible oil seeds, animal fats, and waste cooking oil, categorized under second-generation feedstock, are preferred to facilitate cheaper biodiesel by converting waste to energy (Bhuiya et al. 2014). Utilization of second-generation feedstocks such as chicken fat (Altikriti, Fadhil, and Dheyab 2015), radish seed oil (Fadhil, Sedeeq, and Al-Layla 2019), *Cyprinus carpio* fish oil (Altikriti, Fadhil, and Albadree 2016), poppy seed oil, mixed oils (Kumar, Singhal, and Sharma 2021), etc., can be effectively and economically used for transesterification thereby contributing toward healthy organic

waste management without affecting the food resources. Poppy seed oil is one of the second generation oil feedstocks grown at different geographic and climatic conditions (Bhuiya et al. 2020). Among the alcohols used for transesterification, methanol is preferred due to its lower cost and higher reactivity (Chongkhong, Tongurai, and Chetpattananondh 2009). The transesterification process can be made more effective and economical if the excess methanol supplied for shifting the equilibrium toward the product side can be recovered and reused. The release of waste and unused methanol obtained at the end of transesterification process causes adverse environmental and health hazards.

In the conventional biodiesel production, unused methanol during the washing phase of the process is released to the environment (Dhar and Kirtania 2009). Methanol being toxic, the release may harm the ecosystem through its adverse intervention in the food chain. Recovery of unused methanol after transesterification can also help to limit methanol content within 0.2% in the biodiesel to meet ASTM D6751 or EN14214 standards (Tyagi et al. 2010). The reactor temperature, pressure, and methanol-to-oil ratio of the transesterification process were experimentally reported to have a significant influence on methanol recovery (Baroutian et al. 2010; Wang et al. 2011). Inherently, transesterification is a slow process and hence different types of homogeneous and heterogeneous catalysts are used to augment the reaction kinetics (Thangaraj et al. 2019). Among the homogeneous catalysts, acid catalyst enabled transesterification requires a higher methanol-to-oil ratio of 30:1 (Xie and Wang 2021), whereas alkali catalysts make the process more efficient with better biodiesel quality (Cai et al. 2015). On the other hand, heterogeneous catalysts enable easy separation, recycling (Xie and Wan 2019; Xie and Wang 2020) and reuse of the catalyst without much compromise in oil to ester conversion. Through simulation tools, we can realistically and economically predict the performance of a process under different operating conditions without having to conduct expensive and time-consuming experiments (Bonate 2011). ASPEN Plus is one of the versatile process simulators equipped with module-wise modeling and simulation of integrated systems through default or user-defined settings (Rupesh and Gokul Krishnan 2021; Rupesh, Muraleedharan, and Arun 2016). The simulator is widely used for the design and simulation of transesterification plants. GIWA and Olanipekun (2015) performed a reactive distillation process in ASPEN Plus to investigate the effect of reflux ratio and reboiler duty on the purity of stearic acid methyl ester production. The author found that reflux ratio and reboiler duty have significant role in improving product purity. The effect of methanol-to-oil ratio on alkyl ester yield from *Jatropha curcas* oil is simulated by Adeniyi, Ighalo, and Eletta (2019). Application of ASPEN Plus for algal oil to biodiesel conversion and purification of glycerol was implemented by Jabbar et al. (2014) and Xiao, Xiao, and Varma (2013), respectively. Among the equilibrium, stoichiometric and kinetic modeling strategies in the simulator, kinetic models are more realistic as they use experimentally derived chemical kinetics associated with the transesterification process (Jansson 1980). Several kinetic models were reported for ASPEN Plus simulation of biodiesel synthesis with feedstock as a single triglyceride constituent and transesterification reaction represented in single or multiple steps. Generally, triolein is considered as the triglyceride feedstock and transesterification process is formulated using either single or multi-step reactions. Single step reaction is used to simulate the production of palm oil methyl ester with dimethyl carbonate transesterification reaction in ASPEN Plus using triolein as the feedstock by Ali, and Aziz (2015). The effect of operating parameters on transesterification process was analyzed by Kick et al. (2013) using single-step reaction kinetics in CSTR reactor. Implementation of transesterification in catalytic reactive distillation column using ASPEN Plus was simulated by Xiao et al. (2013) to demonstrate the conversion and separation within a single unit. Silva et al. (2017) also justified the practical implementation of reactive distillation column for transesterification when compared to plug flow reactor. The techno-economic feasibility of acid-catalyzed transesterification was simulated using single reaction in ASPEN Plus by Gebremariam and Marchetti (2018). Two-step and three-step reaction kinetics to represent transesterification in ASPEN Plus simulator was investigated by Hussain and Kumar (2018) and De Riju et al. (2019), respectively. The simulation of transesterification was made more realistic in ASPEN Plus by Silva et al. (2012) by incorporating a six-step reaction mechanism to simulate triolein to methyl ester conversion. Multi-step reaction kinetics consists of six reactions was implemented by Salehi et al. (2019) to conclude the best biodiesel purity from alkali-catalyzed

transesterification, by comparing different catalytic methods. Another six-step reaction model in ASPEN Plus to simulate soybean oil to alkyl ester conversion was implemented by Myint and El-Halwagi (2009). In actual practice, the feedstock consists of more than one type of triglyceride, and hence, more realistic simulation of the process demands consideration of all the constituent triglycerides in the simulation and six reactions per triglyceride constituent. Souza, Hirata, and Batista (2020) developed a multi-component and multi-reaction kinetic model as formulating feedstock with more constituents and incorporated their transesterification reaction kinetics makes the process more realistic. They considered palmitic and oleic acids as palm oil constituents and six reactions to represent transesterification. The transesterification process integrated with a methanol recovery unit was reported to simulate the recovery of excess methanol during biodiesel synthesis (Sotoft et al. 2010). Dhar and Kirtania (2009) developed a stoichiometric ASPEN Plus model for excess methanol recovery with triolein as feedstock. They concluded that alcohol-to-oil ratio is the most important process parameter in methanol recovery. A performance comparison of a distillation column and an evaporator for methanol recovery in the transesterification of waste cooking oil was done by Yun et al. (2013). They reported that the former could contribute to maximum methanol recovery with high biodiesel yield and minimum heat consumption. In another comparison, distillation-based recovery is found to have higher methanol recovery when compared with stripping and flash-based recovery techniques (Philip, Veawab, and Aroonwilas 2014). They formulated feedstock as triolein with single reaction kinetics to incorporate transesterification in the model. Lee, Posarac, and Ellis (2011) developed single constituent single reaction transesterification of waste oil and found that alkali-catalyzed reaction was more effective in methanol recovery than supercritical methanol transesterification. In another model, Okullo (2017) reported maximum methanol recovery in the alkali-catalyzed transesterification of jatropha curcas seed oil represented as triolein with single reaction kinetics. From the review, it is found that transesterification is simulated in ASPEN Plus by considering only single triglyceride constituent or two triglyceride constituents with limited number of reaction kinetics. In actual practice, the feedstock consists of more than one type of triglyceride and hence, more realistic simulation of the process demands consideration of all the constituent triglycerides in the simulation and six reactions per triglyceride constituent. Moreover, no work is found to be reported on the parametric study of methanol recovery in the transesterification of poppy seed oil considering individual feedstock constituents and their transesterification kinetics in ASPEN Plus platform. The present simulation deals with transesterification of poppy seed oil by considering all the four triglyceride constituents with six-step reaction kinetics for each constituent and the recovery of excess methanol.

Model development

A steady-state kinetic model to simulate the transesterification of poppy seed oil is developed in ASPEN Plus process simulator considering the following assumptions:

- The feedstock oil is a mixture of pure triglycerides
- The reactor is a perfectly mixed flow reactor, i.e., continuous stirred tank reactor
- Feed is 100% solid particle free.

The ASPEN Plus flowsheet of the model is depicted in [Figure 1](#). Poppy seed oil is modeled by considering the fatty acid profile reported in the experimental work of Aksoy (2011), given in [Table 1](#). Vapour–liquid equilibria of the system are represented using the Dortmund-UNIFAC (UNIF-DMD) model and the physical properties of feedstock, alcohol, catalyst and products are imported from the ASPEN Plus database (Kuramochi et al. 2009). Binary interaction parameters for the methanol-water and triglyceride-ester pairings are incorporated from the Non-random two liquid (NRTL) property package database available in the ASPEN Plus (Kiss and Sorin Bildea 2012). Alkali-based transesterification of the oil is simulated by considering methanol and NaOH as alcohol and catalyst respectively. The methanol “METHANOL” and sodium hydroxide “NAOH” streams from

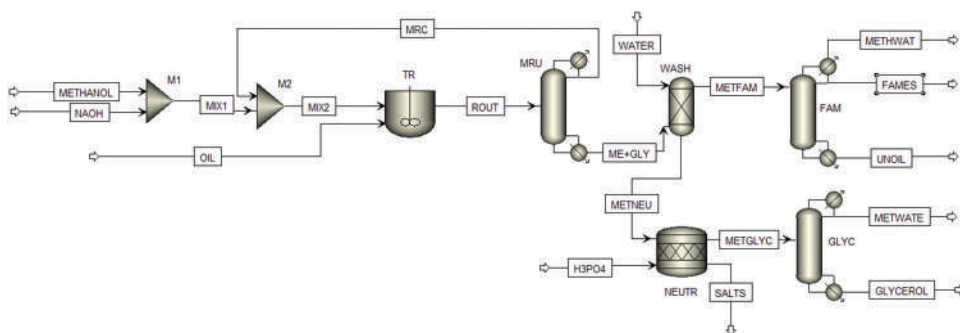


Figure 1. ASPEN Plus flow sheet.

Table 1. Triglyceride composition (Aksoy 2011).

Fatty Acid	Wt. %
Triolein	13.03
Tripalmitin	9.92
Trilinolein	75.07
Tristearate	1.98

mixer “M1” are combined with recovered methanol “MRC” by mixer “M2.” To simulate the transesterification process, the feedstock “OIL” is fed at a flow rate of 10 kg/h along with the resulting stream “MIX2” to the RCSTR reactor “TR.” Transesterification is implemented by incorporating component-specific reaction kinetics (Narváez, Rincón, and Sánchez 2007) in the RCSTR reactor by considering six reactions per triglyceride for four triglycerides, namely, triolein, trilinolein, tripalmitin, and tristearate, resulting in a total of 24 reactions. The general reactions and reaction kinetics used to simulate triglyceride transformation to their respective diglycerides, monoglycerides, and methyl esters are given in Table 2.

The product stream from the reactor “ROUT,” consisting of methyl ester, glycerol and unreacted methanol is fed to the methanol recovery unit “MRU” to remove and recover excess methanol. The methanol recovery unit is simulated using a radfrac distillation column and the recovered methanol “MRC” is reused by feeding it to the RCSTR reactor through mixer “M2.” After recovery, glycerol and catalyst are separated as “METNEU” by water washing from the mixture of POME, catalyst and glycerol represented by “ME+GLY.” The impure POME “METFAM” from ‘WASH’ is fed to a radfrac distillation column “FAM” where pure biodiesel “FAME” is segregated from water-methanol mixture “METHWAT” and unreacted oil “UNOIL.” The glycerol and catalyst mixture “METNEU” is neutralized in the RSTOIC reactor “NEUTR” to precipitate the catalyst in the form of Na_3PO_4 crystals using H_3PO_4 acid. The resultant impure glycerol “METGLYC” is converted to pure glycerol “GLYCEROL” in radfrac distillation column “GLYC.”

The developed model is validated with an average deviation of 3.51% when model-predicted palm oil methyl ester yield is compared with the corresponding experimental yield reported by Narváez, Rincón, and Sánchez (2007). The prediction accuracy of the model is further confirmed with an average deviation of 4.1% when the methyl ester yield of poppy seed oil is compared with the respective experimental values (Aksoy 2011). The comparison of experimental and model-predicted yield is depicted in Figures 2 and 3.

Results and discussion

The validated model is used to analyze the effect of key parameters such as methanol-to-oil ratio, temperature, pressure, reboiler duty and reflux ratio on methanol recovery.

Table 2. Reactions and reaction kinetics.

Reactions	
R1	Triglyceride + Methanol $\xrightleftharpoons[k_2]{k_1}$ Diglyceride + POME
R2	Diglyceride + Methanol $\xrightleftharpoons[k_4]{k_3}$ Monoglyceride + POME
R3	Monoglyceride + Methanol $\xrightleftharpoons[k_6]{k_5}$ Glycerol + POME
Reaction rate constants	
k_1	0.049
k_2	0.112
k_3	0.226
k_4	0.133
k_5	0.122
k_6	0.016
Kinetic rate law	
$\frac{d[TG]}{dt}$	$= -k_1[TG][A] + k_2[DG][POME]$
$\frac{d[DG]}{dt}$	$= k_1[TG][A] - k_2[DG][POME] - k_3[DG][A] + k_4[MG][POME]$
$\frac{d[MG]}{dt}$	$= k_3[DG][A] - k_4[MG][POME] - k_5[MG][A] + k_6[GLY][POME]$
$\frac{d[COME]}{dt}$	$= k_1[TG][A] + k_3[DG][A] + k_5[MG][A]$ $- k_2[DG][POME] - k_4[MG][POME] - k_6[GLY][POME]$
TG – Triglyceride, DG – Diglyceride, MG – Monoglyceride, A – Methanol, GLY – Glycerol, POME – Poppseed oil methyl ester	

The effectiveness of methanol recovery is represented by methanol recovery ratio (MRR), the ratio of amount of methanol recovered to the amount of excess methanol at the reactor exit.

Effect of methanol-to-oil ratio

The influence of methanol-to-oil ratio on methanol recovery is analyzed by varying the methanol-to-oil ratio from 3:1 to 9:1 at different reboiler duties, as depicted in Figure 4. It is observed that the methanol recovery ratio decreases with an increase in methanol-to-oil ratio at lower reboiler duties. This decrease in methanol recovery with increase in methanol-to-oil ratio, at lower reboiler duty values, is attributed to the lack of energy availability to evaporate excess methanol. The effect of the methanol-to-oil ratio on biodiesel yield is depicted in Figure 5. It is found that an increase in methanol-to-oil ratio beyond a value of 6:1 contributes to less than a 1% increase in the yield of biodiesel and hence 6:1 methanol-to-oil ratio is selected for further analysis (Freedman 2017; Nouredini and Zhu 1997; Zhang et al. 2003). For the methanol-to-oil ratio of 6:1, the increase in methanol recovery beyond a reboiler duty of 500 cal/s is found to be insignificant, with a value of 2.22%. So, a reboiler duty of 500 cal/s is considered throughout the simulation as the increase in reboiler duty increases cost without significant methanol recovery (Dhar and Kirtania 2009).

Effect of temperature

The effect of temperature on biodiesel yield is depicted in Figure 6. It is found that the yield of methyl ester increases with an increase in reactor temperature. This is attributed to the fact that at higher temperature, reaction rate increases until the equilibrium is established (Aksoy 2011). The reactor temperature for the optimal yield of biodiesel is found to be 60°C, which is in line with the findings of Silitonga et al. (2017) and Freedman (2017). From Figure 7, it is found that the methanol recovery ratio increases with an increase in temperature. For a given reactor temperature, the stream temperature in MRU further increases due to the addition of heat in terms of reboiler duty, and consequently, the recovery temperature exceeds the boiling point of methanol. Thus, the methanol recovery ratio is

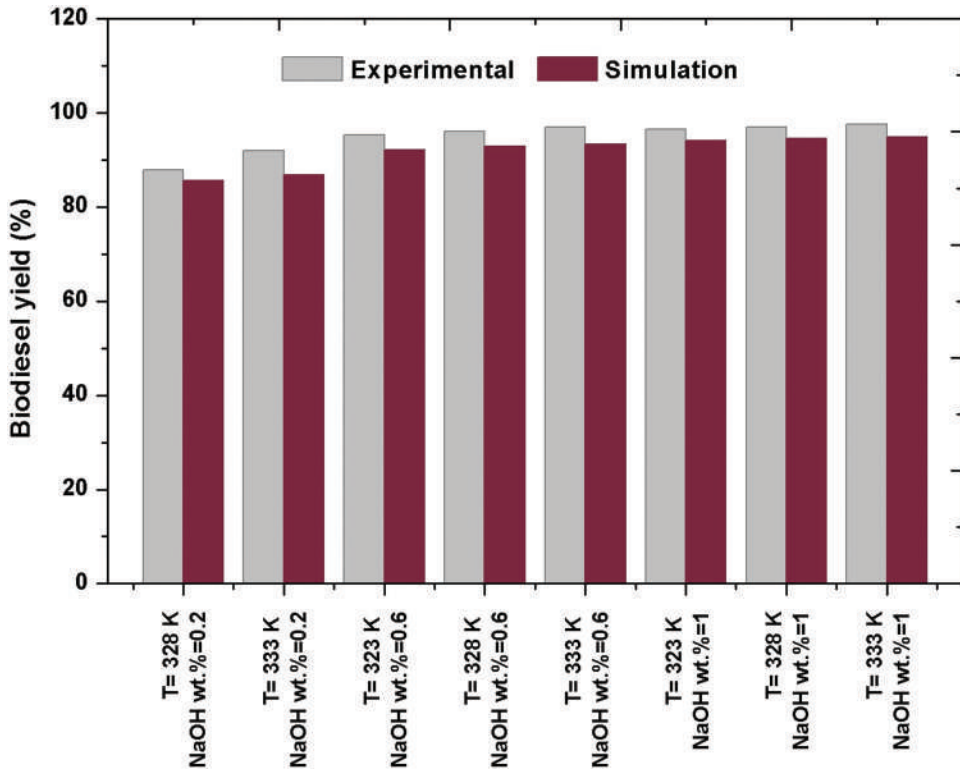


Figure 2. Comparison of model predicted biodiesel yield with the experimental results.

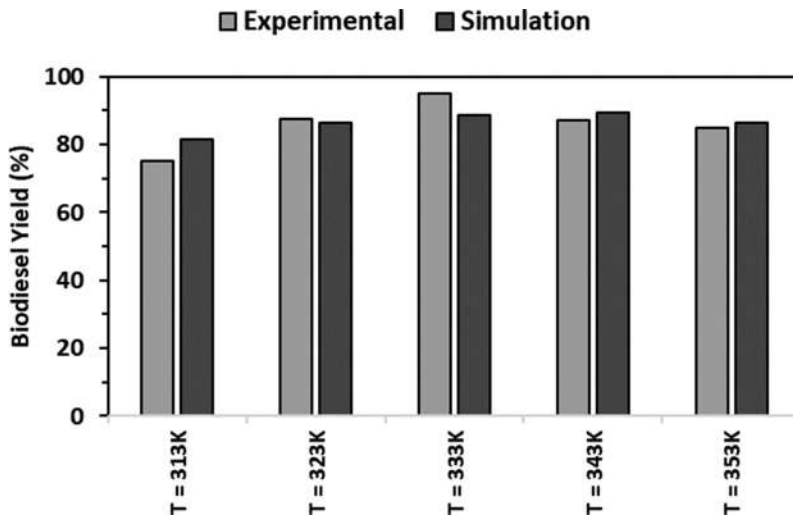


Figure 3. Model validation with poppy seed oil.

a function of reactor temperature, as higher reactor temperature assists MRU for effective vaporization and recovery of excess methanol. An MRR of 0.945 is achieved, corresponding to the optimal biodiesel yield of 90.50% at a reaction temperature of 60°C.

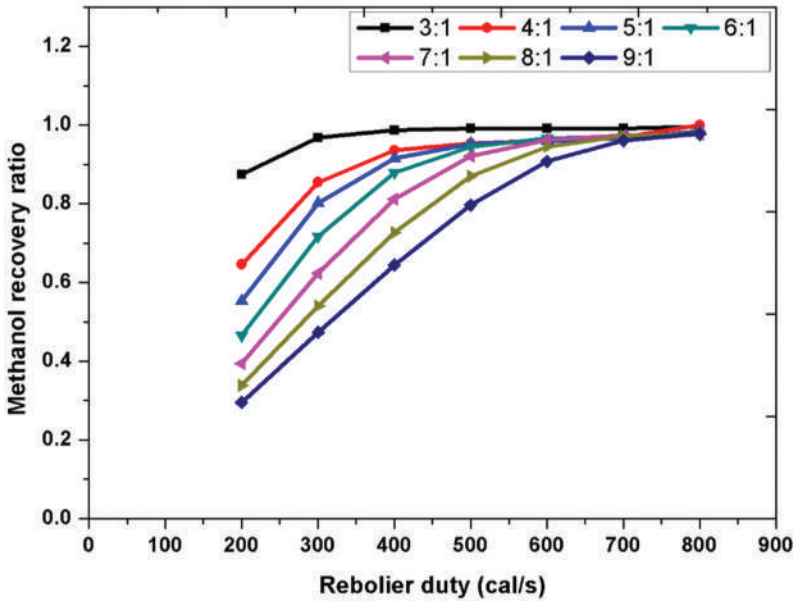


Figure 4. Effect of methanol to oil ratio and reboiler duty on MRR.

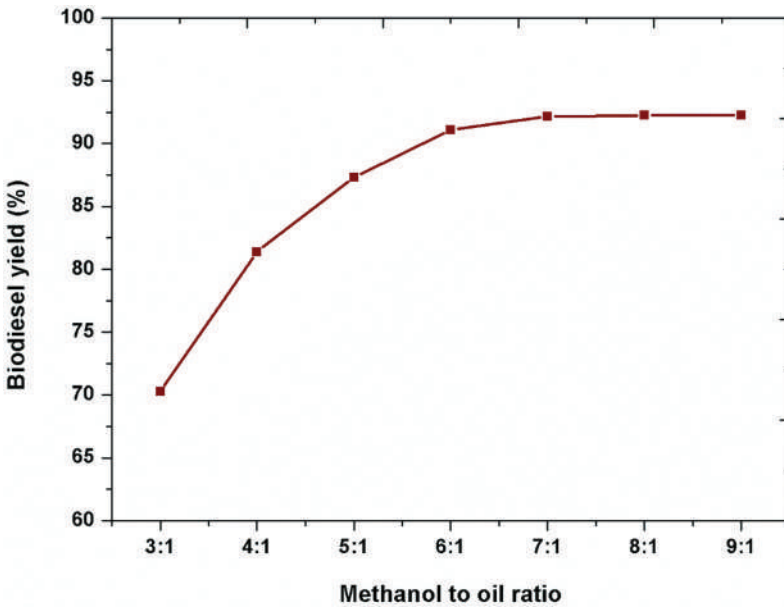


Figure 5. Effect of methanol to oil ratio on biodiesel yield.

Effect of pressure

The effect of reactor pressure on biodiesel yield and methanol recovery ratio is depicted in Figures 8 and 9, respectively. From Figure 8, it is observed that biodiesel yield increases with an increase in operating pressure up to a value of 0.6 bar and remains invariant thereafter. This is due to the establishment of the chemical equilibrium of the transesterification reaction. On the other hand, the methanol recovery ratio decreases up to 0.6 bar and remains insensitive to

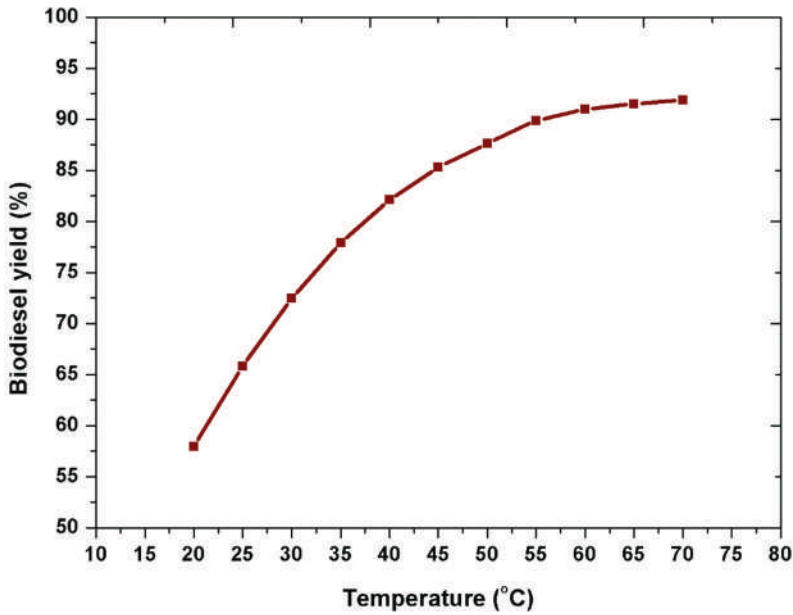


Figure 6. Effect of reactor temperature on yield.

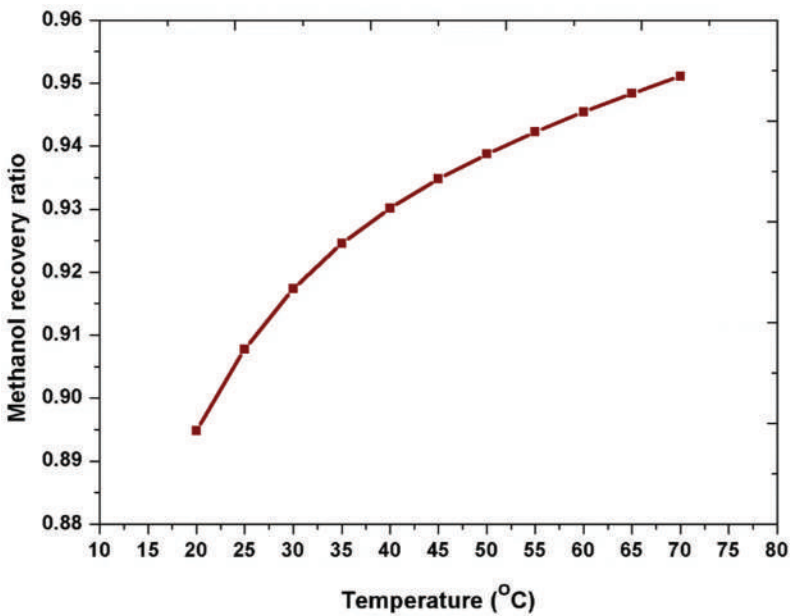


Figure 7. Effect of reactor temperature on methanol recovery ratio.

reactor pressure thereafter. This is attributed to the fact that no further methanol is consumed for reaction as transesterification attains equilibrium, and hence leads to an invariant trend in the methanol recovery ratio. So, an operating pressure of 1 bar is identified as a practical condition to mitigate the operational complexity and cost associated with subatmospheric pressure without compromising biodiesel yield (Noureddini and Zhu 1997).

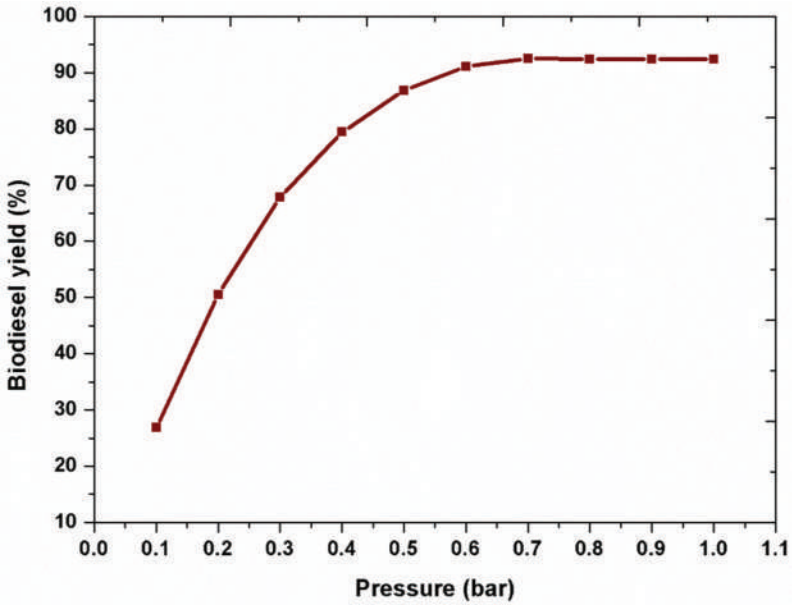


Figure 8. Effect of pressure on biodiesel yield.

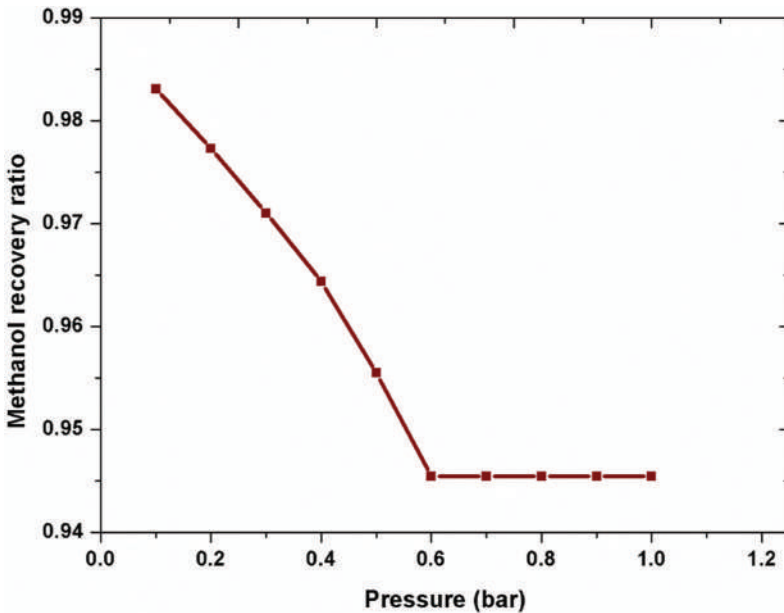


Figure 9. Effect of pressure on methanol recovery ratio.

Effect of reflux ratio

The reflux ratio is another MRU-dependent variable with a vital influence on the methanol recovery ratio. It is defined as the ratio of flow rates of distillate recovered by the MRU to the methanol recovered during the process (Dasan, Abdullah, and Bhat 2014). Figure 10 shows the effect of the reflux ratio on methanol recovery. It is observed that a maximum methanol recovery of 0.945 is achieved at a reflux ratio of 2 for a reboiler duty corresponding to 500 cal/s. A higher reflux ratio is

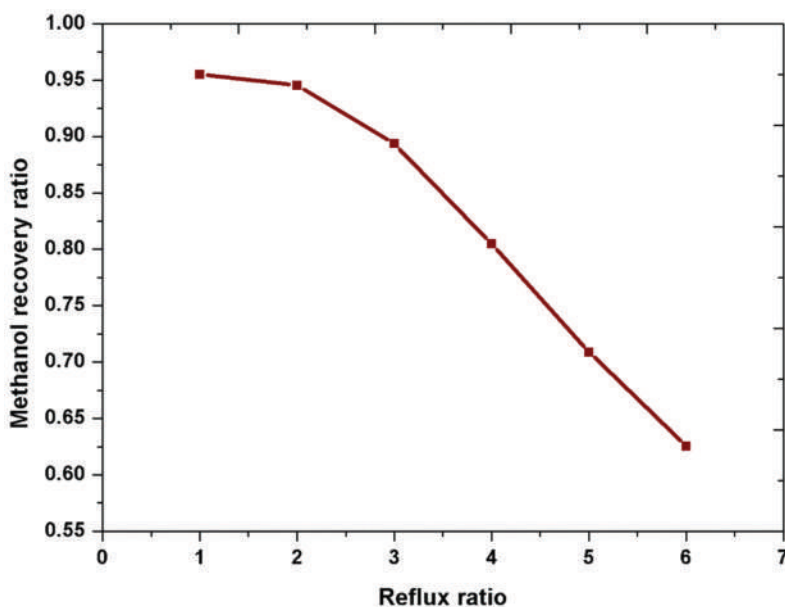


Figure 10. Effect of reflux Ratio on methanol recovery ratio.

required to increase the purity of biodiesel as a higher reflux ratio leads to more vapor liquid contact and thereby better mass transfer (Noureddini and Zhu 1997). However, higher MRR at higher reflux ratio demands increased reboiler duty, which is energy-intensive and uneconomical (Dhar and Kirtania 2009). Thus, a reflux ratio of 2 is selected for an optimal MRR, which is in line with the observation of Okullo (2017).

From the recovery data obtained from maximum biodiesel yield condition, an economic analysis was conducted (Avinash and Murugesan 2017) to quantify the significance and outcome of the simulation. A transesterification plant integrated with methanol recovery unit with a feedstock flowrate capacity of 10 kg/h is considered for the analysis. For an average annual operating hour of 7920 h, the system is able to recover 9068.4 kg of methanol per year which is equivalent to a savings of \$3310 a year.

Conclusions

A component-specific kinetic model for transesterification of poppy seed oil is developed in ASPEN Plus by incorporating individual triglyceride constituents and their step-wise transesterification reactions. The model is further upgraded by implementing a distillation-based recovery unit to recover and reuse the unreacted excess methanol available at the reactor downstream. The developed model is validated with a prediction capability of 3.51% when the simulated biodiesel yield is compared with the corresponding experimental results.

The validated model is used to predict the effect of methanol-to-oil ratio, reboiler duty, temperature, pressure and reflux ratio on methanol recovery. From the simulation, it is found that maximum biodiesel yield is obtained at a process temperature of 60°C and a methanol-to-oil ratio of 6:1. Under the maximum yield condition, a maximum methanol recovery ratio of 0.945 can be practically achieved by maintaining a reboiler duty of 500 cal/s and reflux ratio 2. An economic analysis is conducted for maximum yield condition to quantify the benefit of establishing a methanol recovery system. From the analysis, it is found that a savings of \$3310 can be achieved annually from the recovery and reuse of methanol in a transesterification unit with a feedstock flow rate of 10 kg/h. The research can further be extended by investigating the recovery of other alcohols, such as ethanol, butanol, etc., in transesterification process and to predict the optimal operating conditions and economic benefits of the recovery.

Disclosure statement

No potential conflict of interest was reported by the author(s).

Notes on contributors

Christy Thomas Sani is a Chemical Engineering graduate from the National Institute of Technology Calicut, Kerala, India. His research interest includes fuel cell technology and biodiesel synthesis. During his undergraduate studies, he developed a fuel cell-powered hybrid car in MATLAB SIMULINK. He has two international publications in the area of biodiesel in his credit.

Dr. Rupesh S completed Master of Technology in Propulsion Engineering from College of Engineering Trivandrum, Kerala, India, in 2010. He secured Ph.D in Biomass Gasification from National Institute of Technology Calicut in 2017. His areas of research include Thermochemical Gasification, Transesterification, Anaerobic Digestion and Buoyancy driven flows. He has published 10 peer reviewed International journals, 18 International conferences and one book chapter in the area of Biofuels. He served as the reviewer for 11 peer reviewed International journals published by various renowned publishers and also as technical session chair of various International conferences. Currently, he is working as Assistant Professor in the Department of Mechanical Engineering, PES College of Engineering, Mandya, Karnataka. Presently he is also the district coordinator of Biofuel Research Information and Demonstration Centre, sponsored by Karnataka Bioenergy Development Board (KSBDB) Bangalore.

Chris Ben Xavier is a Chemical Engineering graduate from the National Institute of Technology Calicut, Kerala, India. His research interest includes biodiesel synthesis, green hydrogen production and storage, fuel cell and so on. He has modelled a fuel cell-powered hybrid car in MATLAB SIMULINK software during his undergraduate studies. Currently he is working in the development of a decoupled water splitting electrolyser for hydrogen production.

Dr. Rag R L secured his Ph.D from National Institute of Technology Calicut, Kerala, India in the area of computational heat transfer in 2010. His graduation and post-graduation were from TKM College of Engineering, Kollam, India in 1999 and 2002, respectively. He has six International journal publications and two International conference publications in the area of electronics cooling and computational heat transfer. He is the reviewer of two international peer review journals. A book titled “Introduction to Sustainable Engineering” was authored by him. He is having a teaching experience of more than twenty years. Dr. Rag R L served as resource person for faculty development programmes in the area of computational heat transfer. Currently he is working as the Professor and Head in the Department of Mechanical Engineering at SCMS School of Engineering and Technology, Cochin, Kerala, India.

ORCID

Rupesh S  <http://orcid.org/0000-0002-6460-8299>

References

- Adeniyi, A. G., J. O. Ighalo, and O. A. A. Eletta. 2019. Process integration and feedstock optimisation of a two-step biodiesel production process from jatropha curcas using aspen plus. *Chemical Product and Process Modeling* 14 (2):20180055. doi:10.1515/cppm-2018-0055.
- Aksoy, L. 2011. Opium poppy (*Papaver Somniferum* L.) oil for preparation of biodiesel: optimization of conditions. *Applied Energy* 88 (12):4713–18. doi:10.1016/j.apenergy.2011.06.012.
- M. Ali, and N. Aziz. 2015. Optimization of DMC Transesterification Based Biodiesel Production. *Advanced Materials Research* 1113:370–375. doi:10.4028/AMR.1113.370.
- Altikriti, E. T., A. B. Fadhil, and M. M. Dheyab. 2015. Two-step base catalyzed transesterification of chicken fat: optimization of parameters. *Energy Sources, Part A: Recovery, Utilization, and Environmental Effects* 37 (17):1861–66. doi:10.1080/15567036.2012.654442.
- Al-Tikrity, E., A. B. Fadhil, and M. A. Albadree. 2016. Cyprinus carpio fish oil: a novel feedstock for biodiesel production. *Energy Sources, Part A: Recovery, Utilization, and Environmental Effects* 38 (22):3367–74. doi:10.1080/15567036.2015.1004385.
- Avinash, A., and A. Murugesan. 2017. Economic analysis of biodiesel production from waste cooking oil. In *Energy sources, part B: economics, planning and policy* Vol. 12 (10): 890–94. Taylor & Francis. doi:10.1080/15567249.2017.1319438.
- Baroutian, S., M. K. Aroua, A. A. A. Raman, and N. M. N. Sulaiman. 2010. Methanol recovery during transesterification of palm oil in a TiO₂/Al₂O₃ membrane reactor: experimental study and neural network modeling. *Separation and Purification Technology* 76 (1):58–63. Elsevier B.V. doi:10.1016/j.seppur.2010.09.020.

- Bhuiya, M. M. K., M. G. Rasul, M. M. K. Khan, and N. Ashwath. 2020. Biodiesel production and characterisation of poppy (*papaver somniferum* l.) seed oil methyl ester as a source of 2nd generation biodiesel feedstock. *Industrial Crops and Products* 152:112493. doi:10.1016/j.indcrop.2020.112493.
- Bhuiya, M. M. K., M. G. Rasul, M. M. K. Khan, N. Ashwath, A. K. Azad, and M. A. Hazrat. 2014. Second generation biodiesel: potential alternative to-edible oil-derived biodiesel. *Energy Procedia* 61:1969–72. Elsevier B.V.: 1969–1972. doi:10.1016/j.egypro.2014.12.054.
- Bonate, P. L. 2011. The art of modeling. *Pharmacokinetic-Pharmacodynamic Modeling and Simulation*. doi:10.1007/978-1-4419-9485-1_1.
- Borges, M. E., and L. Díaz. 2012. Recent developments on heterogeneous catalysts for biodiesel production by oil esterification and transesterification reactions: a review. *Renewable and Sustainable Energy Reviews*. Elsevier Ltd. 16 (5):2839–49. doi:10.1016/j.rser.2012.01.071.
- Cai, Z. -Z., Y. Wang, Y. -L. Lai Teng, K. -M. Man Chong, J. -W. Wei Wang, J. -W. Wen Zhang, De Po Yang, and D. -P. Yang. 2015. A two-step biodiesel production process from waste cooking oil via recycling crude glycerol esterification catalyzed by alkali catalyst. *Fuel Processing Technology* 137:186–93. Elsevier B.V. doi:10.1016/j.fuproc.2015.04.017.
- Chang, A. F., and Y. A. Liu. 2010. Integrated process modeling and product design of biodiesel manufacturing. *Industrial and Engineering Chemistry Research* 49 (3):1197–213. doi:10.1021/ie9010047.
- Chongkhong, S., C. Tongurai, and P. Chetpattananondh. 2009. Continuous esterification for biodiesel production from palm fatty acid distillate using economical process. *Renewable Energy*. Elsevier Ltd: 1059–1063. 34 (4):1059–63. doi:10.1016/j.renene.2008.07.008.
- Dasan, Y. K., M. A. Abdullah, and A. H. Bhat. 2014. Effects of reflux ratio and feed conditions for the purification of bioethanol in a continuous distillation column. 1621:218–22. doi:10.1063/1.4898469.
- De Rijj, S. Bhartiya, Y. Shastri, and R. De. 2019. Multi-objective optimization of integrated biodiesel production and separation system. *Fuel* 243 (January):519–32. doi:10.1016/j.fuel.2019.01.132.
- Dhar, B. R., and K. Kirtania. 2009. Excess methanol recovery in biodiesel production process using a distillation column: a simulation study. *Chemical Engineering Research Bulletin* 13 (2):55–60. doi:10.3329/cerb.v13i2.3538.
- Fadhil, A. B., S. H. Sedeeq, and N. M. T. Al-Layla. 2019. Transesterification of non-edible seed oil for biodiesel production: characterization and analysis of biodiesel. In *Energy Sources, Part A: Recovery, Utilization and Environmental Effects*, Vol. 41(7), Taylor & Francis, 892–901. doi:10.1080/15567036.2018.1520367.
- Freedman. 2017. Variables affecting the yields of fatty esters from transesterified vegetable oils. *Proceedings of the Conference on Integrating Technology into Computer Science Education, ITiCse* 61 (10):677–78. doi:10.1007/BF02541649.
- Gebremariam, S. N., and J. M. Marchetti. 2018. Biodiesel production through sulfuric acid catalyzed transesterification of acidic oil: techno economic feasibility of different process alternatives. *Energy Conversion and Management* 174 (August):639–48. doi:10.1016/j.enconman.2018.08.078.
- GIWA, A. G., and S. Olanipekun. 2015. Investigating the effects of operating parameters of a reaction integrated distillation process for SAME production using aspen PLUS. *International Journal of Science and Research* 4 (7):2349–56. <https://www.ijsr.net/archive/v4i7/SUB157055.pdf>.
- Hussain, Z., and R. Kumar. 2018. Esterification of free fatty acids: experiments, kinetic modeling, simulation & optimization. In *International journal of green energy* Vol. 15 (11): 629–40. Taylor & Francis. doi:10.1080/15435075.2018.1525736
- Jabbar, N. A., A. Aidan, H. Razouk, N. Chihadih, S. Faraghat, and Y. El-Tal. 2014. Biodiesel production from algal oil- a simulation study 5th International Renewable Energy Congress (IREC) Hammamet, Tunisia, 25-27 March 2014 (IEEE) 1–6 2014. <https://ieeexplore.ieee.org/document/6827022>. doi:10.1109/IREC.2014.6827022 .
- Jansson, R. E. W. 1980. Electrochemical reaction engineering. *Chemical Engineering Science* 35 (9):1979–2004. doi:10.1016/0009-2509(80)80138-2.
- Kick, C., A. Kline, H. Hladky, and B. Aller. 2013. “Using AspenPlus resources to model biodiesel production applicable for a senior capstone design project.” *ASCE North-Central Section Conference*. <http://people.cst.cmich.edu/yelam1k/asee/proceedings/2013/papers/51.pdf>.
- Kiss, A. A., and C. S. Sorin Bildea. 2012. A review of biodiesel production by integrated reactive separation technologies. *Journal of Chemical Technology and Biotechnology* 87 (7):861–79. doi:10.1002/jctb.3785.
- Kumar, S., M. Kumar Singhal, and M. Pal Sharma. 2021. Utilization of mixed oils for biodiesel preparation: A review, *Energy Sources, Part A: Recovery, Utilization, and Environmental Effects*. doi:10.1080/15567036.2021.1884771.
- Kuramochi, H., K. Maeda, S. Kato, M. Osako, K. Nakamura, and S. Ichi Sakai. 2009. Application of UNIFAC models for prediction of vapor–liquid and liquid–liquid equilibria relevant to separation and purification processes of crude biodiesel fuel. *Fuel*. Elsevier Ltd: 1472–1477. 88 (8):1472–77. doi:10.1016/j.fuel.2009.01.017.
- Lee, S., D. Posarac, and N. Ellis. 2011. Process simulation and economic analysis of biodiesel production processes using fresh and waste vegetable oil and supercritical methanol. *Chemical Engineering Research & Design*. Institution of Chemical Engineers. 89 (12):2626–42. doi:10.1016/j.cherd.2011.05.011.
- Myint, L. L., and M. M. El-Halwagi. 2009. Process analysis and optimization of biodiesel production from soybean oil. *Clean Technologies and Environmental Policy* 11 (3):263–76. doi:10.1007/s10098-008-0156-5.

- Narváez, P. C., S. M. Rincón, and F. J. Sánchez. 2007. Kinetics of palm oil methanolysis. *JAACS, Journal of the American Oil Chemists' Society* 84 (10):971–77. doi:10.1007/s11746-007-1120-y.
- Noureddini, H., and D. Zhu. 1997. Kinetics of transesterification of soybean oil. *Journal of the American Oil Chemists' Society* 74 (11):1457–63. doi:10.1007/s11746-997-0254-2.
- Okullo, A. 2017. Process simulation of biodiesel production from jatropha curcas seed oil. *American Journal of Chemical Engineering* 5 (4):56. doi:10.11648/j.ajche.20170504.12.
- Philip, F. A., A. Veawab, and A. Aroonwilas. 2014. Simulation analysis of energy performance of distillation-, stripping-, and flash-based methanol recovery units for biodiesel production. *Industrial and Engineering Chemistry Research* 53 (32):12770–82. doi:10.1021/ie5003476.
- Rupesh, S., and S. Gokul Krishnan. 2021. Analysis of sorbent enhanced steam assisted air gasification using biomass specific pyrolysis correlations. In *Energy sources, part a: recovery, utilization and environmental effects* Vol. 00 (00): 1–15. Taylor & Francis. doi:10.1080/15567036.2021.1920646.
- Rupesh, S., C. Muraleedharan, and P. Arun. 2016. ASPEN plus modelling of air–steam gasification of biomass with sorbent enabled CO₂ capture. *Resource-Efficient Technologies*. Elsevier B.V. 2 (2):94–103. doi:10.1016/j.refit.2016.07.002.
- Salehi, A., A. Karbassi, A. Doustgani, A. Ghasemi, and A. Doustgani. 2019. “Simulation process of biodiesel production plant,” no. *Environmental Progress & Sustainable Energy* 38 (6):1–12. doi:10.1002/ep.13264.
- Silitonga, A. S., T. M. I. Mahlia, H. C. Ong, T. M. I. Riayatsyah, F. Kusumo, H. Ibrahim, S. Dharma, and D. Gumilang. 2017. A comparative study of biodiesel production methods for reutealis trisperma biodiesel. In *Energy sources, part A: recovery, utilization and environmental effects*, Vol. 39(20), Taylor & Francis: 2006–2014, doi:10.1080/15567036.2017.1399174.
- Silva, C., L. A. Fabiano, G. Cameron, and W. D. Seider. 2012. Optimal design of an algae oil transesterification process. *Computer Aided Chemical Engineering* 31:880–84. doi:10.1016/B978-0-444-59506-5.50007-9.
- Silva, R. J. M. C. L., T. P. C. Souza, J. P. Silva, J. G. A. Pacheco, and J. M. F. Silva. 2017. Ethanollic biodiesel production: a comparative study between a plug flow reactor and reactive distillation. *Brazilian Journal of Chemical Engineering* 34 (3):811–19. doi:10.1590/0104-6632.20170343s20150691.
- Sotoft, L. F., B. -G. Guang Rong, K. V. Christensen, and B. Norddahl. 2010. Process simulation and economical evaluation of enzymatic biodiesel production plant. *Bioresource Technology*. Elsevier Ltd: 5266–5274. 101 (14):5266–74. doi:10.1016/j.biortech.2010.01.130.
- Souza, M. F., G. F. Hirata, and A. Batista. 2020. Evaluation of kinetics and thermodynamic parameters for simulation of palm oil biodiesel production. *Fluid Phase Equilibria* 525:112792. Elsevier B.V.: 112792. doi:10.1016/j.fluid.2020.112792.
- Thangaraj, B., P. R. Raj Solomon, B. Muniyandi, S. Ranganathan, and L. Lin. 2019. Catalysis in biodiesel production—a review. *Clean Energy* 3 (1):2–23. doi:10.1093/ce/zky020.
- Tyagi, O. S., N. Atray, B. Kumar, and A. Datta. 2010. Production, characterization and development of standards for biodiesel — a review. *Mapan - Journal of Metrology Society of India* 25 (3):197–218. doi:10.1007/s12647-010-0018-6.
- Wang, C., W. Chen, W. Wang, Y. Wu, R. Chi, and Z. Tang. 2011. Experimental study on methanol recovery through flashing vaporation in continuous production of biodiesel via supercritical methanol. *Energy Conversion and Management*. Elsevier Ltd: 1454–1458. 52 (2):1454–58. doi:10.1016/j.enconman.2010.10.008.
- Xiao, Y., L. Haoyang, G. Xiao, L. Gao, and X. Pan. 2013. “Simulation of the catalytic reactive distillation process for biodiesel production via transesterification.” *ICMREE 2013 - Proceedings: 2013 International Conference on Materials for Renewable Energy and Environment* 1: 196–99. doi:10.1109/ICMREE.2013.6893646.
- Xiao, Y., G. Xiao, and A. Varma. 2013. A universal procedure for crude glycerol purification from different feedstocks in biodiesel production: experimental and simulation study. *Industrial and Engineering Chemistry Research* 52 (39):14291–96. doi:10.1021/ie402003u.
- Xie, W., and F. Wan. 2019. Immobilization of polyoxometalate-based sulfonated ionic liquids on UiO-66-2COOH metal-organic frameworks for biodiesel production via one-pot transesterification-esterification of acidic vegetable oils. *Chemical Engineering Journal* 365 (January):40–50. doi:10.1016/j.cej.2019.02.016.
- Xie, W., and H. Wang. 2020. Immobilized polymeric sulfonated ionic liquid on core-shell structured Fe₃O₄/SiO₂ composites: a magnetically recyclable catalyst for simultaneous transesterification and esterifications of low-cost oils to biodiesel. *Renewable Energy* 145:1709–19. Elsevier Ltd: 1709–1719. doi:10.1016/j.renene.2019.07.092.
- Xie, W., and H. Wang. 2021. Grafting copolymerization of dual acidic ionic liquid on core-shell structured magnetic silica: a magnetically recyclable brønsted acid catalyst for biodiesel production by one-pot transformation of low-quality oils. *Fuel* 283:118893. doi:10.1016/j.fuel.2020.118893.
- Yun, H., M. Wang, W. Feng, and T. Tan. 2013. Process simulation and energy optimization of the enzyme-catalyzed biodiesel production. *Energy* 54:84–96. Elsevier Ltd. doi:10.1016/j.energy.2013.01.002.
- Zhang, Y., M. A. Dubé, D. D. McLean, and M. Kates. 2003. Biodiesel Production from waste cooking oil: 1. process design and technological assessment. *Bioresource Technology* 89 (1):1–16. doi:10.1016/S0960-8524(03)00040-3.

Vol. 45, No. 6
June 2023

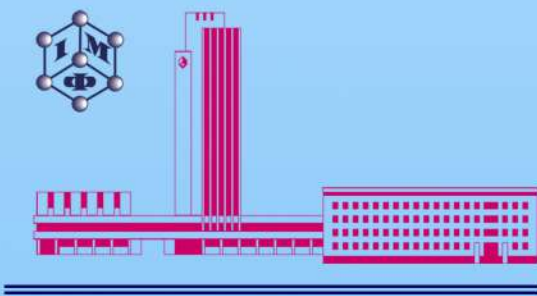
ISSN 1024-1809

METALLOPHYSICS and ADVANCED TECHNOLOGIES

МЕТАЛОФІЗИКА ТА НОВІТНІ ТЕХНОЛОГІЇ

METALLOFIZIKA I NOVEISHIE TEKHNologii

Том 45, № 6 (2023)



**G.V. Kurdyumov Institute for Metal Physics
National Academy of Sciences of Ukraine**
<https://mfint.imp.kiev.ua>

Засновник: НАЦІОНАЛЬНА АКАДЕМІЯ НАУК УКРАЇНИ, ІНСТИТУТ МЕТАЛОФІЗИКИ ІМ. Г. В. КУРДЮМОВА НАН УКРАЇНИ
Видавець: ВД «Академперіодика» НАН України

«МЕТАЛОФІЗИКА ТА НОВІТНІ ТЕХНОЛОГІЇ» • METALLOPHYSICS AND ADVANCED TECHNOLOGIES

Щомісячний науковий журнал • A Monthly Research Journal

РЕДАКЦІЙНА КОЛЕГІЯ

В. А. ТАТАРЕНКО *головний редактор, чл. кор. НАН України (Інститут металофізики ім. Г. В. Курдюмова НАН України, Київ)*

С. В. АХОНІН *акад. НАН України (Інститут електроварування ім. С. О. Патона НАН України, Київ)*

М. О. БЕЛОГОЛОВСЬКИЙ *проф. (Київський академічний університет НАН та МОН України, Київ)*

Т. М. БРИК *д-р фіз.-мат. наук (Інститут фізики конденсованих систем НАН України, Львів)*

М. О. ВАСИЛЬЄВ *проф. (Інститут металофізики ім. Г. В. Курдюмова НАН України, Київ)*

В. Г. ГАВРИЛЮК *проф. (Інститут металофізики ім. Г. В. Курдюмова НАН України, Київ)*

О. С. ГАЦЕНКО *канд. фіз.-мат. наук (Інститут металофізики ім. Г. В. Курдюмова НАН України, Київ)*

Г. С. ГРЕЧНЕВ *проф. (Фізико-технічний інститут низьких температур ім. Б. І. Веркіна НАН України, Харків)*

Т. В. ЗАПОРОЖЕЦЬ *проф. (Черкаський національний університет імені Богдана Хмельницького МОН України, Черкаси)*

О. М. ІВАСИШІН *акад. НАН України (Інститут металофізики ім. Г. В. Курдюмова НАН України, Київ)*

Ю. М. КОВАЛЬ *чл. кор. НАН України (Інститут металофізики ім. Г. В. Курдюмова НАН України, Київ)*

О. А. КОРДЮК *акад. НАН України (Київський академічний університет НАН та МОН України, Київ)*

С. О. КОТРЕЧКО *заступник головного редактора, чл. кор. НАН України (Інститут металофізики ім. Г. В. Курдюмова НАН України, Київ)*

Ю. В. КУДРЯВЦЕВ *проф. (Інститут металофізики ім. Г. В. Курдюмова НАН України, Київ)*

Є. Г. ЛЕНЬ *заступник головного редактора, проф. (Інститут металофізики ім. Г. В. Курдюмова НАН України, Київ)*

В. В. ЛІЗУНОВ *проф. (Інститут металофізики ім. Г. В. Курдюмова НАН України, Київ)*

В. Ф. ЛОСЬ *проф. (Інститут магнетизму НАН та МОН України, Київ)*

П. Є. МАРКОВСЬКИЙ *д-р техн. наук (Інститут металофізики ім. Г. В. Курдюмова НАН України, Київ)*

Б. М. МОРДЮК *д-р фіз.-мат. наук (Інститут металофізики ім. Г. В. Курдюмова НАН України, Київ)*

В. М. НЕСТЕРЕНКОВ *чл. кор. НАН України (Інститут електроварування ім. С. О. Патона НАН України, Київ)*

О. Д. ПОГРЕБНЯК *проф. (Сумський державний університет, МОН України, Суми)*

Ю. М. ПОДРЕЗОВ *д-р фіз.-мат. наук (Інститут проблем матеріалознавства ім. І. М. Францевича НАН України, Київ)*

Т. М. РАДЧЕНКО *д-р фіз.-мат. наук (Інститут металофізики ім. Г. В. Курдюмова НАН України, Київ)*

О. Д. РУДЬ *проф. (Інститут металофізики ім. Г. В. Курдюмова НАН України, Київ)*

В. М. УВАРОВ *чл. кор. НАН України (Інститут металофізики ім. Г. В. Курдюмова НАН України, Київ)*

А. І. УСТИНОВ *проф. (Інститут електроварування ім. С. О. Патона НАН України, Київ)*

О. В. ФІЛАТОВ *д-р фіз.-мат. наук (Інститут металофізики ім. Г. В. Курдюмова НАН України, Київ)*

С. О. ФІРСТОВ *акад. НАН України (Інститут проблем матеріалознавства ім. І. М. Францевича НАН України, Київ)*

Т. С. ЧЕРЕПОВА *д-р техн. наук (Інститут металофізики ім. Г. В. Курдюмова НАН України, Київ)*

EDITORIAL BOARD

V. A. TATARENKO *Editor-in-Chief, Corresponding Member of the N.A.S.Ukr., G.V. Kurdyumov Institute for Metal Physics, N.A.S.Ukr., Kyiv*

S. V. AKHONIN *Member of the N.A.S.Ukr., E. O. Paton Electric Welding Institute, N.A.S.Ukr., Kyiv*

M. O. BELOGOLOVSKIY *Professor, Kyiv Academic University, N.A.S.Ukr. & M.E.S.Ukr., Kyiv*

T. M. BRYK *Dr. Sc. (Phys.-Math.), Institute for Condensed Matter Physics, N.A.S.Ukr., Lviv*

M. O. VASILIEV *Professor, G.V. Kurdyumov Institute for Metal Physics, N.A.S.Ukr., Kyiv*

V. G. GAVRILJUK *Professor, G.V. Kurdyumov Institute for Metal Physics, N.A.S.Ukr., Kyiv*

O. S. GATSENKO *Executive Managing Editor, Ph.D. (Phys.-Math.), G.V. Kurdyumov Institute for Metal Physics, N.A.S.Ukr., Kyiv*

G. E. GRECHNEV *Professor, B. Verkin Institute for Low Temperature Physics and Engineering, N.A.S.Ukr., Kharkiv*

T. V. ZAPOROZHETS *Professor, Bohdan Khmelnytsky National University of Cherkasy, M.E.S.Ukr., Cherkasy*

O. M. IVASHIN *Member of the N.A.S.Ukr., G.V. Kurdyumov Institute for Metal Physics, N.A.S.Ukr., Kyiv*

YU. M. KOVAL' *Corresponding Member of the N.A.S.Ukr., G.V. Kurdyumov Institute for Metal Physics, N.A.S.Ukr., Kyiv*

O. A. KORDYUK *Member of the N.A.S.Ukr., Kyiv Academic University, N.A.S.Ukr. & M.E.S.Ukr., Kyiv*

S. O. KOTRECHKO *Deputy Editor-in-Chief, Corresponding Member of the N.A.S.Ukr., G.V. Kurdyumov Institute for Metal Physics, N.A.S.Ukr., Kyiv*

YU. V. KUDRYAVTSEV *Professor, G.V. Kurdyumov Institute for Metal Physics, N.A.S.Ukr., Kyiv*

E. G. LEN *Deputy Editor-in-Chief, Professor, G.V. Kurdyumov Institute for Metal Physics, N.A.S.Ukr., Kyiv*

V. V. LIZUNOV *Professor, G.V. Kurdyumov Institute for Metal Physics, N.A.S.Ukr., Kyiv*

V. F. LOS *Professor, Institute of Magnetism, N.A.S.Ukr. & M.E.S.Ukr., Kyiv*

P. E. MARKOVSKY *Dr. Sc. (Tech.), G.V. Kurdyumov Institute for Metal Physics, N.A.S.Ukr., Kyiv*

B. M. MORDYUK *Dr. Sc. (Phys.-Math.), G.V. Kurdyumov Institute for Metal Physics, N.A.S.Ukr., Kyiv*

V. M. NESTERENKOV *Corresponding Member of the N.A.S.Ukr., E. O. Paton Electric Welding Institute, N.A.S.Ukr., Kyiv*

O. D. POGREBNJAK *Professor, Sumy State University, M.E.S.Ukr., Sumy*

YU. M. PODREZOV *Dr. Sc. (Phys.-Math.), I. M. Frantsevych Institute for Problems of Materials Science, N.A.S.Ukr., Kyiv*

T. M. RADCHENKO *Dr. Sc. (Phys.-Math.), G.V. Kurdyumov Institute for Metal Physics, N.A.S.Ukr., Kyiv*

O. D. RUD' *Professor, G.V. Kurdyumov Institute for Metal Physics, N.A.S.Ukr., Kyiv*

V. M. UVAROV *Corresponding Member of the N.A.S.Ukr., G.V. Kurdyumov Institute for Metal Physics, N.A.S.Ukr., Kyiv*

A. I. USTINOV *Professor, E. O. Paton Electric Welding Institute, N.A.S.Ukr., Kyiv*

O. V. FILATOV *Dr. Sc. (Phys.-Math.), G.V. Kurdyumov Institute for Metal Physics, N.A.S.Ukr., Kyiv*

S. O. FIRSTOV *Member of the N.A.S.Ukr., I. M. Frantsevych Institute for Problems of Materials Science, N.A.S.Ukr., Kyiv*

T. S. CHEREPOVA *Dr. Sc. (Tech.), G.V. Kurdyumov Institute for Metal Physics, N.A.S.Ukr., Kyiv*

EDITORIAL ADVISORY BOARD MEMBERS AND REGIONAL EDITORS

Professor Ing. Ivo DLOUHÝ
Institute of Physics of Materials, Czech Academy of Sciences, Brno, Czech Republic

Professor Han DONG
School of Materials Science and Engineering, Shanghai University, Shanghai, P.R. China

Professor Janusz DUBOWIK
Institute of Molecular Physics, Polish Academy of Sciences, Poznań, Poland

Professor Leszek B. MAGALAS
AGH University of Science and Technology, Faculty of Metals Engineering and Industrial Computer Science, Kraków, Poland

Professor Elena V. PERELOMA
University of Wollongong, School of Mechanical, Materials and Mechatronic Engineering, Wollongong, Sydney Area, Australia

Dr. Patrice E. A. TURCHI
Lawrence Livermore National Laboratory, Condensed Matter and Materials Division, Livermore, CA, U.S.A.

AN INTERNATIONAL RESEARCH JOURNAL

METALLOPHYSICS AND ADVANCED TECHNOLOGIES

(Metallofizika i Noveishie Tekhnologii)

FOUNDED IN SEPTEMBER, 1979

Volume 45, No. 6; June, 2023

CONTENTS

Editorial Announcements	Information for Foreign Subscribers	V
	Information for Contributors	VII
Electronic Structure and Properties	‘Orbital Glass’ Effects. 2. Hardness. Quantum Theory. Galois Groups <i>O. I. MITSEK and V. M. PUSHKAR</i>	737
	Electrophysical Characteristics of <i>c</i> BN–NbN Composite Ceramics Doped with Al ₂ O ₃ , Si ₃ N ₄ , and SiC <i>Yu. Yu. RUMYANTSEVA, L. O. ROMANKO, I. P. FESENKO, D. O. SAVCHENKO, and V. Z. TURKEVYCH</i>	743
Amorphous and Liquid States	First-Principle Modelling of Amorphization Process of Ni–Zr System Alloys <i>I. V. PLYUSHCHAY, A. O. MAISTRENKO, T. L. TSAREGRADSKA, O. I. PLYUSHCHAY, and O. O. KALENYK</i>	753
Crystal-Lattice Defects	Hydrogen-Sorption Properties of the Alloy Ti _{15.5} Zr ₃₀ Mn ₃₈ V _{5.5} Cr _{5.5} Co _{5.5} Based on the Laves Phase (Type C14) <i>V. A. DEKHTYARENKO</i>	763
Interaction of Radiation and Particles with Condensed Matter	Aluminium Ionic Implantation in Stainless Steel <i>V. HONCHAROV, V. ZAZHIGALOV, and M. HONCHAROVA</i>	777
Metallic Surfaces and Films	The Surfaces Properties of Steel Parts with Wear-Resistant Coatings of the 1M and 90%BK6 + 10% 1M Composition Applied by the Method of Electrospark Alloying with the Use of Special Technological	

Physics of Strength and Plasticity	Environments. Pt. 2. Wear Resistance, Topographic and Mechanical Properties <i>V. B. TARELNYK, O. P. GAPONOVA, N. V. TARELNYK, Ie. V. KONOPLIANCHENKO, S. G. BONDAREV, O. V. RADIONOV, M. M. MAYFAT, A. V. OKHRIMENKO, M. Yu. DUMANCHUK, and K. G. SIROVITSKIY</i>	793
Physical and Technical Bases of Experiment and Diagnostics	Influence of Ultrasonic Impact Treatment on Structure and Properties of 3D Printed Co–Cr–Mo–W Dental Alloy <i>A. P. BURMAK, S. M. VOLOSHKO, B. M. MORDYUK, M. O. VASYLYEV, V. I. ZAKIEV, M. M. VORON, and P. O. GURYN</i>	815
Physical and Technical Bases of Experiment and Diagnostics	Mechanical Stability and Brittleness of Metals and Alloys. Pt. 1. Parameters and Criteria of the Stable State <i>Yu. Ya. MESHKOV and G. P. ZIMINA</i>	843
Physical and Technical Bases of Experiment and Diagnostics	A Review on Additive Manufacturing Process <i>T. G. AVINASH, K. A. ALTHAF, R. VARMA YADU, K. NOWSHAD SHABEEB, and G. R. RAGHAV</i>	859

Scientific Editors of Issue—*O. S. Gatsenko, V. A. Tatarenko*

Executive Managing Editor—*O. S. Gatsenko*

Editors—*L. I. Makarenko, M. V. Manilo, I. V. Zagorulko*

The artwork for direct reproduction is made by computer group of EPD of the G. V. Kurdyumov Institute for Metal Physics, N.A.S. of Ukraine

Editorial Office Address:

G. V. Kurdyumov Institute for Metal Physics, N.A.S. of Ukraine, EPD—'MNT',

36 Academician Vernadsky Boulevard, UA-03142 Kyiv, Ukraine

Telephone: +380 44 4249042. Fax: +380 44 4242561. E-mail: mfint@imp.kiev.ua

Registration Certificate of the Publishing Subject: ДК № 5875 on 13.12.2017

State Registration Certificate of the Printed Mass Medium: KB № 23232-13072 ПП on 23.02.2018.

Approved for publication by the Academic Council of the G. V. Kurdyumov Institute for Metal Physics of the National Academy of Sciences of Ukraine

Published in English or Ukrainian languages according to resolution of Editorial Board of the journal

Printed by Publishing House 'Akademperiodyka', of the NAS of Ukraine

4 Tereshchenkivs'ka Str., UA-01024 Kyiv, Ukraine

Registration Certificate of Publishing Subject: ДК № 544 on 27.07.2001

Journal website: <http://mfint.imp.kiev.ua>

Journal DOI: <https://doi.org/10.15407/mfint>

Issue DOI: <https://doi.org/10.15407/mfint.45.06>

МЕТАЛОФІЗИКА ТА НОВІТНІ ТЕХНОЛОГІЇ

МІЖНАРОДНИЙ НАУКОВИЙ ЖУРНАЛ
ЗАСНОВАНИЙ У ВЕРЕСНІ 1979 р.

Том 45, № 6; червень, 2023

ЗМІСТ

Редакційні оголошення	Інформація для закордонних передплатників	V
	Інформація для авторів	VII
Електронні структура та властивості	Ефекти «орбітального скла». 2. Твердість. Квантова теорія. Групи Галуа <i>О. І. МІЦЕК, В. М. ПУШКАР</i>	737
	Електрофізичні характеристики композитної кераміки cBN–NbN, легованої Al ₂ O ₃ , Si ₃ N ₄ та SiC <i>Ю. Ю. РУМ'ЯНЦЕВА, Л. О. РОМАНКО, І. П. ФЕСЕНКО, Д. О. САВЧЕНКО, В. З. ТУРКЕВИЧ</i>	743
Аморфний і рідкий стани	Першопринципне моделювання процесу аморфізації стопів системи Ni–Zr <i>І. В. ПЛЮЩАЙ, А. О. МАЙСТРЕНКО, Т. Л. ЦАРЕГРАДСЬКА, О. І. ПЛЮЩАЙ, О. О. КАЛЕНИК</i>	753
Дефекти кристалічної ґратниці	Воднесорбційні властивості стопу Ti _{15,5} Zr ₃₀ Mn ₃₈ V _{5,5} Cr _{5,5} Co _{5,5} на основі Лавесової фази (тип C14) <i>В. А. ДЕХТЯРЕНКО</i>	763
Взаємодії випромінення та частинок із конденсованою речовиною	Йонна імплантація Алюмінію в неіржавійну крицю <i>В. ГОНЧАРОВ, В. ЗАЖИГАЛОВ, М. ГОНЧАРОВА</i>	777
Металічні поверхні та плівки	Властивості поверхонь деталей із криці зі зносостійкими покриттями складу 1М і 90% ВК6 + 10% 1М, нанесеними методом електроіскрового легування з використанням спеціальних технологічних середовищ. Ч. 2. Зносостійкість, топографічні та механічні властивості	

	<i>В. Б. ТАРЕЛЬНИК, О. П. ГАПОНОВА, Н. В. ТАРЕЛЬНИК, Є. В. КОНОПЛЯНЧЕНКО, А. В. ОХРИМЕНКО, М. Ю. ДУМАНЧУК, К. Г. СИРОВАЦЬКИЙ</i>	793
Фізика міцності та пластичності	Вплив ультразвукового ударного оброблення на структуру та властивості стоматологічного стопу Co–Cr–Mo–W, одержаного 3D-друком <i>А. П. БУРМАК, С. М. ВОЛОШКО, Б. М. МОРДЮК, М. О. ВАСИЛЬЄВ, В. І. ЗАКІЄВ, М. М. ВОРОН, П. О. ГУРИН</i>	815
	Механічна стабільність і крихкість металів і стопів. Ч. 1. Параметри та критерії стабільного стану <i>Ю. Я. МЄШКОВ, Г. П. ЗІМІНА</i>	843
Фізико-технічні основи експерименту та діагностики	Огляд процесу адитивного виробництва <i>Т. Г. АВИНАШ, К. А. АЛЬТАФ, Р. ВАРМА ЯДУ, К. НОВШАД ШАБІБ, Г. Р. РАГХАВ</i>	859

Наукові редактори випуску: *О. С. Гаценко, В. А. Татаренко*

Відповідальний секретар редакційної колегії *О. С. Гаценко*

Редактор-коректор *О. С. Гаценко*

Технічні редактори *І. В. Загорулько, Л. І. Макаренко, М. В. Маніло*

Художні редактори *І. В. Загорулько, Л. І. Макаренко, М. В. Маніло*

Оригінал-макет для прямого репродукування виготовлено комп'ютерною групою РВВ Інституту металофізики ім. Г. В. Курдюмова НАН України

Адреса редакції:

Інститут металофізики ім. Г. В. Курдюмова НАН України, РВВ—Редакція «МНТ»

бульв. Акад. Вернадського, 36; 03142 Київ, Україна

Тел.: +380 44 4249042; факс: +380 44 4242561

Ел. пошта: mfint@imp.kiev.ua

Свідоцтво суб'єкта видавничої справи: ДК № 5875 від 13.12.2017 р.

Свідоцтво про державну реєстрацію друкованого засобу масової інформації: КВ № 23232-13072 ПР від 23.02.2018 р.

Затверджено до друку вченою радою Інституту металофізики ім. Г. В. Курдюмова НАН України

Друкується за постановою редакційної колегії журналу англійською, або українською мовами

Підписано до друку 27.05.2023 р. Формат 70 × 100/16.

Ум. друк. арк. . Обл.-вид. арк. .

Тираж 58 пр. Зам. № від .2023 р.

Віддруковано ВД «Академперіодика» НАН України

вул. Терещенківська, 4; 01024 Київ, Україна

Свідоцтво суб'єкта видавничої справи ДК № 544 від 27.07.2001 р.

Сайт журналу: <http://mfint.imp.kiev.ua>

DOI (журналу): <https://doi.org/10.15407/mfint>

DOI (випуску): <https://doi.org/10.15407/mfint.45.06>

INFORMATION (GUIDELINES) FOR CONTRIBUTORS

Submission of Manuscripts: Manuscripts should be sent by e-mail (mfint@imp.kiev.ua). Additionally, they can be sent by regular mail to Executive Managing Editor, Editorial Office, G. V. Kurdyumov Institute for Metal Physics, N.A.S. of Ukraine, 36 Academician Vernadsky Boulevard, UA-03142 Kyiv, Ukraine. Manuscripts may also be submitted to a member of the Editorial Advisory Board or to the appropriate Regional Editor who is familiar with the research presented.

Submission of a paper to '*Metallophysics and Advanced Technologies*' (transliteration: '*Metallofizika i Noveishie Tekhnologii*', i.e., '*MfNT*') will be taken to imply that it represents original work not previously published, that it is not being considered for publication elsewhere, and that, if accepted for publication, it will not be republished without the consent of the Editors and Publisher. It is a condition of acceptance by the Editor of a manuscript for publication that the Publishers acquire automatically the copyright in the manuscript throughout the world. Journal '*MfNT*' supports the generally accepted principles described in documents on publication ethics and unacceptable practices, which are presented on the [journal website](#).

Scope of the Journal: *Electronic Structure and Properties, Crystal-Lattice Defects, Phase Transformations, Physics of Strength and Plasticity, Metallic Surfaces and Films, Structure and Properties of Nanoscale and Mesoscopic Materials, Amorphous and Liquid States, Interactions of Radiation and Particles with Condensed Matter, Materials in Extremal Conditions, Reactor and Aerospace Metals Science, Medical Metals Science, New Metallic Materials and Synthetic Metals, Metal-Containing Smart Materials, Physical and Technical Basis of Experiment and Diagnostics, Articles under Discussion.*

Language: The language of publication may be English (preferably) or Ukrainian.

Abstract: Each paper requires an abstract of 200–250 words summarizing the significant coverage and findings (the use of mathematical symbols and expressions in abstract is not recommended).

Keywords and PACS numbers: 5–7 keywords and PACS numbers reflecting the content of the contribution should be supplied (see '[Physics and Astronomy Classification Scheme 2010](#)').

Manuscript Preparation: Papers should be formatted according to the [template](#), which can be downloaded from the Journal's website. The length of **research papers** should not in general exceed 5000 words and 10 figures; **review articles** should not exceed 10000 words and 30 figures, including tables and diagrams. Authors are urged to arrange the subject matter clearly under headings such as: 1. Introduction, 2. Experimental/Theoretical Details, 3. Results, 4. Discussion, 5. Conclusion, References. Subsections should be identified with section and subsection numbers (such as 6.1. Second-Value Subheading).

References and Notes: Notes are indicated in the text by consecutive superior Arabic numbers (without parentheses). References should be numbered consecutively (in square brackets) throughout the text. The full list should be collected and typed at the end of the paper in numerical order. Listed references should be completed in all details including DOI (if available) but excluding article titles in journals. **All authors'** initials should precede their names. Examples of references preparation:

1. S. O. Firstov and T. G. Rogul, *Metallofiz. Noveishie Tekhnol.*, **44**, No. 1: 127 (2022) (in Ukrainian). <https://doi.org/10.15407/mfint.44.01.0127>
2. V. B. Tarelynyk, O. P. Gaponova, and Ye. V. Konoplianchenko, *Prog. Phys. Met.*, **23**, No. 1: 27 (2022). <https://doi.org/10.15407/ufm.23.01.027>
3. A. Meisel, G. Leonhardt, and R. Szargan, *Röntgenspektren und Chemische Bindung* [X-Ray Spectra and Chemical Bond] (Leipzig: Akademische Verlagsgesellschaft Geest & Portig K.-G.: 1977) (in German).
4. J. M. Ziman, *Printsipy Teorii Tverdogo Tela* [Principles of the Theory of Solids] (Moscow: Mir: 1974) (Russian translation).
5. M. A. Stucke, D. M. Dimiduk, and D. M. Hazzledine, *High Temperature Ordered Intermetallic Alloys. V* (Eds. I. Baker and R. Darolia) (Pittsburgh, PA, USA: MRS: 1993), p. 471.
6. *Handbook of Mathematical Functions with Formulas, Graphs and Mathematical Tables* (Eds. M. Abramowitz and I. A. Stegun), Nat'l Bureau of Standards. Appl. Math. Ser. Vol. **55** (Washington, D.C.: U.S. Govt. Printing Office: 1964).
7. B. B. Karpovych and O. B. Borovkoff, *Proc. of Symp. 'Micromaterials Engineering' (Dec. 25–31, 1999)* (Kyiv: RVV IMF: 2000), vol. **2**, p. 113 (in Russian).
8. A. E. Krug, *Abstr. Int. Conf. Phys. Phenomena (Dec. 25–31, 1991, Alushta)* (Kharkiv: 1991), p. 12.
9. T. M. Radchenko, *Vplyv Uporyadkuvannya Defektnoyi Struktury na Transportni Vlastyvosti Zmishanykh Krystaliv* [Influence of Ordering of the Defect Structure on Transport Properties of the Mixed Crystals] (Thesis of Disser. for the Degree of Dr. Phys.-Math. Sci.) (Kyiv: G. V. Kurdyumov Institute for Metal Physics, N.A.S.U.: 2015) (in Ukrainian). <https://doi.org/10.13140/RG.2.2.35430.22089>

ІНФОРМАЦІЯ ДЛІЯ АВТОРІВ

10. E. M. Gololobov, V. B. Shipilo, N. I. Sedrenok, and A. I. Dudyak, *Sposob Polucheniya Karbonitridov Metallov* [Production Method of Metal Carbonitrides], Authors' Certificate 722341 SSSR (Publ. November 21, 1979) (in Russian).

11. V. G. Trubachev, K. V. Chuistov, V. N. Gorshkov, and A. E. Perekos, *Sposob Polucheniya Metallicheskih Poroshkov* [The Technology of Metallic Powder Production]: Patent 1639892 SU. MKI, B22 F9/02, 9/14 (Otkrytiya i Izobreteniya, 34, No. 13: 11) (1991) (in Russian).

12. Yu. M. Koval' and V. V. Nemoshkalenko, *O Prirode Martensitnykh Prevrascheniy* [On the Nature of Martensitic Transformations] (Kyiv: 1998) (Prepr./N.A.S. of Ukraine. Inst. for Metal Physics. No. 1, 1998) (in Russian).

Journal title abbreviations should conform to generally accepted styles:

<https://www.cas.org/support/documentation/references/corejournals>;

<https://cdn.journals.aps.org/files/rmpguapb.pdf>;

https://images.webofknowledge.com/WOK46P9/help/WOS/A_abrvjt.html;

<https://mathscinet.ams.org/msnhtml/serials.pdf>.

Equations and Formulae: Formulas in the text should be inserted by **MathType**, fully compatible with MS Office. Vectors should be typed in bold without arrows above. Note that complicated formulae, mathematical expressions or (de)notations are not recommended in the title, abstract, and keywords.

Tables: Number tables consecutively with Arabic numerals and give a clear descriptive caption at the top.

Figures: All figures should be numbered with consecutive Arabic numbers, have descriptive captions and be mentioned in the text. Keep figures separate at the end of the text and clearly label each figure with author's name and figure number. The labels at axis should contain the designation (or notation) of quantities and their units.

Preparation: Figures submitted must be of a high enough standard for reproduction with 300–600 dpi resolution (including half-tone illustrations). Redrawing or retouching of unusable figures will be charged to the authors.

Colour Plates: Whenever, the use of colour is an integral part of the research, or where the work is generated in colour, the Journal will publish (in paper version) the colour illustrations with charge to the author. Reprints in colour will carry a surcharge. Please write to the Publisher for details.

Submission of Electronic Text: Authors should submit the electronic version of their paper by e-mail to the Editorial Office. The text file should be saved in the native formats of the MS Word with a name consisting the name of the first author, for example, Hotovchenko.docx. The electronic form of figures (in TIF, EPS, JPG, PNG formats preferably and with name consisting the name of the first author also, for example, Hotovchenko_fig2a.jpg) should be planned so that they reduce to 12.7 cm column width (or less), and keep them separated from the text file. It is desirable to submit additionally all the figures within the format of the program, in which they were created.

Proofs: Contributors will receive page proofs for correction by e-mail as a PDF document. These must be returned to Kyiv office (mfint@imp.kiev.ua with subject beginning by word 'mfint') within 5 days of receipt.

Page Charges: There are no page charges to individuals or institutions.

Reprints: Authors can freely download a PDF version of their published article from journal website: <https://mfint.imp.kiev.ua>. The printed issues may be ordered by completing the appropriate form sent with proofs and prepaid by authors under the terms as for subscription.

Further Information: All questions arising during the **peer review** or after acceptance of manuscripts, especially those relating to reprints, should be directed to G. V. Kurdyumov Institute for Metal Physics, N.A.S. of Ukraine, Executive Managing Editor, Editorial Office, 36 Academician Vernadsky Blvd., UA-03142 Kyiv, Ukraine;

Fax: +380 44 4242561, e-mail: mfint@imp.kiev.ua (with subject beginning by word 'mfint').

We ask the authors to apply with their manuscript Copyright Transfer Agreement form.

Copyright Transfer Agreement

We, the undersigned authors of the manuscript '_____', transfer to the Founders, Publisher, and Editorial Board of the Journal 'Metallophysics and Advanced Technologies' (according to agreements between them) the right to publish this manuscript in original language or in translation to the other languages. We confirm that publication of this manuscript will not infringe a copyright of other persons or organizations and publication ethics.

Author(s): _____
(Last Name, First Name, Affiliation)

Correspondence Address: _____

Phone and e-mail: _____

(Signature)

(Date)

ІНФОРМАЦІЯ (ПРАВИЛА) ДЛЯ АВТОРІВ

Науковий журнал «Металофізика та новітні технології» (МФНТ) щомісяця публікує статті, які раніше ще не публікувалися та не перебувають на розгляді для опублікування в інших виданнях. Статті мають містити результати експериментальних і теоретичних досліджень в області фізики та технологій металів, сполук і сполук з металічними властивостями; рецензії на монографії; інформацію про конференції, семінари; відомості з історії металофізики; рекламу нових технологій, матеріалів, приладів. Журнал дотримується загальноприйнятих принципів, зазначених на його сайті в документах з публікаційної етики та щодо неприйнятних практик.

Тематика журналу: *Електронні структура та властивості, Дефекти кристалічної ґратниці, Фазові перетворення, Фізика міцності та пластичності, Металічні поверхні та плівки, Будова та властивості наномасштабних і мезоскопічних матеріалів, Аморфний і рідкий стани, Взаємодії випромінювання та частинок із конденсованою речовиною, Матеріали в екстремальних умовах, Реакторне й авіакосмічне металознавство, Медичне металознавство, Нові металеві матеріали та синтетичні метали, Металовмісні смарт-матеріали, Фізико-технічні основи експерименту та діагностики, Дискусійні повідомлення.*

Статті публікуються однією з двох мов: англійською (відається перевага) або українською.

Статті, в оформленні яких не дотримано наступних правил для опублікування в МФНТ, повертаються авторам без розгляду по суті. (Датою надходження вважається день повторного надання статті після дотримання зазначених нижче правил.)

1. Стаття має бути підписаною всіма авторами (із зазначенням їхніх адрес електронної пошти); слід вказати прізвище, ім'я та по батькові автора, з яким редакція буде вести листування, його поштову адресу, номери телефону та факсу й адресу електронної пошти.

2. Виклад матеріалу має бути чітким, структурованим (розділами, наприклад, «1. Вступ», «2. Експериментальна/Теоретична методика», «3. Результати та їх обговорення», «4. Висновки», «Цитована література»), стислим, без довгих преамбул, відхилень і повторів, а також без дублювання в тексті даних таблиць, рисунків і підписів до них. Анотація та розділ «Висновки» мають не дублювати один одного. Числові дані слід наводити в загальноприйнятих одиницях.

3. Об'єм оригінальної (неоглядової) статті має бути не більше 5000 слів (з урахуванням основного тексту, таблиць, підписів до рисунків, списку використаних джерел) і 10 рисунків. **Об'єм оглядової статті** — до 10000 слів та 30 рисунків.

4. За потреби до редакції може надаватися друкований (A4, подвійний інтервал) примірник рукопису з ілюстраціями.

5. До редакції обов'язково надається (по e-mail) файл статті, набраний у текстовому редакторі Microsoft Word, з назвою, що складається з прізвища першого автора (латиницею), наприклад, Hotovchenko.docx.

6. Електронна версія рукопису та його друкований варіант (в разі його надання) мають бути ідентичними. Вони мають оформлюватися за **шаблоном**, який можна завантажити з сайту журналу, і містити 5–7 **індексів PACS** в редакції 'Physics and Astronomy Classification Scheme 2010'. Тексти статей мають також містити **назву статті, список авторів, повні назви та поштові адреси установ**, в яких вони працюють, **анотацію статті** (200–250 слів), **5–7 ключових слів** двома мовами (англійською та українською), а заголовки таблиць і підписи до рисунків мають подаватися як **мовою рукопису, так і англійською мовою**; англійська анотація може бути представленою в більш розгорнутому варіанті (до 500 слів). Назва статті, її анотація та ключові слова мають не містити складні формули, математичні вирази чи позначення.

7. Електронні версії рисунків мають бути представленими у вигляді окремих файлів (у форматах TIF, EPS, JPG, PNG з розрізненням у 300–600 dpi) з назвами, що складаються з прізвища першого автора (латиницею) та номера рисунка, наприклад, Hotovchenko_fig2a.jpg. Додатково рисунки надаються у форматі програми, в якій вони створювалися.

8. Написи на рисунках (особливо на півтонових) слід по можливості замінити літерними позначеннями (набраними на контрастному фоні), а криві позначити цифрами або різними типами ліній/маркерів, які мають бути роз'ясненими в підписах до рисунків або в тексті. На графіках усі лінії/маркери мають бути достатньої товщини/розміру для якісного відтворення їх у зменшеному в 2–3 рази вигляді (рекомендована початкова ширина рисунка — 12,7 см). Світлини мають бути чіткими та контрастними, а написи та позначення мають не закривати істотні деталі (для чого можна використовувати стрілки). Замість зазначення в підтекстові збільшення під час зйомки бажано проставити масштаб (на контрастному фоні) на одній з ідентичних світлин. На графіках підписи до осей, **виконані мовою статті**, мають містити позначення (або найменування) величин, що відкладаються вздовж осей, і відділені комою їхні одиниці вимірювання.

9. Формули в текст треба вставляти за допомогою редактора формул **MathType**, сумісного з MS Office. **Вектори** слід набирати напівтовстим шрифтом без стрілок зверху.

10. Рисунки, таблиці, формули, а також підрядкові примітки (виноски) мають нумеруватися послідовно по всій статті.

11. Посилання на літературні джерела слід давати у вигляді порядкового номера, надрукованого в рядок у квадратних дужках. Список цитованої літератури складається по чергово за першою згадкою джерела. Приклади оформлення посилань наведено нижче (просимо звернути увагу на порядок розташування ініціалів і прізвищ авторів, бібліографічних відомостей і на розділові знаки, а також на необхідність зазначення **всіх** співавторів цитованої роботи та її ідентифікатора **DOI**, якщо він є):

ІНФОРМАЦІЯ ДЛЯ АВТОРІВ

1. S. O. Firstov and T. G. Rogul, *Metallofiz. Noveishie Tekhnol.*, **44**, No. 1: 127 (2022) (in Ukrainian). <https://doi.org/10.15407/mfint.44.01.0127>
2. V. B. Tarel'nyk, O. P. Gaponova, and Ye. V. Konoplianchenko, *Prog. Phys. Met.*, **23**, No. 1: 27 (2022). <https://doi.org/10.15407/ufm.23.01.027>
3. A. Meisel, G. Leonhardt, and R. Szargan, *Röntgenspektren und Chemische Bindung* [X-Ray Spectra and Chemical Bond] (Leipzig: Akademische Verlagsgesellschaft Geest & Portig K.-G.: 1977) (in German).
4. J. M. Ziman, *Printsipy Teorii Tverdogo Tela* [Principles of the Theory of Solids] (Moscow: Mir: 1974) (Russian translation).
5. M. A. Stucke, D. M. Dimiduk, and D. M. Hazzledine, *High Temperature Ordered Intermetallic Alloys. V* (Eds. I. Baker and R. Darolia) (Pittsburgh, PA, USA: MRS: 1993), p. 471.
6. *Handbook of Mathematical Functions with Formulas, Graphs and Mathematical Tables* (Eds. M. Abramowitz and I. A. Stegun), Nat'l Bureau of Standards. Appl. Math. Ser. Vol. 55 (Washington, D.C.: U.S. Govt. Printing Office: 1964).
7. B. V. Karpovych and O. B. Borovkoff, *Proc. of Symp. 'Micromaterials Engineering' (Dec. 25–31, 1999)* (Kyiv: R V V IMF: 2000), vol. 2, p. 113 (in Russian).
8. A. Eh. Krug, *Abstr. Int. Conf. Phys. Phenomena (Dec. 25–31, 1991, Alushta)* (Kharkiv: 1991), p. 12.
9. T. M. Radchenko, *Vplyv Uporyadkuvannya Defektnoyi Struktury na Transportni Vlastyivosti Zmishanykh Krystaliv* [Influence of Ordering of the Defect Structure on Transport Properties of the Mixed Crystals] (Thesis of Dissert. for the Degree of Dr. Phys.-Math. Sci.) (Kyiv: G. V. Kurdyumov Institute for Metal Physics, N.A.S.U.: 2015) (in Ukrainian). <https://doi.org/10.13140/RG.2.2.35430.22089>
10. E. M. Gololobov, V. B. Shipilo, N. I. Sedrenok, and A. I. Dudyak, *Sposob Polucheniya Karbonitridov Metallov* [Production Method of Metal Carbonitrides], Authors' Certificate 722341 SSSR (Publ. November 21, 1979) (in Russian).
11. V. G. Trubachev, K. V. Chuistov, V. N. Gorshkov, and A. E. Perekos, *Sposob Polucheniya Metallicheskikh Poroshkov* [The Technology of Metallic Powder Production]: Patent 1639892 SU. MKI, B22 F9/02, 9/14 (Otkrytiya i Izobreteniya, **34**, No. 13: 11) (1991) (in Russian).
12. Yu. M. Koval' and V. V. Nemoshkalenko, *O Prirode Martensitnykh Prevrashcheniy* [On the Nature of Martensitic Transformations] (Kyiv: 1998) (Prepr./N.A.S. of Ukraine. Inst. for Metal Physics. No. 1, 1998) (in Russian).

Слід використовувати загальноприйняті скорочення назв журналів:

- <https://www.cas.org/support/documentation/references/corejournals>;
<https://cdn.journals.aps.org/files/rmpguapb.pdf>;
https://images.webofknowledge.com/WOK46P9/help/WOS/A_abrvjt.html;
<https://mathscinet.ams.org/msnhtml/serials.pdf>.

Необхідною вимогою є також надання авторами додаткового списку цитованої літератури (**References**) в латинській транслітерації (система BGN/PCGN; рекомендовані транслітератори: <http://www.slovyuk.ua/services/translit.php>; <http://ru.translit.net/?account=bgn>).

Після транслітерованих назв книг, дисертацій, патентів та ін. слід у квадратних дужках наводити їхній англomовний переклад (див. приклади вище). При транслітерації статей з МФНТ слід використовувати написання П.І.Б. авторів, наведені лише в англomовному змісті відповідного випуску, і офіційну транслітеровану назву журналу (див. також першу сторінку кожної статті та сайт).

12. Коректура авторам надсилається електронною поштою у вигляді pdf-файлу після завершення етапу рецензування. На перевірку коректури авторам відводяться 5 робочих днів. Після закінчення зазначеного терміну стаття автоматично направляється до друку. Виправлення слід відмітити та прокоментувати в самому pdf-файлі або оформити у вигляді переліку виправлень (підписаного уповноваженим представником колективу авторів) і переслати електронною поштою на адресу редакції.

Електронний варіант статті надсилається на e-mail: mfint@imp.kiev.ua (з темою, що починається словом 'mfint'). Друкована версія рукопису (якщо у ній є потреба) надсилається за адресою: Інститут металофізики ім. Г. В. Курдюмова НАН України, редакція МФНТ; бульвар Акад. Вернадського, 36; 03142 Київ, Україна або відповідному регіональному редактору (див. сайт).

Автори можуть вільно завантажити pdf-файли опублікованих статей з сайту журналу (<https://mfint.imp.kiev.ua>), а також замовити друковані примірники випуску журналу зі своєю статтею, надіславши до редакції журналу разом з коректурою відповідну заявку та квитанцію про оплату друку необхідної кількості примірників випуску на умовах, аналогічних передплатним.

Відповідно до угод між редакцією МФНТ, засновниками та видавцем журналу, редакція вважає, що автори, надсилаючи їй рукопис статті, передають засновникам, видавцю та редколегії право опублікувати цей рукопис мовою оригіналу та в перекладі іншими мовами, і просить авторів відразу прикладати до рукопису «Угоду про передачу авторського права».

Угода про передачу авторського права

Ми, що нижче підписалися, автори рукопису «_____», передаємо засновникам, видавцю та редколегії журналу «Металофізика та новітні технології» (згідно з угодами між ними) право опублікувати цей рукопис мовою оригіналу та в перекладі іншими мовами. Ми підтверджуємо, що ця публікація не порушує авторського права інших осіб або організацій і принципів наукової етики. При цьому за авторами зберігаються всі інші права як власників цього рукопису.

Підписи авторів: _____ (П.І.Б., дата, адреса, тел., e-mail)

- Article preview
- Abstract
- Introduction
- Section snippets
- References (10)
- Cited by (2)



Volume 72, Part 6, 2023, Pages 2999-3005

Reverse logistic network design for quality reclaimed rubber

B. Manoj Kumar

Associate Professor, Automobile Engineering, SCMS School of Engineering and Technology, Karukutty, Ernakulam-683576, Kerala, India

Available online 25 August 2022, Version of Record 18 January 2023.


Show less ^

+ Add to Mendeley  Share  Cite

<https://doi.org/10.1016/j.matpr.2022.08.207>

[Get rights and content](#)



Part of special issue 

2nd International Conference on Sustainable Materials, Manufacturing and Renewable Technologies 2022

Edited by Rejeesh C R, Basil Kuriachen, Midhun Paul, Sunil Pothak

Other articles from this issue

[Foam based fracking in unconventional shale reservoir](#)

2023
Mandira Agarwal, Vamsi Krishna Kudapa

[Plasma based fracking in unconventional shale - A review](#)

2023
Mandira Agarwal, Vamsi Krishna Kudapa

FEEDBACK 

An Operative Approach for Effective Segmentation of Retinal Blood Vessels Based on Multilevel DNN

Mr. Sachin Gupta¹, Beena Puthillath², Dr. Meenakshi Sharma³, Dr. K. S. Wagh⁴, Dr. Sharmila K. Wagh⁵

Submitted: 22/04/2023

Revised: 14/06/2023

Accepted: 26/06/2023

Abstract: Vision is obstructed by issues with the retina's blood vessels. Given the rise in patients with visual problems, the frequency of periodic eye exams has increased. Decreasing numbers of ophthalmologists make the screening procedure challenging. Thus, for this field, automated computer-aided diagnostics are required. Over the past few decades, research has advanced to the point that it can now distinguish the different types of illnesses that affect vessels. Risky retinal vessels confirm the occurrence of CAD, DR hypertension, cerebral vascular issues, and stroke. A significant stage of DR called neovascularization involves the growth of many blood vessels without the bifurcation pattern and stiffness and minimal blood loss injuries. Arteriovenous junctions and vesicle width help to identify hypertensive retinopathy in patients. Retinal telangiectasia is a macular condition that affects the retina. The small blood vessels close to the fovea get enlarged or leak blood due to infection. The AV ratio and intersection also provide information on several vessel-related diseases. The suggested DNN is compared to traditional segmentation methods quantitatively and is found to have superior SN while still maintaining respectable SP and Acc. In addition, the area under the curve (AUC) is determined to verify accurate vascular segmentation from the retina. An improved post processing method will aid in accurate binary segmentation and preserve delicate blood vessel structures.

Keywords: AV ratio, CAD, Cerebral vascular issues, Neovascularization

1. Introduction

During an eye exam, the fundus can be seen by looking through the pupil. Most often at the arteries, oxygen, and other nutrients leave the blood and pass into the retina. Later, carbon dioxide and other waste products leave the retina and pass into the blood to be eliminated. The central retinal artery, which leaves the optic disc and has a truly typical vessel configuration at the ganglion cell level, is the source of the blood supply for the retina. The veins have a similar pattern [1].

Vision is obstructed by issues with the retina's blood vessels. Given the rise in patients with visual problems. The frequency of periodic eye exams has increased.

Decreasing numbers of ophthalmologists make the screening procedure challenging. Thus, for this field, automated computer-aided diagnostics are required. Over the past few decades, research has advanced to the point that it can now distinguish the different types of illnesses that affect vessels [2]. Risky retinal vessels confirm the occurrence of DR hypertension, CAD issues with cerebral vessels, and stroke. Neovascularization is a critical stage of DR that involves the growth of many vessels without the stiffness or bifurcation pattern, and it results in minimum blood loss injuries. Arteriovenous intersections and vessel breadth are indicators of hypertensive retinopathy [3]. The macular infection retinal telangiectasia causes blood to drop from or expand the tiny veins close to the fovea. The AV ratio and intersection also provide information regarding several vessel-related diseases. Occasionally the vessels must be taken out for tasks like glaucoma diagnosis [4].

Low-contrast thin vessels could not be identified using vessels derived from several scales. The region-growing technique is a useful segmentation tactic, but the establishment of seed points and the stopping principle is defined. It takes a lot of time and results in over-segmentation for raucous inputs. Active contour models depend on vessel contour fitting for accuracy and are autonomous and self-modifying while seeking [5]. Unsupervised and supervised methodology are categories for pattern recognition-based techniques. Unsupervised learning runs rapidly and doesn't need much segmentation-related information, but it takes a long time

¹Chancellor, Department of Management Sanskriti University, Mathura, Uttar Pradesh, India
chancellor@sanskriti.edu.in

ORCID ID: 0000-0002-4900-0082

²Assistant Professor, Department: EEE Kerala Technological University, Trivandrum
beena.ajit1998@gmail.com

Orcid id: 0000-0001-7476-3287

³OSD, Department of Education Sanskriti University, Mathura, Uttar Pradesh, India
osd@sanskriti.edu.in

ORCID ID: 0000-0002-7596-1784

⁴Associate Professor, Computer Engineering, AISSMS IOIT, Pune.
waghks@gmail.com

ORCID ID: 0000-0002-0309-0705

⁵Professor, Computer Engineering, Modern Education Society's College of Engineering, Pune.
sharmila.wagh123@gmail.com
50000-0001-7232-3819

to guess the results correctly. To correctly segment the vessels in supervised learning, specified feature vectors and hardcoded rules are required. CNN-based supervised learning has greater robustness and performance in vessel segmentation. The DNN is adept at learning the vessel features without any human intervention using many convolutional layers, in contrast to any supervised technique that relies on hardcoded rules created by humans [6].

The training effectiveness and accuracy of the CNN suffer when input patch images are used. Yet, speed and accuracy are increased with the FCN because it trains and tests the entire image. The FCN and fully linked CRF are coupled to obtain vascular segmentation, which is driven by HED. Researchers created a DS-based FCN that successfully segments the optic disc and vessels. A multilayer FCN with DS for vessel segmentation was provided by a few scientists [7]. The dense CRF is fed the pairwise and unary features that were recovered from the input CNN for binary segmentation. There was shown a Concept that uses the training's ground truth data. Instead, utilizing line segments and appropriate knowledge about the underlying data, a synthetic dataset was produced. The thick and fine vessels are segmented separately and then fused to obtain the full vascular tree using a powerful three-stage DNN. Although this segmentation performs exceptionally well, it is difficult and time-consuming [8].

The suggested DNN completes a full image-to-image regression. Instead of designing, the network pre-trained on very huge datasets can be used once more. a network model from scratch to address pertinent segmentation issues using the transfer learning idea. Transfer learning is accelerated by the use of pre-trained weights, which also improve performance. In the training phase, pre-trained weights are gradually changed using lower learning rates [9]. Because of the lack of very big medical datasets available for training, this DNN makes use of the first four stages of the pre-trained VGG-16. For the extraction of vessel features, it is further optimized. To reduce erroneous vascular segmentation during fine-tuning, multi-level/multiscale DS layers are integrated during training, and the deep vessel learned characteristics from the numerous convolutional stages. Moreover, the DS layers' receptive FOV is broadened to localize and divide the vessels. The subsections that follow describe it [10].

The multilevel/multiscale DNN's base network is chosen to be the first four stages of a VGG-16 network. These phases make up the convolutional layers, which are crucial building blocks in the DNN. It consists of a set of expandable learnable filters that spans the entire depth of the input image. These filters will be activated to recognize structures like edges, from lower-layer textures to higher-layer patterns and shapes. For each filter layer,

the network outputs activation maps after learning many features. The weights in these filters are initialized using initialization. The first two stages each have two separate convolutional layers, whereas the following two stages each have three separate convolutional layers [11].

What follows is the outline for the rest of the paper. The related work is briefly described in part 2, and the methodology and the theoretical foundations of the methods used are described in section 3. The simulation results and analysis are presented in section 4. For the chapter's final section, "key findings" we summarize the most important results.

2. Previously Done Related Work

With the development of new techniques, vessel segmentation has improved dramatically. The vessels can be segmented using morphological operations on their architecture, but exact results need the combination of several different techniques. The matching filtering technique finds it challenging to segment regions with reduced contrast, central vessel reflex, and proximity to lesions [12]. Low-contrast thin vessels could not be identified using vessels derived from several scales. The region-growing approach is a useful segmentation tactic, but it requires expert knowledge to choose seed locations and define a stopping principle. It takes a lot of time and results in over-segmentation for raucous inputs. Active contour models, which depend on vessel contour fitting for accuracy are autonomous and self-changing while searching. Unsupervised and supervised methodology are categories for pattern recognition-based techniques [13].

Supervised learning-based segmentation techniques educate the classifier on the right segmentation by using artfully created feature vectors. This feature extraction and selection is challenging and demands in-depth understanding. Deep learning-based approaches could provide solutions to the challenges in segmentation tasks without employing artificial characteristics to train the network as the CNN develops. Because CNN makes use of numerous convolutional layers that mimic the human brain, this methodology offers superior segmentation performance [14]. Sometimes it was even able to identify vessels that a skilled ophthalmologist was unable to. Therefore, conducting the feature extraction operation does not necessitate considerable mathematical expertise [15].

The approach suggested by researchers employed CNN to extract features, and then used the features as input for the RF classifier to segment the data. Both adjustments in rotation and scale do not affect it. The input image was converted into a vessel probability map with a size identical to that of the input image using a five-layer NN that serves as an autoencoder. The ground truth and the

input are automatically used by this network to learn the mapping, which transforms the input into a vessel probability map [16]. Even close to diseased lesions, it exhibits superior segmentation and divides the thin arteries. A few researchers suggested segmenting the vessels in the XCA pictures using a straightforward two-layer patch-based CNN. Although this approach is less complicated, the segmentation accuracy is rather low. A DNN is created with and without a pooling layer, and it is trained using a dataset of 4 lakh retinal image patches. Both DNNs' training phases make use of the pre-processed and enhanced patches. The no-pool DNN outperforms the other as computational complexity rises and is resistant to FP, FN, and central vessel reflex difficulties [17].

The vessel probability map is provided by Holistically-Nested Edge Detection (HED) inspired FCN that was put forth by a few researchers. The Conditional Random Field (CRF) classifier uses this map as input to produce binary segmentation, although some of the vessels are missed. Segmenting the vessels and the optic disc in the input retinal picture can both be done by a DNN that is learned from HED. Using the DS layers obtained from the foundational VGG-16 network model, this DNN is adept at learning vessel-specific properties. The vessels in the vessel probability map are wider than those seen in the ground reality [18].

Some researchers created a domain-specific fake noisy dataset using line segments to train the DNN without using ground truth. Compared to traditional methods, the dataset evaluation in DRIVE and STARE produces somewhat better results. This new project can be used for label-free network training. Some studies suggested segmenting the vessels, which would provide an intermediate vessel probability map by feeding the two-channel CNN the relevant patches from the live and mask XCA pictures [19]. The ROI is determined from the map, and it is then provided to a single-channel CNN for pixel-wise classification. This procedure is intricate and lengthens the testing's computational time. The multiscale top hat transform-enhanced XCA pictures are provided to the two-stage CNN for segmentation [20].

The input image is transformed using Stationary Wavelet Transform (SWT) and then provided as input to the multiscale algorithm because the vessels are of different width and orientations. CNN to divide the containers into halves, as some employees proposed. Images produced

consequently display minimum FP and FN. To obtain the full vessel probability map, multichannel inputs, such as the live and aligned mask CA images (dense matching), are provided to the U-Net-based FCN [21]. Some researchers have developed a CNN that combines the multiscale properties for retinal vascular segmentation while utilizing the idea of cross-connections. It demonstrates how challenging it is to segment fine vessel systems. Divided the retinal fundus image into thick and thin vessels and gave it to the thick, thin, and combination fusion segmenter as input so that the vessels would be accurately segmented. Low contrast microvessel segmentation, thin vessel segmentation, and the presence of central vessel reflex are not challenges for this approach [22].

3. The Purpose of the Proposed Work

- 1) Constructing a Deep Neural Network (DNN) model capable of performing reliable vascular segmentation for images of the retinal fundus collected for medical purposes.
- 2) To guarantee that this framework won't compromise segmentation accuracy and that its execution time will be kept to a minimum.

4. The Proposed Work:

The proposed work is discussed in detail below, where each section is elaborated.

4.1. Pre-processing:

During pre-processing, the input is transformed into a more usable form. Pre-processing is performed to scale the intensity range and enhance the contrast of the ROI, and it is especially important when employing a deep learning strategy. Adjusting the intensity during training reduces the amount of computing effort required. The most common pre-processing technique used for a full RGB input image collection is mean value subtraction. Input images are darker in the vessel parts and contrast is not increased, even though the algorithm scales the input intensity range. The standard RGB plane is eschewed in favour of a more complex setup using three separate planes. With RGB colour space, the green plane is the starting point. When CLAHE is used to the green plane, the result is the plane that comes after it. After the gamma corrections are subtracted out, the green plane becomes linear, and this is the third plane. The three planes are combined and scaled by a factor of two before being used to enclose the pre-processed image as shown in Figure I.

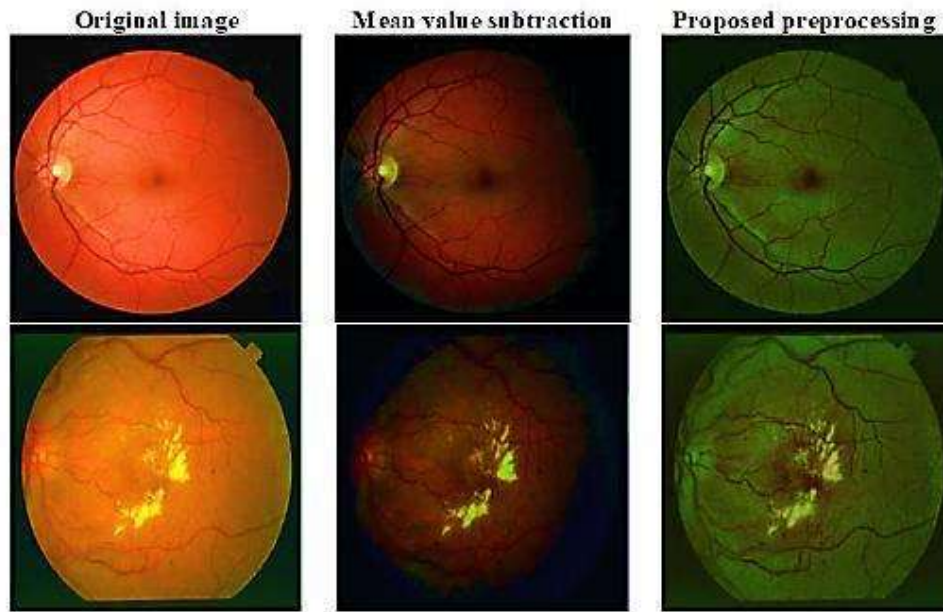


Fig I: Pre-processing input retinal images

4.2. Multi-level DNN application:

So in all, the suggested DNN does a full-fledged image-to-image regression. Rather than starting from scratch when trying to solve a segmentation problem, the network can be re-used after it has been trained on a big dataset. Transfer learning, which makes advantage of previously-trained weights, speeds up the learning process and improves performance. In the training phase, the pre-trained weights are modified gradually using lower learning rates. This DNN uses the first four layers of a pre-trained version of VGG-16 due to the scarcity of suitable very big medical datasets for training. To extract vessel traits, it is further fine-tuned. Fine-tuning is accomplished by combining numerous DS layers to make use of the deep vessel features learned across the many convolutional stages during training, hence decreasing the likelihood of incorrect vessel segmentation. Moreover, the DS layers' receptive FOV is widened so that they can better pinpoint and divide the vessels.

- Base Network: The multilevel/multiscale DNN uses the first four layers of a VGG-16 network as its foundation network. Convolutional layers, the ReLU, and the pooling layers make up these levels. With the VGG-16's layer-by-layer improvement, unnecessary coarse characteristics are filtered out. In light of this, the VGG-16 model only retains the first four convolutional layers.
- D1 layer: The four convolutional layers of the foundational network reveal crucial details about the cardiovascular system. Instead of focusing on the activation map in the last layer, it is more fruitful to delve deeply into the activation outputs in each of the four layers. Retinal fundus vascular architectures have a Gaussian distribution as shown in Figure II.

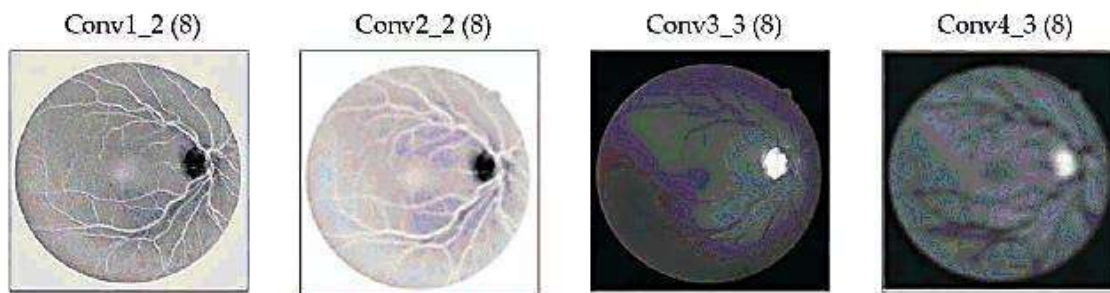


Fig II: The argument maximum of D1 layer output

- D2 Layer: With the Gaussian kernel's standard deviation initialised at 0.0002, the D 2 layer is generated. Each of the four steps employs a Gaussian convolution, but the number of features output by the map has been increased to 16. Standard deviations of 0.0004, 0.0006, and 0.0008 are used for the second,

third, and fourth Gaussian convolution kernels, respectively, to account for vessels of varying diameters. Each of the four final convolutional layers yields 16 feature map outputs, which are then combined as shown in Figure III.

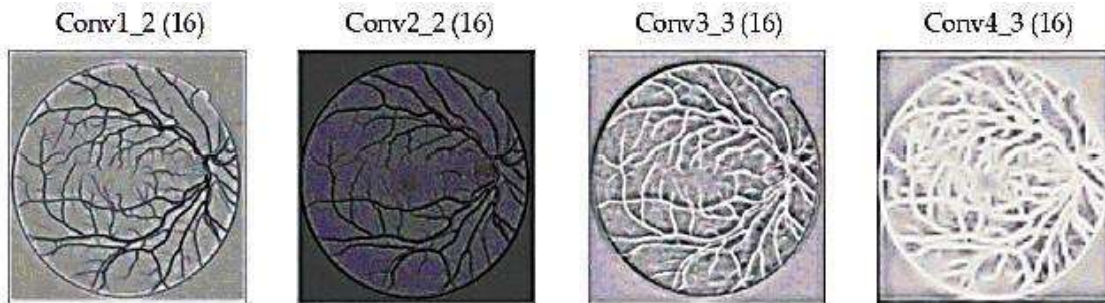


Fig III: The argument maximum of D2 layer output.

- Expanding the receptive FOV of the DS layers: Experiments reveal that the quality of the vessel map is restricted by the immediate fusion and convolution of the derived feature maps from DS layers. Separately convolving D1 and D 2 yields a more accurate probability map, which can be used for exact extraction of the blood vessels. Through

experimenting, we also discover that adding two more convolutional layers on top of the D1 and D2 output activation maps expands the receptive field of view (FOV).

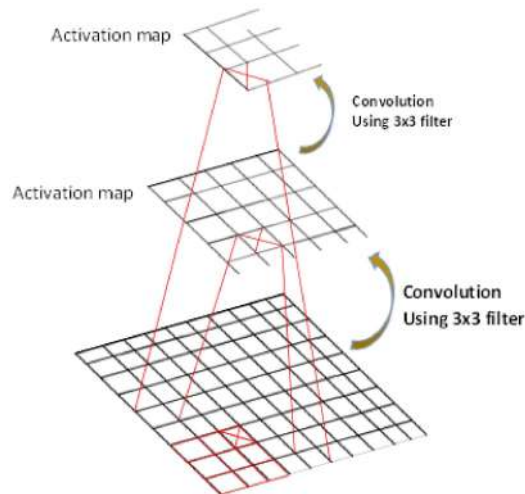


Fig III: Illustration of the increase in receptive FOV

4.3. Input image intensification:

The following changes are applied to the dataset input training images to improve their quality as training input.

- Technique for pre-processing
- Images can be rotated in one of fifteen different ways.
- Inverting all the photos that were rotated
- Targeted cropping of photos after rotation and inversion
- Using a half- and a double-size scaling factor for the flipped and rotated output

4.4. Backpropagation and optimization

One important method for training the DNN is called backpropagation. Errors are kept to a minimum by finding the optimal value of the weight that will lead to the lowest possible loss function (also known as the goal function). During the training phase, minima of the functions are typically found using optimization techniques such as gradient descent.

5. Result and Discussion:

For transfer learning, the weights are stacked using the first five stages of the pre-trained VGG-16 model as the

underlying caffe model. The proposed DS layers and additional convolutional layers are built on top of this foundational network to achieve model convergence. For training the DNN, we make use of the augmented dataset. The developed CAFFE model was then evaluated on test photos taken from the DRIVE, STARE, HRF, and real-world datasets after 18,000 iterations. Otsu thresholding is used to transform the pictures into binary. The quantitative evaluation measures compare the generated photos to the gold standard. These metrics include SN, SP, Acc, and AUC and presented in Figure IV.

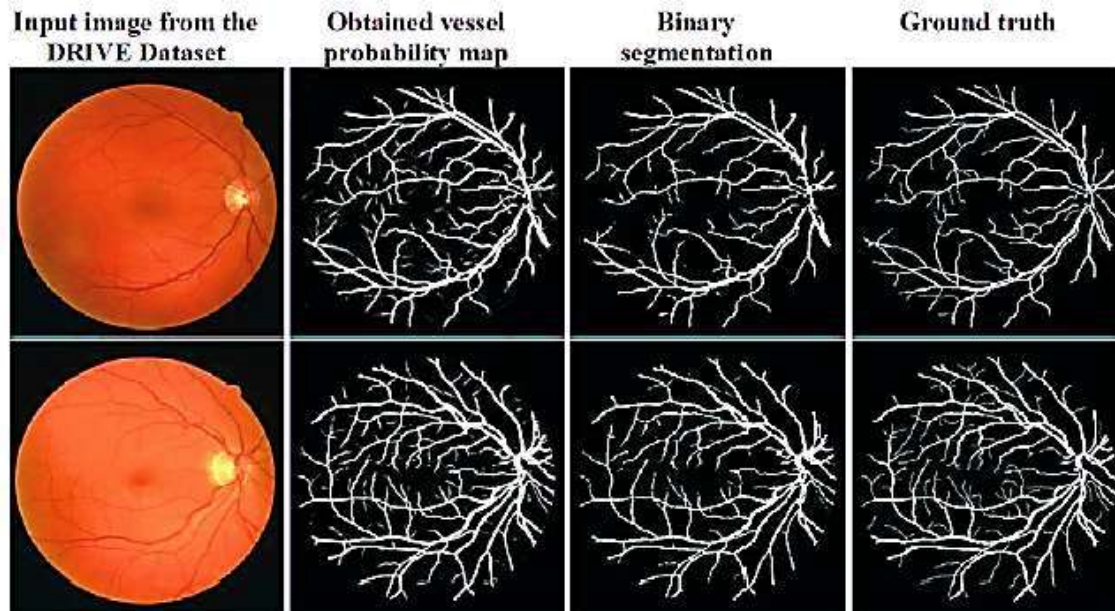


Fig IV: Output vessel segmentation using the proposed DNN

The proposed network model's output images are compared with well-known supervised segmentation methods so that a subjective analysis of the vessel segmented images may be performed. Despite the lack of ground truth during training, the approach proposed by (Chen, 2017) is able to segment the vessels, albeit with many missing segments. The DRIVE provides a unique environment for testing. When it comes to segmenting vessels, the dense CRF model that use CNN to extract the feature sets (Yan et al., 2019) does so, however the resulting vessel regions are not connected. The suggested DNN successfully dissects nearly all major blood artery

types while missing only a small percentage of minor ones. Blood vessel segmentation from non-vessel features in confusing locations is aided by contrast-enhanced vessels using the proposed pre-processing.

Table I also includes the derived and added quantitative performance markers. Using only one dataset for both training and testing, this method achieves the greatest AUC value of all of the cited sources. Not only is the peak SN value higher, but the segmented vessel width is larger as well.

Table I: Quantitative evaluation of performance for different methods.

Parameters	Chen, 2017 [23]	Yan et al., 2019 [24]	Proposed method
Sensitivity	0.7431	0.7625	0.835
Specificity	0.9812	0.984	0.979
Accuracy	0.9467	0.9626	0.976
ACC	0.9548	0.983	0.981

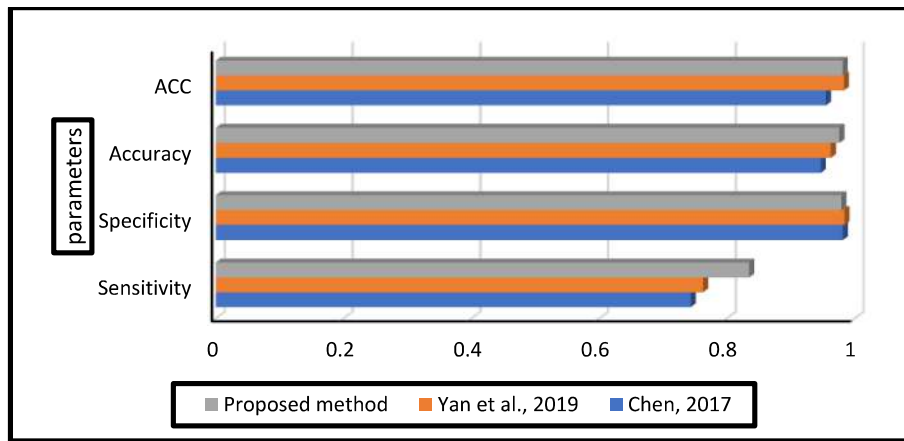


Fig VI: Quantitative evaluation of performance for different methods.

Important quantitative parameters for analysing DR, neovascularization, hypertension, cerebrovascular, and cardiovascular issues can be extracted from the vessel tree after it has been segmented from the retinal image. The width, curvature, tortuosity, AV ratio, etc. of a vessel can be determined using these parameters. In the same way, segmenting the optic disc for glaucoma detection is aided by the careful removal of the vascular tree. The examination of vascular abnormalities is facilitated by this computer-aided automated diagnostics, which is both quick and informative. While automation will never be able to take the position of a trained ophthalmologist, it can speed up the analytical process and improve the accuracy of quantitative estimates.

6. Conclusion:

Since the accuracy of vessel segmentation relied on familiarity with hand-built features, the segmentation process was laborious and inefficient. That's why scientists have come up with deep learning algorithms to automatically learn the feature sets and carry out the segmentation using increasingly complex convolutional layers. Initially, we apply a pre-processing procedure to the input in order to increase the contrast on all three planes and to normalise the intensity range. In contrast to previous methods, the proposed multilevel/multiscale DNN can segment blood vessels without the aid of supervised features. The network has the ability to pick up vessel features at several scales and depths. Real-world clinical datasets are used to evaluate the segmented vascular pictures produced as output. Other deep learning models are used for subjective appraisal of the vascular segments. When compared to existing models, the suggested network successfully segments the vast majority of blood arteries. The suggested DNN is compared to traditional segmentation methods quantitatively and is found to have superior SN while still maintaining respectable SP and Acc. In addition, the area under the curve (AUC) is determined to verify accurate

vascular segmentation from the retina. An improved post processing method will aid in accurate binary segmentation and preserve delicate blood vessel structures. The segmented images that are generated as a result can be used to assess parameters such as vessel diameter, bending radius, and amplification factor. It has been discovered that the alterations in vessel morphology can diagnose not just DR and hypertension but also several cardiovascular and cerebrovascular illnesses.

Conflict of Interests:

The authors declare that there is no conflict of interests regarding the publication of this paper.

Ethical approval: This article does not contain any studies with human participants or animals performed by any of the authors.

References

- [1] Albargathe SMBK, Kamberli E, Kandemirli F, Rahebi J (2021) Blood vessel segmentation and extraction using H-minima method based on image processing techniques. *Multimed Tools Appl* 80(2):2565–2582. <https://doi.org/10.1007/s11042-020-09646-3>
- [2] Al-Bander, B., Williams, B. M., Al-Nuaimy, W., Al-Tae, M. A., Pratt, H. and Zheng, Y. (2018), 'Dense fully convolutional segmentation of the optic disc and cup in color fundus for glaucoma diagnosis', *Symmetry* 10(4), 87.
- [3] Mateen, M.; Wen, J.; Nasrullah; Song, S.; Huang, Z. Fundus image classification using VGG-19 architecture with PCA and SVD. *Symmetry* 2019, 11, 1.
- [4] Popescu, D.; Ichim, L. Intelligent image processing system for detection and segmentation of regions of interest in retinal images. *Symmetry* 2018, 10, 73.
- [5] Adapa D, Raj ANJ, Alisetti SN, Zhuang Z, Naik G (2020) A supervised blood vessel segmentation

- technique for digital Fundus images using Zernike Moment based features. *PLoS ONE* 15(3):e0229831. <https://doi.org/10.1371/journal.pone0229831>
- [6] Moss, H.E. Retinal vascular changes are a marker for cerebral vascular diseases. *Curr. Neurol. Neurosci. Rep.* 2015, 15, 40.
- [7] Hassan, S.S.A.; Bong, D.B.L.; Premshenthil, M. Detect on of neovascularization in diabetic retinopathy. *J. Digit. Imaging* 2012, 25, 437–444.
- [8] Ünver, H.; Kökver, Y.; Duman, E.; Erdem, O. Statistical edge detection and circular hough transform for optic disk localization. *Appl. Sci.* 2019, 9, 350.
- [9] Al-Bander, B.; Williams, B.M.; Al-Nuaimy, W.; Al-Tae, M.A.; Pratt, H.; Zheng, Y. Dense fully convolutional segmentation of the optic disc and cup in color fundus for glaucoma diagnosis. *Symmetry* 2018, 10, 87.
- [10] Sarathi, M.P.; Dutta, M.K.; Singh, A.; Travieso, C.M. Blood vessel inpainting based technique for efficient localization and segmentation of optic disc in digital fundus images. *Biomed. Signal Process. Control* 2016, 25, 108–117.
- [11] Almotiri, J.; Elleithy, K.; Elleithy, A. Retinal vessels Segmentation techniques, and algorithms: A survey. *Appl. Sci.* 2018, 8, 155.
- [12] Li R., Shen S., Chen G., et al. Multilevel risk prediction of cardiovascular disease based on AdaBoost plus RF ensemble learning. *Proceedings of the 2019 5th International Conference on Electrical Engineering, Control, and Robotics*; January 2019; Guangzhou, China.
- [13] Yao Q., Wang R., Fan X., et al. Multi-class arrhythmia detection from 12-lead varied-length ECG using attention-based time-incremental convolutional neural network. *Information Fusion.* 2019; 53
- [14] Zhang X., Li R., Dai H., Liu Y., Zhou B., Wang Z. Localization of myocardial infarction with the multi-lead bidirectional gated recurrent unit neural network. *IEEE Access.* 2019; 7: 161152–161166. doi: 10.1109/access.2019.2946932.
- [15] Hannun A., Rajpurkar P., Tison G. H., et al. Cardiologist-level arrhythmia detection and classification in ambulatory electrocardiograms using a deep neural network. *Nature Medicine.* 2019; 25
- [16] Saman P., Rubin J. Electrocardiogram monitoring and interpretation: from traditional machine learning to deep learning, and their combination. *Proceedings of the Computing in Cardiology*; September 2018; Maastricht, Netherlands.
- [17] Chen Y.-J., Liu C.-L., Tseng V. S., Hu Y.-F., Chen S.-A. Large-scale classification of 12-lead ECG with deep learning. *Proceedings of the 2019 IEEE EMBS International Conference on Biomedical & Health Informatics (BHI)*; May 2019; Chicago, IL, USA. IEEE;
- [18] Rozenwald MB, Galitsyna AA, Sapunov GV, Khrameeva EE, Gelfand MS. A machine learning framework for the prediction of chromatin folding in *Drosophila* using epigenetic features. *PeerJ Comput Sci.* 2020; 6:307.
- [19] Amrit C, Paauw T, Aly R, Lavric M. Identifying child abuse through text mining and machine learning. *Expert Syst Appl.* 2017; 88:402–18.
- [20] Hossain E, Khan I, Un-Noor F, Sikander SS, Sunny MSH. Application of big data and machine learning in smart grid, and associated security concerns: a review. *IEEE Access.* 2019;7:13960–88.
- [21] Al-Dulaimi K, Chandran V, Nguyen K, Banks J, Tomeo-Reyes I. Benchmarking hep-2 specimen cells classification using linear discriminant analysis on higher order spectra features of cell shape. *Pattern Recogn Lett.* 2019;125:534–41.
- [22] Deldjoo Y, Elahi M, Cremonesi P, Garzotto F, Piazzolla P, Quadrana M. Content-based video recommendation system based on stylistic visual features. *J Data Semant.* 2016;5(2):99–113.
- [23] Chen, Y. (2017), ‘A labeling-free approach to supervising deep neural networks for retinal blood vessel segmentation’, arXiv preprint arXiv:1704.07502 .
- [24] Fan, J., Yang, J., Wang, Y., Yang, S., Ai, D., Huang, Y., Song, H., Hao, A. and Wang, Y. (2018), ‘Multichannel fully convolutional network for coronary artery segmentation in x-ray angiograms’, *IEEE Access* 6, 44635–44643.
- [25] Kulkarni, A. P. ., & T. N., M. . (2023). Hybrid Cloud-Based Privacy Preserving Clustering as Service for Enterprise Big Data. *International Journal on Recent and Innovation Trends in Computing and Communication*, 11(2s), 146–156. <https://doi.org/10.17762/ijritcc.v11i2s.6037>
- [26] Ahammad, D. S. K. H. (2022). Microarray Cancer Classification with Stacked Classifier in Machine Learning Integrated Grid L1-Regulated Feature Selection. *Machine Learning Applications in Engineering Education and Management*, 2(1), 01–10. Retrieved from <http://yashikajournals.com/index.php/mlaeem/article/view/18>



Computer-aided diagnosis for early detection and staging of human pancreatic tumors using an optimized 3D CNN on computed tomography

Chaithanyadas Kanady Vishnudas^{1,2} · G. R. Gnana King³

Received: 21 March 2023 / Accepted: 21 July 2023 / Published online: 9 August 2023
© The Author(s), under exclusive licence to Springer-Verlag GmbH Germany, part of Springer Nature 2023

Abstract

It is challenging to screen for and treat pancreatic cancer (PC), an extremely malignant tumor, both early in the course of the disease and as part of the later stages of treatment. In this article, a computer-aided diagnosis (CAD) technique for detecting PC early, particularly when assessing PC staging, is suggested. With this, clinical staff will be better equipped to give a treatment plan and can intervene with therapy early on as a result. This article addresses the process of effectively segmenting and classifying a pancreatic tumor using a deep learning (DL) network by following the four stages outlined below. Initially, computed tomography (CT) images are used for diagnosis, which is obtained from TCIA public access. Following the raw image acquisition, these images need to be pre-processed using the Boosted Anisotropic Diffusion Filter (BADF) and Contrast Limited Adaptive Histogram Equalization (CLAHE). Then, using the DMFCM segmentation approach, the images are segmented. Through Bag of Visual Words (BOVW) and Support Vector Machine (SVM), features are extracted, and the best features are given as input to the classifier. Eventually, classification is carried out using optimized 3D convoluted neural networks (3D CNN) using Improved Harris Hawks Optimization (IHHO). The implemented model achieved better results of 98.32% accuracy, 99% sensitivity, and 99% specificity. The proposed model is compared to some cutting-edge models such as normal CNNs, LSTMs, RESNETs, RNNs, and 3D CNNs to determine which one performs well. In terms of specificity, sensitivity, accuracy, and recall, the proposed model scored better than other models.

Keywords Classification · Computer-aided detection · Computer tomography images · Deep learning · Pancreatic cancer

1 Introduction

Cancer is a serious disease that has an incurable appearance since it is caused by changes in genes that control how cells function [1, 2]. Specifically, PC develops in the digestive organ, which is situated behind the bottom portion of the stomach [3]. An exocrine gland and an endocrine gland reside in the stomach, helping to keep blood sugar levels at a healthy level [4]. PC is characterized by symptoms of jaundice, abdominal pain, loss of appetite, sudden weight loss for unknown reasons, and fatigue [5]. Besides, exocrine tumors are also called adenocarcinomas, which develop in the tissues of the pancreas, as they originate in glands of the endocrine and exocrine glands [6]. Treatment depends on the stage of growth of this tumor, whereas endocrine tumors are often caused by cancers that affect the organs that produce hormones [7]. PC screening involves CT, magnetic resonance imaging (MRI), and so on, which are time-consuming and expensive [8]. PCs are frequently challenging

Communicated by B. Xiao.

✉ Chaithanyadas Kanady Vishnudas
chaithanyadasnidhin@gmail.com

G. R. Gnana King
kings.326@gmail.com

¹ Department of Electronics and Communication, SCMS School of Engineering and Technology, Ernakulam, Kerala, India

² APJ Abdul Kalam Technological University, Thiruvananthapuram, Kerala, India

³ Department of Electronics and Communication, Sahrdaya College of Engineering and Technology, Kodakara, Kerala, India

Quality deterioration of an Indian urban water source near an open dumping siteSruthy Robert, Nisha Luckins^{IWA*} and Ratish Menon^{IWA}

Department of Civil Engineering, SCMS School of Engineering and Technology, Vidya Nagar, Palissery, Karukutty, Ernakulam, Kerala, India

*Corresponding author. E-mail: nisha@scmsgroup.org

ABSTRACT

In developing countries, the stress of drinking water is often due to the increase in population, and rivers are the most important source of water. In this study, the pollution of the Kadambayar River, located in southern India, was evaluated. The river flows through major establishments in the city, and an open dumping site is located near its bank. The river was infested with water hyacinth, which is considered a bioindicator of pollution in water bodies. Sixteen water quality parameters were analyzed across eight sampling stations in the river and compared with the standard limits as per IS 10500:2012 and IS 2296:1992, WHO, ICMR. It was found that parameters such as DO, BOD, and Coliforms did not comply with the limits at any of the stations. The heavy metals were also analyzed for water and sediment samples, in which the concentrations of arsenic in water were seven times higher and chromium was 50 times higher than the national standard limit. Thus, it can be concluded that the quality of this drinking water source is declining abruptly, especially downstream near the dumpsite, affecting the ecosystem as well as human health when exposed to carcinogenic metals.

Key words: drinking water, heavy metals, municipal solid waste, open dumping, urbanization, water quality

HIGHLIGHTS

- The river Kadambayar is an important drinking water source for the surrounding urbanizing region.
- The river is infested with water hyacinth, which is a bioindicator of pollution.
- More than 500 MPN/100mL of coliforms are present in the river at all stations.
- The highest BOD of 228 mg/L and the lowest DO concentration was 0 mg/L for samples from a drain that carried the effluent from the industries to the river.
- The highest arsenic and chromium contamination in sediment and water samples was obtained downstream near the open dumping site.
- Exposure to heavy metal-contaminated drinking water can cause skin disorders, and cancer in humans and also threaten the survival of aquatic biodiversity.

This is an Open Access article distributed under the terms of the Creative Commons Attribution Licence (CC BY 4.0), which permits copying, adaptation and redistribution, provided the original work is properly cited (<http://creativecommons.org/licenses/by/4.0/>).

Training and Classification of PCA with LRM model for Diabetes Prediction

Neethu Krishna¹, Amitha R², Neethu Maria John³, Simy Mary Kurian⁴

¹Department of Computer Science & Engineering
SCMS School of Engineering & Technology
Kochi, India
neethukrishnascms@gmail.com

²Department of Computer Science & Engineering
Mahaguru Institute of Technology
Alappuzha, India.
amitha@mahagurutech.ac.in

³Department of Computer Science & Engineering
Mangalam College of Engineering
Kottayam, India
neethu.john01@mangalam.in

⁴Department of Computer Science & Engineering
Amal Jyothi College of Engineering
Kanjirappally, India
simymarykurian@amaljyothi.ac.in

Abstract— There are exponential increase in the number of families who are diagnosed by diabetes mellitus because of lifestyle and other non-determinable factors. Most of the patients are least bothered about the consequences they face or about the danger factor that approaches them. In this, we have established a novel model predicting the type 2 diabetes mellitus (TD2M) dependent on information digging methods. The main constraints are that we are trying to enhance the precision of the expected model and to not limit the model with just one data set. The model contains the improved NB, DT, KSTAR, LOGISTIC REGRESSION, SVM compared to the pre-processing techniques. To compare our outcome and the outcomes from different scientists we use Pima Indians diabetes data set and the Waikato environment for knowledge analysis toolbox. Apart from these, the model which we expect to implement have adequate data set quality. For more analysis, we applied it to two more diabetic datasets. These two provides satisfied outcomes. Henceforth, the model is set to be valuable for the betterment in the field of diabetology..

Keywords- Diabetes prediction, Logistic regression model, Support Vector Machine, KSTAR, Naïve Bayes classification.

I. INTRODUCTION

Diabetes is the most common sickness worldwide and spreading rapidly even though they are not contagious. Diabetes is diagnosed if there is persistent hyperglycemia and is described by a term called heterogeneous aggravation of digestion. There are two reasons for this: one is inconsistent or the depleting activity of insulin or it may be both. Persistent hyperglycemia can cause various problems it may be due to brokenness issue in organs, any elements in eyes, nerves and heart. The diabetes can be classified into two classes: type 1 and type 2. Type 1 is caused due to the lack of insulin discharge. Therefore type 2 is common among the patients where it is caused either due to the lack of insulin secretion or protection from insulin activity.

A survey was taken to access the number of diabetes patients worldwide which was initiated by the six version IDF (international diabetes federation) and found to be 382 million individuals who are being diagnosed and among this, type 2 diabetes are said to be common. As a result, type 2 diabetes is considered to be a serious issue. If we could predict and analyze diabetes at right time, effective measures can be taken earlier hence not allowing to worsen the condition of the patient. This would be an exceptional innovation where it helps in the advancement of medical field industry. By demonstrating, the future could be anticipated by information mining. Lately, there are numerous computational techniques and instruments are available for information examination. For clinical exploration and mainly in clinical field, information mining has been generally applied. Hence this paper proposes a

half hand half analysis model which would predict diabetes by using various information mining techniques. This model would be really useful for clinical experts and specialists in setting on choices and improve indicative precision. We will discuss about information mining and its devices and techniques in the paper.

II. RELATED WORKS

Riccardo B, Blaz Z et.al has proposed Predictive information mining is turning into a fundamental instrument for scientists and clinical experts in medication. Understanding the primary issues fundamental these strategies and the utilization of concurred and normalized methods is compulsory for their organization and the dispersal of result Data mining is the way toward choosing, investigating and displaying a lot of information to find obscure examples or connections which give a reasonable and valuable outcome to the information expert. Authored during the 1990s, the term information mining has today become an equivalent word for 'Information Discovery in Databases' underlined the information examination measure instead of the utilization of explicit investigation strategies. Information mining issues are frequently addressed by utilizing a mosaic of various methodologies drawn from software engineering, including multi-dimensional data sets, AI, delicate registering and information representation, and from insights, including speculation testing, grouping, characterization and relapse techniques.[1]

In this work, Mechelle Gittens, Reco King et.al , Diabetes as of now positions among the most noteworthy dangers to human existence given the expansion in the quantity of analyzed cases around the world. This unexpected increment has been connected to changes in human way of life since most of cases analyzed are that of type 2 diabetes. Portable wellbeing (m-wellbeing) advances are being executed on the whole zones of the wellbeing business to help patients in their quest for better lives. The general public picked for our examination has a populace predominately of African plunge and is in emergency, as it has perhaps the most elevated pace of diabetes and removal around the world.

The proposed framework is contained an information procurement module (DAM), a cell phone and a wellbeing information worker. The DAM estimates the patient's information by methods for various sensors and sends that information to the cell phone by means of Bluetooth. When the readings arrive at the cell phone, they are sent over an IP organization (like the Internet) to a far off wellbeing server farm. The medical services experts would then be able to see the readings and respond properly. The framework gives day in and day out observing of the patients which, as the creators propose, could trade the requirement for up close and personal

gatherings among specialists and patients. This considers patients to get the consideration they need from the solace of their homes. Not at all like the vast majority of the examination investigated, this arrangement can be executed without the clients expecting to possess a PDA. A large portion of the people experiencing constant infections are for the most part more seasoned people who may discover PDAs confounded and this exploration gives an option in contrast to the utilization of costly savvy phones.[2]

Marcano-Cede~no Alexis, et.al, Diabetes is the most well-known illness these days on the whole populaces and altogether age gatherings. Various strategies of computerized reasoning has been applied to diabetes issue. This examination proposed the counterfeit metaplasticity on multi-facet perceptron (AMMLP) as expectation model for forecast of diabetes.

Diabetes has a lot of adverse issues like kidney sickness, visual impairment, nerve harm, vein harm and coronary illness as well. The World Health Organization in 2000 demonstrated there were ~170 million individuals with diabetes, and assessed that the quantity of instances of the infection worldwide will be dramatically increased to 366 million by 2030. Diabetes happens in two significant structures: type 1, or insulin subordinate diabetes, and type 2, or non-insulin-subordinate diabetes. The type 1 diabetes, is portrayed by an outright insufficiency of insulin discharge. People who have worsened condition of diabetes that affects the vital parts can be diagnosed by immune system pathologic cycle which occurs in the pancreatic islets and by hereditary markers.[3]

Veena Vijayan V et.al has proposed Diabetes mellitus is caused because of the expanded degree of sugar content in the blood. This can cause arrangement inconveniences like kidney disappointment, stroke, malignancy, coronary illness and visual impairment. The early identification and conclusion, assists with recognizing and maintain a strategic distance from these confusions. Various modernized data frameworks were planned utilizing various classifiers for foreseeing and diagnosing diabetes. Choosing appropriate calculations for characterization obviously expands the exactness and productivity of the framework. The principle objective of this investigation is to survey the advantages of various preprocessing procedures for choice emotionally supportive networks for foreseeing diabetes which depend on Support Vector Machine (SVM), Naive Bayes classifier and Decision Tree. Information mining includes computational procedures, measurable strategies, grouping, characterization, design ID and change. Clinical information mining incorporates extraction of concealed examples from immense measure of heterogeneous information which subsequently making the way for a huge wellspring of clinical information investigation. Biomedical and medical care frameworks require a raised degree of coordinated effort among wellbeing and clinical elements. One of significant

obstacle looked by biomedical experts is to keep up routineness inside deliberate foundation. Diabetes is a genuine medical condition wherein the measure of sugar content can't be regulated.[4]

K Sowjanya et.al , Diabetes mellitus (DM) is arriving at perhaps plague extents in India. The level of infection and obliteration because of diabetes and its potential complexities are colossal, and started a critical medical services trouble on the two families and society. The disturbing component is that diabetes is currently being demonstrated to be connected with various inconveniences and to happen at a nearly more youthful age in the country. [5]

Gang Shi, Shanshan Liu, et.al has proposed the principle hazard components of diabetes and set up the diabetes hazard evaluation model which was set on the portable terminal with behind the stage where the information of individual circumstance gathered by poll could be broke down accomplishing way of life intercessions and exercise propensities proposition focused on the chose high-hazard diabetes. Thus, for this present strategy's benefits of simple activity, broad and high-efficiency. World as indicated by the overview of The World Public Health Organization research. It is a significant danger factor for death and various nonfatal complexities that will frame a huge weight to the patients, their families, and the medical services framework. A few ongoing intercession examines have undisputedly demonstrated that type 2 diabetes can be productively forestalled by way of life change in high- hazard people. [6]

Juntao Wang and Xiaolong Su, et.al has proposed It is utilized generally in group examination for that the K-implies calculation has higher effectiveness and adaptability and merges quick when managing enormous informational collections. Anyway it additionally has numerous inadequacies: the quantity of groups K should be introduced, the underlying bunch communities are subjectively chosen, and the calculation is impacted by the commotion focuses. Taking into account the deficiencies of the conventional K- Means grouping calculation, this work presents an improved K-implies calculation utilizing clamor information channel.

Bunching (grouping) is to assemble objects of a data set into various groups or classes (bunch) so that objects in a similar gathering have a huge likeness (comparability) and items in various gatherings have a huge divergence. Bunch investigation is one of the vital advances in the field of information mining and AI which has been applied in numerous territories: information mining and information revelation, design acknowledgment and example grouping, information pressure and vector quantization and assumes a significant part in science, topography, geology, and marketing.[7]

Shunye Wanget.al , The conventional k-implies calculation is frequently determined by the Euclidean distance. For longitudinal information it can't perform exact and proficient registering. This technique can improve the conventional k-implies grouping on longitudinal information. For missing longitudinal information, we previously embraced a straight addition procedure to fill in missing qualities and afterward normalized the information, and so on Through exhaustive reproduction contemplates, we show the force and adequacy of our strategy by contrasting the closeness inside and between the classes. The aftereffects of our investigations show that our technique can bunch the longitudinal information all the more adequately[8].

Bunching examination technique is a sort of unaided learning measure. It is as indicated by a portion of the characteristics that is a sort of likeness between little quite far, inside the class similitudes beyond what many would consider possible enormous of the things to be assembled into a class. Bunching examination is a module of the information mining framework. It is either a solitary device to track down the profound data of dissemination of information in the data set and a preprocessing step of other information mining calculation. Subsequently, it is a significant examination subject in the field of information mining that has been generally applied in numerous fields, for example, design acknowledgment, information investigation, picture handling, and client relationship the executives. K-implies bunching calculation is a sort of ordinary, fundamental division calculation dependent on segment. In view of the target work extremum, it is utilized to partition the information into various classes. In any case, the conventional k- implies grouping calculation has a few restrictions: it is not difficult to fall into neighborhood extremum with setting starting bunch number and bunching focuses as per earlier knowledge.[8]

Phattharat Songthung et.al, has proposed Diabetes is an ongoing illness that adds to a critical bit of the medical care use for a country as people with diabetes need ceaseless clinical consideration. To forestall or postpone the beginning of type 2 diabetes, it is important to recognize high danger populaces and present conduct changes as right on time as could really be expected. Screening the populace to distinguish high danger people is a significant undertaking. Perhaps the most exact trial of diabetes is through the examination of fasting glucose, however it is intrusive and expensive. Besides, it is just helpful when the individual is showing manifestations i.e., making a finding, which is considered past the point where it is possible to be a viable screening system.

The diabetes hazard scoring framework is utilized for distinguishing people who have high danger for diabetes and ought to be circled back to lab tests and conduct alteration. There are six significant credits used to process the score: age

(a long time), sex, BMI, midsection periphery (cm), presence of hypertension, and family background of diabetes in guardians or kin. The presence of each property is given a score dependent on the seriousness of the characteristic, and scores are summarized into an all out hazard score going from 0-17. In the event that the absolute danger score is six or higher, the individual is prescribed to get a subsequent lab test for fasting blood glucose and go through conduct modification.[9]

Longfei Han, Senlin Luo, et.al has proposed K-implies (PSCK- implies) technique all the while incorporates the restricted administered data and the size requirements to screen the high-hazard populace dependent on similitude estimation, and gets an achievable and adjusted separation answer for evade bunch with not many focuses. Results on CHNS public dataset and follow-up dataset show that proposed PSCK implies strategy can normally review the danger of diabetes into four levels, and accomplish 73.8%, 85.1% and 0.95 affectability, explicitness and RME on testing information. The proposed strategy contrasts well and 8 past semi-regulated grouping techniques, it shows that semi-managed bunching by bringing together numerous types of imperatives can direct a decent segment that is more pertinent for the area and find new classifications through earlier information.

Danger delineation can assess an individual's danger for enduring diabetes, it isolates the danger of populace into various danger levels, like high-hazard level, moderate-hazard level or okay level. Having a framework to define people as per hazard is vital to the achievement of diabetes anticipation activity, and this permits people profit by additional examination and mediation. The basic methodologies have been applied to take care of danger separation issue are the danger scores, which grade the scores into one of a few classifications, to give a degree of danger among "low" and "very high"[10].

III. PROPOSED METHODOLOGY

The motivation behind this examination is to furnish an alternate methodology in managing instances of diabetes, that is with information mining strategies NB, DT, KSTAR, Logistic Regression, SVM calculation to foresee and investigate the danger of diabetes that is carried out in the portable system. The dataset utilized for information demonstrating utilizing calculated relapse calculation. In the information readiness dataset done pre-preparing measure utilizing supplant missing worth, standardization, and highlight extraction to deliver a decent exactness. The aftereffect of this examination is execution measure with ROC Curve, and furthermore the property investigation that impact to diabetes utilizing p-esteem. From these outcomes it is realized that by utilizing demonstrating strategic relapse calculation and

approval test utilizing leave one out acquired precision of 94.77%. Also, for ascribes that influence diabetes is 9 credits, age, hemoglobin, sex, glucose pressure, creatin serum, white cell tally, urea, all out cholesterol, and BMI. What's more, for ascribes fatty oils have no impact on diabetes. The proposed technique incorporates extraction of new gathering of highlights from PIDD by utilizing PCA-LRM so the qualities are examined for their significance and pertinence, and are oppressed for information mining strategies like Linear Regression Model (LRM) to arrange the given information for foreseeing diabetes infection.

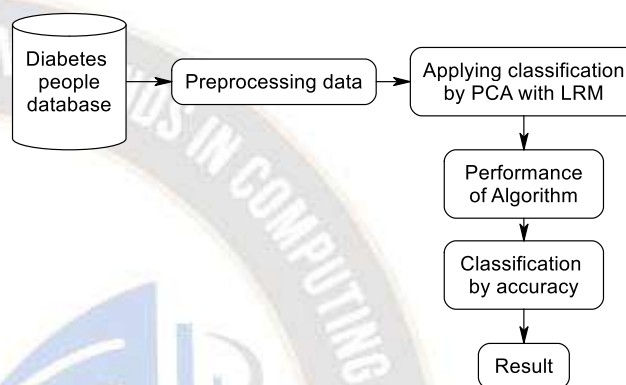


Figure 1. Proposed Frame Work

A. Preprocessing

In Data Selection methodology, it is executed to find the missteps like missing characteristics, wrong substance, and inconsistency of data. In the data examination stage, it calculates the data to get the vital results by taking apart the datasets using an exceptional gadget. Shows Preprocessing strategy consolidates change which performs Restoring the missing characteristics.

B. Normalizing the Data

Tracking down some unacceptable characteristics As data in actuality is foul, insufficient and clamorous, we need to perform data preprocessing technique. In this system, it incorporates finding the missteps and missing the assessment of data from the copious dataset. Using Preprocessing, it ends up being not hard to reestablish the missing characteristics and right some unacceptable data . With list worth and characteristic name and others.

C. Classification

Characterization: Classification is the technique to find a lot of models that explain by apportioning a thing to a particular class subject to its closeness to past examples of various articles. The classifier is made to assess the out and out names. These names portray a data thing into any of the inbuilt classes. First thing, gathering may show closeness to objects that are certainly people from a given class. All described articles should go through pre-gathering (i.e.) the

imprint should be understood. It would be acknowledged that every model has a spot with a predefined class such as NB, DT, KStar, Logistics Regression, Support Vector Machine.

D. Diabetes Classification

Diabetes is the most common sickness worldwide and spreading rapidly even though they are not contagious. Diabetes is diagnosed if there is persistent hyperglycemia and is described by a term called heterogeneous aggravation of digestion. There are two reasons for this[11]: one is inconsistent or the depleting activity of insulin or it may be both. Persistent hyperglycemia can cause various problems it may be due to brokenness issue in organs, any elements in eyes, nerves and heart. The diabetes can be classified into two classes: type 1 and type 2. Type 1 is caused due to the lack of insulin discharge. Therefore type 2 is common among the patients where it is caused either due to the lack of insulin secretion or protection from insulin activity.

A survey was taken to access the number of diabetes patients worldwide which was initiated by the six version IDF (international diabetes federation) and found to be 382 million individuals who are being diagnosed and among this, type 2 diabetes are said to be common. As a result, type 2 diabetes is considered to be a serious issue. If we could predict and analyze diabetes at right time, effective measures can be taken earlier hence not allowing to worsen the condition of the patient. This would be an exceptional innovation where it helps in the advancement of medical field industry. By demonstrating, the future could be anticipated by information mining. Lately, there are numerous computational techniques and instruments are available for information examination.

For clinical exploration and mainly in clinical field, information mining has been generally applied. Hence this paper proposes a half hand half analysis model which would predict diabetes by using various information mining techniques. This model would be really useful for clinical experts and specialists in setting on choices and improve indicative precision. We will discuss about information mining and its devices and techniques in the paper

1) *Logistic Regression Model:* For modelling binary classification, this would be of good choice. Here we assume, the conditional probability of one of the output classes to be equal to the linear combination of the input features. Therefore, the equation would be:

$$Z_i = \ln(P_i / (1 - P_i)) \quad (1)$$

where P is the probability of the occurrence of event i.

2) Naïve Bayes Classification

This algorithm is known for its simplicity and usefulness. At the same time, it is fast to build and makes a quicker prediction. It learns probability as per the target class, we assume that the occurrence of particular attribute is independent of the occurrence of other attributes, this algorithm shows better performance[12]. This algorithm will not require the accurate one such that the highest probability is allocated to the correct class. It is based on the Bayes theorem as in equation 2 which states that:

$$P(A|B) = P(B|A) P(A) P(B) \quad (2)$$

where P(A|B) and P(B|A) are the conditional probabilities of occurrence of an event A given that event B is true and vice versa. A, P(A), P(A|B) and P(B|A) are called proposition, prior probability, posterior probability and likelihood, respectively. Support vector machine is also an algorithm which is basically a linear machine learning algorithm used for solving classification problems. This is called as support vector classification. Support vector regression is the subset of SVM. The above mentioned two algorithms use the same method to solve regression problem. optimization problem is the Primal formulation since the problem statement has original variables.

3) The K – Star

The System Based on Classification Primarily, dividing the data into K subsets are done for performance evaluation. Every subset contains the data of each class. From there K subset, one is taken for testing and remaining other was taken for training. In order to study for testing and training, we assume the value of K to be 10. The measurement of performance would be based on sensitivity, PPV[13], AUC[14], specificity, F-measure and NPV. An explanation of each performance parameter is given as follows:

a) *Positive prediction value (PPV 1):* It is the number of positive samples correctly categorized as positive divided by the total testing data sample classified as positive as shown in equation 3.

$$PPV = TP / (TP + FP) \quad (3)$$

b) *Negative Prediction Value (NPV):* It represents the number of negative samples correctly categorized as negative divided by the total testing data sample classified as negative.

$$NPV = \frac{TN}{TN + FN} \quad (4)$$

c) *Sensitivity*: This is the number of positive samples correctly categorized as positive divided by the total testing sample data testing positive

$$Sensitivity = TPR = \frac{TP}{TP + FN} \quad (5)$$

d) *F-measure (F1)*: This represents the harmonic mean of sensitivity and PPV

$$F1 = 2 * \frac{PPV * Sensitivity}{PPV + Sensitivity} \quad (6)$$

4) *Decision Tree*

This algorithm is a part of supervised learning algorithm. This algorithm can be used for solving regression problems and classification problems. The objective of this algorithm is for creating a training model that is used for predicting the class or value of wanted variable by some simple decision that is acquired from training data before. For recording a class, we have to start from the root of the tree. Hence, we compare the values of the root with the records attribute. So after comparison, we follow the branch corresponding to the value and jump to the next node.

E. *Data Mining*

K implies rich and assorted history as it is been discovered in different logical fields. This was found 50 years before. K implies is one of the most used one. K implies are comfortable to use as it is simple in execution, productivity, experimental achievement and straightforwardness. It follows a basic method, to distinguish the informational collection from particular groups that does not include K bunches fixed a priori.

For calculation it randomly takes K articles, addressing the K bunch community. This advance is for taking each guide that has a place from given informational collection and pair it to the closest focus that is dependent on the closeness of the item with bunch focus utilizing Euclidean distance. When all these processes are done, the K group habits is calculated again. This process would continue, until there is no adjustment in K bunch communities.

With the end goal of expectation, a forecast model was characterized. The working rule of the proposed mode contains four stages:

- a) *Data preprocessing*: missing qualities are replaced and inconceivable qualities with mean.
- b) *Data decrease*: by using K implies remove the inaccurately arranged information to group the data set.

c) *Classification*: by using the diminished information build a choice tree.

d) *Performance assessment*: by using a portion of the classifier assessment measurements, we have to evaluate presentation.

F. *Training and Classification of PCA with LRM*

Select UCI Repository based datasets. Start Data cleaning measure.

Find missing qualities A set W with $K \geq 2$ classes, an integer $k \geq 1$.

{Training with CIC} 1: for $j=1, \dots, K$ do

2: Partition class L_j into "k" groups. 3: end for

4: Choose Better Attributes dependent on Train classifier R utilizing all preparation information to perceive all "k.K" groups.

Require: A point "x". {Logistic Regression Classification with PCA }

1: Let $I = R(x), i=1, \dots, k, \dots, k.K$.

2: Return class of group I. 3: Display the order result.

IV. EXPERIMENTAL SETUP

By using PCA-LRN, it helped in limiting the cons of having same highlights which are of no purpose for grouping. This is possible because of interaction. Since the decrease in the quantity of factors in the first informational index helped with taking care of boisterous and exception information, PCA-LRM in this way improved our k-implies result. The fundamental benefit of PCA-LRM is that whenever we have discovered these Principal Components from the information and we can pack the information i.e., by decreasing the quantity of measurements absent a lot of loss of data, it turned into a fundamental interaction to decide the quantity of groups and give a factual system to display the bunch structure. The productivity and exactness of any prescient and indicative model is of fundamental significance and ought to be guaranteed before a particularly model is sent for execution. We dissected and assessed our model yield utilizing diverse assessment measurements, and the outcome is appeared. To begin with, to decide the presentation of our model, we used the k-fold cross approval strategy, which permits us to decide how well our model will perform when given new and recently untaught information. Our decision of the 10-overlap cross approval implied that our dataset was separated into 10 subsets.

In the beginning of all the steps, one subset is been used as the test set and the remaining are used as the preparation set. At this point, the general mistake present on every 10 preliminaries was registered in order to acquire the complete qualities of the model. This will make overcome two issues: it nearly nullifies the issue of inclination as practically the entirety

of the information is utilized for fitting, and also, the issue of difference is incredibly decreased.

A. Dataset Description

The Pima Indian Diabetes dataset acquired from UCI store of AI was used for this examination. The dataset is included 768 example female patients from the Arizona, USA populace who were analyzed for diabetes. The dataset has an aggregate of 8 ascribes (addressing clinical analysis models) with one objective class (which addresses the situation with each tried person). In the dataset there is a sum of 268 tried positive examples and 500 tried negative cases. The ascribes in the dataset incorporate the accompanying:

- Number of times pregnant (Preg)
- Plasma glucose focus at 2hr in an oral glucose resilience test (Plas)
- Diastolic Blood pressure (Pres)
- Triceps skin crease thickness (Skin)
- 2-hr serum insulin (Insu)
- Body mass file (BMI)
- Diabetes family work (Pedi)
- Age
- Target Variable (Diag)

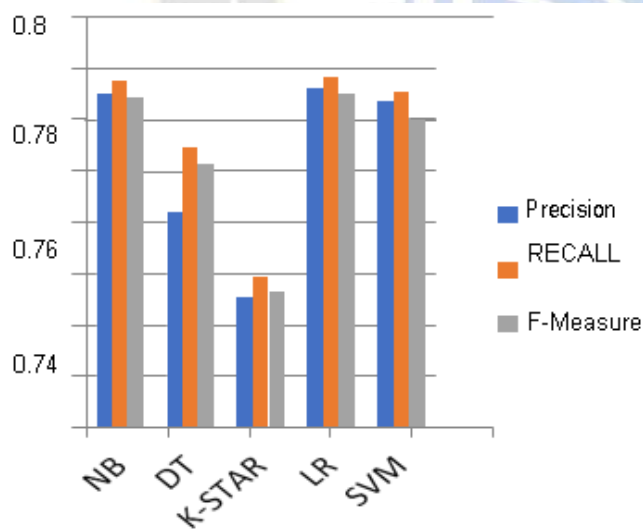


Figure 2. Performance comparison of Algorithms

Despite the fact that PCA with LRM is a notable method, its productivity in improving k-implies bunching and thusly the strategic relapse grouping model has not been given adequate consideration. Through our investigation we have shown that an improved calculated relapse model for anticipating diabetes is conceivable through the joining of PCA with LRM.

TABLE I. PERFORMANCE OF MACHINELEARNING ALGORITHMS

Classification Algorithms	Accuracy	Precision	Recall	Score F1	Score F2	Score F3
Logistic Regression Learning	98.25%	0.9830	0.9820	0.9825	0.9822	0.9821
SVM	97.88%	0.9791	0.9789	0.9710	0.9710	0.9710
Naïve Bayes Classification	91.81%	0.9190	0.9180	0.9185	0.9182	0.9181
K Star	97.08%	0.9710	0.9710	0.9710	0.9710	0.9710
Decision Tree Method	91.81%	0.9200	0.9180	0.9190	0.9184	0.9182

Table shows the results for testing data of each node, random decision tree considered randomly chosen k attributes without performing pruning. The SMO method made use of John Platt’s optimization algorithm for training SVM. KNN selected an appropriate k based on cross validation and performs distance weighting for learning. Figure 3 compared the performance of the all eight classifiers in terms of F3 score. The simple logistic regression (SLR) learning model, SVM learning with stochastic gradient descent (SGD) optimization and multilayer perceptron network (MLP) showed better performance in terms of F3 score than the other five classification algorithms.

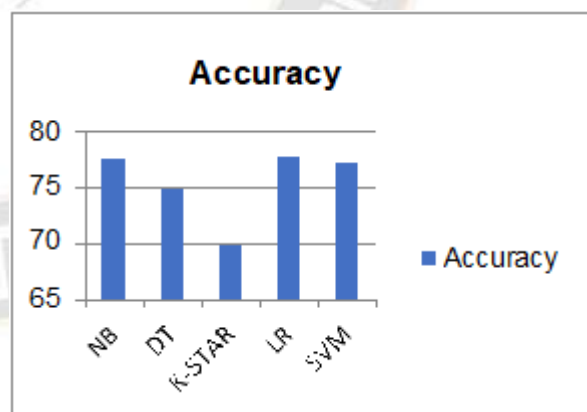


Figure 3. Classification Results in term of the Accuracy

B. Using Different Classifiers

Using different classification algorithms for the classification of the HD dataset shows very promising results in term of the classification accuracy for the K-NN (K = 1), p.s. all other k values gave similar accuracy, when sensitivity analysis was done on the K-NN classifier, Decision tree compared to

Naïve Bayes, SVM, Decision Table and Adaboost classifiers, with accuracy of classification of 99.7073, 98.0488 and 97.2683% respectively, with Kappa statistic value of 0.9941, 0.961 and 0.9454 respectively, and it was mentioned earlier, kappa statistics value implies the accuracy of the classification algorithm used as it intent to reach 1.

V. CONCLUSION

The interest achieved in the assessment joins, the ability to secure an improved k- suggests pack result far above what various experts have gotten in relative examinations. Moreover the essential backslide model performed at an improved level in expecting diabetes starting, when diverged from the results gained when various figuring where used in our examination and that of various assessments. Another advantage is the way that our model can show another dataset adequately.

This proposal was to prepare a productive model for the prediction or foreseeing the diabetes. After researching on other works, we put forwarded a innovative novel model, where it uses PCA with LRN for decrease in dimensions, K implies for assorting and to characterize, we use calculated relapse. At start we applied PCA strategy in order to improve the K implies consequence of different scientists.

The curiosity accomplished in the examination incorporates, the capacity to get an upgraded k-implies group result far above what different specialists have gotten in comparative investigations. Likewise the calculated relapse model performed at an improved level in anticipating diabetes beginning, when contrasted with the outcomes got when different calculations where utilized in our investigation and that of different examinations. Another benefit is the way that our model can demonstrate another dataset effectively.

REFERENCES

- [1] Riccardo B, Blaz Z. "Prescient information mining in clinical medication: recent concerns and rules". *Int J Med Inf* 2008;77:81–97.
- [2] Mechelle Gittens, Reco King, Curtis Gittens and Adrian Als, "Post- conclusion Management of Diabetes through a Mobile Health Consultation Application", 2014 IEEE sixteenth International Conference on e-Health Networking, Applications and Services(Healthcom).
- [3] Marcano-Cede~no Alexis, Torres Joaquín, Andina Diego. "A forecast model to diabetes utilizing fake metaplasticity" *IWINAC 2011, Part II. LNCS 6687*; 2011. p. 418–25.
- [4] Veena Vijayan V. furthermore, Anjali C."Decision emotionally supportive networks for anticipating diabetes mellitus– a survey" *Procedures of 2015 worldwide meeting on correspondence innovations (GCCT 2015)*.
- [5] Ms. K Sowjanya, MobDBTest: "An AI based framework for anticipating diabetes hazard utilizing cell phones" 2015 IEEE International Advance Computing Conference (IACC).
- [6] Gang Shi, Shanshan Liu and Ding Ye"Design and Implementation of Diabetes Risk Assessment Model Based On Mobile Things" 2015 seventh International Conference on Information Technology in Medicine and Education.
- [7] Juntao Wang and Xiaolong Su "An improved K-Means grouping calculation" 2011 IEEE third International Conference on Communication Software and Networks (ICCSN).
- [8] Yanhui Sun, Liying Fang and Pu Wang,"Improved k-implies bunching dependent on Efros distance for longitudinal information" 2016 Chinese Control and Decision Conference (CCDC).
- [9] Shunye Wang, "Improved K-implies bunching calculation dependent on the enhanced starting centroids" 2013 third International Conference on Computer Science and Network Technology(ICCSNT).
- [10] Phattarat Songthung and Kunwadee Sripanidkulchai, "Improving Type 2 Diabetes Mellitus Risk Prediction Using Classification" 2016 thirteenth International Joint Conference on Computer Science and Software Engineering (JCSSE).
- [11] Madhavaram Swapna, D.William Albert (2021). Minimal Rule Based Classifier on Diabetic Dataset Using Machine Learning Techniques. *International Journal of Computer Engineering in Research Trends*, 8(12), 204-210.
- [12] Sarangam Kodati, R P. Singh (2017).Comparative Performance Analysis of Different Data Mining Techniques and Tools Using in Diabetic Disease. *International Journal of Computer Engineering in Research Trends*, 4(12), 556-561.
- [13] Ghatage Trupti B, Takmare Sachin B(2016). High Dimensional Data Clustering with Hub Based DEC. *International Journal of Computer Engineering in Research Trends*, 3(2), 62-66.
- [14] Kumar, M. & Pathak, Rashmi & Gunjan, Vinit. (2022). Diagnosis and Medicine Prediction for COVID-19 Using Machine Learning Approach. 10.1007/978-981-16-8484-5_10.

[Home](#) > [Multimedia Systems](#) > ArticleRegular Paper | [Published: 03 August 2023](#)

Affect sensing from smartphones through touch and motion contexts

[Susmi Jacob](#) , [P. Vinod](#), [Arjun Subramanian](#) & [Varun G. Menon](#)[Multimedia Systems](#) **29**, 2495–2509 (2023)106 Accesses | [Metrics](#)

Abstract

Affect state of a person has an impact on the intellectual processes that control human behavior. Experiencing negative affect escalates mental problems, and experiencing positive affect states improve imaginative reasoning and thereby enhances one's behavior and discipline. Hence, this work centers around affect acknowledgment from typing-based context data during the pandemic. In this paper, we present a novel sensing scheme that perceives one's affect state from their unique contexts. We also aim to study how affect states vary in smartphone users during the pandemic. We collected data from 52 participants over 2 months with an Android application. We exploited the Circumplex Model of Affect (CMA) to infer 25 affect states, leveraging built-in motion and touch sensors on smartphones. We conducted comprehensive experiments by developing machine learning models to predict 25 states. Through our study, we observe that the states of users are heavily pertinent to one's typing and motion contexts. A thorough evaluation shows that affect prediction model yields an F1-score of 0.90 utilizing diverse contexts. To the best of our knowledge, our work predicts the highest number of affect states (25 states) with better performance compared to state-of-the-art methods.

This is a preview of subscription content, [access via your institution](#).

Access options

Buy article PDF

Your Privacy

We use cookies to make sure that our website works properly, as well as some optional cookies to personalise content and advertising, provide social media features and analyse how people use our site. By accepting some or all optional cookies you give consent to the processing of your personal data, including transfer to third parties, some in countries outside of the European Economic Area that do not offer the same data protection standards as the country where you live. You can decide which optional cookies to accept by clicking on "Manage preferences", where you can also find more information about how your personal data is processed. Further information can be found in our privacy policy.

[Accept all cookies](#)[Manage preferences](#)

Data availability

The dataset generated and analyzed during the current study are not publicly available due to the privacy concerns of the participants but the anonymized data are available from the corresponding author on reasonable request.

References

1. Gillan, C.M., Rutledge, R.B.: Smartphones and the neuroscience of mental health. *Ann. Rev. Neurosci.* **44**, 129–151 (2021)
2. Lex, E., Kowald, D., Seitlinger, P., Tran, T.N.T., Felfernig, A., Schedl, M.: *Psychology-Informed Recommender Systems*. Now Publishers, Hanover (2021)
3. Sher, L.: The impact of the COVID-19 pandemic on suicide rates. *QJM: Int. J. Med.* **113**(10), 707–712 (2020)
4. Rudokaite, D., Indriuniene, V.: Effectiveness of psychodrama for mitigating school fears among senior secondary school students. *Zeitschrift für Psychodrama und Soziometrie* **18**(2), 369–385 (2019)
5. Huang, P.H.: Boost: improving mindfulness, thinking, and diversity. *Wm. & Mary Bus. L. Rev.* **10**, 139 (2018)
6. Wu, W., Chen, L., Zhao, Y.: Personalizing recommendation diversity based on user personality. *User Model. User Adapt. Interact.* **28**(3), 237–276 (2018)
7. Trisha, M., Guhan, P., Bhattacharya, U., Chandra, R., Bera, A., Manocha, D.: EmotiCon: context-aware multi-modal emotion recognition using Frege's principle. In: *Proceedings of the IEEE/CVF Conference on Computer Vision and Pattern Recognition*, pp. 14234–14243 (2020)
8. Alexandros, Z., Khan, A., Kalogridis, G., Vatsikas, S., Lewis, T., Sooriyabandara, M.: HealthyOffice: mood recognition at work using smartphones and wearable sensors. In: *2016 IEEE International Conference on Pervasive Computing and Communication Workshops (PerCom Workshops)*, pp. 1–6. IEEE (2016)

Your Privacy

We use cookies to make sure that our website works properly, as well as some optional cookies to personalise content and advertising, provide social media features and analyse how people use our site. By accepting some or all optional cookies you give consent to the processing of your personal data, including transfer to third parties, some in countries outside of the European Economic Area that do not offer the same data protection standards as the country where you live. You can decide which optional cookies to accept by clicking on "Manage preferences", where you can also find more information about how your personal data is processed. Further information can be found in our privacy policy.

10. Russell, J.A.: A circumplex model of affect. *J. Personal. Soc. Psychol.* **39**(6), 1161 (1980)

11. Samuel, O., Walker, G., Salmon, P., Filtness, A., Stevens, N., Mulvihill, C., Stanton, N.: Riding the emotional roller-coaster: using the circumplex model of affect to model motorcycle riders' emotional state-changes at intersections. *Transp. Res. Part F Traffic Psychol. Behav.* **66**, 139–150 (2019)

12. Stanisławski, K., Ciecuch, J., Strus, W.: Ellipse rather than a circumplex: a systematic test of various circumplexes of emotions. *Personal. Individ. Diff.* **181**, 111052 (2021)

13. Girardi, D., Lanubile, F., Novielli, N.: Emotion detection using noninvasive low cost sensors. In: 2017 Seventh International Conference on Affective Computing and Intelligent Interaction (ACII), pp. 125–130. IEEE (2017)

14. LiKamWa, R., Liu, Y., Lane, N. D., Zhong, L.: Moodscope: building a mood sensor from smartphone usage patterns. In: Proceeding of the 11th Annual International Conference on Mobile Systems, Applications, and Services, pp. 389–402 (2013)

15. Evmenenko, A., Teixeira, D.S.: The circumplex model of affect in physical activity contexts: a systematic review. *Int. J. Sport Exerc. Psychol.* **20**(1), 168–201 (2022)

16. Fernández-Caballero, A., Martínez-Rodrigo, A., Pastor, J.M., Castillo, J.C., Lozano-Monator, E., López, M.T., Fernández-Sotos, A.: Smart environment architecture for emotion detection and regulation. *J. Biomed. Inform.* **64**, 55–73 (2016)

17. Morshed, M.B., Saha, K., Li, R., D'Mello, S.K., De Choudhury, M., Abowd, G.D., Plötz, T.: Prediction of mood instability with passive sensing. *Proc. ACM Interact. Mobile Wearable Ubiquitous Technol.* **3**(3), 1–21 (2019)

18. Piskioulis, O., Tzafilkou, K., Economides, A.: Emotion detection through

Your Privacy

We use cookies to make sure that our website works properly, as well as some optional cookies to personalise content and advertising, provide social media features and analyse how people use our site. By accepting some or all optional cookies you give consent to the processing of your personal data, including transfer to third parties, some in countries outside of the European Economic Area that do not offer the same data protection standards as the country where you live. You can decide which optional cookies to accept by clicking on "Manage preferences", where you can also find more information about how your personal data is processed. Further information can be found in our privacy policy.

-
20. Wampfler, R., Klingler, S., Solenthaler, B., Schinazi, V. R., Gross, M.: Affective state prediction based on semi-supervised learning from smartphone touch data. In: Proceedings of the 2020 CHI Conference on Human Factors in Computing Systems, pp. 1–13 (2020). <https://doi.org/10.1145/3313831.3376504>
-
21. Hashmi, M.A., Riaz, Q., Zeeshan, M., Shahzad, M., Fraz, M.M.: Motion reveal emotions: identifying emotions from human walk using chest mounted smartphone. *IEEE Sens. J.* **20**(22), 13511–13522 (2020)
-
22. Balducci, F., Impedovo, D., Macchiarulo, N., Pirlo, G.: Affective states recognition through touch dynamics. *Multimed. Tools Appl.* **79**(47), 35909–35926 (2020)
-
23. Wang, P., Dong, L., Liu, W., Jing, N.: Clustering-based emotion recognition micro-service cloud framework for mobile computing. *IEEE Access* **8**, 49695–49704 (2020)
-
24. Ruensuk, M., Oh, H., Cheon, E., Oakley, I., Hong, H.: Detecting negative emotions during social media use on smartphones. In: Proceedings of Asian CHI Symposium 2019: Emerging HCI Research Collection, pp. 73–79 (2019)
-
25. Tikadar, S., Bhattacharya, S.: A novel method to build and validate an affective state prediction model from touch-typing. In: IFIP Conference on Human-Computer Interaction, pp. 99–119. Springer, Cham (2019)
-
26. Ghandeharioun, A., McDuff, D., Czerwinski, M., Rowan, K.: Emma: an emotion-aware well-being chatbot. In: 2019 8th International Conference on Affective Computing and Intelligent Interaction (ACII), pp. 1–7. IEEE (2019). <https://doi.org/10.1109/ACII.2019.8925455>
-
27. Ghosh, S., Sahu, S., Ganguly, N., Mitra, B., De, P.: EmoKey: an emotion-aware smartphone keyboard for mental health monitoring. In: 2019 11th International Conference on Communication Systems & Networks

Your Privacy

We use cookies to make sure that our website works properly, as well as some optional cookies to personalise content and advertising, provide social media features and analyse how people use our site. By accepting some or all optional cookies you give consent to the processing of your personal data, including transfer to third parties, some in countries outside of the European Economic Area that do not offer the same data protection standards as the country where you live. You can decide which optional cookies to accept by clicking on "Manage preferences", where you can also find more information about how your personal data is processed. Further information can be found in our privacy policy.

Wearable Ubiquitous Technol. **1**(4), 1–30 (2018).

<https://doi.org/10.1145/3161414>

29. Gloor, P.: Consistent excitement correlates with happiness-Predicting mood through body sensing with smartwatches. ICKN White Pap (2017)

30. Ma, Y., Xu, B., Bai, Y., Sun, G., Zhu, R.: Daily mood assessment based on mobile phone sensing. In: 2012 Ninth International Conference on Wearable and Implantable Body Sensor Networks, pp. 142–147. IEEE (2012) <https://doi.org/10.1109/BSN.2012.3>

31. Yang, N., Samuel, A.: Context-rich detection of user's emotions using a smartphone. Microsoft Research Internship Report (2011)

32. Sultana, M., Al-Jefri, M., Lee, J.: Using machine learning and smartphone and smartwatch data to detect emotional states and transitions: exploratory study. JMIR mHealth uHealth **8**(9), e17818 (2020)

33. Budner, P., Eirich, J., Gloor, P.A.: Making you happy makes me happy—Measuring Individual Mood with Smartwatches (2017) arXiv preprint [arXiv:1711.06134](https://arxiv.org/abs/1711.06134)

34. Cortes, C., Vapnik, V.: Mach. Learn. Support-vector networks **20**(3), 273–297 (1995)

35. Ali, J., Khan, R., Ahmad, N., Maqsood, I.: Random forests and decision trees. Int. J. Comput. Sci. Issues (IJCSI) **9**(5), 272 (2012)

36. Ghosh, S., Hiware, K., Ganguly, N., Mitra, B., De, P.: Emotion detection from touch interactions during text entry on smartphones. Int. J. Hum. Comput. Stud. **130**, 47–57 (2019)

37. Salido Ortega, M.G., Rodríguez, L.F., Gutierrez-Garcia, J.O.: Towards emotion recognition from contextual information using machine learning. J. Amb. Intell. Humaniz. Comput. **11**(8), 3187–3207 (2020). <https://doi.org/10.1007/s12652-019-01485-x>

Your Privacy

We use cookies to make sure that our website works properly, as well as some optional cookies to personalise content and advertising, provide social media features and analyse how people use our site. By accepting some or all optional cookies you give consent to the processing of your personal data, including transfer to third parties, some in countries outside of the European Economic Area that do not offer the same data protection standards as the country where you live. You can decide which optional cookies to accept by clicking on "Manage preferences", where you can also find more information about how your personal data is processed. Further information can be found in our privacy policy.

Biology Society, pp. 5368–5371. IEEE (2011)

-
40. Riva, G., Calvo, R.A., Lisetti, C.: Cyberpsychology and affective computing. In: *The Oxford Handbook of Affective Computing*, pp 547–558 (2015)
-
41. Marshall, J., Wang, D.: Mood-sensitive truth discovery for reliable recommendation systems in social sensing. In: *Proceedings of the 10th ACM conference on recommender systems*, pp 167–174 (2016)
-
42. Álvarez, P., Zarazaga-Soria, F.J., Baldassarri, S.: Mobile music recommendations for runners based on location and emotions: the dj-running system. *Pervasive Mobile Comput.* **67**, 101242 (2020)

Funding

The authors have not received any funding for the execution of this work.

Author information

Authors and Affiliations

Department of Computer Science and Engineering, SCMS School of Engineering and Technology, Karukutty, Kerala, India

Susmi Jacob, Arjun Subramanian & Varun G. Menon

APJ Abdul Kalam Technological University, Thiruvananthapuram, Kerala, India

Susmi Jacob, Arjun Subramanian & Varun G. Menon

Department of Computer Applications, Cochin University of Science and Technology, Cochin, Kerala, India

P. Vinod

Department of Mathematics, University of Padua, Padua, Italy

P. Vinod

Contributions

SJ and PV wrote, revised, and corrected the main manuscript. AS and SJ did data collection, experiments, and analysis. PV. and VGM supervised the conceptualization, ideation, and implementation of the work. All authors reviewed the manuscript

Corresponding author

Your Privacy

We use cookies to make sure that our website works properly, as well as some optional cookies to personalise content and advertising, provide social media features and analyse how people use our site. By accepting some or all optional cookies you give consent to the processing of your personal data, including transfer to third parties, some in countries outside of the European Economic Area that do not offer the same data protection standards as the country where you live. You can decide which optional cookies to accept by clicking on "Manage preferences", where you can also find more information about how your personal data is processed. Further information can be found in our privacy policy.

relevant to the content of this article.

Additional information

Communicated by B. Bao.

Publisher's Note

Springer Nature remains neutral with regard to jurisdictional claims in published maps and institutional affiliations.

Rights and permissions

Springer Nature or its licensor (e.g. a society or other partner) holds exclusive rights to this article under a publishing agreement with the author(s) or other rightsholder(s); author self-archiving of the accepted manuscript version of this article is solely governed by the terms of such publishing agreement and applicable law.

[Reprints and Permissions](#)

About this article

Cite this article

Jacob, S., Vinod, P., Subramanian, A. *et al.* Affect sensing from smartphones through touch and motion contexts. *Multimedia Systems* **29**, 2495–2509 (2023).

<https://doi.org/10.1007/s00530-023-01142-6>

Received	Accepted	Published
27 January 2023	17 July 2023	03 August 2023

Issue Date
October 2023

DOI
<https://doi.org/10.1007/s00530-023-01142-6>

Keywords

[Context awareness](#) [Emotion sensing](#) [Affect sensing](#) [Mood sensing](#)

[Machine learning model](#) [Smartphone sensing](#) [Circumplex model](#)

Your Privacy

We use cookies to make sure that our website works properly, as well as some optional cookies to personalise content and advertising, provide social media features and analyse how people use our site. By accepting some or all optional cookies you give consent to the processing of your personal data, including transfer to third parties, some in countries outside of the European Economic Area that do not offer the same data protection standards as the country where you live. You can decide which optional cookies to accept by clicking on "Manage preferences", where you can also find more information about how your personal data is processed. Further information can be found in our privacy policy.

Your Privacy

We use cookies to make sure that our website works properly, as well as some optional cookies to personalise content and advertising, provide social media features and analyse how people use our site. By accepting some or all optional cookies you give consent to the processing of your personal data, including transfer to third parties, some in countries outside of the European Economic Area that do not offer the same data protection standards as the country where you live. You can decide which optional cookies to accept by clicking on "Manage preferences", where you can also find more information about how your personal data is processed. Further information can be found in our privacy policy.

ULTRA-LOW-LATENCY AND RELIABLE COMMUNICATIONS FOR FUTURE WIRELESS NETWORKS



Muhammad Ikram
Ashraf

Mohsen Guizani

Varun G. Menon

Shahid Mumtaz

We are delighted to introduce the special section on Ultra-Low Latency and Reliable Communications for Future Wireless Network. This issue introduces five high quality articles presenting discussions on new techniques and concepts, standards, future applications, network architectures, challenges, and promising solutions for ultra-high speed, low latency, and reliable communications in future networks. In the following, we will introduce these articles and highlight their main contributions.

The article entitled, “Communication and Computation O-RAN Resource Slicing for URLLC Services Using Deep Reinforcement Learning,” presents and discusses a two-level RAN slicing approach based on the O-RAN architecture to allocate the communication and computation RAN resources among URLLC end-devices. For each RAN slicing level, resource slicing problem as a single-agent Markov decision process is modeled, along with a deep reinforcement learning algorithm to solve it. The simulation results presented demonstrates the efficiency of the proposed approach in meeting the desired quality of service requirements.

In the article entitled, “Distributed Computation Offloading with Low Latency for Artificial Intelligence in Vehicular Networking,” the authors proposes a distributed computation offloading scheme which can be used to outsource the tasks of AI model computation to nearby vehicles and road side units in vehicular networking. Here, to alleviate the computational burden and reduce the latency of the computation at the vehicle side, the improved genetic algorithm is used to divide the computation of the sigmoid function into multiple sub-tasks.

The article entitled, “Device-to-Device Communications at the TeraHertz Band: Open Challenges for Realistic Implementation,” presents a comprehensive and interesting discussion on Terahertz channel modeling, communications, and offloading mechanisms. Here, the authors investigate the possibility to make effective use of the THz band for D2D communication.

The article, “Dimensioning Spectrum to Support Ultra-Reliable Low-Latency Communication,” presents an analysis to indicate that the bandwidth needed to meet URLLC goals can be in the order of gigahertz, beyond what is available in today’s mobile networks. Network densification can ease those bandwidth needs but requires new deployment strategies involving substantially larger numbers of sites. As an alternative, multi-connectivity and multi-operator network sharing are considered as efficient ways to reduce the demand for bandwidth without outright deployment of additional base stations.

The article, “Federated Learning Encounters 6G Wireless Communication in the Scenario of Internet of Things,” presents and discusses a novel federated learning architecture integrating 6G, called super-wireless-air federated learning framework, which enables data privacy protection and adapts to complex IoT scenarios. Further the authors present the detailed system design and key technologies of the proposed architecture.

We would like to express our sincere thanks to all the authors for submitting their articles and to the reviewers for their valuable comments and suggestions that significantly enhanced the quality of these articles. We are also grateful to Prof. Zander Lei, for the great support throughout the whole review and publication process of this series, and, of course, all the editorial staff. We hope that this special issue will serve as a useful reference for researchers, scientists, engineers, and academics in the field of Ultra-low Latency and Reliable Communications for Future Wireless Networks.

BIOGRAPHIES

MUHAMMAD IKRAM ASHRAF (ikram.ashraf@nokia-bell-labs.com) received his M.Sc. and Ph.D. in telecommunication systems and communication engineering, respectively, from the University of Oulu, Finland. He is currently working as a Senior Research Specialist, 5G Advanced, at Nokia Bell Labs, Espoo Finland. Prior to that, he worked as an experienced researcher in Network Architecture and Protocols at Ericsson Research in Jorvas, Finland. He has contributed to several technical papers, invention disclosures, and 3GPP. His research interests include 5G Advanced, AI/ML, Industry 4.0, XR, positioning, IoT, V2X, UAV, URLLC, and TSN. He is serving as a series editor of *IEEE Communication Standards Magazine* on Ultra-Low-Latency, and Reliable Communications for Future Wireless Networks, an associate editor of *IET Quantum Communication*, and a guest editor of Elsevier’s *Journal of Industrial Information Integration* Special Issue on Data/Information Integration Techniques in Industry 4.0/5.0. Prior to that, he served as an editor of *IEEE Communication Standards Magazine*, a guest editor of *IEEE Wireless Communications*, an editor of *IEEE Transactions on Cognitive Communications and Networking*, and a guest editor of *IEEE Network*.

MOHSEN GUIZANI [F] (mguizani@qu.edu.qa) received his B.S. (with Distinction), M.S., and Ph.D. in electrical and computer engineering from Syracuse University, New York. He is currently a Professor with the Computer Science and Engineering Department, Qatar University. He worked in different institutions: the University of Idaho, Western Michigan University, the University of West Florida, the University of Missouri-Kansas City, the University of Colorado-Boulder, and Syracuse University. He has authored nine books and more than 800 publications. His research interests include wireless communications and mobile computing, applied machine learning, cloud computing, security, and its application to healthcare systems. He has won several research awards, including the 2015 IEEE Communications Society Best Survey Paper Award as well as four best paper awards from IEEE ICC and GLOBECOM conferences. He is also the recipient of the 2017 IEEE Communications Society Wireless Technical Committee Recognition Award, the 2018 AdHoc Technical Committee Recognition Award, and the 2019 IEEE Communications and Information Security Technical Recognition Award. He served as the editor-in-chief of *IEEE Network* and currently serves on the

editorial boards of many IEEE journals/transactions. He was the chair of the IEEE Communications Society Wireless Technical Committee and the chair of the TAOS Technical Committee. He served as an IEEE Computer Society Distinguished Speaker and is currently an IEEE ComSoc Distinguished Lecturer. He was listed as a Clarivate Analytics Highly Cited Researcher in Computer Science in 2019 and 2020.

VARUN G. MENON [SM] (varungmenon46@gmail.com) is currently a Professor, the Head of the Department of Computer Science Engineering, and is in charge of International Collaborations at SCMS School of Engineering and Technology, India. He is a Distinguished Speaker of ACM. He is currently an associate editor of Physical Communications, IET Networks, IET Quantum Communications, series editor of IEEE Transactions on Intelligent Transportation Systems, and technical editor of Computer Communications. He was the guest associate editor of *IEEE Journal of Biomedical and Health Informatics*, *IEEE Internet of Things Journal*, *IEEE Transactions on Green Communications and Networking*, *IEEE IoT Magazine*, *IEEE Transactions on Industry Informatics*, and *Journal of Supercomputing*. He received the Top Peer Reviewer Award by Publons in 2018 and 2019. He is also currently serving in the Review Boards of many high impact factor journals, including *IEEE Transactions on Vehicular Technology*, *IEEE Transactions on Communications*, *IEEE Communications Magazine*, *IEEE Transactions on Industrial Informatics*, and *IEEE Transactions on Intelligent Transportation Systems*. He has served over 20 conferences, like IEEE ICC 2021, IEEE CAMAD 2021, IEEE ICC 2020, EAI SmartGov

2021, ICCCN 2020, IEEE COINS 2020, and SigTelCom, in leadership capacities, including program co-chair, track chair, session chair, and technical program committee member. He has completed his Ph.D. in Computer Science and Engineering and holds an M. Tech degree in Computer and Communication with University First Rank. He also holds an M.Sc. in Applied Psychology, an MBA in Human Resource Management, and a Diploma in Training and Development. His research interests include Sensor Technologies, Internet of Things, Green IoT, Wireless Communication, Fog Computing and Networking.

SHAHID MUMTAZ (smumtaz@av.it.pt) is with Instituto de Telecomunicacoes, Portugal, and an IET Fellow, an IEEE ComSoc and ACM Distinguished Lecturer, a recipient of the IEEE ComSoc Young Researcher Award, founder and Editor-in-Chief of IET's *Journal of Quantum Communication*, Editor-in-Chief of the *Alexandria Engineering Journal* (Elsevier), Vice-Chair, Europe/Africa Region – IEEE ComSoc Green Communications & Computing Society, and Vice-Chair for IEEE Standard P1932.1, "Standard for Licensed/Unlicensed Spectrum Interoperability in Wireless Mobile Networks." His work has resulted in technology transfer to companies and patented technology. His expertise lies in 5G/6G wireless technologies using AI/ML and digital twin (VR/XR) tools and innovation paths in industry and academia. Moreover, he worked as a senior 5G consultant at Huawei and InterDigital, where he contributed to RAN1/RAN2 and looked after the university-industrial collaborative projects.



Search Article

SEARCH

Impact Factor (SJIF): 6.092 E-ISSN: 2583-1615

INTERNATIONAL JOURNAL OF RESEARCH IN ACADEMIC WORLD

Multidisciplinary

Refereed Journal

Peer Reviewed Journal

HOME

EDITORIAL BOARD

ARCHIVES

INSTRUCTIONS

INDEXING

SUBMIT MANUSCRIPT

CONTACT US

INTERNATIONAL JOURNAL OF RESEARCH IN ACADEMIC WORLD

VOL.: 2 ISSUE.: 10(OCTOBER 2023)

DDoS Attack Detection on Botnet Devices

Author(s): Rosebell Paul and Shilpa M

Abstract:

The high surge in the number of devices connected by the Internet of Things (IoT) causes several challenges to the security of data and users, leaving the Internet open to various threats. IoT networks faces several challenges that call for the evolution of traditional internet topology. Network security has recently become more important due to the significant damage that DDoS poses to it. DDoS assaults are now frequent as cyber threats because of the expansion of IoT devices, their complexity, and the use of attack services. A DDoS attack prevents actual internet users from using the suspect's services. IoT device failures and data theft are being caused more frequently by DDoS attacks on IoT devices. In response to this growing threat, new techniques are being developed to identify and halt attack traffic from IoT botnets. Recent anomaly detection experiments using machine learning (ML) have demonstrated its potential to identify malicious Internet traffic. Unreliable customer IoT devices have been used to perform distributed denial of service (DDoS) attacks against crucial Internet infrastructure botnets like Mirai to launch distributed denial of service (DDoS) assaults against vital Internet infrastructure. A distributed denial-of-service (DDoS) attack is a malicious attempt to delay a server, service, or its working system with an excessive volume of Web traffic. By using numerous compromised computer systems as sources of attack traffic, DDoS attacks are made effective. Computers and other networked resources, like as IoT devices, can be exploited machines. This promotes the development of novel methods to immediately identify consumer IoT attack traffic. In this study, we use a variety of machine learning classifiers to identify DDoS attacks coming from botnet-infected IoT devices.

Keywords: DDoS attack, IoT devices, Machine learning classifier**Pages:** 32-36 | **8 View** | **1 Download**[DOWNLOAD](#)**How to Cite this Article:**

Rosebell Paul and Shilpa M. DDoS Attack Detection on Botnet Devices. Int. J Res. Acad. World. 2023;2(10):32-36

QUICK LINKS

[Aim & Scope](#)
[Manuscript Presentation](#)
[Publication Fee](#)
[Helpline No.: 9289291589](#)

[Current Issue](#)
[Submit Manuscript](#)
[Publication Certificate](#)
[Peer-review & Publication Policy](#)

[About Journals](#)
[Copyright Form](#)
[Indexing](#)
[Publication Ethics](#)

© 2021-2023. All Rights Reserved. International Journal of Research in Academic World
 E-mail: editor.academicworld@gmail.com





Role of deep learning models and analytics in industrial multimedia environment

Nawab Muhammad Faseeh Qureshi¹ · Varun G. Menon² · Ali Kashif Bashir³ · Shahid Mumtaz⁴ · Irfan Mehmood⁵

Published online: 4 May 2023

© The Author(s), under exclusive licence to Springer-Verlag GmbH Germany, part of Springer Nature 2023

Deep learning models and data-driven intelligent analytics are widely used components of artificial intelligence. Deep learning models discover features through autonomous or representation learning and process them through artificial neural networks to retrieve the desired results. There are several base types of deep learning models, such as radial basis function networks (RBFN), recurrent neural networks (RNN), generative-adversarial-networks (GANs), long-short-term memory networks (LSTMs), convolutional neural networks (CNNs), self-organizing maps (SOM), restricted Boltzmann machines (RBM), autoencoders, and multilayer-perceptron (MLP). These types depend on the requirement; for example, the autoencoder is designed to transform input data into a different representation, such as re-generating or re-constructing an image. In the same way, self-organizing maps are created to solve high-dimensional data that consist of the number of features that are larger than the number of observations and use the winning weight award technique to choose distinct features in the high-dimensional complex data. The industrial multimedia data that include hypermedia, hypertext, graphics having 2D and 3D formats, 3D animation, and audio and video types are fragile and complex. And, with the variety of base deep learning models, it is difficult to understand how we use a particular type for a specific multimedia data problem.

We observed the recent research contributions and understood the requirement of utilizing deep learning models in the industrial multimedia environment. And, sought the submissions carefully related to the topic of deep learning models having the scope of multimedia data formats only. In the response, we received various numbers of submissions out of which, a total of thirteen papers were accepted after rigorous review. We share a summary of the contributions from different parts of the world mentioned below.

The paper by Tiago do Carmo Nogueira et al. proposes a novel idea using encoder–decoder structure to extract features from reference images and gated-recurrent-units (GRUs) for creating descriptions. And they used part-of-speech (PoS) analysis to generate weights. They evaluated their technique using MS-COCO and Flickr30k datasets. They performed prediction resulting in more descriptive captions for predicted and KNN-selected captions.

The paper by Ahmed Barnawi et al. presents a new method of detecting COVID-19 using emergency services such as UAVs. They designed and proposed a transfer-learning-based deep CNN architecture to categorize patients into positive, negative, and null (pneumonia patient) categories. Using the developed model, they evaluated their technique through time-bounded services and achieved 94.92% accuracy.

The paper by Faria Nazir et al. proposes a deep learning model to address the problem of language pronunciation mistakes using speech mistakes analysis. They further divide the solution into phonemic errors (confusing phonemes) and prosodic errors (partially modified pronunciation variants of phones). They use CNN-based clustering technique to identify the faults and categorize phonemes through K-nearest neighboring technique along with Naïve Bayes mechanism, and support-vector-machine (SVM) algorithm. They evaluated the model using an Arabic dataset of 28 individuals and received an accuracy of 97% than traditional models.

The paper by Linbo Wang et al. present a collaborative transformational–spatial clustering model that identifies

✉ Nawab Muhammad Faseeh Qureshi
faseeh@skku.edu

¹ Department of Computer Education, Sungkyunkwan University, Seoul, Republic of Korea

² Department of Computer Science, SCMS School of Engineering and Technology, Kochi, India

³ Department of Computing and Mathematics, Manchester Metropolitan University, Manchester, UK

⁴ Nottingham Trent University, Nottingham, UK

⁵ Center of Visual Computing, University of Bradford, Bradford, UK

inliers with two-way proximities. They discuss the technique so that, at first, a generalized match is transformed into a collaborative transformational–spatial space. After that, a collaborative kernel density estimator maps the object with images. Finally, they fix matching proximities to enhance application on different images. They perform experiments and achieve superior performance on feature-identical jobs, such as multi-object pairing, duplicate-object pairing, and object-retrieve technique.

The paper by Loveleen Gaur et al. discusses a deep learning model that detects COVID-19 using autonomous deep convolutional neural networks. Using transfer learning, they focus on chest X-rays and evaluate three pre-trained CNN models, EfficientNetBo, VGG16, and InceptionV3. They consider the technique by measuring performance metrics, such as accuracy, recall, precision, and F1 scores. They achieve an overall accuracy of 92.92% with a sensitivity of 94.79%.

The paper by Asma Kausar et al. proposes a deep learning model to automate left-side-atrium segmentation on magnetic resonance imaging (MRI) to assist medication and diagnosis of heart surgical treatment. They discuss a three-D multi-scale residual-learning-based model to maintain granular and standard-level features through a network. They evaluated their model using the award-winning left-atrial-segmentation technique with less constraints. They claimed not to add any extensive pre-processing of input data for the said task.

The paper by Jimmy Ming-Tai Wu et al. proposes a graph-based CNN-LSTM deep learning mode and predicts stock prices having high indicators. They use a financial time series dataset onto a joint convolution neural network (CNN) and long-short-term-memory neural network (LSTM) and constructs a sequence-array of historical data with leading indicators. They evaluated their model using the USA and Taiwan stock datasets and achieved better results than existing approaches.

The paper by Gengsheng Xie et al. presents a re-identification (Re-ID) technique that focuses on a deep metric representation technique for extracting the features through a dataset. They discuss a pose-guided feature region-based fusion network (PFRFN) for using pose landmarks as local features. They evaluate the technique using various datasets, such as Market-1501, DukeMTMC, and CUHK03, and achieve improvement over traditional models.

The paper by Sumit Pundir et al. proposes an intelligent machine learning model that handles the botnet attacks through a malware detection technique in the IoT-enabled industrial multimedia environment. They use four types of methods: naïve Bayes, logistic regression, artificial neural network (ANN), and random forest, to detect the malware. They evaluate the idea and achieve 99.5% detection success having a 0.5% false positive rate.

The paper by Akshi Kumar presents a model that focuses on crowd knowledge and answers how-to-do concerns in the QA websites. For that, he develops the mechanism of Siamese neural architecture and extracts similarity-matching features. Furthermore, the training is performed through a multi-layer perceptron for predictions. And semantically matched questions are grouped to figure out the experts. He evaluated the technique by combining multi-layer perceptron and Manhattan distance function and compared the results with existing models.

Another paper by Ranran Lou et al. proposes a model to protect the ocean environment and predict the unknown elements and deep sea resource monitoring. They use a data-driven analytics approach to analyze ocean data, including sound source identification, element prediction, and physical constraints. They evaluated the model with standard ocean datasets and compared the results with existing approaches.

In the paper by Mohib Ullah Khan et al. presents a technique focusing on social media reviews for the restaurant industry. They use a novel convolutional attention-based bi-directional modified LSTM of the word, successive sequences, and patterns with aspect category detection (ACD). They extract features of public reviews as entities and attributes to further develop sequences and patterns. They compare the technique using SemEval-2015, SemEval-2016, and SentiHood datasets and achieve results with an average improvement of 79% than traditional models.

In the last, the paper by Celestine Iwendi et al. proposes an experimental analysis based on four deep learning models, such as recurrent neural network (RNNs) along with Bidirectional Long Short-Term Memory (BLSTM), Long Short-Term Memory (LSTMs), and Gated Recurrent Units (GRU), for detecting insults in the social media platform commentary. For that, they develop a method of text cleaning, tokenization, stemming, Lemmatization, and removal of stop words and perform prediction using the models. They evaluate deep learning models and share findings compared to existing models.

We are excited to share the details and hope that the research community related to deep learning models will find these articles with colossal interest and relevant to the multimedia-based deep learning models. We thank Editor-In-Chief Prof. Changsheng Xu and the editorial staff especially Garth Haller, senior publisher, for their support and collaboration in executing this special issue in the Multimedia Systems Journal.

Declarations

Conflict of interest The authors do not have any conflict of interest.

Publisher's Note Springer Nature remains neutral with regard to jurisdictional claims in published maps and institutional affiliations.

OPINION

Quantum computing in India: Recent developments and future

Varun G. Menon¹  | Mainak Adhikari²¹SCMS School of Engineering and Technology, Ernakulam, India²Indian Institute of Information Technology Lucknow, Lucknow, India**Correspondence**

Varun G. Menon.

Email: varungmenon46@gmail.com

Quantum computing combines mathematics, quantum physics, and computer science to optimise, learn, and simulate chemical, physical, and biological systems. It offers the ability to solve problems in a unique method and to speed up solutions compared to standard procedures. This computing may solve issues with intractable inputs. With the capabilities of quantum computers and the availability of quantum development kits, quantum computing is expected to become ubiquitous, and the demand for trained people is expected to rise significantly. Quantum technologies are rapidly developing globally with substantial disruptive potential. Quantum technology is opening up new frontiers in computing, communications, and cyber security with widespread applications. The range of quantum technologies is expected to be one of the significant technology disruptions that will change the entire paradigm of computation, communication, and encryption. It is perceived that the countries that achieve an edge in this emerging field will have a more significant advantage in garnering multifold economic growth and dominant leadership roles. It is expected that lots of commercial applications will emerge from the developing theoretical constructs in this area. In India, there is a growing interest in quantum computing and communication with active participation from students, developers, industry, and academia, leading to many recent initiatives and developments. This article provides an overview of some of the recent developments of quantum computing in India and the future ahead.

In its 2020 budget, the Indian government announced the National Mission on Quantum Technologies and Applications, which will be run by the Department of Science and Technology with a budget of 80 billion INR over five years [1]. Among the next-generation technologies that will be pushed by this mission are quantum computers and computing, quantum communication, quantum key distribution, cryptanalysis, quantum devices, quantum sensing, quantum materials, quantum clocks, and so on. The mission will focus on basic science, technology development, building up human and infrastructure resources,

innovation, and new businesses to solve problems that are important to the country. By putting the mission into action, India would be able to develop and use quantum computers, secure communications through fibre and free space, quantum encryption and cryptanalysis, and other related technologies. It would also be able to deal with national and regional problems that are unique to India.

International Business Machines (IBM) and the Indian Institute of Technology, Madras (IIT-Madras) joined forces in September 2022 to help India learn more about quantum computing and accelerate research [2]. With this partnership, IIT Madras becomes one of the more than 180 members of the IBM Quantum Network around the world. IIT Madras is also the "first Indian institution" to join the global community of Fortune 500 companies, start-ups, academic institutions, and research labs working with IBM quantum technology to improve quantum computing and find business uses for it. As a member of the IBM Quantum Network, IIT Madras will have cloud-based access to IBM's most advanced quantum computing systems and IBM's quantum expertise. This will allow to look into real-world applications and see how this technology can help business and society in a wide range of ways. International Business Machines has also taken a number of steps to promote quantum computing in India and make it more well-known. IBM has made Qiskit, an open-source software development kit for the quantum developer community. The textbook "Qiskit" is available in Tamil, Bengali, and Hindi, and students in India accessed it more than 30,000 times in 2021 alone. Through the IBM Quantum Educators Programme, IBM works together with some of India's best schools. For educational purposes, teachers and students at these schools will be able to use IBM Cloud to access quantum systems, quantum learning resources, and quantum tools.

With help from the National Security Council Secretariat, the Indian Army set up a laboratory for quantum computing and a centre for artificial intelligence at the Military College of

This is an open access article under the terms of the [Creative Commons Attribution License](https://creativecommons.org/licenses/by/4.0/), which permits use, distribution and reproduction in any medium, provided the original work is properly cited.

© 2023 The Authors. *IET Quantum Communication* published by John Wiley & Sons Ltd on behalf of The Institution of Engineering and Technology.



Telecommunication Engineering in Mhow, Madhya Pradesh, in December 2021 [4]. The Indian Army's work on quantum technology will help it jump to the next generation of communication and change the Indian Armed Forces' current cryptography system to Post Quantum Cryptography. Quantum key distribution, quantum communication, quantum computing, and post-quantum cryptography are all the focus areas. In July of 2021, a Memorandum of Understanding (MoU) was signed between the Defence Institute of Advanced Technology and the Centre for the Development of Advanced Computing (C-DAC) to collaborate on the study and development of quantum computers. The group is working together to develop quantum computers for both commercial and military applications. In 2020 December, a quantum random number generator was developed at India's DRDO Young Scientist Laboratory for quantum technologies. It can detect and convert random quantum events into a stream of binary numbers, and it represents a significant advancement for quantum technology in India.

There have been some more noteworthy developments in this research direction recently. Department of Science and Technology and around 13 research groups from IISER Pune have established the I-HUB Quantum Technology Foundation (I-HUB QTF). Additionally, in January 2021, a Quantum Computing Applications Lab was launched by the Ministry of Electronics and Information Technology (MeitY) in collaboration with Amazon Web Services. Projects motivated by quantum computing will receive assistance from this facility. The Centre for the Development of Telematics (C-DOT) launched its quantum communication lab in October 2021, and it is capable of communicating over 100 km of standard optical fibre [3, 4]. In February 2022, a joint team of the Defence

Research and Development Organisation (DRDO) and IIT-Delhi successfully demonstrated a Quantum Key Distribution link between two cities in UP — Prayagraj and Vindhyachal — located 100 km apart. The following are some of India's top quantum computing research groups and institutions.

- Indian Institute of Science Quantum Technology Initiative [5].
- IIT Jodhpur's Quantum Information and Computation (QIC) group [6].
- Centre for Quantum Information, Communication, and Computing (C-QuICC) at IITM [7].
- TIFR's Quantum Measurement and Control Laboratory (QuMaC) [8].
- I-Hub Quantum Technology Foundation (I-Hub QTF), IISER, Pune [9].
- Quantum Information and Computing (QuIC) lab at the Raman Research Institute, Bangalore [10].
- Quantum Information and Computation Group at Harish-Chandra Research Institute [11].

A quantum computer is extremely challenging to design, construct, and write code on due to its robust nature. It should not be surprising how challenging it will be to train an AI model to recognise things within a picture. Quantum computers and programs are susceptible to errors in noise and defects, as well as a loss of quantum coherence, because of the complex nature of quantum computing. As the number of qubits increases, it becomes increasingly difficult to maintain the isolation of these qubits from their surroundings. As a result, decoherence is almost certain to occur, which results in several errors being introduced. Some of the major

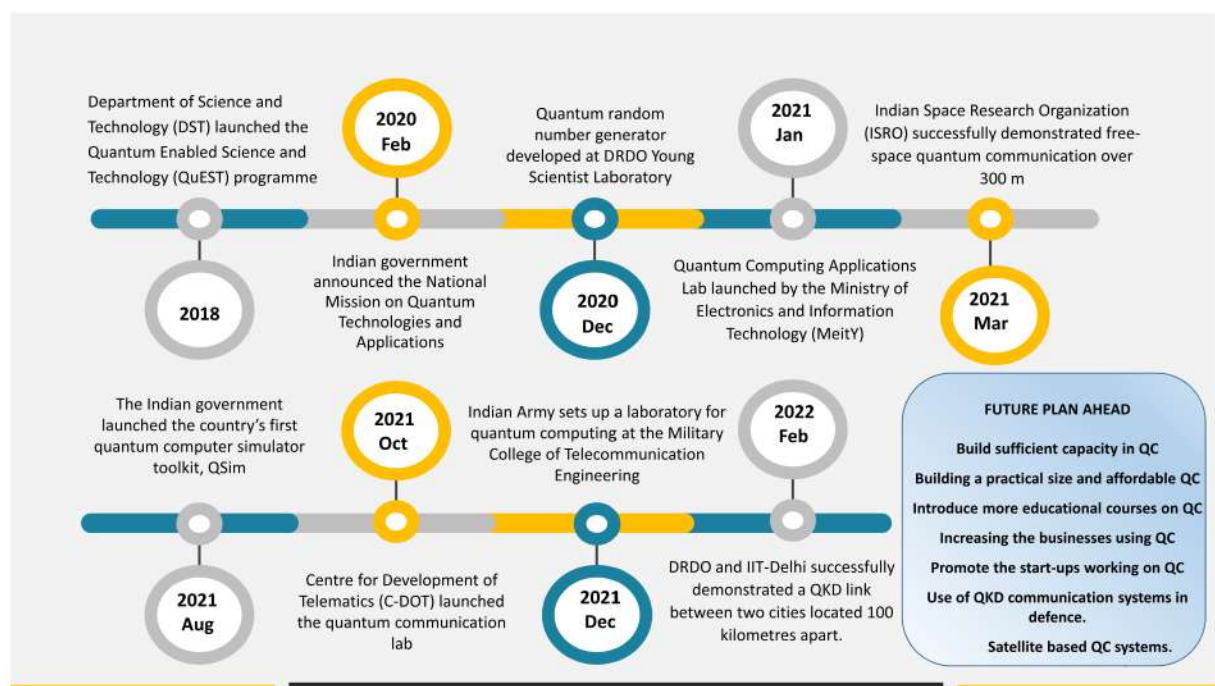


FIGURE 1 Summary of recent developments and future plan ahead in Quantum Computing.

applications areas of quantum computing, along with artificial intelligence, include financial services and healthcare, finding solutions to mathematical issues, and detecting fraudulent activity and cyber-attacks. Figure 1 summarises the recent developments in quantum computing and communications in India and the plan for the future.

1 | FUTURE OF QUANTUM COMPUTING IN INDIA

In India, there is a tremendous interest in quantum computing, with active participation from students, developers, industry, and academia, leading to many initiatives and developments that have taken place recently. The country is also expected to emerge as a talent hub for quantum computing very soon. The need of the hour is to popularise the quantum computing technology and its advantages and applications among all, simultaneously build sufficient quantum computational capacity and develop skills in building and operationalising a practical size and affordable cost quantum computer. Introduce more educational courses at the university level to develop quantum science and engineering as a discipline that will produce a large number of science and technology heads.

India plans to develop a quantum computer with approximately 50 qubits by 2026, joining many countries such as Australia and Israel looking to drive broader adoption of the nascent technology. Over the next 5 years, India will invest one billion dollars in various programmes to advance its capabilities in quantum information and meteorology, quantum applications and materials, and quantum communications. India estimates that the percentage of businesses using quantum technology will increase from less than one percent in 2022 to between 35 and 45% by 2030. There are currently 14 or 15 startups in the country working on commercial uses of quantum technology, but that number is expected to climb to between 400 and 500 over the next decade.

AUTHOR CONTRIBUTIONS

Varun G. Menon: Conceptualisation; Data curation; Investigation; Resources; Validation; Visualisation; Writing – original draft; Writing – review & editing. **Mainak Adhikari:**

Conceptualisation; Formal analysis; Project administration; Supervision; Writing – original draft; Writing – review & editing.

DATA AVAILABILITY STATEMENT

Data sharing not applicable – no new data generated.

ORCID

Varun G. Menon  <https://orcid.org/0000-0002-3055-9900>

REFERENCES

1. Budget 2020 announces Rs. 8000 cr National Mission on Quantum Technologies & Applications [Internet]. [cited 10th December 2022] <https://dst.gov.in/budget-2020-announces-rs-8000-cr-national-mission-quantum-technologies-applications> (2020)
2. IIT Madras becomes first Indian institute to join IBM Quantum Network [Internet]. [cited 10th December 2022] <https://www.indiatoday.in/education-today/news/story/iit-madras-becomes-first-indian-institute-to-join-ibm-quantum-network-1999583-2022-09-13> (2022)
3. India & Quantum Computing. [Internet]. [cited 10th December 2022] <https://www.drishtiias.com/daily-updates/daily-news-analysis/india-quantum-computing> (2022)
4. Indian Army Establishes Quantum Laboratory at Mhow (MP). [cited 10th December 2022] <https://pib.gov.in/PressReleasePage.aspx?PRID=1786012> (2021)
5. Indian Institute of Science Quantum Technology Initiative (IQTI). [cited 18th December 2022] <https://iqti.iisc.ac.in/> (2022)
6. IIT Jodhpur's Quantum Information and Computation (QIC) group. [cited 18th December 2022] <https://iitj.ac.in/qic/> (2022)
7. Center for Quantum Information, Communication, and Computing (C-QuICC). [cited 18th December 2022] <https://quantum.iitm.ac.in/> (2022)
8. TIFR's Quantum Measurement and Control Laboratory (QuMaC). [cited 18th December 2022] <https://www.tifr.res.in/~quantro/> (2022)
9. I-Hub Quantum Technology Foundation. [cited 18th December 2022] <https://www.quantech.org.in/> (2022)
10. Quantum Information and Computing (QuIC) lab at the Raman Research Institute. [cited 18th December 2022] <https://www.rri.res.in/qic/> (2022)
11. Quantum Information and Computation Group at Harish-Chandra Research Institute (HRI). [cited 18th December 2022] <https://www.hri.res.in/~qic/> (2022)

How to cite this article: Menon, V.G., Adhikari, M.: Quantum computing in India: Recent developments and future. *IET Quant. Comm.* 4(2), 93–95 (2023). <https://doi.org/10.1049/qt2.12056>



Institutional Sign In

All



ADVANCED SEARCH

Journals & Magazines > IEEE Transactions on Vehicular Technology > Early Access [?](#)

Optimization of Resource Allocation for V2X Security Communication based on Multi-Agent Reinforcement Learning

Publisher: **IEEE**

[Cite This](#)

PDF

Baofeng Ji ; Bingyi Dong ; Da Li ; Yi Wang ; Lvxi Yang ; Charalampos Tsimenidis ; **Varun G Menon** [All Authors](#) ...



55
Full
Text Views

Alerts

[Manage Content Alerts](#)
[Add to Citation Alerts](#)

[Abstract](#)

Authors

[Keywords](#)

[Metrics](#)

[More Like This](#)



Download
PDF

Abstract: In order to address the data security and communication efficiency of vehicles during high-speed mobile communication, this paper investigates the problem of secure in-vehicle communication. [View more](#)

► Metadata

Abstract:

In order to address the data security and communication efficiency of vehicles during high-speed mobile communication, this paper investigates the problem of secure in-vehicle communication resource allocation based on slow-variable large-scale fading channel information, to meet the quality of service requirements of vehicular communication, i.e., to ensure the reliability of V2V communication and the time delay while maximizing the transmission rate of the cellular link. And an eavesdropping model is introduced to ensure the secure delivery of link information. Considering that the high mobility of vehicles causes rapid channel changes, we model the problem as a Markov decision process and propose a resource allocation optimization framework based on the Multi-Agent Reinforcement Learning Algorithm (MARL-DDQN), in which a large-scale neural network model is built to train vehicular to learn the optimal resource allocation strategy for optimal communication performance and security performance. Simulation results show that the load successful delivery rate and confidentiality performance of the vehicular communication network are effectively improved compared to the baseline and MADDPG strategies while ensuring link security. This study provides useful references and practical value for the optimization of secure communication resource allocation in vehicular networking.

Published in: IEEE Transactions on Vehicular Technology (Early Access)

Page(s): 1 - 12

DOI: 10.1109/TVT.2023.3340424

Date of Publication: 07 December 2023 [?](#)

Publisher: IEEE

▼ ISSN Information:

Print ISSN: 0018-9545

PDF

[Help](#)



Baofeng Ji
School of Information Engineering, Henan University of Science and Technology, China

Bingyi Dong
School of Information Engineering, Henan University of Science and Technology, China

Da Li
Henan Polytechnic University, China

Yi Wang
Zhengzhou University of Aeronautics, China

Lvxi Yang
Radio Department, Southeast University, China

Charalampos Tsimenidis
Nottingham Trent University, U.K.

Varun G Menon
Department of Computer Science and Engineering, SCMS School of Engineering and Technology, India

Authors



Baofeng Ji
School of Information Engineering, Henan University of Science and Technology, China

Bingyi Dong
School of Information Engineering, Henan University of Science and Technology, China

Da Li
Henan Polytechnic University, China

Yi Wang
Zhengzhou University of Aeronautics, China

Lvxi Yang
Radio Department, Southeast University, China

Charalampos Tsimenidis
Nottingham Trent University, U.K.

Varun G Menon
Department of Computer Science and Engineering, SCMS School of Engineering and Technology, India

Keywords



Metrics



PDF

Help

More Like This

Reinforcement Learning-Based Routing Protocols for Vehicular Ad Hoc Networks: A Comparative Survey

IEEE Access

Published: 2021

Optimization of Vehicular Ad Hoc Network using Taguchi method

2015 International Conference on Computer, Communications, and Control Technology (I4CT)

Published: 2015

Show More

IEEE Personal Account

CHANGE
USERNAME/PASSWORD

Purchase Details

PAYMENT OPTIONS
VIEW PURCHASED
DOCUMENTS

Profile Information

COMMUNICATIONS
PREFERENCES
PROFESSION AND
EDUCATION
TECHNICAL INTERESTS

Need Help?

US & CANADA: +1 800
678 4333

WORLDWIDE: +1 732
981 0060

CONTACT & SUPPORT

Follow

f @ in y

PDF

Help

A not-for-profit organization, IEEE is the world's largest technical professional organization dedicated to advancing technology for the benefit of humanity.

© Copyright 2024 IEEE - All rights reserved.

IEEE Account

- » [Change Username/Password](#)
- » [Update Address](#)

Purchase Details

- » [Payment Options](#)
- » [Order History](#)
- » [View Purchased Documents](#)

Profile Information

- » [Communications Preferences](#)
- » [Profession and Education](#)
- » [Technical Interests](#)

Need Help?

- » **US & Canada:** +1 800 678 4333
- » **Worldwide:** +1 732 981 0060
- » [Contact & Support](#)

[About IEEE Xplore](#) | [Contact Us](#) | [Help](#) | [Accessibility](#) | [Terms of Use](#) | [Nondiscrimination Policy](#) | [Sitemap](#) | [Privacy & Opting Out of Cookies](#)

A not-for-profit organization, IEEE is the world's largest technical professional organization dedicated to advancing technology for the benefit of humanity.
© Copyright 2024 IEEE - All rights reserved. Use of this web site signifies your agreement to the terms and conditions.

PDF

Help



IOT-BASED SMART GREENHOUSE SYSTEMS FOR CONTROLLED ENVIRONMENT AGRICULTURE

Mrs. Vivitha Vijay¹, Mrs. Hema H², Reshma K V³, Doney Daniel⁴, Neethu Krishna⁵

^{1,2}Assistant Professor, Department of Artificial Intelligence and Machine Learning, Mahaguru Institute of Technology, Kattachira, Kayamkulam, Alappuzha.

^{3,4,5}Assistant Professor, Department of Computer Science and Engineering, SCMS School of Engineering and Technology, Karukutty, Ernakulam, Kerala, India.

Abstract

Controlled Environment Agriculture (CEA) has emerged as a transformative approach to modern farming, enabling precise management of climatic conditions to enhance crop production. This paper explores the integration of Internet of Things (IoT) technologies in developing smart greenhouse systems to optimize CEA. By implementing a network of sensors and actuators, IoT-based smart greenhouses can autonomously monitor and control environmental parameters such as temperature, humidity, soil moisture, and nutrient levels, resulting in increased efficiency and yield. Through a thorough review of current technologies and case studies, we investigate the architecture, data management, and operational strategies of these advanced greenhouse systems. We also examine the challenges faced, such as high initial costs, system complexity, and data security concerns, proposing viable solutions to address these issues. Our findings indicate that IoT-enabled smart greenhouses not only contribute to sustainable agriculture practices by conserving water and reducing the use of fertilizers and pesticides but also pave the way for future advancements in urban and precision farming. The paper concludes by discussing future directions for IoT in CEA, emphasizing the need for scalable, interoperable solutions that can adapt to the growing global food demands. This study offers significant insights for researchers, practitioners, and policymakers interested in leveraging IoT to enhance the efficacy of CEA.

Keywords: Controlled Environment Agriculture (CEA), Internet of Things (IoT), Smart Greenhouses, Precision Agriculture, Agricultural Technology and Sensor Networks.

1. Introduction

The growing global population, coupled with the looming challenges of climate change, has put unprecedented pressure on the agricultural sector to produce more food while minimizing environmental impact. Controlled Environment Agriculture (CEA) has been identified as a pivotal solution to these challenges, offering a way to maximize crop yields through the control of environmental variables within agricultural systems[1]. Among the technologies enabling this revolution, the Internet of Things (IoT) stands out as a game-changer, propelling the creation of smart greenhouse systems that promise to redefine traditional farming practices[2]. Smart greenhouses equipped with IoT infrastructure represent a significant leap forward in agriculture.

They leverage interconnected sensors and actuators to precisely regulate conditions such as temperature, humidity, soil moisture, light, and nutrient levels, thus providing crops with an optimal growth environment[3]. The essence of these advanced systems lies in their ability to continuously collect data and autonomously execute decisions, thereby reducing the need for manual intervention and paving the way for more resilient and efficient farming methods[4]. However, the integration of IoT technology in CEA is not without challenges. Issues such as high setup and operational costs, data management complexities, and security vulnerabilities pose substantial barriers to widespread adoption. This paper aims to demystify the implementation of IoT-based smart greenhouse systems within the context of CEA, dissecting their architecture, operational mechanisms, and the sophisticated data analytics that underpin them[5]. By dissecting successful case studies and identifying potential pitfalls and their respective antidotes, the paper endeavors to offer a holistic view of this innovative agricultural paradigm. The paper also extends its vision to the future, prognosticating the evolution of smart greenhouse systems and their role in the larger ecosystem of smart farming. In an era where sustainability and productivity must coexist, the fusion of CEA and IoT emerges not just as a technological possibility, but as a necessary step toward a food-secure future for the burgeoning global populace. In setting forth these objectives, the paper will contribute valuable insights for researchers, technologists, and agriculturalists seeking to harness the power of IoT in transforming greenhouse agriculture into a smart, sustainable, and highly productive enterprise.

2. Literature Review

Controlled Environment Agriculture (CEA) is not a novel concept; however, its integration with the Internet of Things (IoT) represents a relatively recent paradigm shift. This fusion has received increasing scholarly attention, underpinning the advent of smart agriculture[6]. The literature abounds with studies that underscore the potential of IoT to revolutionize farming practices by enabling real-time monitoring and management of agricultural environments. Initial studies in the field have focused on the basic implementation of IoT in agriculture. Author's in [7] provided one of the early overviews of the technologies involved in precision agriculture, noting the potential for IoT devices to improve resource use efficiency. Similarly, Author's in [8] outlined the importance of wireless sensor networks in CEA systems, discussing the fundamental role of sensors in data collection.

More recent research has delved into sophisticated applications of IoT in greenhouses. For instance, Author's in [9] explored how cloud computing and IoT can work in tandem to enable data-driven decision-making in smart greenhouses. Their findings pointed to significant improvements in crop yield and resource conservation when IoT systems are properly implemented.

Another critical aspect that emerges from the literature is the challenge of data management. As pointed out by Author's in [10], the sheer volume of data generated by IoT devices requires robust analytics tools and techniques to convert raw data into actionable insights. Machine learning

models, as investigated by Author's in [11], have shown promise in predicting and optimizing greenhouse conditions to improve productivity.

However, despite the optimistic projections, the literature also points to several challenges that inhibit the full realization of IoT potential in smart greenhouses. Economic barriers, technical complexities, and concerns regarding data privacy and security are recurrent themes. For example, Author's in [12] discussed the economic considerations and the need for scalable IoT solutions, while Author's in [13] focused on the security vulnerabilities inherent in IoT systems. The literature review highlights a significant gap: while there is ample research on the components and potential of IoT in agriculture, fewer studies provide a comprehensive analysis of the economic and practical feasibility of these systems, particularly in diverse geographic and socio-economic contexts. In addressing this gap, our study aims to build on the existing body of knowledge by presenting an integrative review of smart greenhouse architectures, pinpointing real-world applications, and evaluating the scalability and sustainability of these solutions.

3. Internet of Things (IoT) in Agriculture

The advent of the Internet of Things (IoT) has ushered in a new era of precision in agriculture, allowing for a level of monitoring and control that was previously unattainable. IoT refers to a network of physical objects — "things" — that are embedded with sensors, software, and other technologies with the purpose of connecting and exchanging data with other devices and systems over the internet[14]. These IoT systems offer numerous applications in agriculture, from field monitoring to supply chain management, and are particularly transformative in the context of Controlled Environment Agriculture (CEA).

The Role of IoT in Modern Agriculture: In modern agricultural practices, the role of IoT is multifaceted and expansive. At the heart of IoT applications in agriculture is the use of sensors and devices to collect data on various aspects of the farming environment[15]. This data can include a wide range of variables such as soil moisture levels, crop growth, pest infestations, weather conditions, and more. Through the aggregation and analysis of this data, farmers and agriculturalists are able to make more informed decisions about the management of their crops and resources.

Examples of IoT Devices in Greenhouses: Within the controlled settings of greenhouses, the application of IoT devices is particularly effective. Common examples of these include:

Temperature and Humidity Sensors: These are vital for maintaining the delicate balance required for optimal plant growth, ensuring that conditions do not become too hot, cold, or humid, which could harm the plants.

Soil Moisture Sensors: These allow for precise irrigation, ensuring that plants receive the correct amount of water without wastage.

Light Sensors: They monitor the levels of natural and supplemental light, allowing for adjustments to ensure that plants receive the right amount of light for photosynthesis.

CO₂ Sensors: These help maintain the optimal carbon dioxide levels for photosynthesis.

Nutrient Sensors: In hydroponic setups, these sensors are crucial for monitoring the nutrient solution's composition to adjust for optimal plant nutrition.

The integration of these sensors into a cohesive IoT ecosystem enables the automation of greenhouse climate controls, irrigation systems, and even feeding mechanisms, often in real-time. This not only optimizes the growth conditions but also facilitates remote monitoring and control, reducing the need for physical presence and manual checks.

Data Management in IoT Agriculture: The value of IoT in agriculture is significantly enhanced by the sophisticated data management systems it utilizes. The collection of vast quantities of data from various sensors necessitates an equally robust system for data processing and analytics. This is where technologies such as cloud computing come into play, providing the infrastructure necessary to store and analyze large datasets. Big data analytics and machine learning algorithms can process this information to identify patterns and predict outcomes, leading to actionable insights for greenhouse management. These systems can forecast environmental changes, suggest adjustments to optimize plant growth, and even automate processes in response to predicted conditions.

Integration and Interoperability in IoT Systems: An essential consideration in the application of IoT in agriculture is the integration and interoperability of various devices and systems. The IoT ecosystem within a greenhouse must be cohesive, with sensors, actuators, and control systems working in unison. This requires standardized protocols and communication technologies that ensure seamless interaction between devices, regardless of manufacturer or model.

In conclusion, IoT stands as a cornerstone of modern agricultural strategies, offering a toolkit for smart greenhouse management that promises sustainability and efficiency. By converging sensors, data, and automation, IoT transforms greenhouses into data-driven, responsive environments capable of adapting to the needs of plants with minimal human intervention. The potential for scalability and technological advancement within this domain continues to grow, signaling a future where IoT and agriculture are inextricably linked.

4. Smart Greenhouse Architecture

Smart greenhouse architecture represents a symbiotic integration of hardware, software, and communication technologies that collectively form a responsive and adaptive agricultural environment. Central to this architecture is the IoT framework, which enables real-time data collection, automated control systems, and remote management capabilities.

Structural Components: The structural components of a smart greenhouse are the physical entities that constitute the environment. These include:

The Greenhouse Structure: Designed to optimize light entry and maintain internal climate.

Sensor Array: Distributed throughout the greenhouse to monitor environmental variables and plant health indicators.

Actuator Network: Mechanisms that can alter the environment in response to sensor data, such as opening vents, adjusting shade cloths, or modulating heating systems.

Irrigation and Nutrient Delivery Systems: Precision-based systems that provide water and nutrients tailored to the plants' needs, informed by soil and plant sensors.

Connectivity and Data Flow: Key to the architecture's functionality is the seamless connectivity among its components. This is achieved through:

Wireless Sensor Networks (WSNs): Enable data flow from sensors to central processing units without the complexity of wired systems.

IoT Gateways: Act as intermediaries that aggregate sensor data and communicate with the cloud or local servers.

Data Processing Units: These may be on-premise or cloud-based systems where data analytics and decision-making processes occur.

Control Systems and Automation: Smart greenhouses leverage advanced control systems to automate the adjustment of environmental conditions. These systems include:

Climate Control Systems: Regulate temperature, humidity, and CO₂ concentration to maintain optimal growing conditions.

Light Management Systems: Ensure that plants receive the ideal light spectrum and intensity for photosynthesis throughout their growth cycles.

Watering Systems: Adjust water delivery based on soil moisture content and plant water requirements.

Software and User Interface: The user interface and software platform are critical for human interaction with the smart greenhouse:

Data Analytics and Machine Learning Platforms: Analyze historical and real-time data to make predictions and suggest optimizations.

Dashboard: Provides a user-friendly interface for monitoring conditions and manual override options.

Mobile Applications: Allow for remote monitoring and control, providing alerts and updates to users on the go.

Energy Management: Smart greenhouses often incorporate sustainable energy solutions to power the array of IoT devices:

Renewable Energy Sources: Such as solar panels, to provide a green and cost-effective energy supply.

Energy Storage Systems: Batteries or other storage solutions to manage energy supply when renewable sources are intermittent.

Energy Efficiency Optimization: Intelligent systems designed to reduce energy consumption by adjusting the operation of devices to the times of day when energy is cheaper or more readily available from renewable sources.

Security and Reliability: Ensuring the security and reliability of the smart greenhouse is paramount:

Cybersecurity Measures: Protect data integrity and privacy, securing communication channels against unauthorized access.

Redundancy and Fail-safes: Critical to maintain functionality and protect plants in the event of system failures.

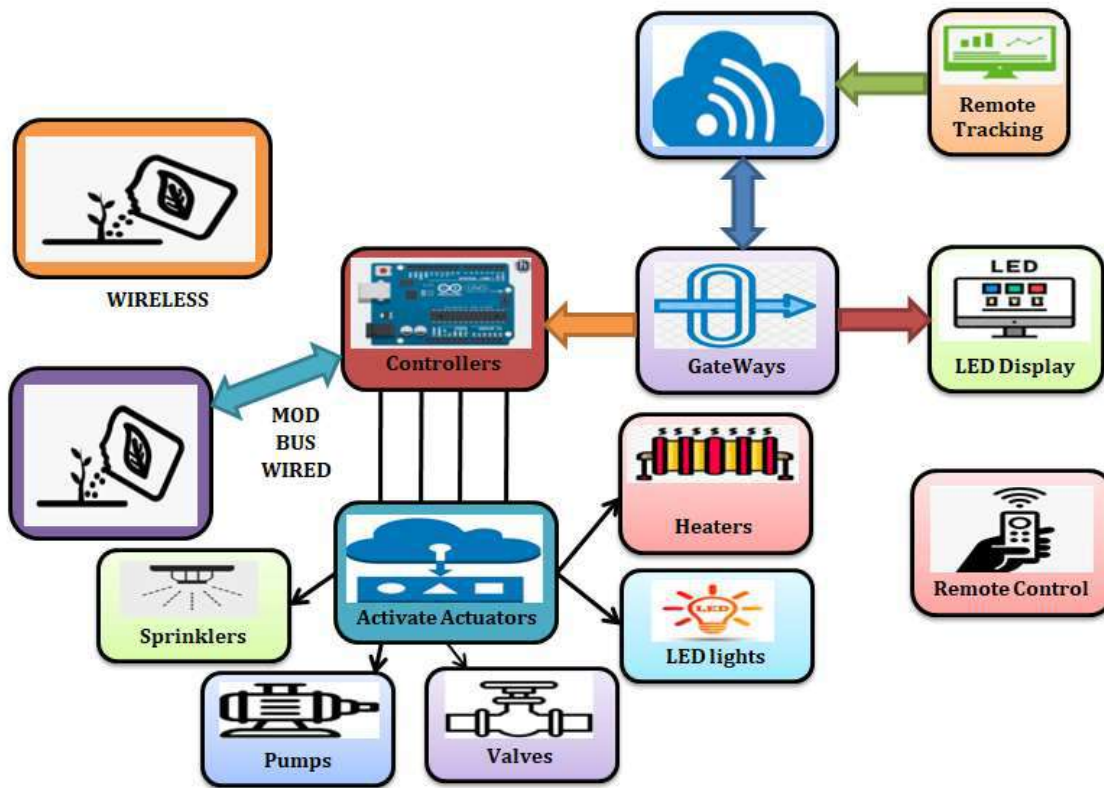


Figure.1: A Smart Greenhouse conceptualized with IoT integration

In the modern agricultural sector, devices enabled by the Internet of Things (IoT) play a critical role in the monitoring and control systems. IoT technology encompasses a variety of tools including sensors, actuators, data management through cloud computing, as well as drones, and sophisticated navigation and analytics systems. This suite of technologies empowers the agricultural framework to make informed decisions that enhance crop production. IoT devices have the capacity to gather detailed information about environmental factors such as humidity, temperature, and broader climatic conditions. They also monitor field-specific variables, including soil characteristics and plant biomass. This data is crucial for predicting and tracking crop quality for consumer markets. Furthermore, IoT technology facilitates the aggregation of data, which is then stored in cloud-based systems. This storage capability enables the generation of alerts and the dispatch of text message notifications to farmers. The cloud-stored data is not only pivotal for immediate insights but is also valuable for constructing predictive models. These models are capable of forecasting various factors that could impact crop health and yield. An example of this advanced IoT-driven approach to agriculture is demonstrated in the concept of a smart greenhouse, which is depicted in Figure 1. In conclusion, the smart greenhouse architecture is a holistic framework, meticulously designed to harness the power of IoT for precision agriculture. This system exemplifies the convergence of agronomy, engineering, and data science, leading to an optimized, controlled environment that fosters sustainable and efficient crop production. Future developments may introduce greater levels of automation and AI-driven decision-making, further enhancing the capabilities of smart greenhouses to meet the food demands of a growing global population.

5. Benefits of IoT-Based Smart Greenhouses

IoT-based smart greenhouses represent a significant advancement in agricultural technology, offering a multitude of benefits that address efficiency, productivity, and sustainability in agriculture. This section will explore the myriad advantages of employing IoT systems in controlled environment agriculture.

Enhanced Crop Yield and Quality

Precision Farming: IoT-enabled systems provide precise control over the internal conditions of the greenhouse, optimizing the environment for plant growth and leading to significant improvements in crop yield and quality.

Consistent Production: The use of smart greenhouses mitigates many of the risks associated with traditional farming, allowing for year-round production irrespective of external weather conditions.

Customization for Crop Needs: Smart systems can adjust the micro-climate to suit specific crop requirements, enhancing growth rates and improving the nutritional value of the produce.

Resource Efficiency

Water Conservation: IoT-based systems can regulate irrigation with pinpoint accuracy, significantly reducing water usage while ensuring plants receive the optimal amount for their growth.

Energy Efficiency: Smart energy management systems can reduce the energy consumption of greenhouses by adjusting lighting, heating, and ventilation in response to real-time conditions.

Reduction in Input Wastage: Precision application of nutrients, water, and other inputs means that resources are not wasted, leading to a more sustainable farming practice.

Operational Cost Reduction

Labor Efficiency: Automation of routine tasks can reduce the labor required for greenhouse operations, cutting down on costs and minimizing human error.

Maintenance Predictability: Predictive maintenance enabled by IoT can foresee equipment failures before they occur, avoiding costly downtime and repairs.

Data-Driven Insights and Decision Making

Improved Monitoring: Continuous monitoring of greenhouse conditions allows for data-driven decision making, improving the responsiveness and agility of farming operations.

Historical Data Analysis: Long-term data collection contributes to a deeper understanding of optimal growing conditions and can help predict future outcomes.

Environmental Benefits

Sustainable Practices: Smart greenhouses can significantly reduce the carbon footprint of agricultural practices by minimizing the input of resources and optimizing the internal environment for growth.

Reduced Chemical Use: Effective monitoring and control can lead to a reduction in the use of pesticides and herbicides, as the controlled environment itself can prevent pest infestations and disease.

Socioeconomic Impacts

Food Security: By enabling consistent and increased production, IoT-based smart greenhouses can contribute to addressing the global challenge of food security.

Rural Development: The introduction of high-tech agriculture can lead to the development of rural areas, providing new employment opportunities and technological upskilling.

Scalability and Flexibility

Adaptability to Various Scales: Smart greenhouse technologies are scalable, suitable for both small family farms and large commercial operations.

Flexibility in Crop Selection: Advanced control systems allow for the cultivation of a wide variety of crops, enabling growers to respond to market demands quickly.

In conclusion, IoT-based smart greenhouses provide a wealth of benefits that can revolutionize the agricultural sector. By leveraging advanced technologies to create finely-tuned growing conditions, these systems can improve yields, enhance sustainability, and provide a pathway towards a more secure food future.

6. IoT based Greenhouse Monitoring and Control System

A block diagram for an IoT-based Greenhouse Monitoring and Control System typically illustrates how different components of the system interact to create a network for automated and remote management of a greenhouse environment (Figure.2). Here's a step-by-step explanation of how the components in such a diagram might function together:

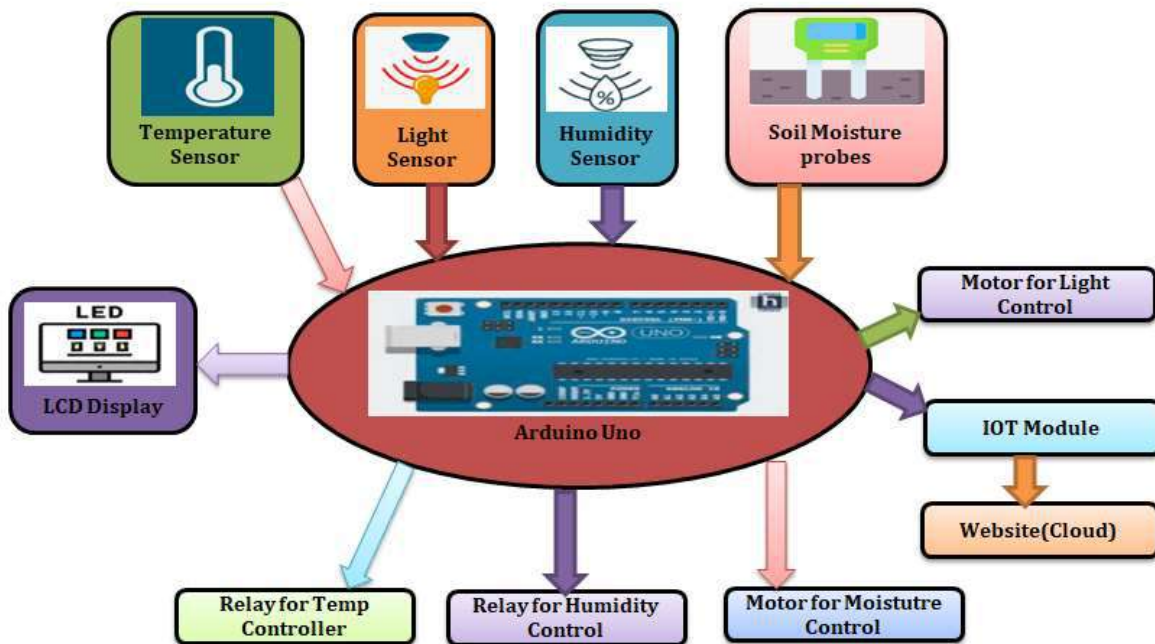


Figure.2: block diagram for an IoT-based Greenhouse Monitoring and Control System

Sensors: These are the frontline devices in the system. Various sensors are deployed throughout the greenhouse to collect data on environmental parameters such as temperature, humidity, soil moisture levels, light intensity, and CO2 concentration.

Actuators: Based on the data received from the sensors, actuators are the components that perform actions. For instance, if the temperature sensor detects a temperature that's too high, an actuator would activate a cooling system. Actuators can control heating systems, humidifiers, irrigation systems, and window or vent openers.

Microcontroller or Microprocessor: This is the brain of the operation. It receives data from the sensors, processes it, and decides what actions the actuators need to take. This unit often runs on a simple set of programmed rules—like "if temperature > 30°C, then activate cooling system."

Communication Module: For the IoT aspect, the system requires a communication module that enables it to send and receive data from the internet. This could be via Wi-Fi, Bluetooth, ZigBee, or cellular networks.

Cloud Computing/Data Storage: The data collected by the sensors is sent to the cloud for storage and analysis. Cloud platforms can also host the control algorithms that make decisions based on sensor data.

Data Processing and Analysis: Advanced analytics are performed either in the cloud or on local computers to make sense of the data collected. This can involve trend analysis, predictive modeling, and decision-making processes.

User Interface (UI): There is usually an application or web-based dashboard where the user can view real-time data, receive alerts, and manually override automatic controls if necessary.

Control System: This system takes the analyzed data and user inputs to send back control signals to the actuators in the greenhouse.

Notification System: This system is responsible for sending alerts or notifications to the greenhouse manager or farmer, usually through SMS, email, or app notifications, when attention is required.

Power Supply: All these components require a reliable power source to function. The block diagram would show how power is supplied or distributed to sensors, actuators, and the control unit.

In an IoT-based greenhouse, all these components are designed to work together seamlessly to maintain the ideal growing conditions, improve efficiency, reduce waste, and maximize the yield of the crops grown within. The block diagram serves as a simplified representation of this complex and interconnected system, providing a high-level overview of how the greenhouse's monitoring and control functions are organized.

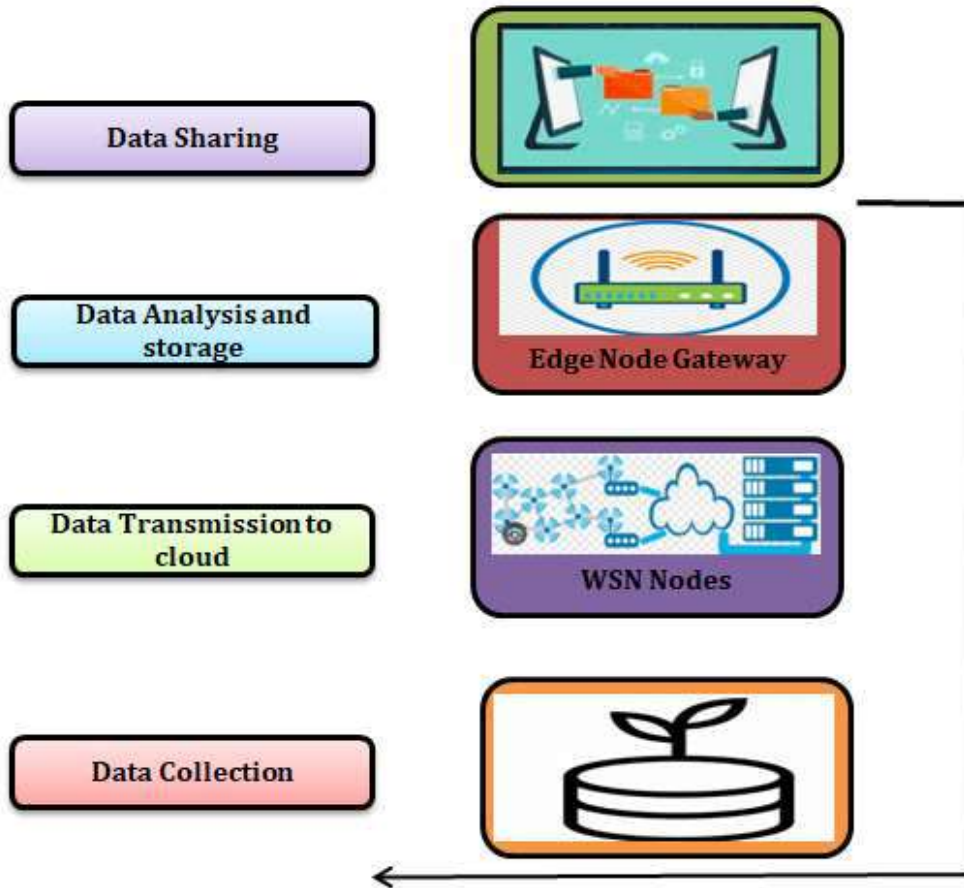


Figure.3: Decision Making

In an IoT-based Greenhouse Monitoring and Control System, decision-making is an automated and dynamic process integral to maintaining optimal growing conditions(Figure.3). It begins with a network of sensors strategically placed throughout the greenhouse, collecting real-time data on various environmental factors like temperature, humidity, soil moisture, and light intensity. This data is wirelessly transmitted to a central processing unit, usually a microcontroller, where it's analyzed against predetermined parameters that define the ideal conditions for plant growth. The core of the decision-making lies within the system's pre-programmed rules or algorithms, which interpret the sensor data and determine the necessary adjustments. For example, if the ambient temperature rises above the desired range, the system might decide to activate cooling mechanisms or increase ventilation. These commands are then relayed to the corresponding actuators, such as fans, shading systems, or irrigation controls, which physically alter the greenhouse environment. A critical aspect of this process is the feedback loop. After the environmental changes have been made, the sensors measure the new conditions and send this information back to the central unit.

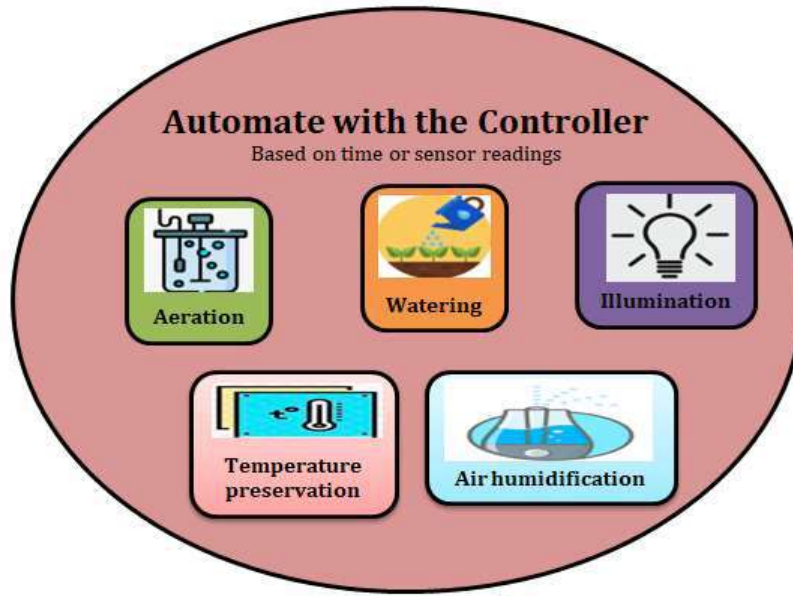


Figure.4: Automate with the Controller

The system evaluates this feedback to confirm that the environment now meets the set criteria or to determine if further adjustments are needed. Additionally, many modern systems are equipped with interfaces that alert the human operators when issues arise that require manual intervention, such as equipment malfunctions or conditions that fall outside the scope of the system's programming. Operators can also adjust settings and parameters through these interfaces, tailoring the automated responses of the system as needed. Over time, with advancements in technology, some systems may incorporate machine learning algorithms that use historical data to refine and improve decision-making processes, enabling the system to adapt to changing conditions and potentially improve its efficiency and the quality of the crops produced. This continuous cycle of monitoring, acting, and adjusting forms the backbone of an IoT-enabled greenhouse, creating a precision-controlled environment conducive to high-yield, high-quality agricultural production. The controller in an IoT-based Greenhouse Monitoring and Control System is the pivotal component that automates the environmental management within the greenhouse (Figure.4). It serves as the central intelligence hub, interpreting sensor data, making decisions, and executing actions through connected devices and actuaries. The automation process within an IoT-enabled greenhouse is orchestrated by a sophisticated controller, which functions as the brain of the entire operation. This controller receives a continuous stream of data from a myriad of sensors that monitor critical conditions such as temperature, humidity, light, and soil moisture. Utilizing a set of pre-determined algorithms and thresholds, the controller compares the incoming data against ideal growth parameters for the plants. When discrepancies arise—like a temperature deviation—the controller instantly initiates a response. It sends signals to the appropriate actuators to adjust the environmental conditions, such as activating the irrigation system when soil moisture drops or engaging cooling systems if the temperature exceeds optimal levels. The controller's role extends beyond immediate responses; it continuously records and analyzes this environmental data,

adjusting its control algorithms to improve the system's efficiency and accuracy over time. As a result, the greenhouse environment is perpetually tweaked to perfection, all while minimizing the need for human intervention and fostering an automated, sustainable ecosystem where plants can thrive.

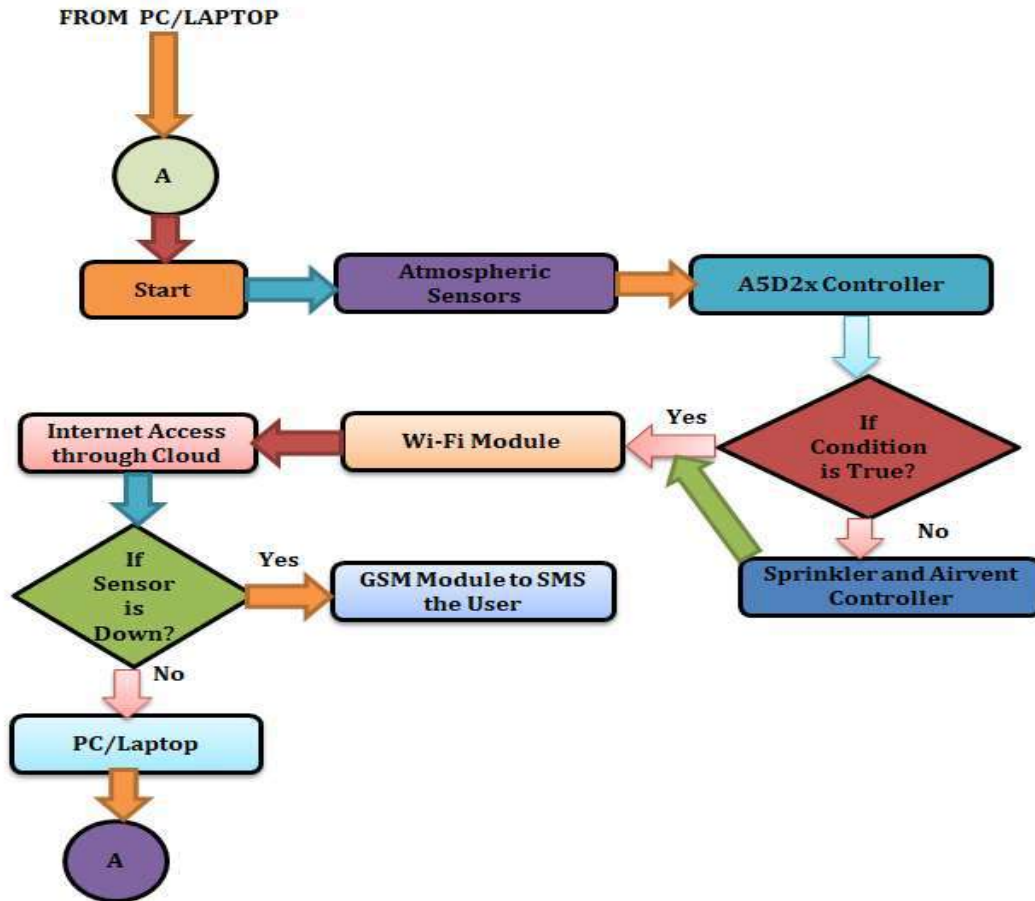


Figure.5: Flow diagram

A flow diagram for Smart Greenhouse Automation methodology typically illustrates a sequence of operational steps and decision-making processes that are automated by a central control system to optimize the greenhouse environment for plant growth(Figure.5). In a Smart Greenhouse Automation system, the entire operational workflow begins with the initialization phase, where the central control unit boots up, performing diagnostics to ensure all connected sensors and actuators are operational. Following this, a network of sensors strategically placed throughout the greenhouse starts gathering critical environmental data, such as temperature, humidity, CO2 concentration, light intensity, and soil moisture levels.

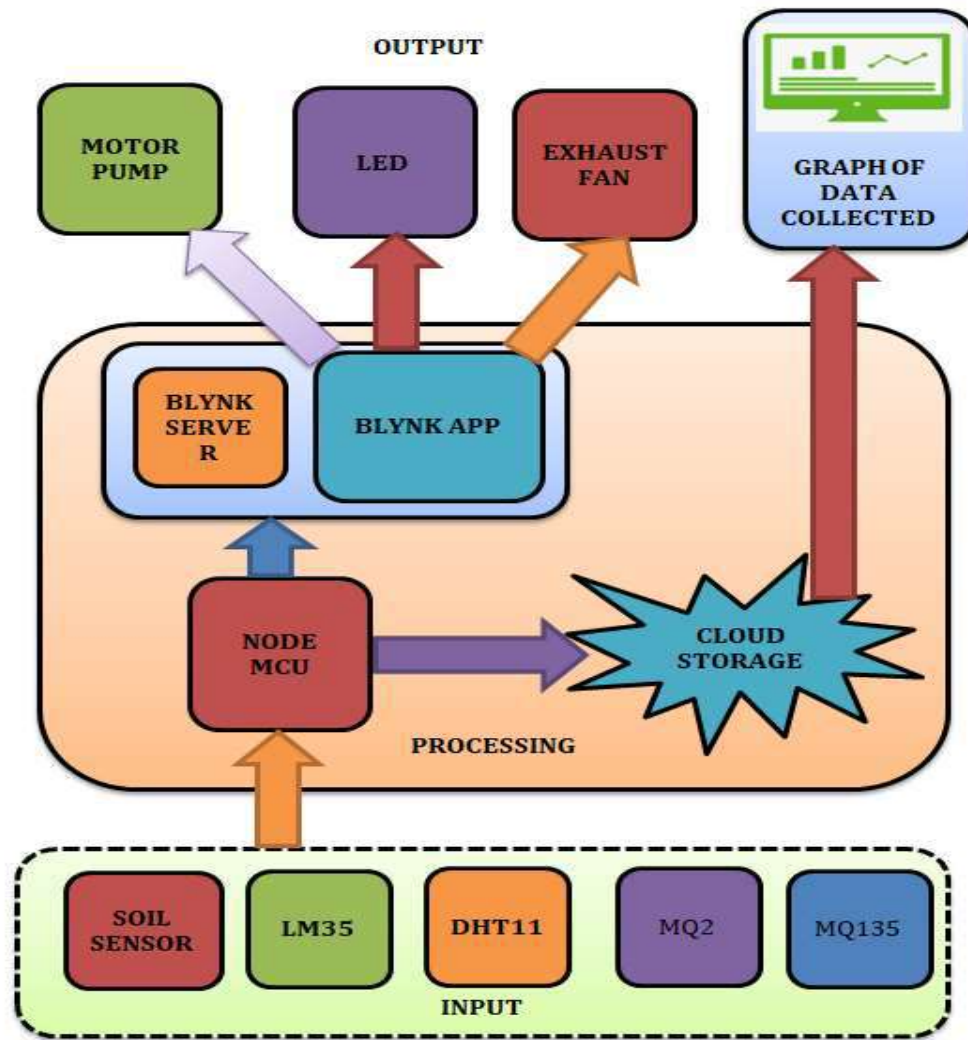


Figure.6: Managing energy in a greenhouse that utilizes electrical equipment

This data is then wirelessly transmitted to the central controller, which undertakes the task of data analysis, comparing the real-time sensor information against predefined optimal growth conditions for the plants. If discrepancies are detected—say, the temperature is higher than the desired level—the controller enters the decision-making phase, wherein it executes a set of programmed instructions to rectify the imbalance. Subsequently, commands are dispatched to the actuators, triggering a series of corrective actions such as activating the cooling system or opening ventilation shafts. As these actuators implement changes, the sensors continue to monitor the resulting environmental adjustments, sending this feedback to the controller, thereby completing a feedback loop. The controller assesses the impact of its directives, ensuring that the environment is adjusted to the set parameters. This process of monitoring and adjustment is continuous, with the system persistently cycling through these steps to maintain an optimal growing environment. In instances where the system's automated responses do not suffice, or when human expertise is required, alerts are generated and sent to the operators through a user interface, which also allows for manual

system overrides and parameter adjustments. Moreover, the system is designed to log all environmental data and interaction history, which can be analyzed to enhance the greenhouse's operational algorithms for future improvement, thus evolving the automation process over time. Energy management within a greenhouse that utilizes electrical appliances is crucial for optimizing resource use, reducing costs, and minimizing the environmental impact of operations(Figure.6). The integration of IoT and smart systems has greatly enhanced the ability to manage energy effectively. Here's how energy management with electrical appliances in a greenhouse typically works:

Smart Sensors and Monitors: Energy consumption begins with monitoring. Smart sensors are installed to provide real-time data on the energy use of all electrical appliances, including lights, heating and cooling systems, ventilation fans, and irrigation pumps. These sensors can detect when equipment is on, how much power it's using, and even when it may be operating inefficiently.

Automated Control Systems: The data from sensors is fed to a central control system, which uses it to automate the operation of electrical appliances. For example, lighting can be adjusted based on the amount of natural sunlight available, or heating can be modulated according to both the internal temperature of the greenhouse and external weather conditions.

Energy-Efficient Technologies: Modern greenhouses often employ energy-efficient technologies, such as LED lighting, which provides the necessary light spectrum for plant growth while using less electricity. Similarly, energy-efficient HVAC systems can be used to maintain the ideal temperature and humidity with minimal energy use.

Scheduling: Non-critical operations that consume a lot of energy can be scheduled during off-peak hours when electricity rates are lower. This scheduling can be done manually by the greenhouse operators or could be automated by the control system.

Energy Production and Storage: Some greenhouses take a step further by integrating renewable energy sources, like solar panels, to power their operations. Energy storage systems, such as batteries, can store excess energy produced during the day for use during the night or cloudy days, ensuring a constant and cost-effective energy supply.

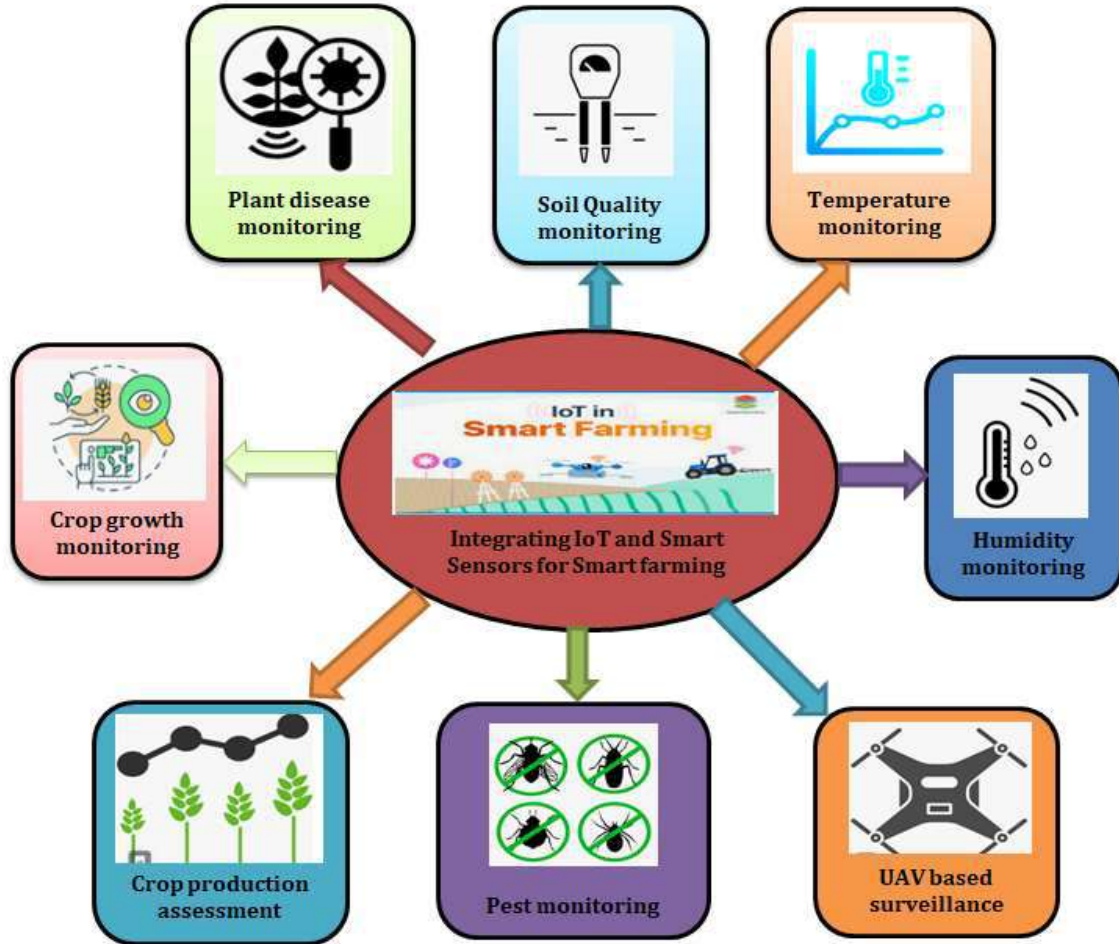


Figure.7: diverse applications of combining IoT and smart sensors for precision

Data Analysis and Optimization: All the collected data on energy use is analyzed, often with the help of cloud-based software, to identify patterns, inefficiencies, and opportunities for further energy savings. For instance, the system can learn the best times to ventilate the greenhouse or the most efficient temperature settings for different times of the day or year.

Remote Management and Alerts: Operators can manage the energy use remotely via a smartphone or computer interface. The system can send alerts if it detects abnormal energy usage, which might indicate a fault in an appliance that requires maintenance.

Maintenance Scheduling: Preventative maintenance is scheduled for all electrical appliances to ensure they operate at peak efficiency. Well-maintained equipment typically uses less energy and has a longer operational life. In summary, energy management in a greenhouse is about having the right technological tools to collect data and the analytical systems to process that data, leading to informed decisions on energy use. Through continuous monitoring, automated controls, energy-efficient technology, and smart operation scheduling, a greenhouse can achieve significant energy savings and reduce its overall carbon footprint.

Figure 7 illustrates the diverse applications of combining IoT and smart sensors for precision agriculture. These advanced IoT-enabled smart sensors are capable of precisely tracking environmental variables including temperature, moisture, and humidity, critical for farm management. They also have the capability to gauge soil health by measuring attributes like nitrate concentrations and moisture levels. To identify plant diseases and insect infestations, sophisticated sensors equipped with high-resolution cameras and GPRS systems are used. Unmanned Aerial Vehicles (UAVs) offer aerial surveillance to observe crop development and map the topography of the farmland. Furthermore, the yield of crops is projected utilizing automated mass flow sensors, enhancing the accuracy of production forecasts.

7. Results and Discussion

Figure 8 depicts a system for monitoring soil moisture levels, a critical component for maintaining agricultural health and efficiency. A predefined value acts as a benchmark for the desired soil moisture content. When the moisture sensor detects a drop below this threshold, it triggers an automatic response to activate the irrigation system, ensuring plants receive adequate water without manual intervention. The soil moisture readings are recorded and regulated through IoT platforms like Blynk and ThingSpeak, which provide real-time data visualization and analysis. To ensure comprehensive moisture management, multiple sensors are positioned throughout different zones of the greenhouse or across distinct crop patches. The collective data from these sensors, as illustrated in Figure 8, enables a detailed and dynamic overview of the soil's hydration status, facilitating targeted and efficient watering practices.

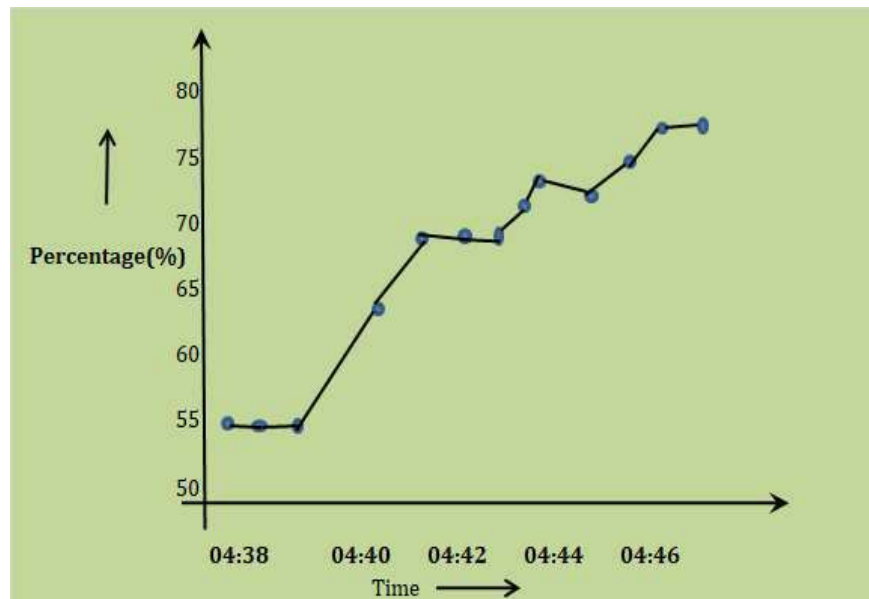


Figure.8: Humidity inside the greenhouse

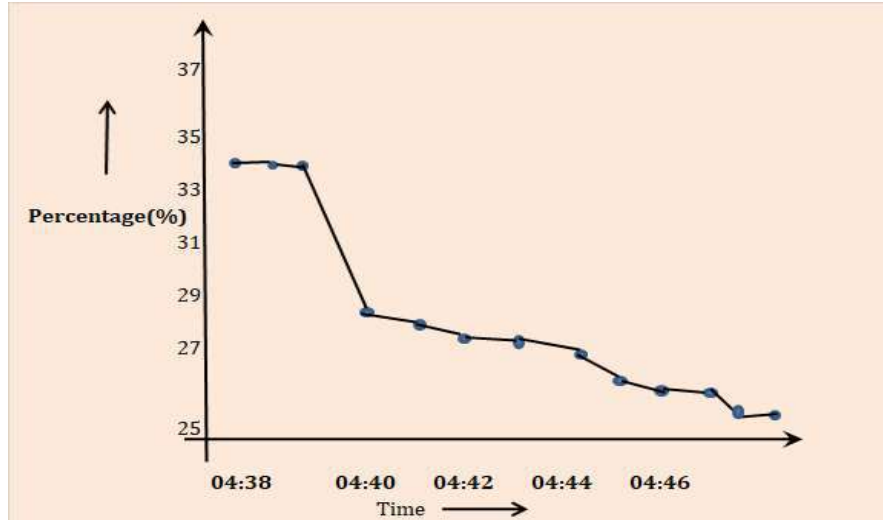


Figure.9:Temperature inside the greenhouse

Maintaining the correct humidity is vital for plant growth, and it can be crucial in compensating for less-than-ideal weather conditions. The DHT11 sensor plays an integral role in the greenhouse environment by constantly gauging both temperature and humidity levels. Should either the humidity or temperature fall below predetermined levels, the greenhouse's internal fans are activated to circulate air and dissipate excess moisture and heat, thus stabilizing the environment to favor plant development. Data collected by the DHT11 sensor is logged and managed via ThingSpeak, as detailed in Figures 9 and 10. For instance, if the greenhouse's maximum acceptable temperature is set at 28°C, surpassing this limit would trigger the exhaust fans to turn on, thereby cooling down the interior. Concurrently, an alert is sent to the control engineer to inform them of the change in conditions, allowing for timely interventions and adjustments to the system.

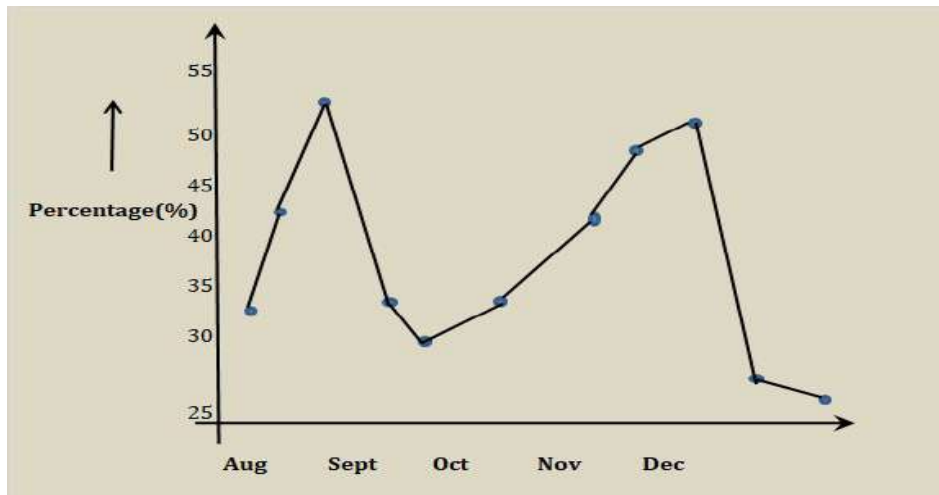


Figure.10: Soil moisture(low is wet)

This work presents an IoT-based smart soil management system designed to continuously monitor and adjust the soil environment, ensuring its suitability for agricultural use and optimal crop

growth. The system operates by periodically reading sensor data via an integrated IoT framework. The durability and performance of each sensor node within this network are dependent on its energy usage, which is a critical consideration for the IoT platform's overall functionality. The primary environmental factors under surveillance include soil moisture, ambient temperature, and humidity within the greenhouse. Based on the data acquired, the system can autonomously execute necessary actions to correct any deviations from the ideal conditions for crop cultivation. Such actions might include watering the plants when the soil moisture falls below a certain level or adjusting the greenhouse's climate controls in response to temperature and humidity changes. This approach presents a sophisticated solution for the agricultural sector, enabling the collection of precise information and monitoring of crop development. It stands to significantly improve decision-making in the agricultural and food industries by providing real-time data and ensuring that the crops are grown in conditions that are as close to optimal as possible.

8. Future Directions

The rapidly evolving landscape of IoT technology coupled with the growing demands of global food production presents numerous opportunities for innovation in smart greenhouse systems. This section outlines potential future directions for this burgeoning field.

Technological Advancements

Integration of Next-Generation IoT: Future smart greenhouses may utilize advanced IoT devices with enhanced capabilities, including energy harvesting and self-healing networks, to further reduce maintenance and energy costs.

AI and Machine Learning Evolution: Continued development in AI will likely provide more sophisticated predictive analytics for precision farming, improving decision-making processes and operational efficiency.

Robotics and Automation: The incorporation of robotics for tasks such as planting, pruning, harvesting, and packaging could automate nearly all physical activities within the greenhouse.

Advanced Sensing Technologies: The development of more sensitive and selective sensors could allow for the detection of specific plant diseases or nutrient deficiencies at earlier stages.

Economic and Market Trends

Cost Reduction: As technology becomes more widespread and production scales up, the cost of implementing smart greenhouse systems is expected to decrease, making it more accessible.

Market Differentiation: Producers may increasingly rely on the superior quality and sustainability of smart greenhouse crops to differentiate their products in the market.

Investment in Research and Development: Private and public sectors are likely to increase investment in R&D to further explore the untapped potential of IoT in agriculture.

Environmental Sustainability

Climate Change Adaptation: Smart greenhouses may become a key tool in adapting to the challenges posed by climate change, allowing cultivation in areas previously unsuitable for agriculture.

Renewable Energy Integration: The future may see a closer integration of smart greenhouses with renewable energy sources, like solar or wind power, to create a truly sustainable agricultural system.

Policy and Regulatory Frameworks

Standardization and Certification: The development of international standards and certification for smart agriculture technologies could facilitate their adoption and integration across different regions.

Data Governance: There will be a need for clear policies regarding data ownership, privacy, and security, particularly as farm data becomes increasingly valuable.

Social and Educational Aspects

Workforce Development: Education and training programs will be crucial in preparing a new generation of farmers who are proficient in technology.

Public Awareness: Efforts to raise public awareness about the benefits of smart greenhouse agriculture can drive consumer preference and market demand.

Research Areas

Interdisciplinary Research: Future research should be inherently interdisciplinary, combining plant science, environmental science, engineering, data science, and other fields.

Human-Computer Interaction: Studies on how humans interact with these systems can lead to more user-friendly designs and increased adoption rates.

Ecosystem Services: Exploring the broader ecological impacts of smart greenhouses, such as their role in pollinator pathways or biodiversity, could open new avenues for sustainable agriculture.

In conclusion, the future of IoT-based smart greenhouses is bright and ripe with possibilities. Innovations in technology and practices promise not only to enhance productivity and sustainability but also to profoundly reshape the agricultural landscape. By anticipating these directions, stakeholders can prepare to meet the challenges and harness the opportunities that lie ahead.

9. Conclusion

Throughout this paper, we have explored the multifaceted role that IoT-based smart greenhouse systems play in revolutionizing Controlled Environment Agriculture (CEA). By integrating

advanced technologies to monitor and control the growing environment, these systems offer unparalleled precision in agricultural management, leading to enhanced crop yields, resource efficiency, and sustainable farming practices. The review of the literature and case studies has underscored the significant improvements that IoT technologies bring to greenhouse operations, including increased operational efficiency, cost reduction, and the provision of optimal conditions for plant growth. The potential of IoT in agriculture extends beyond immediate operational improvements, offering a path to address broader challenges such as food security, climate change resilience, and the reduction of agriculture's environmental footprint. Furthermore, we have identified and discussed the primary challenges associated with implementing IoT in greenhouses, from technical and economic barriers to social and policy-related issues. The solutions to these challenges, while not trivial, have been evolving through innovative approaches in technology, financing, and policy-making. The benefits presented by IoT-based smart greenhouses—such as water conservation, energy efficiency, and the socio-economic upliftment of rural areas—illustrate the transformative impact of these systems. The positive implications for sustainability, efficiency, and food security position smart greenhouses not just as a tool for individual growers but as a critical component in the future of global agriculture. Looking forward, the continued evolution of IoT technology, coupled with advancements in related fields such as artificial intelligence, big data analytics, and machine learning, will undoubtedly lead to even more sophisticated and efficient smart greenhouse ecosystems. This progression promises to further enhance the ability of growers to produce food in a variety of climates and conditions, catering to the world's growing population in a sustainable manner.

In conclusion, IoT-based smart greenhouse systems stand at the forefront of agricultural innovation, offering viable solutions to today's agricultural challenges while opening new horizons for future developments. It is incumbent upon researchers, industry leaders, and policymakers to continue to foster the growth of this dynamic field, ensuring that the potential of smart greenhouses is fully realized for the benefit of all.

References

1. Vishwakarma, A. Sahu, N. Sheikh, P. Payasi, S. K. Rajput and L. Srivastava, "IOT Based Greenhouse Monitoring And Controlling System," *2020 IEEE Students Conference on Engineering & Systems (SCES)*, Prayagraj, India, 2020, pp. 1-6, doi: 10.1109/SCES50439.2020.9236693.
2. P. V. Vimal and K. S. Shivaprakasha, "IOT based greenhouse environment monitoring and controlling system using Arduino platform", *IEEE International Conference on Intelligent Computing Instrumentation and Control Technologies (ICICT)*, pp. 1514-1519, 2017.
3. A. Chakraborty, M. Islam, A. Dhar and M. S. Hossain, "IoT Based Greenhouse Environment Monitoring and Smart Irrigation System for Precision Farming Technology," *2022 International Conference on Innovations in Science, Engineering and Technology (ICISSET)*, Chittagong, Bangladesh, 2022, pp. 123-128, doi: 10.1109/ICISSET54810.2022.9775852.

4. R. Aafreen, S. Y. Neyaz, R. Shamim and M. S. Beg, "An IoT based system for telemetry and control of Greenhouse environment," *2019 International Conference on Electrical, Electronics and Computer Engineering (UPCON)*, Aligarh, India, 2019, pp. 1-6, doi: 10.1109/UPCON47278.2019.8980258.
5. Y. Alaviyan, M. Aghaseyedabdollah, M. Sadafi and A. Yazdizade, "Design and Manufacture of a Smart Greenhouse with Supervisory Control of Environmental Parameters Using Fuzzy Inference Controller," *2020 6th Iranian Conference on Signal Processing and Intelligent Systems (ICSPIS)*, Mashhad, Iran, 2020, pp. 1-6, doi: 10.1109/ICSPIS51611.2020.9349619.
6. A. F. Subahi and K. E. Bouazza, "An Intelligent IoT-Based System Design for Controlling and Monitoring Greenhouse Temperature," in *IEEE Access*, vol. 8, pp. 125488-125500, 2020, doi: 10.1109/ACCESS.2020.3007955.
7. L. Dan, C. Xin, H. Chongwei and J. Liangliang, "Intelligent Agriculture Greenhouse Environment Monitoring System Based on IOT Technology," *2015 International Conference on Intelligent Transportation, Big Data and Smart City*, Halong Bay, Vietnam, 2015, pp. 487-490, doi: 10.1109/ICITBS.2015.126.
8. M. M. Abbassy and W. M. Ead, "Intelligent Greenhouse Management System," *2020 6th International Conference on Advanced Computing and Communication Systems (ICACCS)*, Coimbatore, India, 2020, pp. 1317-1321, doi: 10.1109/ICACCS48705.2020.9074345.
9. R. Zhao, Y. Ding, S. Ma and M. Wang, "Design of Intelligent Greenhouse Control System Based on Internet of Things," *2019 2nd International Conference on Information Systems and Computer Aided Education (ICISCAE)*, Dalian, China, 2019, pp. 117-121, doi: 10.1109/ICISCAE48440.2019.221600.
10. O. Elijah, T. A. Rahman, I. Orikumhi, C. Y. Leow and M. N. Hindia, "An Overview of Internet of Things (IoT) and Data Analytics in Agriculture: Benefits and Challenges", *IEEE Internet of Things Journal*, vol. 99, no. 2018, pp. 1-1.
11. Minkeun Ha et al., "SNAIL gateway: Dual-mode wireless access points for WiFi and IP-based wireless sensor networks in the internet of things", *Consumer Communications and NETWORKING Conference IEEE*, pp. 169-173, 2012.
12. A. Augustin, J. Yi, T. Clausen and W. M. Townsley, "A Study of LoRa: Long Range and Low Power Networks for the Internet of Things", *Sensors*, vol. 16, no. 9, pp. 1466, 2016.
13. M. A. Akkaş and R. Sokullu, "An IoT-based greenhouse monitoring system with micaz motes", *Procedia Comput. Sci.*, vol. 113, pp. 603-608, 2017.
14. K.-L. Tsai, F.-Y. Leu and I. You, "Residence energy control system based on wireless smart socket and IoT", *IEEE Access*, vol. 4, pp. 2885-2894, 2016.
15. R. J. Tom, S. Sankaranarayanan and J. J. P. C. Rodrigues, "Smart energy management and demand reduction by consumers and utilities in an IoT-fog-based power distribution system", *IEEE Internet Things J.*, vol. 6, no. 5, pp. 7386-7394, Oct. 2019.



Institutional Sign In

All



[ADVANCED SEARCH](#)

Journals & Magazines > IEEE Internet of Things Journal > Volume: 10 Issue: 21 [?](#)

IoMT-Assisted Medical Vehicle Routing Based on UAV-Borne Human Crowd Sensing and Deep Learning in Smart Cities

Publisher: [IEEE](#)

[Cite This](#)

[PDF](#)

[Khosro Rezaee](#) ; [Mohammad R. Khosravi](#) ; [Hani Attar](#) ; [Varun G. Menon](#) ; [Mohammad Ayoub Khan](#) ; [Haitham Issa](#) ; [Lianyong ...](#) [All Authors](#) [...](#)

2
Cites in
Papers

181
Full
Text Views



Alerts

[Manage Content Alerts](#)
[Add to Citation Alerts](#)

Abstract

Document Sections

- I. Introduction
- II. Related Work
- III. Proposed Method
- IV. Results
- V. Conclusion

Authors

- [Figures](#)
- [References](#)
- [Citations](#)
- [Keywords](#)
- [Metrics](#)
- [More Like This](#)



Downl
PDF

Abstract:An emergency medical vehicle can save the patient's life if it arrives at his location as quickly as possible. Unmanned aerial vehicles (UAVs) offer wide visibility and m... [View more](#)

► Metadata

Abstract:

An emergency medical vehicle can save the patient's life if it arrives at his location as quickly as possible. Unmanned aerial vehicles (UAVs) offer wide visibility and mobility, making them a viable choice for smart cities and intelligent transportation systems (ITSs) as edge devices for the Internet of Things (IoT). Based on population behavior and overcrowding, video surveillance through the Internet of multimedia things (IoMT) and public safety in smart cities can help determine the most efficient routes for emergency medical vehicles. This study investigates UAV overcrowding and abnormal population activity patterns, which affect the flow of emergency medical vehicles and traffic flow. Moreover, the purpose of this article is to analyze received video frames from UAVs in order to identify the most efficient route for emergency medical vehicles in smart cities to transfer patients in the event of abnormalities or overcrowding. In order to detect overcrowding on the streets, a hybrid Cascade-ResNet is utilized, which detects congestion based on many data points. Based on our proposed approach, we achieve a 2.5% improvement over similar methods because it is effective, flexible, and accurate. UAV video frames can be used to communicate with emergency response vehicles, to monitor traffic congestion, and to monitor other aspects of smart city life.

Published in: IEEE Internet of Things Journal (Volume: 10 , Issue: 21, 01 November 2023)

Page(s): 18529 - 18536

DOI: 10.1109/JIOT.2023.3284056

Date of Publication: 08 June 2023 [?](#)

Publisher: IEEE

▼ ISSN Information:

Electronic ISSN: 2327-4662

CD: 2372-2541

PDF

[Help](#)



Khosro Rezaee
Department of Biomedical Engineering, Meybod University, Meybod, Iran

Mohammad R. Khosravi
Shandong Provincial University Laboratory for Protected Horticulture, Weifang University of Science and Technology, Weifang, Shandong, China

Hani Attar
Department of Energy Engineering, Zarqa University, Zarqa, Jordan

Varun G. Menon
Department of Computer Science and Engineering, SCMS School of Engineering and Technology, Ernakulam, India

Mohammad Ayoub Khan
College of Computing and Information Technology, University of Bisha, Bisha, Saudi Arabia

Haitham Issa
Department of Electrical Engineering, Zarqa University, Zarqa, Jordan

Lianyong Qi
Department of Computer Science, China University of Petroleum (East China), Dongying, China

Contents

I. Introduction

Delays in locating an accident for a patient, calling emergency services, and assessing how to get to the ideal location can cause irreparable damage to the patient [1]. With time lost, the ability to provide essential assistance to the person decreases, and despite heavy traffic, emergency vehicles, especially, ambulances, are unable to arrive on time. Determining the proper route for medical emergency vehicles can, therefore, save the lives of patients, injured people, and others [1]. In urban areas, video surveillance is used for behavior analysis because it provides information about activities' location [2]. Smart cities use video surveillance to identify and track pedestrians, identify congestion [2]. Traffic flow in crowded places may be affected by social issues related to congestion. Intelligent technologies such as CCTV are increasingly employed to monitor crowded areas [3], [4], [5]. Due to the rarity of overcrowding, it is difficult to control the population and avoid congestion. There are many different characteristics of crowds. Identifying the population and monitoring human behavior are essential in metropolitan areas because of abnormal congestion [6]. Consequently, the intelligent technology is needed to prevent human error and accidental inefficiency. Additionally, smart cities require an automated monitoring system that is constantly available in real time [7].

Authors

Khosro Rezaee
Department of Biomedical Engineering, Meybod University, Meybod, Iran

Mohammad R. Khosravi
Shandong Provincial University Laboratory for Protected Horticulture, Weifang University of Science and Technology, Weifang, Shandong, China

Hani Attar
Department of Energy Engineering, Zarqa University, Zarqa, Jordan

Varun G. Menon
Department of Computer Science and Engineering, SCMS School of Engineering and Technology, Ernakulam, India

Mohammad Ayoub Khan
College of Computing and Information Technology, University of Bisha, Bisha, Saudi Arabia

PDF

Help

Haitham Issa
Department of Electrical Engineering, Zarqa University, Zarqa, Jordan

Lianyong Qi
Department of Computer Science, China University of Petroleum (East China), Dongying, China

Figures	▼
References	▼
Citations	▼
Keywords	▼
Metrics	▼

More Like This

Intelligent Patient Monitoring for Arrhythmia and Congestive Failure Patients Using Internet of Things and Convolutional Neural Network
2019 31st International Conference on Microelectronics (ICM)
Published: 2019

Classification Techniques for Arrhythmia Patterns Using Convolutional Neural Networks and Internet of Things (IoT) Devices
IEEE Access
Published: 2022

Show More

PDF

Help

IEEE Personal Account

CHANGE
USERNAME/PASSWORD

Purchase Details

PAYMENT OPTIONS
VIEW PURCHASED
DOCUMENTS

Profile Information


COMMUNICATIONS
PREFERENCES
PROFESSION AND
EDUCATION
TECHNICAL INTERESTS

Need Help?

US & CANADA: +1 800
678 4333
WORLDWIDE: +1 732
981 0060
CONTACT & SUPPORT

Follow



[About IEEE Xplore](#) | [Contact Us](#) | [Help](#) | [Accessibility](#) | [Terms of Use](#) | [Nondiscrimination Policy](#) | [IEEE Ethics Reporting](#)  | [Sitemap](#) | [IEEE Privacy Policy](#)

A not-for-profit organization, IEEE is the world's largest technical professional organization dedicated to advancing technology for the benefit of humanity.

© Copyright 2024 IEEE - All rights reserved.

IEEE Account

- » [Change Username/Password](#)
- » [Update Address](#)

Purchase Details

- » [Payment Options](#)
- » [Order History](#)
- » [View Purchased Documents](#)

Profile Information

- » [Communications Preferences](#)
- » [Profession and Education](#)
- » [Technical Interests](#)

Need Help?

- » **US & Canada:** +1 800 678 4333
- » **Worldwide:** +1 732 981 0060

PDF

Help

[» Contact & Support](#)

[About IEEE Xplore](#) | [Contact Us](#) | [Help](#) | [Accessibility](#) | [Terms of Use](#) | [Nondiscrimination Policy](#) | [Sitemap](#) | [Privacy & Opting Out of Cookies](#)

A not-for-profit organization, IEEE is the world's largest technical professional organization dedicated to advancing technology for the benefit of humanity.
© Copyright 2024 IEEE - All rights reserved. Use of this web site signifies your agreement to the terms and conditions.

PDF

Help

Indicating Context for Emoji Powered Bengali Hate Speech Detection using Extended Fuzzy SVM and Text Embedding Models

Just Accepted

Authors: [Sayani Ghosal](#), [Amita Jain](#), [Devendra Kumar Tayal](#), [Varun G. Menon](#), [Akshi Kumar](#) [Authors Info & Claims](#)

ACM Transactions on Asian and Low-Resource Language Information Processing • Accepted on March 2023
• <https://doi.org/10.1145/3589001>

Published: 27 March 2023 [Publication History](#) 

 0  299

    eReader  PDF

     45   

Abstract

The massive growth of social webs offer opportunities to communicate with diverse languages, unstructured text, informal posts, misspelled contents and emojis. Social media users feel comfortable to express their emotions specially emotions with high intensity (hate speech) in their mother tongue. Hate speech in any form targets groups and individuals that may trigger antisocial activities, crimes, and terrorist acts. Bengali social media users use Bengali for posting implicit or indirect text. Existing Bengali hate speech detection research considers explicit hate speech detection but in actual hate is expressed more in implicit way. In order to detect both implicit and explicit hate speech for low resource content, social webs need highly efficient automated tools. Researchers applied discriminative learning approaches (i.e. SVM, MLP, CNN) to distinguish hate text with only clear-cut

Feedback

PDF










Help



dataset (FSVMCIL) and multilingual BERT (mBERT) text embedding model to detect first hate label; (ii) Morphological analysis method to detect implicit and explicit hate content with the hate similarity (HS)

Bengali hate lexicon. It also considers emoji to text conversion for efficient contextual analysis. This study also conducts extensive experiments for various categories with the Bengali hate speech dataset. It also evaluates the proposed model performance considering weighted F1 score, precision, recall and accuracy parameters. Results reveal significant improvement in Bengali hate speech detection with 2.35% increase in F1- score and 9.11 % increase in accuracy.

References


1. Statista Research Department. 2022. Number of monthly active Facebook users worldwide as of 2nd quarter 2022. Statista. Retrieved 29 July 2022 from <https://www.statista.com/statistics/264810/number-of-monthly-active-facebook-users-worldwide/> 
2. Quantum Marketer. 2022. How Many People Use Twitter in 2022? (Twitter Statistics). Retrieved 29 July 2022 from <https://quantummarketer.com/twitter-statistics/> 
3. Sayani Ghosal and Amita Jain. 2021. Research Journey of Hate Content Detection From Cyberspace. In Natural Language Processing for Global and Local Business (pp. 200-225). IGI Global. <https://doi.org/10.4018/978-1-7998-4240-8.ch009> 
4. Light. 2022. Rising Levels of Hate Speech & Online Toxicity During This Time of Crisis. Retrieved 25 July 2022 from https://l1ght.com/Toxicity_during_coronavirus_Report-L1ght.pdf 
5. Statista Research Department. 2022. The most spoken languages worldwide in 2022. Statista. Retrieved 10 Aug 2022 from <https://www.statista.com/statistics/266808/the-most-spoken-languages-worldwide/> 
6. Nauros Romim, Mosahed Ahmed, Hriteshwar Talukder, and Saiful Islam. 2021. Hate speech detection in the bengali language: A dataset and its baseline evaluation. In Proceedings of International Joint Conference on Advances in Computational Intelligence (pp. 457-468). Springer, Singapore. https://doi.org/10.1007/978-981-16-0586-4_37  
7. Tomas Mikolov, Kai Chen, Greg Corrado, and Jeffrey Dean. 2013. Efficient estimation of word representations in vector space. arXiv preprint arXiv:1301.3781 
8. Alec Radford, Karthik Narasimhan, Tim Salimans, and Ilya Sutskever. 2018. Improving language understanding with unsupervised learning. Technical report, OpenAI. 



PDF



Help


10. Md, Imdadul Haque Emon, Khondoker Nazia Iqbal, Md Mehedi, Humaion Kabir, Mohammed Julfikar Ali Mahub, and Annajiat Alim Rasel. 2022. Detection of Bangla Hate Comments and Cyberbullying in Social



ACM Transactions on Asian and Low-Resource Language Information Processing



11. Jacob Devlin, Ming-Wei Chang, Kenton Lee, and Kristina Toutanova. 2018. Bert: Pre-training of deep bidirectional transformers for language understanding. arXiv preprint arXiv:1810.04805. 


12. Alvi Md Ishmam and Sadia Sharmin. 2019. Hateful speech detection in public facebook pages for the bengali language. In 2019 18th IEEE international conference on machine learning and applications (ICMLA) (pp. 555-560). IEEE. <https://doi.org/10.1109/ICMLA.2019.00104>  | 


13. Estiak Ahmed Emon, Shihab Rahman, Joti Banarjee, Amit Kumar Das, and Tanni Mittra. 2019. A deep learning approach to detect abusive bengali text. In 2019 7th International Conference on Smart Computing & Communications (ICSCC) (pp. 1-5). IEEE. <https://doi.org/10.1109/ICSCC.2019.8843606>  | 


14. Amena Akter Aporna, Istinub Azad, Nibraj Safwan Amlan, Md Humaion Kabir Mehedi, Mohammed Julfikar Ali Mahub, and Annajiat Alim Rasel. 2022. Classifying Offensive Speech of Bangla Text and Analysis Using Explainable AI. In International Conference on Advances in Computing and Data Sciences (pp. 133-144). Springer, Cham. https://doi.org/10.1007/978-3-031-12638-3_12 

15. Tharindu Ranasinghe, and Marcos Zampieri. 2021. Multilingual offensive language identification for low-resource languages. Transactions on Asian and Low-Resource Language Information Processing, 21(1), 1-13. <https://doi.org/10.1145/3457610>  | 

16. Md Rezaul Karim, Bharathi Raja Chakravarthi, John P. McCrae, and Michael Cochez. 2020. Classification benchmarks for under-resourced bengali language based on multichannel convolutional-lstm network. In 2020 IEEE 7th International Conference on Data Science and Advanced Analytics (DSAA) (pp. 390-399). IEEE. <https://doi.org/10.1109/DSAA49011.2020.00053>  | 

17. Nauros Romim, Mosahed Ahmed, Md Saiful Islam, Arnab Sen Sharma, Hriteshwar Talukder, and Mohammad Ruhul Amin. 2021. HS-BAN: A Benchmark Dataset of Social Media Comments for Hate Speech Detection in Bangla. arXiv preprint arXiv:2112.01902. 

18. Muhammad F. Mridha, Md Anwar Hussen Wadud, Md Abdul Hamid, Muhammad Mostafa Monowar, Muhammad Abdullah-Al-Wadud, and Atif Alamri. 2021. L-Boost: Identifying Offensive Texts From Social Media Post in Bengali. IEEE Access, 9, 164681-164699. <https://doi.org/10.1109/ACCESS.2021.3134154> 


19. Manash Sarker, Md Forhad Hossain, Fahmida Rahman Liza, Syed Nazmus Sakib, and Abdullah. 2022. A Machine Learning Approach to Classify Anti-social Bengali Comments on Social Media. In 2022 International Conference on Advancement in Electrical and Electronic Engineering (ICAEEE) (pp. 1-6). IEEE. <https://doi.org/10.1109/ICAEEE54957.2022.9836407>  | 

PDF



Help



21. Han Liu, Pete Burnap, Wafa Alorainy, and Matthew L. Williams. 2019. A fuzzy approach to text classification with two-stage training for ambiguous instances. *IEEE Transactions on Computational Social Systems*, 6(2),



ACM Transactions on Asian and Low-Resource Language Information Processing 



22. Sayani Ghosal and Amita Jain. 2022. HateCircle and Unsupervised Hate Speech Detection incorporating Emotion and Contextual Semantic. *ACM Transactions on Asian and Low-Resource Language Information Processing*. <https://doi.org/10.1145/3576913>  | 



23. Md Gulzar Hussain, Tamim Al Mahmud, and Waheda Akthar. 2018. An approach to detect abusive bangla text. In *2018 International Conference on Innovation in Engineering and Technology (ICIET)* (pp. 1-5). IEEE. <https://doi.org/10.1109/ICIET.2018.8660863>  | 



24. Nayan Banik, and Md Hasan Hafizur Rahman. 2019. Toxicity detection on bengali social media comments using supervised models. In *2019 2nd International Conference on Innovation in Engineering and Technology (ICIET)* (pp. 1-5). IEEE. <https://doi.org/10.1109/ICIET48527.2019.9290710>  | 


25. Fha Shibly, Uzzal Sharma, and Hmm Naleer. 2022. Development of an efficient method to detect mixed social media data with Tamil-English code using machine learning techniques. *Transactions on Asian and Low-Resource Language Information Processing*. <https://doi.org/10.1145/3563775>  | 

26. Pradeep Kumar Roy, Snehaan Bhawal, and Chinnaudayar Navaneethakrishnan Subalalitha .2022. Hate speech and offensive language detection in Dravidian languages using deep ensemble framework. *Computer Speech & Language*, 75, 101386. <https://doi.org/10.1016/j.csl.2022.101386>  | 

27. Md Anwar Hussen Wadud, Muhammad Mohsin Kabir, M. F. Mridha, M. Ameer Ali, Md Abdul Hamid, and Muhammad Mostafa Monowar. 2022. How can we manage Offensive Text in Social Media-A Text Classification Approach using LSTM-BOOST. *International Journal of Information Management Data Insights*, 2(2), 100095. <https://doi.org/10.1016/j.jjime.2022.100095>  | 

28. Gourav Jain, Tripti Mahara, S. C. Sharma, and Arun Kumar Sangaiah. 2022. A Cognitive Similarity-Based Measure to Enhance the Performance of Collaborative Filtering-Based Recommendation System. *IEEE Transactions on Computational Social Systems*, 9(6), 1785-1793. <https://doi.org/10.1109/TCSS.2022.3187430>  | 

29. Sayani Ghosal and Amita Jain. 2022. Weighted aspect based sentiment analysis using extended OWA operators and Word2Vec for tourism. *Multimedia Tools and Applications*, 1-28. <https://doi.org/10.1007/s11042-022-13800-4>  | 

30. Prasanta Mandal, Apurbalal Senapati, and Amitava Nag. 2022. Hate-Speech Detection in News in the Context of West Bengal Assembly Election 2021. In *Pattern Recognition and Data Analysis with Applications* (pp. 247-256). Springer, Singapore. https://doi.org/10.1007/978-981-19-1520-8_19 

31. Tharindu Ranasinghe, and Marcos Zampieri. 2020. Multilingual offensive language identification with cross-

PDF

Help



33. DOI: [10.1.1.1.1](#). Retrieved 15 April 2022 from [https://doi.org/10.1.1.1.1](#)

ACM Transactions on Asian and Low-Resource Language Information Processing

34. Unicode. Full Emoji List, v14.0.2. Retrieved 29 January 2022 from <https://www.emoji.com/full-emoji-list>



35. Adam Wiemerslage, Miikka Silfverberg, Changbing Yang, Arya D. McCarthy, Garrett Nicolai, Eliana Colunga, and Katharina Kann. 2022. Morphological Processing of Low-Resource Languages: Where We Are and What's Next. arXiv preprint arXiv:2203.08909.

36. Elisa Bassignana, Valerio Basile, and Viviana Patti. 2018. Hurltlex: A multilingual lexicon of words to hurt. In 5th Italian Conference on Computational Linguistics, CLiC-it 2018. CEUR-WS, Vol. 2253, pp. 1-6

37. Subrata. Bengali slang words with meaning (Bengali slang dictionary). Academia. Retrieved 29 January 2022 from https://www.academia.edu/2965218/Bengali_slang_words_with_meaning_Bengali_slang_dictionary

38. <https://github.com/stopwords-iso/stopwords-bn>

39. Rui Zhao, Anna Zhou, and Kezhi Mao. 2016. Automatic detection of cyberbullying on social networks based on bullying features. In Proceedings of the 17th international conference on distributed computing and networking (pp. 1-6). <https://doi.org/10.1145/2833312.2849567> |

40. Telmo Pires, Eva Schlinger, and Dan Garrette. 2019. How multilingual is multilingual BERT?. arXiv preprint arXiv:1906.01502.

41. Chao Zhang, Juanjuan Ding, Jianming Zhan, Arun Kumar Sangaiah, and Deyu Li. 2022. Fuzzy Intelligence Learning Based on Bounded Rationality in IoMT Systems: A Case Study in Parkinson's Disease. IEEE Transactions on Computational Social Systems. <https://doi.org/10.1109/TCSS.2022.3221933>

42. Amita Jain, and D. K. Lobiyal. 2015. Fuzzy Hindi WordNet and word sense disambiguation using fuzzy graph connectivity measures. ACM Transactions on Asian and Low-Resource Language Information Processing (TALLIP), 15(2), 1-31.

43. Chun-Fu Lin, and Sheng-De Wang. 2002. Fuzzy support vector machines. IEEE transactions on neural networks, 13(2), 464-471. <https://doi.org/10.1109/72.991432> |

44. Marti A. Hearst, Susan T. Dumais, Edgar Osuna, John Platt, and Bernhard Scholkopf. 1998. "Support vector machines." Intelligent Systems and their Applications, IEEE, 13(4), pp. 18–28. <https://doi.org/10.1109/5254.708428> |

45. Rukshan Batuwita, and Vasile Palade. 2010. FSVM-CIL: fuzzy support vector machines for class imbalance learning. IEEE Transactions on Fuzzy Systems, 18(3), 558-571. <https://doi.org/10.1109/TFUZZ.2010.2042721>

PDF

Help

Show Fewer References

Index Terms

Inculcating Context for Emoji Powered Bengali Hate Speech Detection using Extended Fuzzy SVM and Text Embedding Models

Applied computing

Computing methodologies

Artificial intelligence

Natural language processing

Index terms have been assigned to the content through auto-classification.

Recommendations

HateCircle and Unsupervised Hate Speech Detection Incorporating Emotion and Contextual Semantics

The explosive growth of social media has fueled an extensive increase in online freedom of speech. The worldwide platform of human voice creates possibilities to assail other users without facing any consequences, and flout social etiquettes,...

[Read More](#)

Detecting Hate Speech Contents Using Embedding Models

Computational Data and Social Networks

Abstract

The rise of hate speech contents on social network platforms has recently become a topic of interest. There have been a lo...

[Read More](#)

A cross-lingual transfer learning method for online COVID-19-related hate speech detection

Abstract

During the COVID-19 pandemic, online social media platforms such as Twitter facilitate the exchange of informat

Highlights

- Suggested a cross-lingual COVID-19-related hate speech detection problem...

PDF

Help

[Read More](#)

DL Comment Policy

Comments should be relevant to the contents of this article, (sign in

Got it

ACM Transactions on Asian and Low-Resource Language Information Processing

0 Comments

Share

Best

Newest

Oldest

Nothing in this discussion yet.

Privacy

Do Not Sell My Data

Categories

- Journals
- Magazines
- Books
- Proceedings
- SIGs
- Conferences
- Collections
- People

Join

- Join ACM
- Join SIGs
- Subscribe to Publications
- Institutions and Libraries

About

- About ACM Digital Library
- ACM Digital Library Board
- Subscription Information
- Author Guidelines
- Using ACM Digital Library
- All Holdings within the ACM Digital Library
- ACM Computing Classification System
- Digital Library Accessibility

Connect

- Contact
- Facebook
- Twitter
- Linkedin
- Feedback
- Bug Report

PDF

Help





ACM Transactions on Asian and Low-Resource Language Information Processing

PDF

Help



Guest Editorial

Introduction to the Special Section on Computational Intelligence and Advanced Learning for Next-Generation Industrial IoT

THE rapid development of real-time Industrial Internet-of-Things (IIoT) applications including green infrastructure, smart grids, smart city, intelligent transport networks, etc. enables green communication between tens of billions of end devices such as wearable devices and sensors. As a result, a tremendous amount of data is generated from massively distributed sources, which require computational intelligence techniques to fulfill high computing and communication demand that frequently exceeds energy consumption. Many emerging IIoT applications including remote surgery, machine monitoring and control, fault detection, and healthcare generate delay-sensitive tasks, which require timely processing with minimum delay. Besides, according to the energy consumption formulation, the required energy consumption for processing real-time tasks on remote computing devices should be the accumulation of data transmission time, transmission power, and processing capacity. Thereby, the energy emission rate can be controlled by balancing the trade-off between the transmission power and transmission time. IIoT covers a broad domain of real-time IIoT applications and refers to the combination of IoT technologies and computational intelligence techniques for processing real-time data with minimum delay. In addition, energy-efficient communication and computation of the real-time IIoT applications target to increase efficiency, automation, and productivity.

Recent advances in artificial intelligence (AI)-enabled techniques including advanced machine learning (ML) and deep learning (DL), bring many key research directions to analyze the computational intelligence framework by monitoring the real-time information and sensed data. Despite various advantages of the integration of computational intelligence techniques for various IIoT applications, the appropriate application of the AI model poses several challenges including data volume and quality, integration, and accuracy of the inferences drawn from the collected data. Besides that, advanced computational intelligence techniques such as distributed and federated learning are selected to train the local edge/fog devices locally and produce a global model under the coordination of a central edge/fog/cloud server. In recent times, advanced computational intelligence techniques for IIoT have attracted great interest from academia and industry.

The special section focused on the recent advances and novel contributions from academic researchers and industry practi-

tioners in the area of computational intelligence techniques for the Next-generation IIoT applications to fully leverage the potential capabilities and opportunities brought by this area. Thanks to the extensive efforts of the reviewers and the great support from the Editor-in-Chief, Dr. Jianwei Huang, we were able to accept 27 contributed articles covering several important topics related to IIoT application [A1], mobile edge resource allocation [A2], Federated Learning (FL) in edge computing [A3], intelligent transportation system [A4], digital-twin in edge computing [A5], Blockchain and digital-twin in IIoT [A6], robust graph clustering [A7], distributed split mechanism in wireless communication system [A8], task offloading in D2D-based IIoT application [A9], prediction-based task allocation [A10], secured FL mechanism in healthcare system [A11], computational intelligence and deep learning in edge networks [A12], intrusion detection for IIoT applications [A13], privacy preservation in edge networks [A14], federated analysis in distributed IIoT network [A15], resource allocation using deep reinforcement learning [A16], securing IIoT applications using hybrid deep learning [A17], security enhancement using deep learning [A18], anomaly detection in IIoT application [A19], partial task offloading and resource allocation [A20], anomaly detection in IIoT application [A21], resource allocation in vehicular social networks [A22], computational offloading and resource allocation in end-edge-cloud framework [A23], privacy preserving data aggregation using FL [A24], secure framework for Internet of Drones [A25], accelerating CNN for IIoT applications [A26], object detection in edge networks [A27], dynamic tracking in IIoT [A1]. A brief review follows:

Li et al. in [A1], addressed that earlier research has attempted to follow the demographic trends, even though many have looked at tracking population dynamics. In this regard, their work suggested a widely used, reliable IIoT-based approach for tracking built environment demographic dynamics.

Zhang et al. [A2], proposed a proactive downlink system framework in which a proactive task-based data transmission problem is decomposed into multiple sub-problems and improves the low latency communication scenario.

Chakraborty and Misra in [A3], addressed the resource allocation problem to improve the quality of IIoT. Motivated by this, they proposed the framework using the Nah-Bargaining game approach that optimizes the service delay in edge networks.

Zhou et al. in [A4], considered the challenges in the vehicle re-identification area for cross-domain. To address this problem,

they proposed a generative adversarial network to transform the identical vehicle into other domains.

Wen et al. [A5] considered the delays and communication failures in ocean monitoring platforms. To address this issue, they propose an artificial platform method based on maritime IoT where multi-autonomous underwater glider (AUG) systems are used to reduce communication delays.

Kumar et al. [A6] found different kinds of threats and attacks on ongoing communication by unreliable public communication channels and a lack of confidence among participating entities. In response to these difficulties, they provide an integrated framework of blockchain and Deep Learning (DL) for delivering decentralised data processing and learning in the IIoT network, where the DL scheme is created to apply the Intrusion Detection System (IDS) on legitimate data obtained from the blockchain.

Wang et al. [A7] found that many of the consolidation solutions now in use are unaware of the significance of an appropriate consolidation schema. They concentrate on offering a strong and efficient consolidation schema in their article. They consider the workload uncertainty issue and provide a graph-clustering-based approach that is more resilient to workload uncertainty in the future than the majority of existing methods, which primarily concentrate on the past workload. To achieve this, they present robust optimization, a mathematical approach that offers support theoretically for resolving uncertainty problems.

Sun et al. [A8] found wireless communication system dependability faces difficulties due to the stringent requirements for industrial applications. So, they suggest a distributed split mechanism with a cross-level dependability assessment model in their study. The distributed split mechanism splits and deploys the model's device-level assessment sub-models and system-level assessment sub-models independently once they have been trained together.

Ibrar et al. [A9] addressed the Social IIoT (SIIoT) problems due to uneven job offloading which actually worsens system performance. In this research, they offer an adaptive capacity task offloading solution for D2D-based social industrial IoT (ToSIIoT) that takes into account the strength of social links and device utilization ratio to enhance resource utilization, raise QoS, and achieve higher task completion rates. The suggested method has three components: selecting a socially conscious relay in a multi-hop D2D communication context, selecting a resource-rich SIIoT device for task offloading, and adaptive workload redistribution.

Peng et al. in [A10] found the efficiency of crowdsourcing job allocation is decreased by the fact that existing spatial crowdsourcing task allocation technologies overlook the temporal and spatial continuity of previous work data. For addressing this issue, they suggested a Spatiotemporal Prediction based Spatial Crowdsourcing technique, known as SPSC, utilizing blockchain and artificial intelligence to address these issues. The SPSC lowers the possibility of crowdsourcing employees banding together to steal the private data of crowdsourcing projects utilizing blockchain technology by classifying crowdsourcing activities and grouping crowdsourcing workers.

Zhang et al. [A11] introduced the deep learning of medical models in an Internet of Things (IoT)-based healthcare system. To further secure local models, cryptographic primitives like masks and homomorphic encryption are used. This prevents the adversary from deducing sensitive medical data through various

methods like model reconstruction attacks or model inversion attacks. The security study demonstrates that the suggested solution fulfills data privacy.

Tang et al. [A12] found that it is difficult for multiple devices to complete local training and upload weights to the edge server promptly due to the constrained resources in industrial IoT networks, including CPU power, bandwidth, and channel status. So, they offer a novel multi-exit-based federated edge learning (ME-FEEL) framework to address this problem, allowing the deep model to be partitioned into numerous sub-models of varying depths and output prediction from the exit in each sub-model.

Zhang et al. [A13] noticed that intrusion detection is a practical way to increase security in the Industrial Internet of Things (IIoT) which are so susceptible to cyberattacks. However, since labeled examples are hard to come by, finding a trustworthy model is also challenging. They use graph neural network technologies to deal with the high dimensional, redundant, but categorically imbalanced and scarce labeled data in IIoT. This network constructor with refinement regularisation is created to alter the network structure to reduce the impact produced by the erroneous network structure.

Wang et al. in [A14] discussed that outsourcing data to far-away clouds always carries a risk to privacy and has a significant latency. As a result, they develop a new framework (called PC-NNCEC) based on cloud-edge-client collaboration for effective and privacy-preserving CNN inference. In PCNNCEC, the cloud model and client data for the IIoT are divided into two shares and sent to two edge servers without collusion.

Wang et al. [A15] described that all types of federated industrial IoT learning tasks suffer considerably from the intrinsic data heterogeneity (skewness) of many industrial IoT data holders. They suggest a Federated skewness Analytics and Client Selection mechanism (FedACS) to quantify the skewness of the data while protecting privacy and use this knowledge to support subsequent tasks including federated learning.

Chang et al. [A16] present unique machine learning-based resource allocation and trajectory planning strategies for a multi-UAV communications system. They first provide a machine learning-based strategic resource allocation algorithm that uses deep learning and reinforcement learning to create the best possible policy for every UAV to address the issue created by the large dimensionality in state space. With no prior knowledge of the dynamic nature of networks, they then also provide a multi-agent deep reinforcement learning technique for distributed implementation.

Hasan et al. [A17] found that the attacks by smart and persistent multi-variant bots are seen as disastrous for connected IIoTs. Additionally, botnet attack detection is quite difficult and precise. Therefore, the prompt and effective identification of IIoT botnets is an urgent current demand. To protect IIoT infrastructure from deadly and complex multi-variant botnet attacks, they provide a hybrid intelligent Deep Learning (DL)-enabled technique.

Ye et al. [A18] discussed that the widespread adoption of WiFi fingerprinting of Received Signal Strength (RSS) for indoor localization is challenging. Current RSS fingerprint-based techniques lack security-related concerns and are open to hostile intrusions. They suggested suggesting SE-Loc, a strategy based on semi-supervised learning to increase the security and

robustness of fingerprint-based localization. The SE-Loc architecture consists of two components: (1) a correlation-based AP selection for handling RSS fingerprints and generating fingerprint images, and (2) a deep learning model based on a denoising autoencoder and convolutional neural networks for robust feature learning and location matching.

Gao et al. [A19] discovered that anomaly detection is crucial to assure hardware and software security since the IoT's time-series feature increases data density and dimension. The conventional anomaly detection technique, however, has trouble satisfying this requirement. So, in their research, they offer a memory-augmented autoencoder technique that uses reconstruction errors to identify data anomalies in IoT data.

Zhang et al. [A20] discussed that IIoT resources must be used effectively because IIoT devices have a finite capacity. Finding the best option for effective resource allocations is also difficult because of the variety of services customers can choose from and the dynamic nature of wireless networks. To address this issue, they suggested a partial task offloading and resource allocation strategy, aiming to maximize user work completed within a reasonable time frame while reducing energy consumption.

Yang and Zhou [A21] discovered that the data on intrusion detection is in the form of a dynamic data stream with infiniteness, correlations, and changing data distribution features. These characteristics, however, provide some challenges for the existing anomaly detection methods. To achieve accurate and effective anomaly detection with improved scalability, thus they offer ASTREAM (anomaly detection in data streams), a unique anomaly detection approach that combines sliding window, model updating, and change detection algorithms into LSHiForest.

Zhang and Zhou [A22] found that, due to the narrow range of vehicular social networks and the uneven distribution of cache resources, issues including low vehicle data transfer rates, subpar service quality, and poor service content delivery efficiency of streaming media are present. To address these issues, they offer an approach to resource distribution in vehicle social networks (RATG) based on tripartite graphs. Using vehicle mobility and social similarity as its foundations, this technique creates a mobile vehicular social network model.

Peng et al. [A23] discussed about the large scale of IIoT devices and the nature of the applications, as well as the constrained and heterogeneous resources of edge servers, prevent the direct deployment of the existing MEC approaches for IIoT situations. In light of this, they develop an end-edge-cloud collaborative intelligent optimization technique and formulate the offloading of computation and resource allocation as a multi-objective optimization issue.

Song et al. in [A24] showed that FL is vulnerable to a reverse attack, in which a foe might obtain user information by scrutinizing the user-uploaded model. Thus, they created EPPDA, an effective privacy-preserving data aggregation mechanism for FL, based on secret sharing to resist the reverse attack, which can aggregate users trained models covertly without disclosing the user models.

Tanveer et al. [A25] discussed the requirements of the authentication key exchange between users and drones in the Internet of Drones (IoD) networks for users to be able to communicate securely with the drone through the public communication infrastructure. In their study, they present a REAS-IoD

authentication mechanism for IoD networks. The AKE process is carried out securely by the proposed REAS-IoD using the ACE authentication primitive and lightweight hash function.

Li et al. in [A26], offer ABM-SpConv-SIMD, an on-device inference optimization framework, to expedite the network inference by fully using the low-cost and common CPU resource. This model optimizer with pruning and quantization is used initially by ABM-SpConv SIMD to create models with sparse convolutions.

Wu et al. [A27], presented an edge computing and multi-task-driven framework to fulfill tasks of image enhancement and object detection with quick response, in contrast to previous techniques to acquire enhanced images before detection with various types of manually constructed filters.

In summary, the collected articles provide innovative application scenarios and shed light on the computational intelligence and advanced learning for next-generation Industrial IoT. We hope that this timely special section will trigger more future work in the emerging area.

MAINAK ADHIKARI, *Lead Guest Editor*
Department of Computer Science
Indian Institute of Information Technology
Lucknow 226002, India
mainak@iiit.ac.in

VARUN G. MENON, *Guest Editor*
Computer Science and Engineering
SCMS Group of Educational Institutions
Kerala 683 106, India
varunmenon@ieee.org

DANDA B. RAWAT, *Guest Editor*
Department of Electrical Engineering and Computer Science
Howard University
Washington, DC 20059 USA
db.rawat@ieee.org

XINGWANG LI, *Guest Editor*
Henan Polytechnic University
Henan 454099, China
lixingwang@hpu.edu.cn

APPENDIX RELATED ARTICLES

- [A1] P. Li et al., "IIoT based trustworthy demographic dynamics tracking with advanced Bayesian learning," *IEEE Trans. Netw. Sci. Eng.*, early access, Jan. 25, 2022, doi: [10.1109/TNSE.2022.3145572](https://doi.org/10.1109/TNSE.2022.3145572).
- [A2] P. Zhang, H. Tian, P. Zhao, and S. Fan, "Context-aware mobile edge resource allocation in OFDMA downlink system," *IEEE Trans. Netw. Sci. Eng.*, early access, Nov. 24, 2022, doi: [10.1109/TNSE.2022.3224258](https://doi.org/10.1109/TNSE.2022.3224258).
- [A3] A. Chakraborty and S. Misra, "QoS-aware resource bargaining for federated learning over edge networks in industrial IoT," *IEEE Trans. Netw. Sci. Eng.*, early access, Sep. 14, 2022, doi: [10.1109/TNSE.2022.3206474](https://doi.org/10.1109/TNSE.2022.3206474).

- [A4] Z. Zhou et al., "GAN-Siamese network for cross-domain vehicle re-identification in intelligent transport systems," *IEEE Trans. Netw. Sci. Eng.*, early access, Aug. 18, 2022, doi: [10.1109/TNSE.2022.3199919](https://doi.org/10.1109/TNSE.2022.3199919).
- [A5] J. Wen, J. Yang, Y. Li, J. He, Z. Li, and H. Song, "Behavior-based formation control digital twin for multi-AUG in edge computing," *IEEE Trans. Netw. Sci. Eng.*, early access, Aug. 19, 2022, doi: [10.1109/TNSE.2022.3198818](https://doi.org/10.1109/TNSE.2022.3198818).
- [A6] P. Kumar et al., "Blockchain and deep learning for secure communication in digital twin empowered industrial IoT network," *IEEE Trans. Netw. Sci. Eng.*, early access, Jul. 18, 2022, doi: [10.1109/TNSE.2022.3191601](https://doi.org/10.1109/TNSE.2022.3191601).
- [A7] S. Wang, H. Lan, Y. Peng, and Z. Peng, "Consolidating industrial small files using robust graph clustering," *IEEE Trans. Netw. Sci. Eng.*, early access, Aug. 01, 2022, doi: [10.1109/TNSE.2022.3195350](https://doi.org/10.1109/TNSE.2022.3195350).
- [A8] D. Sun, J. Zhao, B. Chen, H. Wu, and J. Wu, "Cross-level dependability assessment with a distributed split mechanism for wireless communication systems," *IEEE Trans. Netw. Sci. Eng.*, early access, Jul. 28, 2022, doi: [10.1109/TNSE.2022.3194535](https://doi.org/10.1109/TNSE.2022.3194535).
- [A9] M. Ibrar et al., "Adaptive capacity task offloading in multi-hop D2D-based social industrial IoT," *IEEE Trans. Netw. Sci. Eng.*, early access, Jul. 19, 2022, doi: [10.1109/TNSE.2022.3192478](https://doi.org/10.1109/TNSE.2022.3192478).
- [A10] M. Peng et al., "Spatiotemporal prediction based intelligent task allocation for secure spatial crowdsourcing in industrial IoT," *IEEE Trans. Netw. Sci. Eng.*, early access, Aug. 16, 2022, doi: [10.1109/TNSE.2022.3198675](https://doi.org/10.1109/TNSE.2022.3198675).
- [A11] L. Zhang, J. Xu, P. Vijayakumar, P. K. Sharma, and U. Ghosh, "Homomorphic encryption-based privacy-preserving federated learning in IoT-enabled healthcare system," *IEEE Trans. Netw. Sci. Eng.*, early access, Jun. 30, 2022, doi: [10.1109/TNSE.2022.3185327](https://doi.org/10.1109/TNSE.2022.3185327).
- [A12] S. Tang et al., "Computational intelligence and deep learning for next-generation edge-enabled industrial IoT," *IEEE Trans. Netw. Sci. Eng.*, early access, Jun. 08, 2022, doi: [10.1109/TNSE.2022.3180632](https://doi.org/10.1109/TNSE.2022.3180632).
- [A13] Y. Zhang, C. Yang, K. Huang, and Y. Li, "Intrusion detection of industrial internet-of-things based on reconstructed graph neural networks," *IEEE Trans. Netw. Sci. Eng.*, early access, Jun. 21, 2022, doi: [10.1109/TNSE.2022.3184975](https://doi.org/10.1109/TNSE.2022.3184975).
- [A14] J. Wang, D. He, A. Castiglione, B. B. Gupta, M. Karuppiah, and L. Wu, "PCNNCEC: Efficient and privacy-preserving convolutional neural network inference based on cloud-edge-client collaboration," *IEEE Trans. Netw. Sci. Eng.*, early access, May 26, 2022, doi: [10.1109/TNSE.2022.3177755](https://doi.org/10.1109/TNSE.2022.3177755).
- [A15] Z. Wang, Y. Zhu, D. Wang, and Z. Han, "Federated analytics informed distributed industrial IoT learning with non-IID data," *IEEE Trans. Netw. Sci. Eng.*, early access, Jul. 04, 2022, doi: [10.1109/TNSE.2022.3187992](https://doi.org/10.1109/TNSE.2022.3187992).
- [A16] Z. Chang et al., "Trajectory design and resource allocation for multi-UAV networks: Deep reinforcement learning approaches," *IEEE Trans. Netw. Sci. Eng.*, early access, May 03, 2022, doi: [10.1109/TNSE.2022.3171600](https://doi.org/10.1109/TNSE.2022.3171600).
- [A17] T. Hasan et al., "Securing industrial internet of things against botnet attacks using hybrid deep learning approach," *IEEE Trans. Netw. Sci. Eng.*, early access, Apr. 22, 2022, doi: [10.1109/TNSE.2022.3168533](https://doi.org/10.1109/TNSE.2022.3168533).
- [A18] Q. Ye et al., "SE-Loc: Security-enhanced indoor localization with semi-supervised deep learning," *IEEE Trans. Netw. Sci. Eng.*, early access, May 23, 2022, doi: [10.1109/TNSE.2022.3174674](https://doi.org/10.1109/TNSE.2022.3174674).
- [A19] H. Gao et al., "TSMAE: A novel anomaly detection approach for internet of things time series data using memory-augmented autoencoder," *IEEE Trans. Netw. Sci. Eng.*, early access, Mar. 29, 2022, doi: [10.1109/TNSE.2022.3163144](https://doi.org/10.1109/TNSE.2022.3163144).
- [A20] F. Zhang et al., "Deep reinforcement learning based cooperative partial task offloading and resource allocation for IIoT applications," *IEEE Trans. Netw. Sci. Eng.*, early access, Apr. 19, 2022, doi: [10.1109/TNSE.2022.3167949](https://doi.org/10.1109/TNSE.2022.3167949).
- [A21] Y. Yang et al., "ASTREAM: Data-stream-driven scalable anomaly detection with accuracy guarantee in IIoT environment," *IEEE Trans. Netw. Sci. Eng.*, early access, Mar. 08, 2022, doi: [10.1109/TNSE.2022.3157730](https://doi.org/10.1109/TNSE.2022.3157730).
- [A22] Y. Zhang and Y. Zhou, "Resource allocation strategy based on tripartite graph in vehicular social networks," *IEEE Trans. Netw. Sci. Eng.*, early access, Feb. 23, 2022, doi: [10.1109/TNSE.2022.3153511](https://doi.org/10.1109/TNSE.2022.3153511).
- [A23] K. Peng et al., "Intelligent computation offloading and resource allocation in IIoT with end-edge-cloud computing using NSGA-III," *IEEE Trans. Netw. Sci. Eng.*, early access, Mar. 08, 2022, doi: [10.1109/TNSE.2022.3155490](https://doi.org/10.1109/TNSE.2022.3155490).
- [A24] J. Song et al., "EPPDA: An efficient privacy-preserving data aggregation federated learning scheme," *IEEE Trans. Netw. Sci. Eng.*, early access, Feb. 25, 2022, doi: [10.1109/TNSE.2022.3153519](https://doi.org/10.1109/TNSE.2022.3153519).
- [A25] M. Tanveer, A. U. Khan, T. Nguyen, M. Ahmad, and A. Abdei-Latif, "Towards a secure and computational framework for Internet of Drones enabled aerial computing," *IEEE Trans. Netw. Sci. Eng.*, early access, Feb. 15, 2022, doi: [10.1109/TNSE.2022.3151843](https://doi.org/10.1109/TNSE.2022.3151843).

- [A26] X. Li et al., "ABM-SpConv-SIMD: Accelerating convolutional neural network inference for industrial IoT applications on edge devices," *IEEE Trans. Netw. Sci. Eng.*, early access, Feb. 25, 2022, doi: [10.1109/TNSE.2022.3154412](https://doi.org/10.1109/TNSE.2022.3154412).
- [A27] Y. Wu et al., "Edge computing driven low-light image dynamic enhancement for object detection," *IEEE Trans. Netw. Sci. Eng.*, early access, Feb. 14, 2022, doi: [10.1109/TNSE.2022.3151502](https://doi.org/10.1109/TNSE.2022.3151502).

Mainak Adhikari (Senior Member, IEEE) received the B.Tech degree in computer science and engineering from the West Bengal University of Technology, Kolkata, India, and the M.Tech. degree in computer science and engineering from the University of Kalyani, Kalyani, India, and the Ph.D. degree from the Indian Institute of Technology Dhanbad, Dhanbad, India. He completed his Postdoctoral Research Fellowship from the Mobile & Cloud Lab, Institute of Computer Science, University of Tartu, Tartu, Estonia. He is currently the Head of Department and Assistant Professor of Indian Institute of Information Technology Lucknow, Lucknow, India. His research interests include distributed computing such as serverless computing, fog computing, and cloud computing, wearable sensors for healthcare, Internet-of-Things, and data analysis with AI approaches. He has contributed to numerous research articles/papers in various national and international journals such as IEEE, ACM, Elsevier, and Springer and conferences such as IEEE and Springer.

Varun G. Menon (Senior Member, IEEE) is currently an Associate Professor of computer science and engineering, international collaborations and a Corporate Relations in-charge with the SCMS School of Engineering and Technology, SCMS Group of Educational Institutions, Cochin, India. His research interests include the Internet of medical Things, Wearable sensor for healthcare, Ad Hoc network, wireless networks, 5G, fog computing and networking, underwater acoustic sensor networks, information science, scientometrics, opportunistic routing, and wireless sensor networks.

Danda B. Rawat (Fellow, IEEE) is currently a Professor with the Department of Electrical Engineering and Computer Science, the Founding Director of the Data Science and Cybersecurity Center, Graduate Program Director of Howard-CS Graduate Programs, Director of Graduate Cybersecurity Certificate Program, and Founding Director of Cyber-security and Wireless Networking Innovations Research Lab, Howard University, Washington, DC, USA. Dr. Rawat is engaged in research and teaching in the areas of cybersecurity, machine learning, and wireless networking for emerging networked systems including cyber-physical systems, Internet of Things, smart cities, software-defined systems, and vehicular networks.

Xingwang Li (Senior Member, IEEE) received the M.Sc. degree from the University of Electronic Science and Technology of China, Chengdu, China, in 2010, and the Ph.D. degree from the Beijing University of Posts and Telecommunications, Beijing, China, in 2015. From 2010 to 2012, he was an Engineer with Comba Telecom Ltd., Guangzhou, China. From 2017 to 2018, he was a Visiting Scholar with Queen's University Belfast, Belfast, U.K. His research interests include MIMO communication, cooperative communication, hardware constrained communication, nonorthogonal multiple access, physical layer security, unmanned aerial vehicles, and Internet of Things.

Guest Editorial

Intelligent Autonomous Transportation System With 6G—Series—Part III

WE ARE delighted to introduce the third part of the Special Section on Intelligent Autonomous Transportation Systems with 6G, which aims to provide the scientific community with a comprehensive overview of innovative technologies, advanced architectures, and potential challenges for the 6G-supported Intelligent Autonomous Transport Systems. Twenty articles were selected for publication in this issue. All the articles were rigorously evaluated according to the standard reviewing process of the IEEE TRANSACTIONS ON INTELLIGENT TRANSPORTATION SYSTEMS. The evaluation process considered originality, technical quality, presentational quality, and overall contribution. We will introduce these articles and highlight their main contributions in the following.

In [A1], Kamal et al. discuss the requirements of securing data exchange between autonomous vehicles. Securing data transfer and keeping a record of each transaction becomes necessary in IoV/IATS. Furthermore, they discuss optimized security algorithms using symmetric encryption for secure multimedia data transfer between vehicles. The main feature of these optimized algorithms is that they use a lower amount of data to generate fingerprints.

In [A2], Liu et al. present a discussion on a UAV-enabled Computing-Communications Intelligent Offloading (UAV-CCIO) scheme to offload tasks energy-efficiently. Here some nodes with a large amount of data are selected as Task Gathering Nodes (TGNs), and TGNs collect all the tasks of the left nodes. In this way, the UAV can only fly the TGNs, and so all the IoT devices' tasks can be offloaded. The distance needed for the UAV can be significantly reduced and energy is saved.

In [A3], Fang et al. discuss a new protograph-LDPC-coded modulation framework utilizing irregular mapping (IM) for the flash-memory systems. Analyses and simulations indicate that the proposed IM protograph-LDPC-coded modulation scheme can achieve very desirable performance and thus is a reliable and efficient storage solution for new-generation mobile networks, such as the Internet of Vehicles.

In [A4], Wang et al. discuss a heterogeneous Blockchain-based Hierarchical Trust Evaluation strategy, named BHTE, utilizing the federated deep learning technology for 5G-ITS. Specifically, the trust of ITS users and task distributors is evaluated using federated deep learning, and hierarchical incentive mechanisms are designed for reasonable and fair rewards and punishments. Moreover, the trusts of ITS

users and task distributors are stored on heterogeneous and hierarchical blockchains for trust verification.

In [A5], Liu et al. explore Massive machine type communication (mMTC) as a core component of 6G, to fulfill the demand of massive connectivity of billions of Internet-of-Things (IoT) devices. Granting free random access is a promising technique for implementing mMTC, and the key to grant-free random access is active device detection at the base station. The article further discusses an odd-periodic total squared correlation bound, and systematic constructions of sequences achieving that bound are presented. It is demonstrated that the proposed sequences can be effectively used in massive device activity detection.

In [A6], Zhen et al. present a discussion on the uplink synchronization maintenance problem in a satellite-ground integrated vehicular network. They propose an efficient timing advance update approach by jointly designing the preamble format and fourth-order statistics-based timing metric. The proposed approach's superiority is demonstrated in class separability, the robustness of the multi-path effect and CFO, and the computational complexity through theoretical derivation and numerical investigations.

In [A7], Aloqaily et al. present a novel cooperative health emergency response system within Cooperative Intelligent Transportation Environment, namely, C-HealthIER. C-HealthIER is a cooperative health intelligent emergency response system that aims to reduce the time of receiving the first emergency treatment for passengers with abnormal health conditions. C-HealthIER continuously monitors passengers' health and conducts cooperative behavior in response to health emergencies by vehicle-to-vehicle and vehicle-to-infrastructure information sharing to find the nearest treatment provider.

In [A8], Duan et al. discuss an improved isolation forest method with data mass (MS-iForest) for data tampering attack detection, in which the data mass is used instead of the number of divisions and an anomaly score ranking to quantify the degree of anomalies is provided. This method is promising to be used as part of the intrusion detection system, like a security component in the onboard gateway, which can effectively avoid data tampering attacks.

In [A9], the authors discuss the exploration of the intrusion detection effect of urban rail transit management systems to improve the safety performance of the traffic field in urban construction. They further discuss on the deep convolution neural network model AlexNet with more network layers and

stronger learning ability to ensure the safe operation of urban rail transit. Meanwhile, the GRU (Gate Recurrent Unit) neural network is introduced into the improved AlexNet to build an intrusion detection model for urban rail transit management systems.

In [A10], Liu et al. present a discussion on a Lightweight Trustworthy Message Exchange (LTME) scheme for UAV networks by efficiently aggregating the cryptography and trust management technologies. In the LTME scheme, a centralized Ground Control Station (GCS) periodically updates the reputation levels of registered UAVs (or UAVs for short) and securely distributes secret values to the UAVs. Based on the received secret values, each trustworthy broadcasting UAV can generate its encrypted messages so that only trustworthy receiving UAVs can decrypt them, and each trustworthy receiving UAV can accurately judge whether the received messages and the corresponding broadcasting UAVs are trustworthy in a lightweight manner.

In [A11], Gao et al. discuss the analysis of the 3-D point cloud for the 3-D scene understanding of autonomous driving. Further, a local feature transformer model and a trans-pooling model are presented, and a novel point cloud analysis framework LFT-Net is designed for 3-D point cloud analysis, which enhances the expression ability of local fine-grained characteristics of 3-D point cloud data.

In [A12], Liu et al. present an offloading scheme by exploiting multi-hop vehicle computation resources in vehicular edge computing based on mobility analysis of vehicles. In addition to the vehicles within one hop from the task vehicle that generates computation tasks, certain multi-hop vehicles that meet the given requirements in terms of link connectivity and computation capacity are also leveraged to carry out the tasks offloaded by the task vehicle.

In [A13], Li et al. discuss a cooperative Conflict Detection and Resolution (CD&R) method in the UAV IoT environment considering UAV relative motion relationships and UAV priorities. To verify the effectiveness of CD&R methods, a safety assessment method (evaluate from both conflict feature and network structure perspectives) is also proposed. A Monte Carlo Simulation with “clone mechanism” is designed to incorporate the effect of CD&R systems.

In [A14], He et al. analyze the security issues of the Internet of vehicles (IoV) in 5G environment from the perspective of big data. Further, an access control mechanism based on risk prediction is proposed aiming at the problems existing in the node access control process. A Wasserstein Distance-based Combined Generative Adversarial Network (WCGAN) is proposed. It modifies the loss function to solve the gradient disappearance problem, and a combination of multiple generators is designed to solve the pattern collapse.

In [A15], Yu et al. explore the construction status and prediction performance of intelligent transportation systems in the road network of smart cities based on 5G network. Aiming at the diversity and complexity of regional traffic influencing factors of road network in the construction of smart city, this research carries out resource real-time load balancing scheduling from the perspective of a 5G heterogeneous network.

In [A16], Zheng et al. discuss the challenges of spectrum scarcity, large-scale connectivity, ultra-low latency, and various security threats for the upcoming Intelligent Transportation System supported by 6G. To address these issues, the article discusses an overlay cognitive ambient backscatter communication non-orthogonal multiple access network for ITS and elaborates on the secrecy performance by deriving the secrecy outage probability.

In [A17], Zhou et al. explore the performance of short-term traffic flow prediction of the 5G Internet of Vehicles (IoV) based on edge computing (EC) for the smart city and to further improve the intelligence of the smart city. Aiming at the current emergency of traffic congestion and road congestion, the present work adds EC to the current vehicle network and integrates a deep convolution random forest neural network (DCRFNN).

In [A18], Chu et al. present a trajectory planning and tracking framework, which applies an artificial potential to obtain target trajectory and model predictive control (MPC) with PID feedback to effectively track planned trajectory. The method can reduce steady errors of the conventional MPC caused by the simplified vehicle model.

In [A19], Gao et al. discuss a spectrum sensing scheduling (SSS) scheme for communication resource management in vehicle platooning. Based on the SSS scheme and vehicle-to-vehicle (V2V) communications, a greedy algorithm for resource allocation is designed to minimize platoon delay.

In [A20], Dong et al. discuss a dependence-aware edge intelligent function offloading scheme for 6G-based Internet of Vehicles (IoV). Each edge server can provide some specific intelligent functional services. These services can receive data from cars and serve as different intelligent functions. Then, an intelligent application offloading scheme is changed into an embedding scheme of a service chain. An NP-hard objective function is constructed using a multi-winner committee selection model for this offloading service chain embedding problem.

We would like to express our sincere thanks to all the authors for submitting their articles and to the reviewers for their valuable comments and suggestions that significantly enhanced the quality of these articles. We are also grateful to Editor-in-Chief, Prof. Azim Eskandarian, for the tremendous support throughout this Special Issue’s review and publication process and, of course, all the editorial staff. We hope this Special Issue will serve as a valuable reference for researchers, scientists, engineers, and academics in intelligent autonomous transportation systems.

SHAHID MUMTAZ, *Corresponding Guest Editor*
Instituto de Telecomunicacoes
Aveiro 3810078, Portugal
e-mail: dr.shahid.mumtaz@ieee.org

MUHAMMAD IKRAM ASHRAF, *Guest Editor*
Nokia Bell Labs
4876 Espoo, Finland
e-mail: ikram.ashraf@nokia-bell-labs.com

VARUN G. MENON, *Guest Editor*
SCMS School of Engineering and Technology
Karukutty, Kerala 683576, India
e-mail: varunmenon@ieee.org

TAIMOOR ABBAS, *Guest Editor*
Huawei Technologies
9087 Lund, Sweden
e-mail: taimoor.abbas@ieee.org

ANWER AL-DULAIMI, *Guest Editor*
EXFO Electro-Optical Engineering
Montreal, QC H4S 0A9, Canada
e-mail: anwer.aldulaimi@ieee.org

APPENDIX: RELATED ARTICLES

- [A1] M. Kamal, M. Tariq, G. Srivastava, and L. Malina, "Optimized security algorithms for intelligent and autonomous vehicular transportation systems," *IEEE Trans. Intell. Transp. Syst.*, early access, Nov. 2, 2021, doi: [10.1109/TITS.2021.3123188](https://doi.org/10.1109/TITS.2021.3123188).
- [A2] R. Liu, A. Liu, Z. Qu, and N. N. Xiong, "An UAV-enabled intelligent connected transportation system with 6G communications for Internet of Vehicles," *IEEE Trans. Intell. Transp. Syst.*, early access, Oct. 28, 2021, doi: [10.1109/TITS.2021.3122567](https://doi.org/10.1109/TITS.2021.3122567).
- [A3] Y. Fang, Y. Bu, P. Chen, F. C. M. Lau, and S. A. Otaibi, "Irregular-mapped protograph LDPC-coded modulation: A bandwidth-efficient solution for 6G-enabled mobile networks," *IEEE Trans. Intell. Transp. Syst.*, early access, Nov. 3, 2021, doi: [10.1109/TITS.2021.3122994](https://doi.org/10.1109/TITS.2021.3122994).
- [A4] X. Wang, S. Garg, H. Lin, G. Kaddoum, J. Hu, and M. M. Hassan, "Heterogeneous blockchain and AI-driven hierarchical trust evaluation for 5G-enabled intelligent transportation systems," *IEEE Trans. Intell. Transp. Syst.*, early access, Dec. 1, 2021, doi: [10.1109/TITS.2021.3129417](https://doi.org/10.1109/TITS.2021.3129417).
- [A5] B. Liu, Z. Zhou, Y. Yang, A. R. Adhikary, and P. Fan, "Constructions of binary signature sets with optimal odd total squared correlation and their application to device activity detection," *IEEE Trans. Intell. Transp. Syst.*, early access, Nov. 25, 2021, doi: [10.1109/TITS.2021.3128632](https://doi.org/10.1109/TITS.2021.3128632).
- [A6] L. Zhen, Y. Wang, K. Yu, G. Lu, Z. Mumtaz, and W. Wei, "Reliable uplink synchronization maintenance for satellite-ground integrated vehicular networks: A high-order statistics-based timing advance update approach," *IEEE Trans. Intell. Transp. Syst.*, early access, Dec. 10, 2021, doi: [10.1109/TITS.2021.3131816](https://doi.org/10.1109/TITS.2021.3131816).
- [A7] M. Aloqaily, H. Elayan, and M. Guizani, "C-HealthIER: A cooperative health intelligent emergency response system for C-ITS," *IEEE Trans. Intell. Transp. Syst.*, early access, Feb. 9, 2022, doi: [10.1109/TITS.2022.3141018](https://doi.org/10.1109/TITS.2022.3141018).
- [A8] X. Duan, H. Yan, D. Tian, J. Zhou, J. Su, and W. Hao, "In-vehicle CAN bus tampering attacks detection for connected and autonomous vehicles using an improved isolation forest method," *IEEE Trans. Intell. Transp. Syst.*, early access, Dec. 15, 2021, doi: [10.1109/TITS.2021.3128634](https://doi.org/10.1109/TITS.2021.3128634).
- [A9] Y. Sun, J. Xu, H. Wu, G. Lin, and S. Mumtaz, "Deep learning based semi-supervised control for vertical security of maglev vehicle with guaranteed bounded airgap," *IEEE Trans. Intell. Transp. Syst.*, vol. 22, no. 7, pp. 4431–4442, Jul. 2021.
- [A10] Z. Liu et al., "Lightweight trustworthy message exchange in unmanned aerial vehicle networks," *IEEE Trans. Intell. Transp. Syst.*, early access, Dec. 22, 2021, doi: [10.1109/TITS.2021.3136304](https://doi.org/10.1109/TITS.2021.3136304).
- [A11] Y. Gao, X. Liu, J. Li, Z. Fang, X. Jiang, and K. M. S. Huq, "LFT-Net: Local feature transformer network for point clouds analysis," *IEEE Trans. Intell. Transp. Syst.*, early access, Feb. 1, 2022, doi: [10.1109/TITS.2022.3140355](https://doi.org/10.1109/TITS.2022.3140355).
- [A12] L. Liu, M. Zhao, M. Yu, M. A. Jan, D. Lan, and A. Taherkordi, "Mobility-aware multi-hop task offloading for autonomous driving in vehicular edge computing and networks," *IEEE Trans. Intell. Transp. Syst.*, early access, Jan. 19, 2022, doi: [10.1109/TITS.2022.3142566](https://doi.org/10.1109/TITS.2022.3142566).
- [A13] S. Li, X. Cheng, X. Huang, S. A. Otaibi, and H. Wang, "Cooperative conflict detection and resolution and safety assessment for 6G enabled unmanned aerial vehicles," *IEEE Trans. Intell. Transp. Syst.*, early access, Jan. 4, 2022, doi: [10.1109/TITS.2021.3137458](https://doi.org/10.1109/TITS.2021.3137458).
- [A14] Y. He, M. Kong, C. Du, D. Yao, and M. Yu, "Communication security analysis of intelligent transportation system using 5G Internet of Things from the perspective of big data," *IEEE Trans. Intell. Transp. Syst.*, early access, Mar. 23, 2022, doi: [10.1109/TITS.2022.3141788](https://doi.org/10.1109/TITS.2022.3141788).
- [A15] M. Yu, "Construction of regional intelligent transportation system in smart city road network via 5G network," *IEEE Trans. Intell. Transp. Syst.*, early access, Feb. 14, 2022, doi: [10.1109/TITS.2022.3141731](https://doi.org/10.1109/TITS.2022.3141731).
- [A16] Y. Zheng et al., "Overlay cognitive ABCOM-NOMA based ITS: An in-depth secrecy analysis," *IEEE Trans. Intell. Transp. Syst.*, early access, Jan. 19, 2022, doi: [10.1109/TITS.2022.3140325](https://doi.org/10.1109/TITS.2022.3140325).
- [A17] S. Zhou, C. Wei, C. Song, X. Pan, W. Chang, and L. Yang, "Short-term traffic flow prediction of the smart city using 5G Internet of Vehicles based on edge computing," *IEEE Trans. Intell. Transp. Syst.*, early access, Feb. 15, 2022, doi: [10.1109/TITS.2022.3147845](https://doi.org/10.1109/TITS.2022.3147845).
- [A18] D. Chu, H. Li, C. Zhao, and T. Zhou, "Trajectory tracking of autonomous vehicle based on model predictive control with PID feedback," *IEEE Trans. Intell. Transp. Syst.*, early access, Feb. 17, 2022, doi: [10.1109/TITS.2022.3150365](https://doi.org/10.1109/TITS.2022.3150365).
- [A19] W. Gao, C. Wu, L. Zhong, and K.-L.-A. Yau, "Communication resources management based on spectrum sensing for vehicle platooning," *IEEE Trans. Intell. Transp. Syst.*, early access, Feb. 9, 2022, doi: [10.1109/TITS.2022.3148230](https://doi.org/10.1109/TITS.2022.3148230).
- [A20] L. Dong, H. Gao, W. Wu, Q. Gong, N. C. Dechasa, and Y. Liu, "Dependence-aware edge intelligent function offloading for 6G-based IoV," *IEEE Trans. Intell. Transp. Syst.*, early access, Feb. 9, 2022, doi: [10.1109/TITS.2022.3148229](https://doi.org/10.1109/TITS.2022.3148229).

Optimizing Routing in Nature-Inspired Algorithms to Improve Performance of Mobile Ad-Hoc Network

Dr. Arshey M¹, Ravuri Daniel², Deepak Dasaratha Rao³, Dr. Emerson Raja⁴, D Chandrasekhar Rao⁵, Aniket Deshpande⁶

Submitted: 20/04/2023

Revised: 19/06/2023

Accepted: 30/06/2023

Abstract: It is a wireless network made up of mobile nodes that operate independently and use radio waves to communicate. Nodes can communicate with one another without a permanent basic structure by exchanging packets with nearby nodes. When the hosts are in wireless communication range, they exchange packets directly and without the need for a middle man. By sending messages to intermediaries, communication occurs outside of the wireless range. The message is sent to the closest host by the originating node. The host then passes it on to the host that is the closest to it, allowing for numerous hops between the intermediate nearby nodes to carry out the conversation. In these networks, each node is in charge of deciding which path is the most effective for transferring packets. The best path is picked and the packet is forwarded when a node receives it. Every node of the network has routing capabilities built into it in this fashion. At first, a new protocol called Energy Aware Simple Ant Routing Algorithm (ESARA) was developed in which the node's energy consumption was factored into the cost function. It was discovered that the adjustment boosted the packet delivery ratio and decreased routing overhead. Such an adjustment also helped boost communication throughput. It was observed that ESARA's performance improved even when the number of hosts increased.

Keywords: Wireless network, wireless range, MANET, SARA, ESARA.

1. Introduction

The efficiency of the network is dependent on how well the routing protocol performs. The following characteristics are ideal for an efficient MANET routing protocol. The MANET routing protocols should ideally have these qualities in order to function well. i) Distributed control: In MANET, routing is carried out jointly by all nodes because there is no centralized control [1]. The protocols used in MANET should therefore have distributed control for this reason. ii) Loop Free: Packets transmitted along paths with loops will just circle without being eaten by any nodes. This lowers network

effectiveness. A perfect protocol would find a direct route from source to destination without any loops. iii) Adjust to the circumstance: The MANET routing protocol should zealously support any changes to the network's structure [2]. They must effectively use resources like bandwidth and power. iv) Secure: The creation of MANET requires the cooperation of all hosts connected to the network. These networks are typically vulnerable to assaults at the network and link layers. Hence, MANET protocols should be resilient to a variety of network threats [3].

¹Department of Computer Science and Engineering, SCMS School Of Engineering And Technology, arsheym@scmsgroup.org, 0000-0001-6702-4064

²Department of Computer Science and Engineering, Prasad V. Potluri Siddhartha Institute of Technology, Vijayawada, Andhra Pradesh, India, danielravuri@gmail.com; 0000-0001-8404-8674

³Research and Development, India, Ddrb2011@gmail.com; 0000-0001-5959-3136

⁴Faculty of Engineering and Technology, Multimedia University, Malaysia, emerson.raja@mmu.edu.my; 0000-0002-4512-0802

⁵Department of Information Technology, Veer Surendra Sai University of Technology, Burla, India, dcrao_it@vssut.ac.in; 0000-0001-7414-3360

⁶Department of Computer Science and Engineering, Mewar University, Gangrar, Rajasthan, India, anik.deshpande@gmail.com; orchid id : 0000-0001-6366-5999

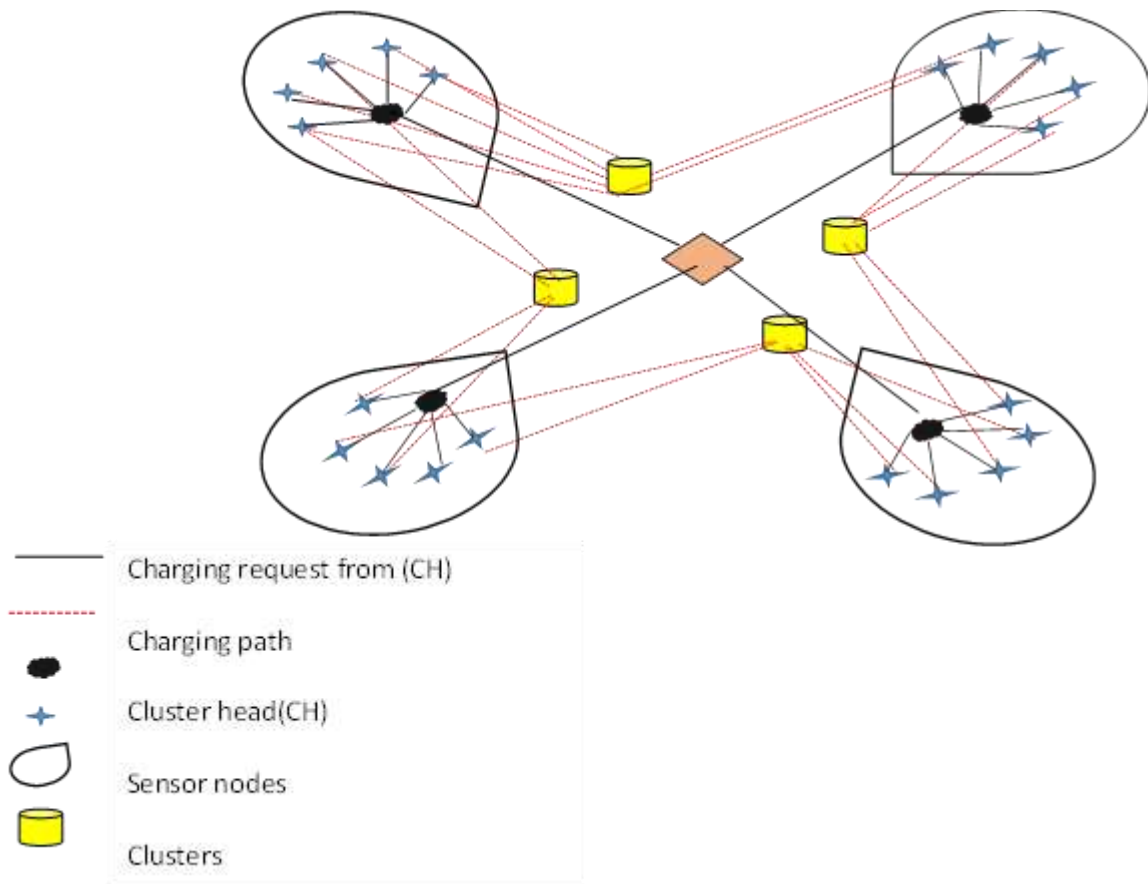


Fig I: A WSN model with multiple mobile chargers.

It can be difficult to route in the changing environment of MANET. Many problems prevent efficient routing operations. These are a few of the concerns that should be addressed when creating MANET routing protocols. MANET communicates over a wireless medium. Due to electromagnetic interference or unfavourable weather, the wireless medium is vulnerable to distortions. Furthermore, erratic are the link's performance and bandwidth availability [4]. These variables all affect the MANET's ability to communicate effectively. Batteries, which cannot maintain electricity for an extended period of time, power hosts in MANET. Because of this, hosts in MANET live shorter lives. They have limited storage and processing power because of their compact size [5]. Nodes in MANET move quickly and abruptly alter the network's structure. Moreover, their erratic mobility will cause links between nearby nodes to fail. Path failure is the result of this. Wireless media is vulnerable to issues like noise, fading, and interference [6]. They have a lower link capacity than wired networks. All of these variables lower the bandwidth that is available while limiting the maximum transmission rate. Using mobile devices carries more danger. They are more vulnerable to physical theft and experience network attacks more frequently. Mobile networks are susceptible to spoofing, eavesdropping, and DOS assaults [7].

The network's anatomy quickly changes as a result of the hosts' erratic movements in MANET. Traditional protocols like shortest-path and link-state protocols become obsolete in such a dynamic setting. Many protocols are developed to deal with this [8]. Four criteria have been used to group these treatments. 1) The method for updating routing information, 2) The utilization of temporal information, 3) The topology utilized for routing, and 4) The kind of resources employed. The classification of protocols is not governed by any strict rules, and the same protocol may fall under more than one heading [9].

This is the approach that is most frequently used to categorize routing protocols. It makes a distinction between the protocols based on the method used to get and maintain the route. Protocols falling under this category decide on new paths using information from their previous route and the condition of the links. The routing protocols within this category are further divided into three types based on the route discovery and update times. i) Proactive routing protocols, often known as "table-driven" protocols, keep a list of routing information [10]. They operate by continuously maintaining pathways toward all hosts and routinely discovering paths toward every host in the network. The pre-established paths allow for rapid packet delivery without the need for new path discovery. Regrettably, they send out route revisions on a

regular basis to maintain routes. Routing information is typically flooded across the network via proactive protocols, which increases network traffic and decreases the bandwidth that can be used for real data transfer. As a result of node movement, links can break [11].

ii) The reactive routing protocol only looks for a path when it is unquestionably required. A host consults its routing table when it needs to communicate with another host. The previously created path is used if it is still in place. However, a new route is found if there is no previously known route. As a result, route finding only occurs when necessary. They are also referred to as an on-demand routing mechanism for this reason. Request messages are sent out among the neighbours throughout the route discovery phase till they arrive at their destination [12]. An intermediate node checks the routing table when it receives a route request. A route reply packet is returned if there is a viable path. A packet is routed to the following intermediate node if not. iii) Hybrid Routing Protocols combine reactive and proactive routing strategies. It is referred to as a hybrid routing protocol for this reason. Nodes are typically considered to be in a routing zone if they are located in a topographical region or in a pre-established region. With hybrid routing systems, proactive communication occurs within the routing zone while reactive communication occurs across zones [13].

What follows is the outline for the rest of the paper. The related work is briefly described in part 2, and the methodology and the theoretical foundations of the methods used are described in section 3. The simulation results and analysis are presented in section 4. For the chapter's final section, "key findings" we summarize the most important results.

2. Past Related Work

In a MANET, nodes can take on the roles of a source, destination, or intermediary node. They can send, receive, or forward packets in each of these scenarios. To send and receive packets, power is required. Less powerful hosts will soon lose power, and if these nodes are connected to a route, they will result in route failure. The goal of this work is to reduce energy usage in ant colony routing (ACR). By transferring packets through less congested pathways, the protocol that has been created will also take signal strength into account when switching between alternate paths and lessen the latency [14].

The Ant Colony Optimization approach is based on swarm intelligence, which makes use of foraging ants in nature to choose the best course. A group of academic researchers first suggested using this optimization method. These algorithms are created using two different kinds of ants. They are respective Reverse and Forward

ants. Ants moving forward start their journey from the sender node and move toward the destination [15]. At each intermediate node during the traverse, the forward ant gathers crucial information. After they reach their target, forward ants are wiped out and backward ants are created. The backward ant changes the pheromone concentration at each intermediate host while applying the learning from the forward voyage. By transmitting FANT reactively, the ARA protocol overcomes the problem of excessive control overhead in distribution [16]. This protocol cannot significantly reduce the overhead because it assumes that the traffic is balanced. The SARA uses a different strategy. Additionally, it distributes FANTs to nearby nodes while allowing a selected host to redistribute the FANT once more. A controlled neighbour broadcast is what this is. Additionally, the protocol anticipates that there is an imbalance in communication and uses super FANT to balance the pheromone level near the link [17].

A team of researchers has proposed an improved version of the ARA protocol called Ant HocNet. Contrary to the maintenance method, this protocol is different. Here, the sender host sends proactive FANT (PFANT) to its close neighbour on a frequent basis to assess the link quality. PFANTS are distributed more slowly in order to find new routes. HOPNET is a cantered protocol that is another method. Depending on the wireless radius, it divides the surroundings into different parts [18]. While communicating across regions, the proactive approach is used internally and the reactive approach externally. As AODV and ACO combine, MRAA is created. Here, inter-node pathways are created using ACO while AODV is used during a path search operation. The protocol survives while storing and maintaining the standby path, but it shows less delay and overhead. I-ACO employs two techniques to keep the host's pheromone levels high. Transition probability and directional probability are these processes [19]. Although the protocol demands higher control overhead and uses more resources, it reduces delay and improves packet delivery. A reactive region-based protocol called POSANT. Depending on where the source and destination hosts are located, this protocol divides the area around a host into 3 sections. FANT advances through each area as it looks for a way. Due to its inability to preserve host locations, the protocol suffers. Since the objective shifts quickly, it is challenging to distribute regions [20].

According to a group of scientists, MRP protocols operate according to the clustering theory. It establishes many routes between the cluster head and sinks after electing a node with high power as the cluster head. It chooses a communication path based on power and other factors [21]. It has been discovered that the protocol reduces power consumption and keeps the path open for longer. Nevertheless, the protocol does not adequately address

pheromone depletion and motion-based connection failures. E- AOMDV builds various pathways between the communication nodes while utilizing hop count and power efficiency [22]. When determining the path, it takes into account the power factors of all the hosts in the path. It is discovered that Protocol offers a longer lifespan than AOMDV. With ACO's positive acknowledgments, ACECR selects the best course of action. The protocol chooses the active path based on distance, mean power, and least power. It extends the life of communication and efficiently uses energy [23].

Researchers have proposed POSANT, which uses positional data and ant colony optimization to shorten the time needed to determine the path. Additionally, fewer control messages are sent. The protocol assumes that hosts are aware of their surroundings, including their immediate surroundings. As recommended by another group, EMP-DSR selects the active route based on connection stability and FANT duration [24]. It employs a regional repair method. DSR, which selects the close-by nodes to reroute lost paths. Sadly, the protocol necessitates more resources and increases overhead. As a result, efficiency suffers. In addition, there are issues with increased congestion and incorrect management of lost connections as a result of host failure [25].

3. The Objective of the Work

1. To optimize routes using nature-inspired algorithms that take signal strength, traffic, and host power into account.
2. Use simulation to evaluate and contrast the performance of the improved algorithms with those of the baseline methods.

4. The Projected Work:

In a MANET, any node can act as a source, a sink, or an intermediate node. Each of these scenarios allows for packet transmission, reception, and forwarding. To transmit and receive packets, energy is required. Those hosts with weaker batteries will run out of juice sooner,

which can bring down the entire route if those nodes are integral to it. In this section, we will discuss how to reduce Ant Colony Routing's power usage (ACR). To further reduce delays, the newly designed protocol will take signal intensities into account while choosing between available channels.

The network is modelled in the Simple Ant Routing Algorithm (SARA) as a weighted graph with V vertices and E edges. The notation for this is $G = (V, E)$. Adj[u] is an adjacency list that every node uses to keep track of its neighbours. This directory is constantly updated through neighbouring nodes exchanging HELLO messages. The routing table stores information such as the final destination, the next hop, and the total number of hops. In SARA, only one neighbour is allowed to forward the FANT, thanks to the application of control neighbour broadcast. If the ant stops at a node along the way that has a convincing path to the final destination, or is itself the final destination, a BANT will be produced. The BANT makes its way back to the node that sent it. As a control or data message travels along a network, the pheromone level at each node increases by. Then, after a time lag of, its value is reduced. Nevertheless, transmission does not account for the node's remaining power. Whenever a node sends or receives a packet, it loses energy. Consequently, a longer lifespan for a node means that it can keep the route going for longer. In this method, the route's steadiness can be strengthened.

The residual power of the host is based on the energy's evolution from the beginning to the present. Here's how it's compared:

$$E_c = E_i - E_{co} \quad (1)$$

The node uses power when sending packets E_t , receiving packets E_r , and eavesdropping on packets E_o . Thus, the amount of energy used is equivalent to (2). In most cases, E_o is irrelevant and is not given any thought during proceedings.

$$E_{co} = E_t + E_r + E_o \quad (2)$$

Table 1: Simulation background for protocols comparison.

Parameter	Value
Dimension	1000X1000 sq. m.
Node Count	10-90
Connection Count	5-60
Source Type	CBR
Packet size	512 Bytes
Buffer Size	50 packets

MAC layer	802.11b
Simulation Model	Random way point
Propagation radio model	2 ray ground
Maximum speed	20 m/s
Pause Time	20s
Interval time to send	2 packets/s
Simulation time	100 sec
Transmission power	0.7 packets/joule
Reception power	0.3 packets/joule

It appears that SARA and ESARA's routing workload increases when more nodes are added to the network. When there are fewer nodes in ESARA, the routing workload increases. This is because ESARA may fail to detect nodes with higher energy and a greater need for control packets during transmission if they are in a sparse environment. ESARA, on the other hand, chooses reliable nodes that send out minimal control packets as the number of nodes in the network grows.

5. Result and Discussion:

Throughput and packet delivery rate (PDR) for different nodes in the presence and absence of outliers are analysed and compared with the current method. Since the maximum number of nodes are taking part in the activities of the network, it is determined that the throughput improves with an increase in the number of nodes. The suggested network scenario has throughput within the threshold limits while there are no outliers, and throughput below the lower worthy threshold limit when there are outliers.

5.1. PDR (Packet delivery ratio): PDR is the ratio of packets received to packets sent. The primary success of

wireless networks is the transmission of packets. As far as PDR is concerned, this delivery ratio is a success.

$$PDR = \frac{\text{Received Packet Count}}{\text{Delivered Packet Count}} \quad (7)$$

5.2. Throughput: The throughput is the rate at which data packets are successfully relayed from the sending node to the receiving node.

$$\text{Throughput} = \frac{\text{Forwarded data}}{\text{Transmission time}} \quad (8)$$

5.2. End-to-end delay: Reducing Reduced power consumption and increased reliability are two benefits of end-to-end (E2E) delay. Hence, less time spent waiting improves both efficacy and dependability. E2E delay measures how long it takes for a packet to go from one node to another. Time spent on tasks such as data processing, transmission, and reception are all factored into the end-to-end delay.

$$\text{End to end Delay} = \text{Time for (Data transmission + Data processing + Data delivery)} \quad (9)$$

All these evaluation parameters are calculated for above mentioned routing protocols and compared the effectiveness of proposed routing protocols with existing ones.

Table II: Evaluation of proposed method with existing model based on different parameters.

Node Count	Throughput (Kbps)		End to End Delay (ms)		PDR (%)		Energy Consumed (J)	
	SARA	ESARA	SARA	ESARA	SARA	ESARA	SARA	ESARA
10	190.02	189.15	236.42	236.12	99.24	99.35	7.89	7.63
30	226	226.14	245.48	244.57	98.89	99.16	15.27	14.82
50	249.12	250.54	220.43	218.67	99.48	99.57	24.43	24.03
70	260.28	264.18	237.28	236.49	99.67	99.75	34.58	34.16
90	252.41	253.83	215.83	213.56	99.73	99.87	43.52	42.19

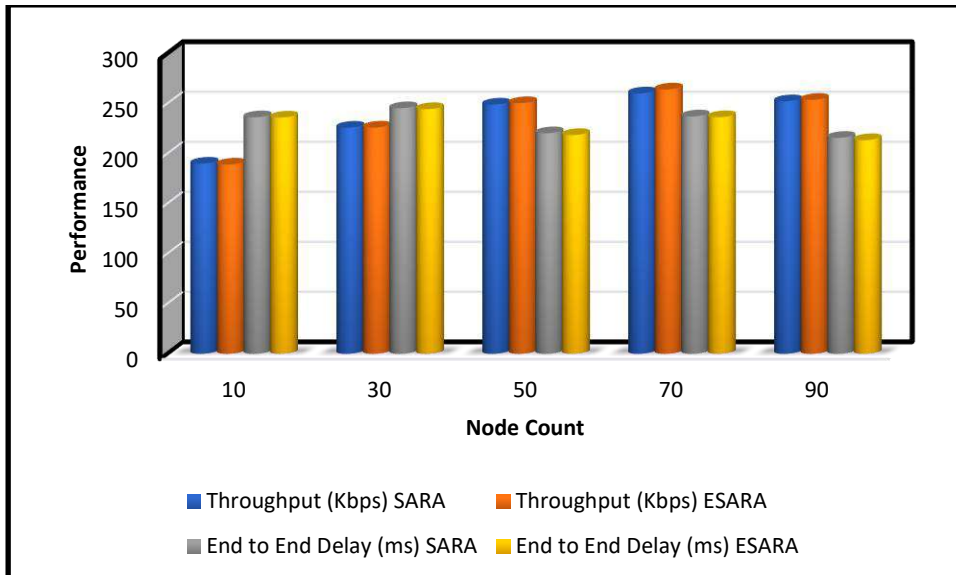


Fig II: Throughput and End-to-End delay enactment Comparison of the proposed method.

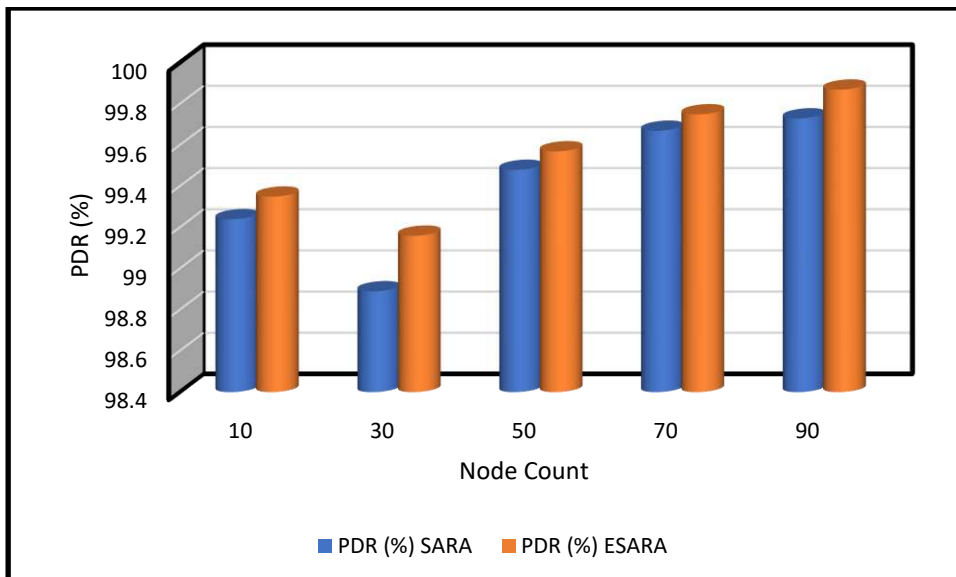


Fig III: PDR (%) enactment Comparison of the proposed method.

When choosing a path, ESARA ignores congestion. This causes longer latencies in data transmission. When hosts increase, experimental results suggest that latency decreases. In contrast, ESARA's simulation delay is very imperceptible. Table II and Figure II demonstrate that ESARA has a shorter latency than SARA.

It was found that ESARA increases the quantity of packets transferred as more nodes are introduced into the

ecosystem. This is because ESARA is able to find a more reliable path and send more packets when there is a large increase in the number of hosts sending data. Figure III displays the outcome of the simulation. If there are enough nodes, ESARA's throughput is much higher. As seen in diagram II, network throughput improves as more nodes are added. The average amount of energy used by ESARA is shown in diagram IV.

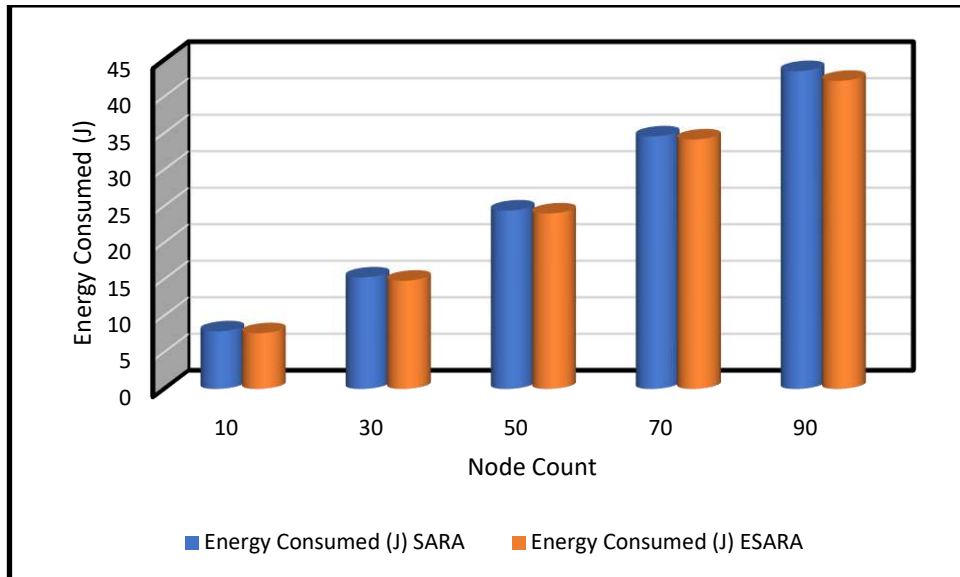


Fig IV: Energy Consumed enactment Comparison of the proposed method.

The findings indicate that ESARA uses less energy than its predecessor. When ESARA disperses the data packets over the network, it steers clear of the nodes with the lowest residual energies. As a result, the network nodes' residual energies drop across the board. The results indicated that the proposed protocol had better PDR even when the network was fairly crowded. Throughput predominated when the routing overhead was minimised. Simulation results demonstrate that while SARA performed well for low-to-medium node counts, ESARA outperformed it for higher-to-extreme node counts.

6. Conclusion:

The lack of a single authority figure is what sets MANET apart. The route is decided at each node independently. The network's hosts collaborate to facilitate communication. By mimicking their foraging behaviour, ant colonies use the Ant Colony Optimization (ACO) approach to lay down a superior path between the origin and destination hosts. Ant agents are used in these protocols to aid the intermediary node in its path selection process. Here, all of the intermediate nodes work together to facilitate communication. As a result, the MANET is a perfect fit for the ant colony optimisation method. An optimal route can be attained with the use of ACO by considering factors like available bandwidth, congestion, and available residual energy.

In this study, we explore some potential ways in which the ACO protocol's implementation could be enhanced. In the first phase, we balanced the energy by picking the nodes with the highest residual energy. Measurements of queue length are made later on to evaluate connection congestion. The adjustment was shown to increase throughput and decrease latency. The energy needed for talking was lowered as a side effect of this procedure. The Simple Ant Routing Protocol is one such protocol that has

seen enhancements. At first, a new protocol called Energy Aware Simple Ant Routing Algorithm (ESARA) was developed in which the node's energy consumption was factored into the cost function. It was discovered that the adjustment boosted the packet delivery ratio and decreased routing overhead. Such an adjustment also helped boost communication throughput. It was observed that ESARA's performance improved even when the number of hosts increased.

References

- [1] R. H. Jhaveri, N. M. Patel, D. C. Jinwala, J. H. Ortiz, and A. P. de la Cruz, "A Composite Trust Model for Secure Routing in Mobile Ad-Hoc Networks," *Ad Hoc Networks*, vol. 2, pp. 19-45, 2017.
- [2] G. Singal, V. Laxmi, M. S. Gaur, S. Todi, V. Rao, M. Tripathi, and R. Kushwaha, "Multi-Constraints Link Stable Multicast Routing Protocol in Manets," *Ad Hoc Networks*, vol. 63, pp. 115-128, 2017.
- [3] Y. M. Khamayseh, S. A. Aljawarneh, and A. E. Asaad, "Ensuring Survivability Against Black Hole Attacks in MANETS for Preserving Energy Efficiency, Sustainable Computing," *Informatics and Systems*, vol. 18, pp. 90-100, 2018.
- [4] P. S. Rajendra Prasad, "Efficient Performance Analysis of Energy Aware on Demand Routing Protocol in Mobile Ad-Hoc Network," *Engineering Reports*, vol. 2, no. 3, pp. 1-14, 2019.
- [5] N. M. Quy, N. T. Ban, and V. K. Quy, "An Adaptive on-Demand Routing Protocol with Qos Support for Urban-Manets," *IAENG International Journal of Computer Science*, vol. 49, no. 1, pp. 1-8, 2022.
- [6] M. Abu Zant, and A. Yasin, "Avoiding and Isolating Flooding Attack by Enhancing AODV MANET Protocol AIF_AODV," *Security and Communication Networks*, vol. 2019, pp. 1-13, 2019.

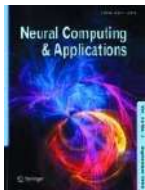
- [7] Z. A. Zardari, J. He, M. S. Pathan, S. Qureshi, M. I. Hussain, F. Razaque, and N. Zhu, "Detection and Prevention of Jellyfish Attacks Using KNN Algorithm and Trusted Routing Scheme in Manet," *International Journal of Network Security*, vol. 23, no. 1, pp. 77-87, 2021.
- [8] A. Al Sarah, T. Oyedare, and S. Shetty, "Detecting and Mitigating Smart Insider Jamming Attacks in Manets Using Reputation-Based Coalition Game," *Journal of Computer Networks and Communications*, vol. 2016, pp. 1-14, 2016.
- [9] K. Manojkumar, S. Devi, "Jamming Attack in Wireless Sensor Networks using Ant Colony Algorithm," *SSRG International Journal of Computer Science and Engineering*, vol. 8, no. 2, pp. 6-9, 2021.
- [10] M. Supriya, Dr. T. Adilakshmi, "Secure Routing using ISMO for Wireless Sensor Networks," *SSRG International Journal of Computer Science and Engineering*, vol. 8, no. 12, pp. 14-20, 2021.
- [11] S. Yasaswini, G. M. Naik, P. G. K. Sirisha, "Efficient Loss Recovery in Ad Hoc Networks," *SSRG International Journal of Computer Science and Engineering*, vol. 4, no. 1, pp. 1-7, 2017.
- [12] Nelesh Sharma, Dr. Nirupama Tiwari, "Implementation of Multipath AODV for Enhanced Performance in Wireless Ad hoc Network," *SSRG International Journal of Computer Science and Engineering*, vol. 6, no. 9, pp. 15-19, 2019.
- [13] Alameri, I. A., & Komarkova, J. (2020, June). A multiparameter comparative study of manet routing protocols. In *2020 15th Iberian Conference on Information Systems and Technologies (CISTI)* (pp. 1-6). IEEE. doi.org/10.23919/CISTI49556.2020.9141119
- [14] Alameri, I., Hubálovský, Š., & Komarkova, J. (2021, June). Evaluation of impact of mobility, network size and time on performance of adaptive routing protocols. In *2021 International Conference on Information and Digital Technologies (IDT)* (pp. 245-253). IEEE. doi.org/10.1109/IDT52577.2021.9497568
- [15] Alkahtani, S. M., & Alturki, F. (2021). Performance Evaluation of Different Mobile Ad-hoc Network Routing Protocols in Difficult Situations. *Performance Evaluation*, 12(1). doi.org/10.14569/IJACSA.2021.0120119
- [16] Mani Bushan Dsouza, Manjaiah D.H., "Improving the QoS of multipath routing in MANET by considering reliable node and stable link", In: Karuppusamy P., Perikos I., Shi F., Nguyen T.N. (eds) *Sustainable Communication Networks and Application. Lecture Notes on Data Engineering and Communications Technologies*, 2021 vol 55. Springer, Singapore. https://doi.org/10.1007/978-981-15-8677-4_43
- [17] Mani Bushan Dsouza, Manjaiah D.H., "Signal Strength Based Routing Using Simple Ant Routing Algorithm", In: Gunjan, V.K., Suganthan, P.N., Haase, J., Kumar, A. (eds) *Cybernetics, Cognition and Machine Learning Applications, Proceedings of ICCMLA 2020*, Springer, pp. 535-546, 2021, https://doi.org/10.1007/978-981-33-6691-6_38
- [18] J. Dhanapal, S. Narayanan and G. Asha, "Efficient load sharing using multipath channel. Awareness routing in mobile ad hoc networks," *Indian Journal of Science and Technology*, vol. 8, no. 15, 2015.
- [19] 8, no. 15, 2015.
- [20] S. A. Alghamdi, "Load balancing ad hoc on-demand multipath distance vector (LBAOMDV) routing protocol," *EURASIP Journal on Wireless Communications and Networking*, pp. 1-11, 2015.
- [21] Correia, A., Moura, R., & Fonseca, M. (2020). Assessing the location of search and rescue stations on the Portuguese coast. In *Developments and Advances in Defense and Security* (pp. 321-331). Springer, Singapore. doi.org/10.1007/978-981-13-9155-2_26
- [22] Hassan, M. H., & Muniyandi, R. C. (2017). An improved hybrid technique for energy and delay routing in mobile ad-hoc networks. *International Journal of Applied Engineering Research*, 12(1), 134-139.
- [23] Hassan, M. H., Mostafa, S. A., Budiyo, A., Mustapha, A., & Gunasekaran, S. S. (2018). A hybrid algorithm for improving the quality of service in MANET. *International Journal on Advanced Science, Engineering and Information Technology*, 8(4), 1218-1225. doi.org/10.18517/ijaseit.8.4.5004
- [24] Hassan, M. H., Mostafa, S. A., Mohammed, M. A., Ibrahim, D. A., Khalaf, B. A., & Al-Khaleefa, A. S. (2019). Integrating African Buffalo optimization algorithm in AODV routing protocol for improving the QoS of MANET. *Journal of Southwest Jiaotong University*, 54(3). doi.org/10.35741/issn.0258-2724.54.3.13
- [25] Pattnaik, P. K., Panda, B. K., & Sain, M. (2021). Design of novel mobility and obstacle-aware algorithm for optimal MANET routing. *IEEE Access*, 9, 110648-110657. doi.org/10.1109/ACCESS.2021.3101850
- [26] Rao, S. V. R. K., Devi, M. S., Kishore, A. R., & Kumar, P. (2018). Wireless sensor network based industrial automation using internet of things (IoT). *International Journal of Advanced Trends in Computer Science and Engineering*, 7(6), 82-86. doi.org/10.30534/ijatcse/2018/01762018
- [27]

- [28] Mr. Rahul Sharma. (2015). Recognition of Anthracnose Injuries on Apple Surfaces using YOLOV 3-Dense. International Journal of New Practices in Management and Engineering, 4(02), 08 - 14. Retrieved from <http://ijnpme.org/index.php/IJNPME/article/view/36>
- [29] Rambabu, B. ., Vikranth, B. ., Anupkanth, S. ., Samya, B. ., & Satyanarayana, N. . (2023). Spread Spectrum based QoS aware Energy Efficient Clustering Algorithm for Wireless Sensor Networks . International Journal on Recent and Innovation Trends in Computing and Communication, 11(1), 154–160. <https://doi.org/10.17762/ijritcc.v11i1.6085>

[Home](#) [Neural Computing and Applications](#) [Article](#)


An intelligent heart disease prediction system based on swarm-artificial neural network

S.I: ML4BD_SHS Published: 27 May 2021

Volume 35, pages 14723–14737, (2023) [Cite this article](#)

Neural Computing and Applications

[Aims and scope](#)[Submit manuscript](#)



[Sudarshan Nandy](#), [Mainak Adhikari](#), [Venki Balasubramanian](#), [Varun G. Menon](#) ,
[Xingwang Li](#) & [Muhammad Zakarya](#)

 1209 Accesses  20 Citations [Explore all metrics](#) →

Abstract

The accurate prediction of cardiovascular disease is an essential and challenging task to treat a patient efficiently before occurring a heart attack. In recent times, various intelligent healthcare frameworks have been designed with different machine learning and swarm optimization techniques for cardiovascular disease prediction. However, most of the existing strategies failed to achieve higher accuracy for cardiovascular disease prediction due to the lack of data-recognized techniques and proper prediction methodology. Motivated by the existing challenges, in this paper, we propose an intelligent healthcare framework for predicting cardiovascular heart disease based on Swarm-Artificial Neural Network (Swarm-ANN) strategy. Initially, the proposed Swarm-

ANN strategy randomly generates predefined numbers of Neural Networks (NNs) for training and evaluating the framework based on their solution consistency. Additionally, the NN populations are trained by two stages of weight changes and their weight is adjusted by a newly designed heuristic formulation. Finally, the weight of the neurons is modified by sharing the global best weight with other neurons and predicts the accuracy of cardiovascular disease. The proposed Swarm-ANN strategy achieves 95.78% accuracy while predicting the cardiovascular disease of the patients from a benchmark dataset. The simulation results exhibit that the proposed Swarm-ANN strategy outperforms the standard learning techniques in terms of various performance matrices.

 This is a preview of subscription content, [log in via an institution](#)  to check access.

Access this article

[Log in via an institution](#)

Buy article PDF 39,95 €

Price includes VAT (India)

Instant access to the full article PDF.

Rent this article via [DeepDyve](#) 

[Institutional subscriptions](#) →

References

1. Ahmed H, Younis EM, Hendawi A, Ali AA (2020) Heart disease identification from patients' social posts, machine learning solution on spark. *Fut Gener Comput Syst* 111:714–722

2. Kumar PM, Gandhi UD (2018) A novel three-tier Internet of Things architecture with machine learning algorithm for early detection of heart diseases. *Comput Elect Eng* 65:222–235

3. Kwon J-M, Kim KH, Jeon K-H, Park J (2019) Deep learning for predicting in-hospital mortality among heart disease patients based on echocardiography. *Echocardiography* 36(2):213–218

4. Hao Y, Usama M, Yang J, Hossain MS, Ghoneim A (2019) Recurrent convolutional neural network-based multimodal disease risk prediction. *Fut Gener Comput Syst* 92:76–83

5. Jonnagaddala J, Liaw S-T, Ray P, Kumar M, Chang N-W, Dai H-J (2015) Coronary artery disease risk assessment from unstructured electronic health records using text mining. *J Biomed Inform* 58:S203–S210

6. Melin P, Miramontes I, Prado-Arechiga G (2018) A hybrid model based on modular neural networks and fuzzy systems for classification of blood pressure and hypertension risk diagnosis. *Exp Syst Appl* 107:146–164

7. Al-Makhadmeh Z, Tolba A (2019) Utilizing IoT wearable medical device for heart disease prediction using higher-order Boltzmann model: a classification approach”.

[Article](#) [Google Scholar](#)

8. Ali F, Kwak D, Khan P, El-Sappagh S, Ali A, Ullah S, Kim KH, Kwak K-S (2019) Transportation sentiment analysis using word embedding and ontology-based topic modeling. *Knowl Based Syst* 174:27–42

[Article](#) [Google Scholar](#)

9. Yadav A, Singh A, Dutta MK, Travieso CM (2019) Machine learning-based classification of cardiac diseases from PCG recorded heart sounds. *Neural Comput Appl* 32:1–14

[Google Scholar](#)

10. Ali F, El-Sappagh S, Islam SR, Kwak D, Ali A, Imran M, Kwak K-S (2020) A smart healthcare monitoring system for heart disease prediction based on ensemble deep learning and feature fusion. *Inform Fusion* 63:208–222

[Article](#) [Google Scholar](#)

11. Kishore A, Jayanthi V (2018) Neuro-fuzzy based medical decision support system for coronary artery disease diagnosis and risk level prediction. *J Comput Theor Nanosci* 15(3):1027–1037

[Article](#) [Google Scholar](#)

12. Ali F, Islam SR, Kwak D, Khan P, Ullah N, Yoo SJ, Kwak KS (2018) Type-2 fuzzy ontology-aided recommendation systems for IoT-based healthcare. *Comput Commun* 119:138–155

[Article](#) [Google Scholar](#)

13. Garate-Escamila AK, El-Hassani AH, Andres E (2020) Classification models for heart disease prediction using feature selection and PCA. Inform Med Unlocked 19:1–15
[Article](#) [Google Scholar](#)

14. Diwakar M, Tripathi A, Joshi K, Memoria M, Singh P et al (2020) Latest trends on heart disease prediction using machine learning and image fusion. Mater Today Proceed 37:3213–3218
[Article](#) [Google Scholar](#)

15. Haq AU, Li JP, Memon MH, Nazir S, Sun R (2018) A hybrid intelligent system framework for the prediction of heart disease using machine learning algorithms. Mob Inf Syst 2018:1–21
[Google Scholar](#)

16. Mohan S, Thirumalai C, Srivastava G (2019) Effective heart disease prediction using hybrid machine learning techniques. IEEE Access 7:81542–81554
[Article](#) [Google Scholar](#)

17. Li JP, Haq AU, Din SU, Khan J, Khan A, Saboor A (2020) Heart disease identification method using machine learning classification in e-healthcare. IEEE Access 8:107562–107582
[Article](#) [Google Scholar](#)

18. Khan MA, Algarni F (2020) A healthcare monitoring system for the diagnosis of heart disease in the IOMT cloud environment using mssso-anfis. IEEE Access 8:122259–122269
[Article](#) [Google Scholar](#)

19. Fitriyani NL, Syafrudin M, Alfian G, Rhee J (2020) Hdpm: an effective heart disease prediction model for a clinical decision support system. *IEEE Access* 8:133034–133050

[Article](#) [Google Scholar](#)

20. Abdeldjouad FZ, Brahami M, Matta N (2020) A hybrid approach for heart disease diagnosis and prediction using machine learning techniques. *International conference on smart homes and health telematics*. Springer, New York, pp 299–306

[Google Scholar](#)

21. Ansari MF, AlankarKaur B, Kaur H (2020) A prediction of heart disease using machine learning algorithms. *International conference on image processing and capsule networks*. Springer, New York, pp 497–504

[Google Scholar](#)

22. Shahid AH, Singh MP, Roy B, Aadarsh A (2020) Coronary artery disease diagnosis using feature selection-based hybrid extreme learning machine. In: *Proceedings of the 2020 3rd international conference on information and computer technologies (ICICT)*, IEEE, pp 341–346.

23. Javeed A, Rizvi SS, Zhou S, Riaz R, Khan SU, Kwon SJ (2020) Heart risk failure prediction using a novel feature selection method for feature refinement and neural network for classification. *Mob Inf Syst 2020*

24. Costa W, Figueiredo L, Alves E (2019) Application of an artificial neural network for heart disease diagnosis. In: *Proceedings of the XXVI Brazilian congress on biomedical engineering*, pp 753–758. Springer, New York

25. Vivekanandan T, Iyengar NCSN (2017) Optimal feature selection using a modified differential evolution algorithm and its effectiveness for prediction of heart disease.

[Article](#) [Google Scholar](#)

26. Goldberger AL, Amaral LA, Glass L, Hausdorff JM, Ivanov PC, Mark RG, Mietus JE, Moody GB, Peng C-K, Stanley HE (2000) Physiobank, physiotoolkit, and physionet: components of a new research resource for complex physiologic signals. *Circulation* 101(23):e215–e220

[Article](#) [Google Scholar](#)

27. Rish I, et al (2001) An empirical study of the naive Bayes classifier. In: *IJCAI 2001 workshop on empirical methods in artificial intelligence*, vol 3, pp 41–46.

28. Meyer D, Leisch F, Hornik K (2003) The support vector machine under test. *Neurocomputing* 55(1–2):169–186

[Article](#) [Google Scholar](#)

29. Jan MA, Khan F, Khan R, Mastorakis S, Menon VG, Watters P, Alazab M (2020) A lightweight mutual authentication and privacy-preservation scheme for intelligent wearable devices in industrial-CPS. *IEEE Trans Ind Inform* 1–11

30. Shynu PG, Menon VG, Kumar RL, Kadry S, Nam Y (2021) Blockchain-based secure healthcare application for diabetic-cardio disease prediction in fog computing. *IEEE Access* 9:45706–45720

[Article](#) [Google Scholar](#)

Author information

Authors and Affiliations

Computer Science and Engineering, ASETK, Amity University Kolkata, Kolkata, India
Sudarshan Nandy

Mobile & Cloud Lab, Institute of Computer Science, University of Tartu, Tartu, Estonia

Mainak Adhikari

School of Science, Engineering and Information Technology, Federation University,
Mount Helen, Australia

Venki Balasubramanian

Computer Science and Engineering, SCMS School of Engineering and Technology,
Ernakulam, India

Varun G. Menon

School of Physics and Electronic Information Engineering, Henan Polytechnic
University, Jiaozuo, China

Xingwang Li

Department of Computer Science, Abdul Wali Khan University, Mardan, Pakistan

Muhammad Zakarya

Corresponding author

Correspondence to [Varun G. Menon](#).

Ethics declarations

Conflict of interest

The authors declare that there are no potential conflicts of interest in this work.

Additional information

Publisher's Note

Springer Nature remains neutral with regard to jurisdictional claims in published maps and institutional affiliations.

Rights and permissions

[Reprints and permissions](#)

About this article

Cite this article

Nandy, S., Adhikari, M., Balasubramanian, V. *et al.* An intelligent heart disease prediction system based on swarm-artificial neural network. *Neural Comput & Applic* 35, 14723–14737 (2023). <https://doi.org/10.1007/s00521-021-06124-1>

Received

21 February 2021

Accepted

11 May 2021

Published

27 May 2021

Issue Date

July 2023

DOI

<https://doi.org/10.1007/s00521-021-06124-1>

Keywords

[Artificial neural network](#)

[Heuristic formulation](#)

[Swarm optimization](#)

[Back-propagation](#)

[Classification model](#)

[Heart disease prediction](#)



Institutional Sign In

All



[ADVANCED SEARCH](#)

PDF

[Help](#)

Journals & Magazines > IEEE Transactions on Intellig... > Volume: 24 Issue: 12 [?](#)

Crowd Emotion Prediction for Human-Vehicle Interaction Through Modified Transfer Learning and Fuzzy Logic Ranking

Publisher: **IEEE**

[Cite This](#)

PDF

[Mohammad R. Khosravi](#) ; [Khosro Rezaee](#) ; [Mohammad Kazem Moghimi](#) ; [Shaohua Wan](#) ; [Varun G. Menon](#) **All Authors** [...](#)

9
Cites in
Papers

358
Full
Text Views



Alerts

[Manage Content Alerts](#)
[Add to Citation Alerts](#)

Abstract

Document Sections

- I. Introduction
- II. Related Work
- III. Proposed Method
- IV. Experimental Results
- V. Conclusion

Authors

- [Figures](#)
- [References](#)
- [Citations](#)
- [Keywords](#)
- [Metrics](#)
- [More Like This](#)



Downl
PDF

Abstract:In metropolitan environments, unmanned aerial vehicles (UAVs) equipped with video surveillance equipment can monitor crowd behavior and maintain public safety. In high-tr... [View more](#)

▶ Metadata

Abstract:

In metropolitan environments, unmanned aerial vehicles (UAVs) equipped with video surveillance equipment can monitor crowd behavior and maintain public safety. In high-traffic areas where humans are more likely to make mistakes, a smart city needs modern technology to forecast the behavior of its residents. In order to improve citywide traffic flow, urban transportation systems (UTSs) monitor and learn how people behave in crowds. Using UAVs for video surveillance in smart cities, our research describes a unique way to assess crowd condition, which expands the scope of human-vehicle interactions. Moreover, we use fuzzy logic ranking to improve the system's ability to detect anomalies in crowds. In order to improve decision-making, a novel deep transfer learning (DTL) technique is applied to the UAV's received frames. A 98.5% accuracy rate, satisfactory performance, and robustness to population behavior are all characteristics of the proposed integrated model. In UTSs and urban areas, our novel intelligent system analyzes human behavior based on vehicle-human interactions. In areas with low and high traffic congestion, the modified ResNet (mResNet) architecture predicts the crowd's condition based on fuzzy logic (FLA). Through decision-making based on accurate crowd conditions, best general paths can be selected using the algorithm.

Published in: IEEE Transactions on Intelligent Transportation Systems (Volume: 24 , Issue: 12, December 2023)

Page(s): 15752 - 15761

DOI: 10.1109/TITS.2023.3239114

Date of Publication: 06 February 2023 [?](#)

Publisher: IEEE

▼ ISSN Information:

Print ISSN: 1524-9050

Electronic ISSN: 1558-0016



► Funding Agency:

Mohammad R. Khosravi

Shandong Provincial University Laboratory for Protected Horticulture, Weifang University of Science and Technology, Shandong, Weifang, China

Khosro Rezaee

Department of Biomedical Engineering, Meybod University, Meybod, Iran

Mohammad Kazem Moghimi

Department of Communication Engineering, University of Sistan and Baluchestan, Zahedan, Iran

Shaohua Wan

Shenzhen Institute for Advanced Study, University of Electronic Science and Technology of China, Shenzhen, China

PDF

Help

Varun G. Menon

SCMS School of Engineering and Technology, Ernakulam, India

☰ Contents

I. Introduction

Video monitoring in metropolitan areas is used today for crowd behavior research to pinpoint precise locations of events. Video surveillance of crowds, including pedestrian detection, congestion recognition, and overcrowding prediction, has been shown to be useful in smart cities [1], [2]. As a result of this link between congestion and social and urban transportation issues, the latter may impede the free movement of automobiles in cities. With the advent of smart technologies for UTSs [3], [4], [5], crowded areas are now monitored by various cameras, including CCTVs. Due to the rarity of unusual occurrences, monitoring crowds and preventing traffic jams in vehicles is difficult as well. It is possible for congestion to act in unexpected ways in different people. Detecting overpopulation and observing human behavior is essential for preventing issues like the emergence of abnormal population behavior in urban settings [6]. Nevertheless, a continuous and real-time automated monitoring system based on social computing is needed to prevent mistakes caused by operator fatigue and inefficiency [7]. The ability to recognize congestion in traffic conditions to save energy and time is one of the distinctive social systems that can enhance vehicle safety and traffic management. Smart cities require crowd flow prediction (CFP) to assist UTS in making itineraries and avoiding congestion. An urban transport system plays an important role in enhancing urban mobility in a smart city [8], [9]. The implementation of connected and autonomous vehicles (CAVs) and UTS operations as intelligent city infrastructure is possible with connected and autonomous vehicles. By using machine learning methods to determine overpopulation, we can develop better and more effective density management tactics [10], [11], [12], [13].

Sign in to Continue Reading

Authors

Mohammad R. Khosravi

Shandong Provincial University Laboratory for Protected Horticulture, Weifang University of Science and Technology, Shandong, Weifang, China

Khosro Rezaee

Department of Biomedical Engineering, Meybod University, Meybod, Iran

Mohammad Kazem Moghimi

Department of Communication Engineering, University of Sistan and Baluchestan, Zahedan, Iran

Shaohua Wan

Shenzhen Institute for Advanced Study, University of Electronic Science and Technology of China, Shenzhen, China

Varun G. Menon

SCMS School of Engineering and Technology, Ernakulam, India

Figures	▼
References	▼
Citations	▼
Keywords	▼
Metrics	▼

PDF

Help

More Like This

Deep Transfer Learning-Based Feature Extraction: An Approach to Improve Nonintrusive Load Monitoring

IEEE Access

Published: 2021

Smart City Traffic Monitoring:YOLOv7 Transfer Learning Approach for Real-Time Vehicle Detection

2023 International Conference on Smart Applications, Communications and Networking (SmartNets)

Published: 2023

Show More

IEEE Personal Account

CHANGE
USERNAME/PASSWORD

Purchase Details

PAYMENT OPTIONS
VIEW PURCHASED
DOCUMENTS

Profile Information

COMMUNICATIONS
PREFERENCES
PROFESSION AND
EDUCATION
TECHNICAL INTERESTS

Need Help?

US & CANADA: +1 800
678 4333
WORLDWIDE: +1 732
981 0060
CONTACT & SUPPORT

Follow



[About IEEE Xplore](#) | [Contact Us](#) | [Help](#) | [Accessibility](#) | [Terms of Use](#) | [Nondiscrimination Policy](#) | [IEEE Ethics Reporting](#)  | [Sitemap](#) | [IEEE Privacy Policy](#)

A not-for-profit organization, IEEE is the world's largest technical professional organization dedicated to advancing technology for the benefit of humanity.

© Copyright 2024 IEEE - All rights reserved.

PDF

IEEE Account

- » [Change Username/Password](#)
- » [Update Address](#)

Purchase Details

- » [Payment Options](#)
- » [Order History](#)
- » [View Purchased Documents](#)

Profile Information

- » [Communications Preferences](#)
- » [Profession and Education](#)
- » [Technical Interests](#)

Need Help?

- » **US & Canada:** +1 800 678 4333
- » **Worldwide:** +1 732 981 0060
- » [Contact & Support](#)

[About IEEE Xplore](#) | [Contact Us](#) | [Help](#) | [Accessibility](#) | [Terms of Use](#) | [Nondiscrimination Policy](#) | [Sitemap](#) | [Privacy & Opting Out of Cookies](#)

A not-for-profit organization, IEEE is the world's largest technical professional organization dedicated to advancing technology for the benefit of humanity.

© Copyright 2024 IEEE - All rights reserved. Use of this web site signifies your agreement to the terms and conditions.

Artificial Intelligence in IoT-Based Healthcare System Enhancements

^[1]Mrs.Sreelekshmi B, ^[2]Mrs.Tessy Abraham Azhikakathu, ^[3]Mrs.MathuUthaman,
^[4]Mrs.Aparna M, ^[5]Mrs.Chippy T, ^[6]Mrs.Neethu Krishna

^[1]^[2]^[3]^[5]Assistant Professor, Department of Computer Science and Engineering, Mahaguru Institute of Technology, Kattachira, Kayamkulam, Alappuzha, India.

^[4]Assistant Professor, Department of Artificial Intelligence and Machine Learning, Mahaguru Institute of Technology, Kattachira, Kayamkulam, Alappuzha, India.

^[6]Assistant Professor, Department of Computer Science and Engineering, SCMS School of Engineering and Technology, Karukutty, Ernakulam, Kerala, India.

Abstract

This research paper delves into the transformative impact of Artificial Intelligence (AI) on Internet of Things (IoT)-based healthcare systems. As healthcare continues to evolve with technological advancements, integrating AI into IoT frameworks presents a promising frontier for enhancing patient care, diagnosis, treatment, and overall healthcare management. This paper examines current IoT applications in healthcare and explores how AI can augment these systems to improve accuracy, efficiency, and patient outcomes. Through a comprehensive literature review, case studies, and analysis of emerging trends, this study identifies key areas where AI-powered IoT systems can revolutionize healthcare practices. It also addresses the challenges and ethical considerations in implementing such technologies, including data privacy and security. The findings underscore the potential of AI in optimizing IoT-based healthcare systems, paving the way for more personalized, efficient, and accessible healthcare solutions. This research contributes to the growing body of knowledge in the field and outlines future directions for innovation and research in AI-enhanced healthcare technologies.

Keywords: Artificial Intelligence (AI), Healthcare Technology, AI in Healthcare, Data Privacy in Healthcare, Healthcare System Innovation, Digital Health, AI and IoT Integration.

1. Introduction

The integration of the Internet of Things (IoT) in healthcare has marked a revolutionary shift in the way medical services are delivered and managed. IoT in healthcare refers to the network of physical devices, like wearable sensors and medical equipment, connected to the internet for data collection, exchange, and analysis[1]. This technology has enabled remote monitoring of patients, real-time data access, and improved patient engagement and care. It has also facilitated efficient resource management in healthcare settings, thereby enhancing the overall quality of healthcare services.

Artificial Intelligence (AI) has emerged as a pivotal technology in modern healthcare systems, driving innovations in diagnosis, treatment planning, and patient care management. AI algorithms can analyze complex medical data, recognize patterns, and provide insights that assist healthcare professionals in making informed decisions[2]. The application of AI ranges from predictive analytics in patient care to the development of personalized medicine, and it plays a crucial role in research and drug discovery.

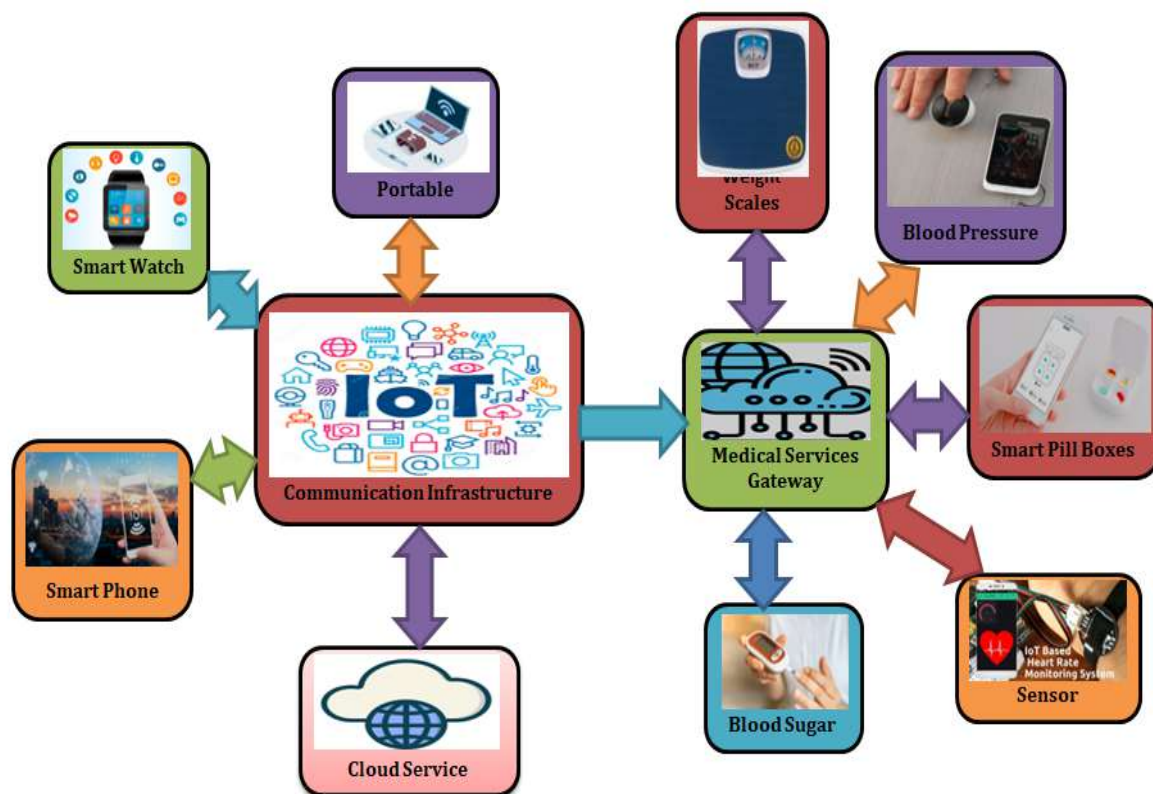


Figure.1:IoT Bases Healthcare System

Artificial Intelligence (AI) and the Internet of Things (IoT) together bring a transformative power to physical objects and equipment, enabling them to perceive, analyze, and act. These "smart" objects communicate through data exchange, effectively sharing their insights. This fusion, known as AIoT, turns once ordinary devices into intelligent entities[3]. By connecting them to the Internet using embedded devices, Internet protocols, sensor networks, and communication protocols, AIoT elevates the functionality of these objects.

In the healthcare sector, AIoT is revolutionizing services. It supports electronic health systems, telecare networks, diagnostics, prevention, rehabilitation, and patient monitoring. Key components like Wireless Body Area Networks and Radio Frequency Identification systems play a vital role in IoT, although they are not strictly essential[4]. Research has shown the feasibility of remote health monitoring, highlighting its potential to significantly enhance healthcare delivery in various scenarios. Remote monitoring, for instance, allows for home-based observation of non-critical patients, easing the strain on hospital resources like staff and beds. This approach not only alleviates pressure on healthcare facilities but also extends healthcare access to elderly individuals living independently[5], enhancing their quality of life. Essentially, AIoT in healthcare can broaden access to medical services, reduce the burden on healthcare systems, and empower individuals to take greater control of their health over time. Figure 1 in the document illustrates various AIoT-based healthcare devices.

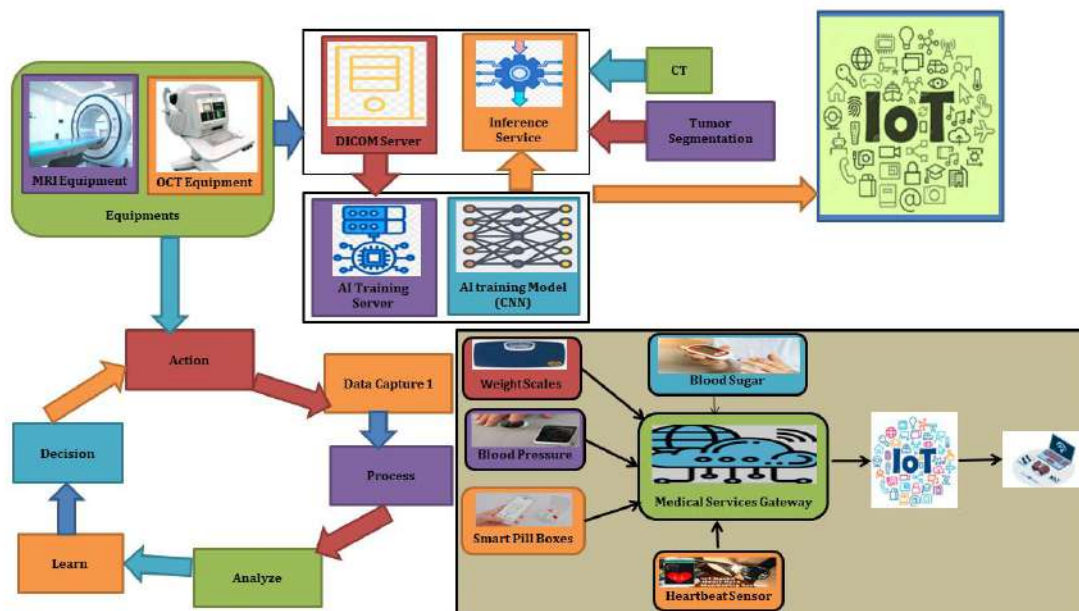


Figure.2: IoT & AI Integrated Health Care Module

As healthcare devices become more interconnected, they generate diverse scenarios that require various management strategies. One intriguing possibility is the use of data from health-monitoring devices by insurance companies to aid in underwriting and operational tasks. This data can be instrumental in detecting and assessing potential fraud claims and identifying individuals who may benefit from specific treatment procedures[6]. Insurance Information Technologies (IIT) stand to benefit both insurers and customers. These technologies are not limited to standard underwriting and pricing; they also play a crucial role in risk assessment. Customers gain transparency, as they can view the information that informs each decision, promoting a data-driven approach[7]. This transparency fosters an understanding of the rationale behind each decision made by an insurance firm. A typical AIoT-based healthcare system, illustrating this interplay, is depicted in Figure 2. Insurance companies are exploring ways to incentivize clients for their participation and contribution of health data via AIoT devices. Such initiatives could enhance treatment adherence and compliance levels among clients using these devices. Insurers might offer rewards for measurable health-related activities that clients can control, aiding in their efforts to minimize liability claims. Additionally, IoT data collection devices could be used to streamline the handling and verification of insurance claims, potentially simplifying the process for both clients and insurance firms.

The integration of AI with IoT in healthcare holds immense potential for transforming the healthcare industry[8]. By combining AI's analytical prowess with IoT's extensive data-gathering capabilities, this integration can lead to more accurate diagnoses, predictive analytics for preventive care, and personalized treatment plans[9]. It promises to enhance patient outcomes by enabling real-time, data-driven decision-making and automating routine tasks, which can reduce the workload on healthcare providers and improve the efficiency of healthcare systems. This synergy of AI and IoT could be particularly impactful in managing chronic diseases, elderly care, and in areas with limited access to healthcare facilities. The paper aims to explore these aspects in detail, highlighting the transformative power of AI in IoT-based healthcare systems and the challenges that need to be addressed to realize its full potential.

2. Literature Review

The literature reveals a growing interest in the deployment of IoT in healthcare. Studies such as [1] have detailed how IoT devices like wearable sensors, remote monitoring tools, and connected medical devices are revolutionizing patient care. These devices collect vital data, which is used for continuous patient monitoring, thereby preventing hospital readmissions and aiding in chronic disease management. However,

research by [10] highlights concerns regarding data security and privacy in IoT-enabled healthcare systems, underscoring the need for robust security protocols.

The application of AI in healthcare is extensively documented in literature, showcasing its role in diagnostic procedures, treatment planning, and predicting patient outcomes. Pioneering studies, such as those by [11], demonstrate AI's capability in analyzing medical images and patient data to identify diseases with higher accuracy than traditional methods. AI's predictive analysis, as discussed in [12], is crucial in preventive healthcare, identifying potential health risks before they become critical. However, literature also indicates challenges in AI implementation, including the need for large datasets and concerns about AI's interpretability and decision-making process.

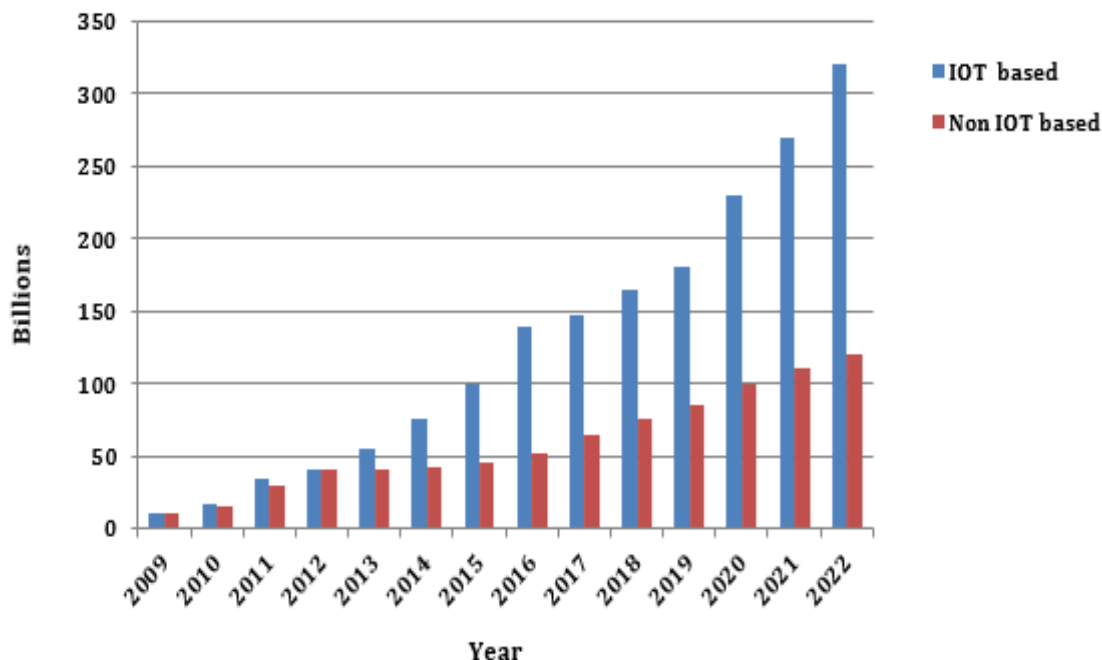


Figure.3: Survey on IoT based Healthcare system

Artificial Intelligence (AI) encompasses various subfields, including machine learning and deep learning. Machine learning involves algorithms that self-adjust to deliver desired outputs based on given inputs, functioning autonomously without human intervention, as illustrated in Figure 3. Deep learning, on the other hand, enables computers to self-learn using neural networks and unlabeled data. Deep learning employs layered algorithms to construct neural networks capable of learning. These multi-layered approaches provide in-depth insights into data. They operate through artificial neural networks, which remarkably mimic the neural networks of the human brain. The complexity of learning increases as more neurons and hidden layers are added, resembling the intricate connections in the brain. Coordinated learning models in deep learning can exclude certain features from a labeled training dataset for multi-layered comprehension. Convolutional Neural Networks (CNNs), Recurrent Neural Networks (RNNs), and particularly large-scale CNNs are pivotal in estimating coordinated learning processes. This article delves into the applications of deep learning in healthcare. It explores how deep learning can be utilized for individual disease predictions—forecasting a person's illness based on their medical history—and community disease predictions, which involve estimating the prevalence of diseases or epidemics within populations.

A critical analysis of the literature reveals several gaps in the current technology. While IoT devices are efficient in data collection, their integration with healthcare systems often faces interoperability challenges, as noted in [13]. Similarly, while AI has shown promise in data analysis, issues related to the ethical use of AI, biases in AI algorithms, and the need for transparency in AI decision-making are recurrent themes in recent research. Furthermore, studies like [14] point out the lack of standardized regulations and guidelines for the combined use of AI and IoT in healthcare, which is crucial for ensuring patient safety and data privacy.

3. Methodology

This research adopts a mixed-method approach, combining qualitative and quantitative analysis to provide a comprehensive understanding of the integration of AI in IoT-based healthcare systems. The methodology is structured to analyze both the technical aspects and the practical implications of this integration.

In this study, we employed a mixed-method approach, integrating both qualitative and quantitative research techniques to thoroughly examine the impact of Artificial Intelligence (AI) in enhancing Internet of Things (IoT)-based healthcare systems. Our data collection spanned a variety of sources to ensure a comprehensive view.

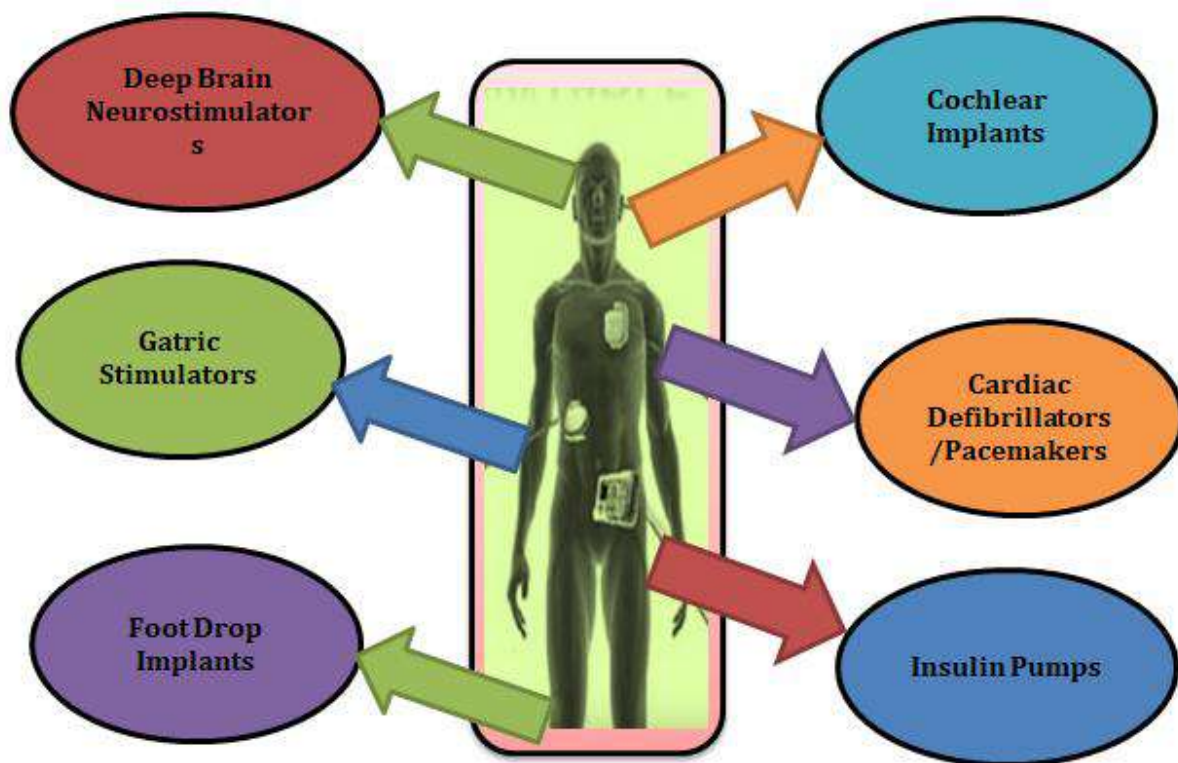


Figure.4: Self-sufficient therapeutic internal gadgets

This included an extensive review of academic journals and papers from medical, technological, and scientific databases, analysis of relevant case studies demonstrating the practical application of AI in IoT healthcare systems, and interviews with professionals in healthcare, AI, and IoT fields[15]. The analysis involved a detailed content analysis of the collected literature to identify recurring themes and trends, comparative analysis to juxtapose different viewpoints and outcomes, and statistical analysis for quantitative data to discern correlations and validate hypotheses. In synthesizing our research, we integrated these findings, performed a gap analysis to identify areas lacking in current research, and developed a theoretical framework to conceptualize the interaction and implications of AI and IoT in healthcare[16]. Throughout our research, ethical considerations, particularly concerning data use and the confidentiality of interview respondents, were rigorously maintained. For over 30 million diabetic individuals in America, managing glucose levels is a significant concern. Traditional methods of glucose monitoring, which involve manual testing and recording, are time-consuming and only provide a snapshot of glucose levels at the time of testing.

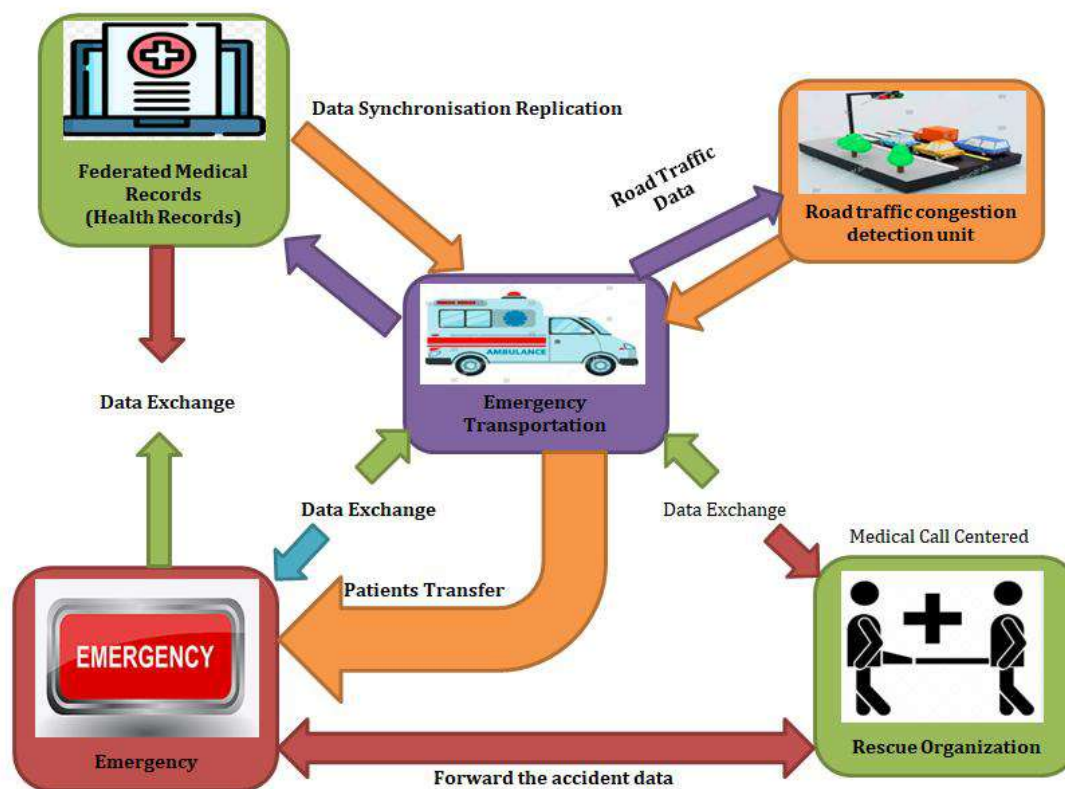


Figure.5: Critical components of IoT data scrutiny in medical applications

This approach may not be sufficient to detect sudden or dramatic changes in glucose levels. Internet of Things (IoT) solutions, particularly those incorporating AI and IoT (AIoT), offer a promising alternative[17]. These solutions enable continuous, automated glucose monitoring, alerting patients when their blood glucose levels deviate from normal ranges, thus reducing the need for manual record-keeping. Wireless, implantable devices based on AIoT technology, illustrated in Figure 4, are at the forefront of this innovation.

Developing an AIoT system for glucose monitoring presents specific challenges. Firstly, the device must be small enough to be used unobtrusively[18], allowing for long-term tracking without causing discomfort to the patient. Secondly, it should be energy-efficient, not requiring frequent recharging. While these challenges are significant, they are not insurmountable. Devices that successfully address these issues have the potential to revolutionize how individuals with diabetes manage and control their blood sugar levels.

Academics have contributed to the development of a reference model for Internet of Things (IoT) applications, particularly in the context of smart city development. Jin et al., in their research article "Creating an IoT Implementation for Smart Cities," outline a comprehensive framework for project planning within this domain. According to the article, the IoT can contribute to the development of a smart city through three primary perspectives: data-centric, cloud-centric, and network-centric. These approaches provide a foundational reference model for the creation of smart cities, accommodating the diverse range of applications and initiatives involved in smart development. These perspectives not only guide the development of smart cities but also influence various applications within them, including healthcare. Figure 5 in the article likely illustrates key areas where AIoT analytics are applied in medicine, demonstrating how IoT, when combined with AI, can enhance healthcare delivery and management within smart city frameworks.

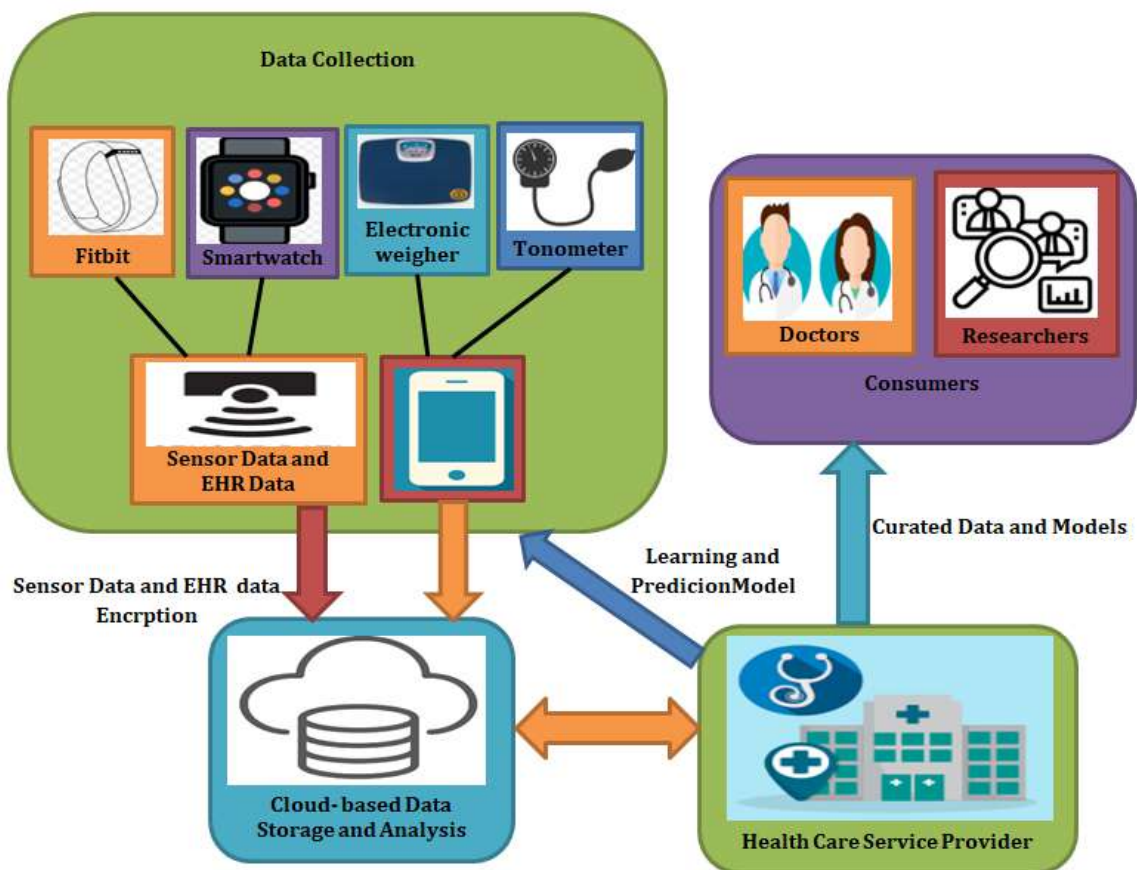


Figure.6: Comprehensive analysis of the IoT platform centered around cloud technology

The cloud-centric IoT architecture fully leverages the capabilities of cloud computing to integrate IoT functionalities and smart city technologies, while capitalizing on the benefits of cloud computing. In this architecture, sensors connected to the network generate data, which are then stored in cloud storage. This process is facilitated by software engineers who develop the necessary framework-supporting software. Furthermore, data mining and deep learning experts play a crucial role in transforming the raw data collected by these sensors into meaningful insights and comprehensible information. The architecture utilizes various cloud computing services, including Infrastructure as a Service (IaaS), Platform as a Service (PaaS), and Software as a Service (SaaS). One of the key features of this system is the security of the data. Data collected by sensors, the software that maintains the devices, and the algorithms that interpret the data are protected from public access, ensuring privacy and security. A cloud-based IoT architecture integrates various aspects of distributed computing and offers scalable storage and processing resources that can be adjusted according to need. Figure 6 in the document likely provides a visual representation of this systematic overview, illustrating how a cloud-centric IoT platform functions, including the integration of sensor data, cloud storage, data processing, and security measures.

4. Challenges and Limitations

Despite the promising potential of integrating Artificial Intelligence (AI) with the Internet of Things (IoT) in healthcare, several challenges and limitations have been identified. A primary concern is ensuring data privacy and security, as the vast amount of sensitive patient data collected by IoT devices and processed by AI systems is susceptible to cyber threats and breaches. This necessitates the development of advanced and robust security measures. Ethical considerations also play a significant role, particularly in regards to the transparency of AI decision-making processes and the potential for inherent biases within AI algorithms, which could lead to unequal treatment outcomes. The issue of interoperability arises from the diverse range of IoT devices and

systems, which often lack standardization, making seamless integration a complex task. The effectiveness of AI is heavily dependent on the quality and quantity of data, and any inadequacies here can lead to inaccurate outcomes. Regulatory and compliance challenges are also prominent, given the rapidly evolving nature of AI and IoT technologies and the need for healthcare-specific guidelines. Furthermore, the implementation of these technologies in healthcare settings requires substantial resources and infrastructure, which can be particularly challenging in low-resource environments. Lastly, patient acceptance and trust in AI-driven healthcare systems are crucial and can be influenced by concerns over privacy, the impersonal nature of technology, and a general lack of understanding of these advanced technologies.

5. Case Studies and Examples

In exploring the application of AI in enhancing IoT-based healthcare systems, we examined several case studies and theoretical scenarios. A key real-world application was found in a remote patient monitoring system, where AI-enhanced IoT wearables were used to monitor patients with chronic conditions. This system demonstrated how AI algorithms, analyzing data from sensors in real-time, could predict health deteriorations and alert healthcare providers for timely interventions. Another significant example was the use of AI in diagnostic tools within radiology. Here, AI algorithms, combined with IoT-enabled imaging devices, showcased improved accuracy in diagnoses, particularly in early detection of diseases such as cancer. We also proposed theoretical scenarios, such as an AI and IoT integrated smart home environment for elderly care, which could monitor daily activities and detect anomalies like falls, and a scenario illustrating personalized treatment plans through AI analysis of data from various IoT medical devices. These cases and scenarios collectively illustrate the profound impact AI can have in healthcare when integrated with IoT, from enhancing patient monitoring to personalizing treatment plans, thereby significantly improving patient care and outcomes.

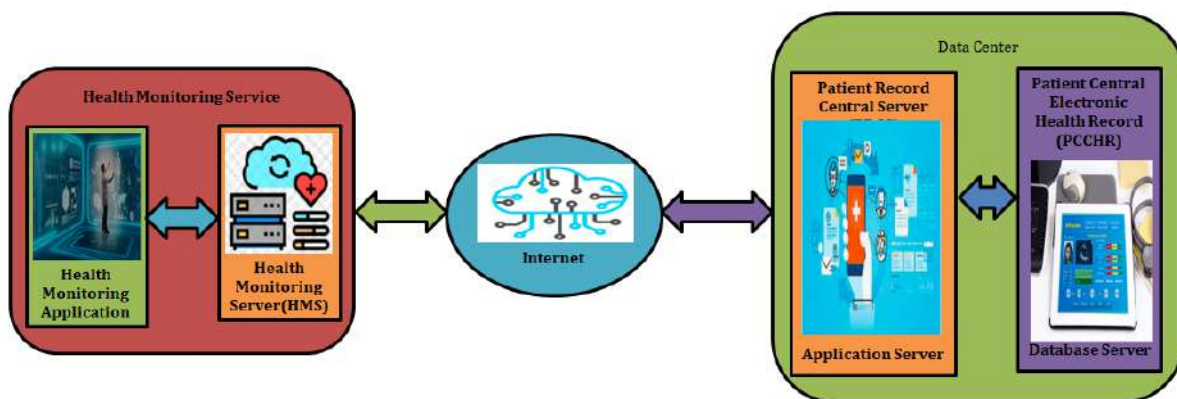


Figure.7: Basic technological structure for advanced healthcare solutions

The health monitoring service in this system is designed to collect information from medical sensors attached to a patient's body as well as from the smart device of a caregiver or custodian. The heart of this system is the Health Monitoring Server (HMS), which acts as the controller. HMS is responsible for delivering a real-time Individualized Healthcare Plan (IHP) based on the analysis of the patient's current health status and historical health records. It also generates signal notifications, warnings, and alerts during critical health situations.

The system comprises several key components:

Health Monitoring Service: This service focuses on evaluation and oversight of the patient's health, gathering data from the sensors and making real-time assessments.

Hospital Service: This component aids in identifying health issues by allowing medical professionals to make informed decisions based on the patient's health status. They use the reports delivered by the HMS and the historical health records provided by the PRMC.

Patient Record Management Center (PRMC): The PRMC acts as a central repository for all health records and data of patients. It maintains the digital health records, including ongoing health conditions, and

shares necessary information with other connected systems. The PRMC is crucial for storing personal records, including past health data.

Local Storage: In addition to the PRMC, the health monitoring service includes local storage, which holds the patient's medical history and health records. This storage is essential for a streamlined technology architecture in smart healthcare services.

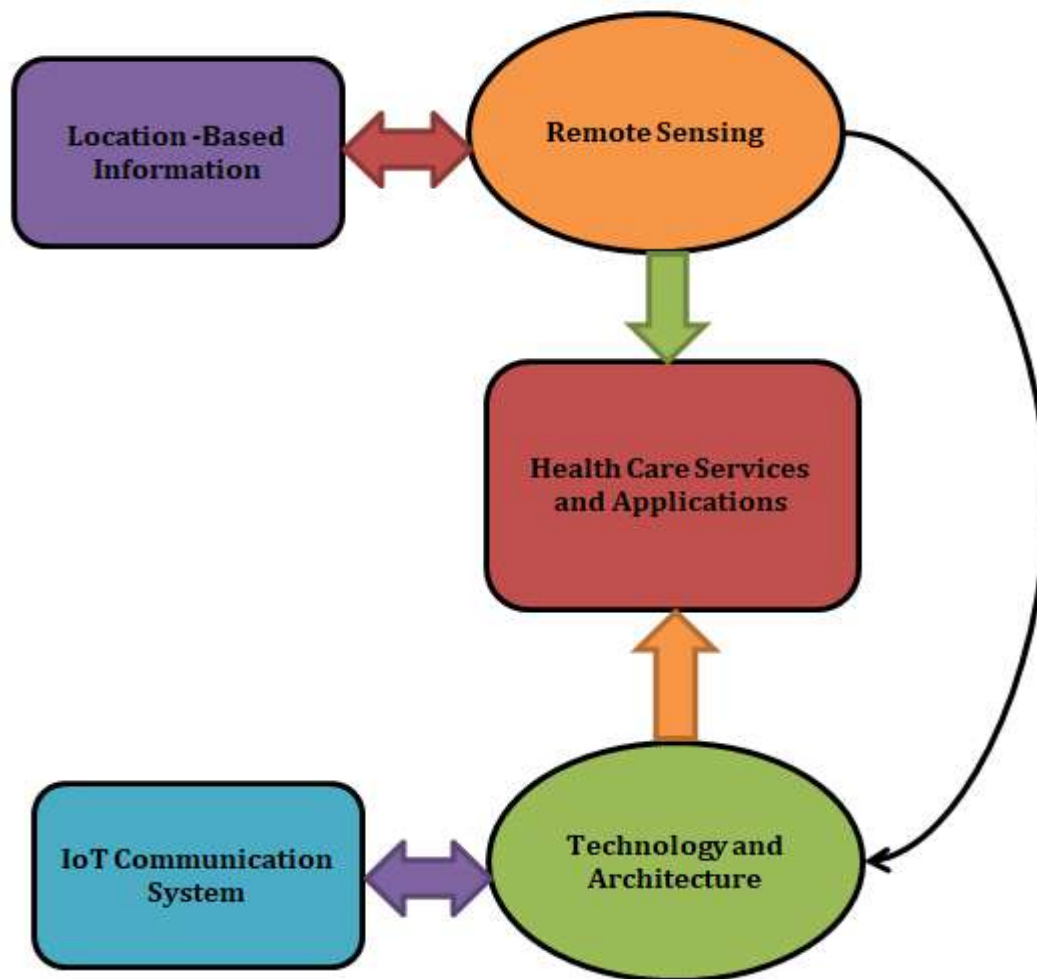


Figure.8: Foundational elements of a healthcare system in a smart city, with IoT integration

Patient Central Electronic Health Record (PC-EHR): This versatile storage system contains the patient's past health records and detailed personal information like name, address, phone number, etc.

Figure 7 in the document likely illustrates how these components interact within the smart healthcare service, showing the flow of information from the sensors to the HMS, and then to the PRMC and hospital services, outlining the comprehensive data management and analysis process in the health monitoring system.

The concept of smart city healthcare represents a paradigm shift for traditional cities, as they integrate conventional medical devices and equipment with smart solutions and Information and Communication Technology (ICT). These technologies are pivotal in enabling smart cities to offer high-quality healthcare services to their citizens. The primary objectives of a smart city in the context of healthcare include enhancing the quality of living, maintaining high standards of healthcare service, and fostering more favorable living conditions for its residents. A specific model is required to develop and deliver innovative and efficient healthcare services.

As depicted in Figure 8, various systems, architectures, and frameworks collaborate towards a unified goal, implementing the essential elements of an IoT-enabled smart city healthcare system. Smart services in such a city are categorized into six main components: (i) smart economies, (ii) smart environments, (iii) smart

governments, (iv) smart people, (v) smart mobility, and (vi) smart living. Each of these components encompasses a range of services that collectively contribute to a more comfortable, luxurious, and efficient living environment. They also empower citizens to actively participate in activities that meet their needs and to be engaged members of the community. In a smart city, citizens interact with a multitude of smart devices to access and use these services. This setup forms an intricate network configuration where a significant amount of personal data is transmitted via the Internet. The usefulness of such a system became particularly evident during the COVID-19 pandemic. For example, in February 2020, prior to the outbreak, there were approximately 1,000 virtual medical visits recorded. However, during the peak of the pandemic in April, this number surged to between 3,000 and 3,500 visits per day. Telemedicine facilities, a crucial component of smart healthcare, played a significant role in providing treatment while enabling patients to adhere to social distancing guidelines, thereby reducing the risk of infection during the outbreak.

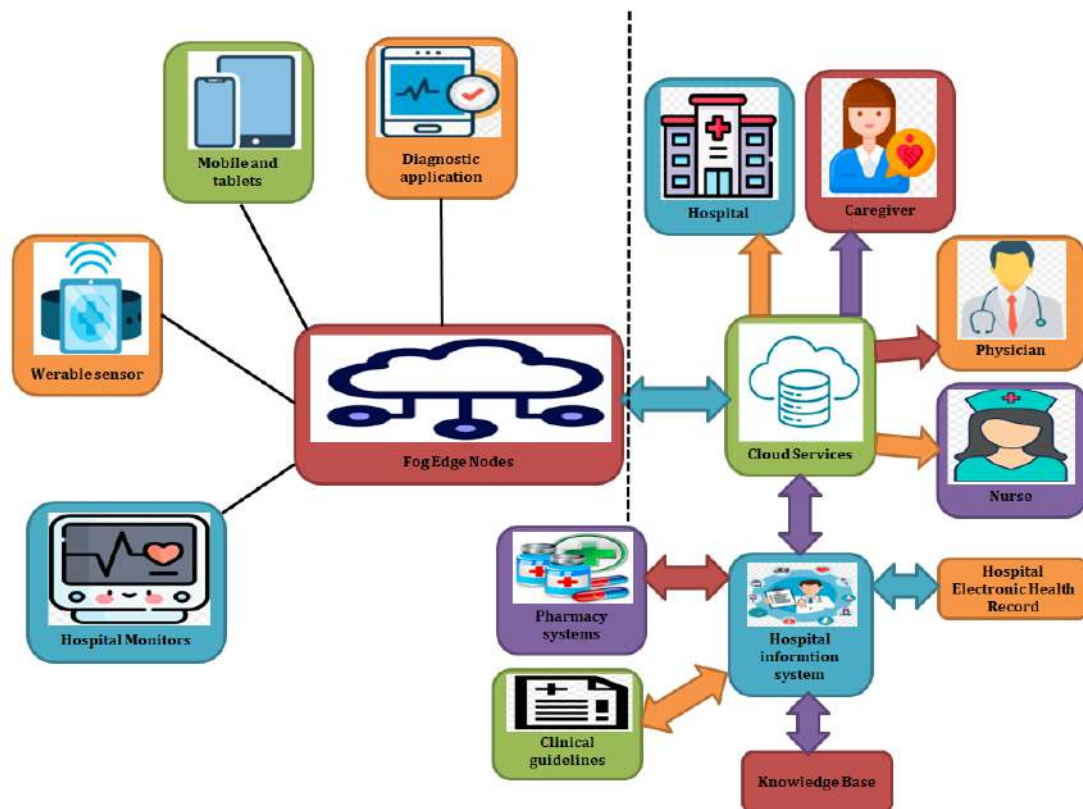


Figure.9: Basic building blocks of an IoT-enhanced healthcare system

In our evaluation of ECG arrhythmia classification, we utilized the MIT dataset, dividing it into two subsets known as DS1 and DS2. These divisions were made from both an inter-patient and intra-patient viewpoint.

Inter-Patient Viewpoint: This approach separates datasets in such a way that different patients are used for development and testing. This ensures that the classification model is evaluated on a diverse set of patients, reducing bias.

Intra-Patient Viewpoint: In this split, datasets include ECG readings from patients with similar characteristics. This can be useful for evaluating the model's performance within specific patient groups.

To achieve unbiased and accurate classification, we adopted a persistent worldview that considers disparities in patient information. Initially, we trained the ECG classifier using 51,020 ECG tests from a wide range of patients, creating a classifier with a broad perspective (referred to as "between persistent").

Using DS2, the classification results were found to be acceptable. Table 1 provides details of the ECG test selections and their corresponding scores within a heterogeneous network. However, it's important to note that in this early stage, there is a prevalence of correct classifications, as indicated in the disordered grid.

Due to the vast amount of data used for classifier training and the significant variations in ECG morphologies across patients, the accuracy may not be sufficient for clinical applications. Additionally, the model was not specifically designed for monitored patients.

To improve accuracy, our strategy involves retraining the classifier using ECG tests from the patient in question as well as data from other patients. This approach aims to refine the model's performance. The proposed system architecture is illustrated in Figure 9, showcasing the framework for this process.

6. Discussion

The findings from our literature review and case studies paint a comprehensive picture of the burgeoning role of Artificial Intelligence (AI) in enhancing Internet of Things (IoT)-based healthcare systems. The integration of AI with IoT technologies has been shown to significantly improve patient care, primarily through advanced diagnostic tools, personalized treatment plans, and effective patient monitoring systems. These advancements highlight AI's potential in revolutionizing healthcare delivery by facilitating more accurate diagnoses, enabling proactive health management, and tailoring treatments to individual patient needs. However, our research also brings to light significant challenges that need addressing. These include concerns around data privacy and security, given the sensitive nature of health data processed by AI and IoT systems. The issues of interoperability between diverse IoT devices and the need for transparent and ethical AI decision-making processes also stand out as critical areas for improvement. Furthermore, our study underscores the importance of developing robust regulatory frameworks and standards for AI and IoT in healthcare, ensuring patient safety and data privacy. The discussion of these findings indicates a clear need for continued innovation and research in this field, emphasizing the necessity to balance technological advancement with ethical, security, and regulatory considerations to fully harness the potential of AI in IoT-based healthcare systems.

7. Conclusion

In conclusion, this research has highlighted the significant potential of Artificial Intelligence (AI) in enhancing Internet of Things (IoT)-based healthcare systems. The integration of AI with IoT technologies promises to revolutionize healthcare by improving diagnostic accuracy, enabling real-time patient monitoring, and facilitating personalized treatment plans. These advancements suggest a future where healthcare is more proactive, efficient, and patient-centric. However, the realization of this potential is not without challenges. Issues surrounding data privacy and security, ethical considerations in AI implementation, interoperability among IoT devices, and the need for comprehensive regulatory frameworks have emerged as critical areas requiring further attention and resolution. Addressing these challenges is essential for the successful and ethical integration of AI and IoT in healthcare. As technology continues to evolve, ongoing research and development in this field are imperative to ensure that AI and IoT technologies are leveraged effectively and responsibly to improve healthcare outcomes while safeguarding patient data and rights. Thus, while AI and IoT hold great promise for transforming healthcare, a balanced approach that considers both the technological possibilities and the associated challenges is crucial for their successful and sustainable implementation in healthcare systems.

References

- [1] J. I. Khan, J. Khan, F. Ali, F. Ullah, J. Bacha and S. Lee, "Artificial Intelligence and Internet of Things (AI-IoT) Technologies in Response to COVID-19 Pandemic: A Systematic Review," in *IEEE Access*, vol. 10, pp. 62613-62660, 2022, doi: 10.1109/ACCESS.2022.3181605.
- [2] R. F. Mansour, A. E. Amraoui, I. Nouaouri, V. G. Díaz, D. Gupta and S. Kumar, "Artificial Intelligence and Internet of Things Enabled Disease Diagnosis Model for Smart Healthcare Systems," in *IEEE Access*, vol. 9, pp. 45137-45146, 2021, doi: 10.1109/ACCESS.2021.3066365.
- [3] R. D. Chand, R. Rajnish and H. Chandra, "IoT-enabled Smart Healthcare System for Accessing Healthcare Services Anywhere and Anytime," *2023 10th International Conference on Computing for Sustainable Global Development (INDIACom)*, New Delhi, India, 2023, pp. 688-693.
- [4] H. K. Bharadwaj *et al.*, "A Review on the Role of Machine Learning in Enabling IoT Based Healthcare Applications," in *IEEE Access*, vol. 9, pp. 38859-38890, 2021, doi: 10.1109/ACCESS.2021.3059858.

- [5] B. Godi, S. Viswanadham, A. S. Muttipati, O. P. Samantray and S. R. Gadiraju, "E-Healthcare Monitoring System using IoT with Machine Learning Approaches," *2020 International Conference on Computer Science, Engineering and Applications (ICCSEA)*, Gunupur, India, 2020, pp. 1-5, doi: 10.1109/ICCSEA49143.2020.9132937.
- [6] R. Rastogi and M. Bansal, "Analysis of various Smart Healthcare Technologies," *2022 Seventh International Conference on Parallel, Distributed and Grid Computing (PDGC)*, Solan, Himachal Pradesh, India, 2022, pp. 629-634, doi: 10.1109/PDGC56933.2022.10053093
- [7] S. Ahamed, P. Bhatt, S. Sultanuddin, R. Walia, M. A. Haque and S. B. InayathAhamed, "An Intelligent IoT enabled Health Care Surveillance using Machine Learning," *2022 International Conference on Advances in Computing, Communication and Applied Informatics (ACCAI)*, Chennai, India, 2022, pp. 1-5, doi: 10.1109/ACCAI53970.2022.9752648.
- [8] F. Ahamed and F. Farid, "Applying Internet of Things and Machine-Learning for Personalized Healthcare: Issues and Challenges," *2018 International Conference on Machine Learning and Data Engineering (iCMLDE)*, Sydney, NSW, Australia, 2018, pp. 19-21, doi: 10.1109/iCMLDE.2018.00014.
- [9] E. -A. Paraschiv, C. -M. Petrache and O. Bica, "On the continuous development of IoT in Big Data Era in the context of Remote Healthcare Monitoring & Artificial Intelligence," *2022 14th International Conference on Electronics, Computers and Artificial Intelligence (ECAI)*, Ploiesti, Romania, 2022, pp. 1-6, doi: 10.1109/ECAI54874.2022.9847503.
- [10] Boukhenoufa, A. Amira, F. Bensaali and S. SoheilianEsfahani, "A novel gateway-based solution for remote elderly monitoring", *Journal of biomedical informatics*, vol. 1, no. 09, 2020.
- [11] L. A. Duran-Vega et al., "An IoT System for Remote Health Monitoring in Elderly Adults Through a Wearable Device and Mobile Application", *Geriatrics*, vol. 4, no. 2, pp. 34, May 2019.
- [12] S. I. Lopes, P. Pinho, P. Marques, C. Abreu, N. B. Carvalho and J. Ferreira, "Contactless Smart Screening in Nursing Homes: an IoT-enabled solution for the COVID-19 era", *2021 17th International Conference on Wireless and Mobile Computing Networking and Communications (WiMob)*, pp. 145-150, 2021.
- [13] E. J. Chow, N. G. Schwartz, F. A. Tobolowsky, R. L. Zacks, M. Huntington-Frazier, S. C. Reddy, et al., "Symptom screening at illness onset of health care personnel with SARS-Cov-2 infection in king county Washington", *Jama*, vol. 323, no. 20, pp. 2087-2089, 2020.
- [14] R. Tkachenko, I. Izonin, V. chopyak, N. Kryvinska and N. Lotoshynska, "Piecewise-linear approach for medical insurance costs prediction using SGTm neural-like structure", *Proc. IDDM*, pp. 170-179, Nov. 2018.
- [15] J. Hathaliya, P. Sharma, S. Tanwar and R. Gupta, "Blockchain-based remote patient monitoring in healthcare 4.0", *Proc. IEEE 9th Int. Conf. Adv. Comput. (IACC)*, pp. 87-91, Dec. 2019.
- [16] V. Hassija, V. Chamola, V. Saxena, D. Jain, P. Goyal and B. Sikdar, "A survey on IoT security: Application areas security threats and solution architectures", *IEEE Access*, vol. 7, pp. 82721-82743, 2019.
- [17] S. Challa, M. Wazid, A. K. Das and M. K. Khan, "Authentication protocols for implantable medical devices: Taxonomy analysis and future directions", *IEEE Consum. Electron. Mag.*, vol. 7, no. 1, pp. 57-65, Jan. 2018.
- [18] N. L. W. S. R. Ginantra, I. G. A. D. Indradewi and E. Hartono, "Machine learning approach for acute respiratory infections (ISPA) prediction: Case study Indonesia", *J. Phys. Conf. Ser.*, vol. 1469, Feb. 2020.

A defensive framework for deepfake detection under adversarial settings using temporal and spatial features

Regular contribution Published: 03 May 2023

Volume 22, pages 1371–1382, (2023) [Cite this article](#)



International Journal of Information Security

[Aims and scope](#)

[Submit manuscript](#)


[S. Asha](#) , [P. Vinod](#) & [Varun G. Menon](#)

 361 Accesses  3 Citations [Explore all metrics](#) →

Abstract

Advances in artificial intelligence have led to a surge in digital forensics, resulting in numerous image manipulation and processing tools. Hackers and cybercriminals utilize these techniques to create counterfeit images and videos by placing perturbations on facial traits. We propose a novel defensive framework that employs temporal and spatially aware features to efficiently identify deepfakes. This paper utilizes the facial landmarks in the video to train a self-attenuated VGG16 neural model to obtain the spatial attributes. Further, we generate optical flow feature vectors that extract temporal characteristics from the spatial vector. Another necessity of deepfake detection systems is the need for cross-dataset generalization. We built a custom dataset comprising samples from

FaceForensics, Celeb-DF, and Youtube videos. Experimental analysis shows that the system achieves a detection accuracy of 98.4%. We evaluate the robustness of our proposed framework under various adversarial settings, employing the Adversarial Robustness Toolbox, Foolbox, and CleverHans tools. The experimental evaluation shows that the proposed method can classify real and fake videos with an accuracy of 74.27% under diverse holistic conditions. An extensive empirical investigation to evaluate the cross-dataset generalization capacity of the proposed framework is also performed.

i This is a preview of subscription content, [log in via an institution](#)  to check access.

Access this article

[Log in via an institution](#)

Buy article PDF 39,95 €

Price includes VAT (India)

Instant access to the full article PDF.

Rent this article via [DeepDyve](#) 

[Institutional subscriptions](#) →

References

1. Goodfellow, I., Pouget-Abadie, J., Mirza, M., Xu, B., Warde-Farley, D., Ozair, S., Courville, A., Bengio, Y.: Generative adversarial nets. Adv. Neural Info. Process. Syst. 27, (2014)
2. “Faceapp link,” (2015). Available from: <https://www.faceapp.com/>

3. Perov, I., Gao, D., Chervoniy, N., Liu, K., Marangonda, S., Umé, C., Dpfks, M., Facenheim, C.S., RP, L., Jiang, J., et al.: “Deepfacelab: A simple, flexible and extensible face swapping framework,” arXiv preprint [arXiv:2005.05535](https://arxiv.org/abs/2005.05535), (2020)
4. WatchMojo, “Another top 10 deepfake videos.”
5. Thies, J., Zollhofer, M., Stamminger, M., Theobalt, C., Nießner, M.: Face2face: Real-time face capture and reenactment of rgb videos, In: Proceedings of the IEEE conference on computer vision and pattern recognition, pp. 2387–2395, (2016)
6. Yu, P., Xia, Z., Fei, J., Lu, Y.: A survey on deepfake video detection. Iet Biomet. **10**(6), 607–624 (2021)

[Article](#) [Google Scholar](#)

7. Li, Y., Yang, X., Sun, P., Qi, H., Lyu, S.: Celeb-df: A large-scale challenging dataset for deepfake forensics, in Proceedings of the IEEE/CVF Conference on Computer Vision and Pattern Recognition, pp. 3207–3216, (2020)
8. Rossler, A., Cozzolino, D., Verdoliva, L., Riess, C., Thies, J., Nießner, M.: Faceforensics++: Learning to detect manipulated facial images, In: Proceedings of the IEEE/CVF International Conference on Computer Vision, pp. 1–11, (2019)
9. Maria-Irina, Nicolae, Sinn, M., Tran, M.N., Rawat, A., Wistuba, M., Zantedeschi, V., Molloy, I., Edwards, B.: Adversarial robustness toolbox v0.10.0, CoRR, 1807.01069, (2018)
10. Rauber, J., Brendel, W., Bethge, M.: Foolbox: A python toolbox to benchmark the robustness of machine learning models, arXiv preprint [arXiv:1707.04131](https://arxiv.org/abs/1707.04131), (2018)

11. Papernot, N., Faghri, F., Carlini, N., Goodfellow, I., Feinman, R., Kurakin, A., Xie, C., Sharma, Y., Brown, T., Roy, A., et al.: Technical report on the cleverhans v2. 1.0 adversarial examples library, arXiv preprint [arXiv:1610.00768](https://arxiv.org/abs/1610.00768), (2016)
12. Wang, W., Jiang, X., Wang, S., Wan, M., Sun, T.: Identifying video forgery process using optical flow, In: International Workshop on Digital Watermarking, pp. 244–257, Springer, (2013)
13. Li, L., Bao, J., Zhang, T., Yang, H., Chen, D., Wen, F., Guo, B.: Face x-ray for more general face forgery detection, In: Proceedings of the IEEE/CVF Conference on Computer Vision and Pattern Recognition, pp. 5001–5010, (2020)
14. Bonettini, N., Cannas, E.D., Mandelli, S., Bondi, L., Bestagini, P., Tubaro, S.: Video face manipulation detection through ensemble of cnns, In: 2020 25th international conference on pattern recognition (ICPR), pp. 5012–5019, IEEE, (2021)
15. Li, L., Bao, J., Zhang, T., Yang, H., Chen, D., Wen, F., Guo, B.: Face x-ray for more general face forgery detection, In: Proceedings of the IEEE/CVF conference on computer vision and pattern recognition, pp. 5001–5010, (2020)
16. Amerini, I., Galteri, L., Caldelli, R., Del Bimbo, A.: Deepfake video detection through optical flow based cnn, in Proceedings of the IEEE/CVF International Conference on Computer Vision Workshops, pp. 0–0, (2019)
17. Wang, R., Juefei-Xu, F., Ma, L., Xie, X., Huang, Y., Wang, J., Liu, Y.: Fakespotter: A simple yet robust baseline for spotting ai-synthesized fake faces, arXiv preprint [arXiv:1909.06122](https://arxiv.org/abs/1909.06122), (2019)

18. Dang, H., Liu, F., Stehouwer, J., Liu, X., Jain, A.K.: On the detection of digital face manipulation, In: Proceedings of the IEEE/CVF Conference on Computer Vision and Pattern recognition, pp. 5781–5790, (2020)
19. Chen, L., Zhang, Y., Song, Y., Wang, J., Liu, L.: Ost: Improving generalization of deepfake detection via one-shot test-time training, In: Advances in Neural Information Processing Systems, (2022)
20. Nadimpalli, A.V., Rattani, A.: On improving cross-dataset generalization of deepfake detectors, In: Proceedings of the IEEE/CVF Conference on Computer Vision and Pattern Recognition, pp. 91–99, (2022)
21. Wang, T., Cheng, H., Chow, K.P., Nie, L.: Deep convolutional pooling transformer for deepfake detection, arXiv preprint [arXiv:2209.05299](https://arxiv.org/abs/2209.05299), (2022)
22. Tolosana, R., Vera-Rodriguez, R., Fierrez, J., Morales, A., Ortega-Garcia, J.: Deepfakes and beyond: a survey of face manipulation and fake detection. *Inf. Fus.* **64**, 131–148 (2020)

[Article](#) [Google Scholar](#)
23. Nirkin, Y., Keller, Y., Hassner, T.: Fsgan: Subject agnostic face swapping and reenactment, in Proceedings of the IEEE/CVF International Conference on Computer Vision, pp. 7184–7193, (2019)
24. Zhu, J.-Y., Park, T., Isola, P., Efros, A.A.: Unpaired image-to-image translation using cycle-consistent adversarial networks, In: Proceedings of the IEEE international conference on computer vision, pp. 2223–2232, (2017)
25. Tang, C., Chen, S., Fan, L., Xu, L., Liu, Y., Tang, Z., Dou, L.: A large-scale empirical study on industrial fake apps, In 2019 IEEE/ACM 41st International Conference on

Software Engineering: Software Engineering in Practice (ICSE-SEIP), pp. 183–192, IEEE, (2019)

26. N. Mondaini, R. Caldelli, A. Piva, M. Barni, and V. Cappellini, “Detection of malevolent changes in digital video for forensic applications,” in *Security, steganography, and watermarking of multimedia contents IX*, vol. 6505, p. 65050T, International Society for Optics and Photonics, 2007
27. Fridrich, J., Kodovsky, J.: Rich models for steganalysis of digital images. *IEEE Trans. Inf. Foren. Secur.* 7(3), 868–882 (2012)
28. P. Bestagini, S. Milani, M. Tagliasacchi, and S. Tubaro, “Local tampering detection in video sequences,” in *2013 IEEE 15th international workshop on multimedia signal processing (MMSP)*, pp. 488–493, IEEE, 2013
29. X. Pan, X. Zhang, and S. Lyu, “Exposing image splicing with inconsistent local noise variances,” in *2012 IEEE International Conference on Computational Photography (ICCP)*, pp. 1–10, IEEE, 2012
30. F. Matern, C. Riess, and M. Stamminger, “Exploiting visual artifacts to expose deepfakes and face manipulations,” in *2019 IEEE Winter Applications of Computer Vision Workshops (WACVW)*, pp. 83–92, IEEE, 2019
31. W. Luo, J. Huang, and G. Qiu, “Robust detection of region-duplication forgery in digital image,” in *18th International Conference on Pattern Recognition (ICPR’06)*, vol. 4, pp. 746–749, IEEE, 2006
32. M. Goljan and J. Fridrich, “Cfa-aware features for steganalysis of color images,” in *Media Watermarking, Security, and Forensics 2015*, vol. 9409, p. 94090V, International Society for Optics and Photonics, 2015

33. J. Huang, W. Zou, J. Zhu, and Z. Zhu, "Optical flow based real-time moving object detection in unconstrained scenes," arXiv preprint [arXiv:1807.04890](https://arxiv.org/abs/1807.04890), 2018
34. J. F. Cohn, A. J. Zlochower, J. J. Lien, and T. Kanade, "Feature-point tracking by optical flow discriminates subtle differences in facial expression," in Proceedings Third IEEE International Conference on Automatic Face and Gesture Recognition, pp. 396–401, IEEE, 1998
35. Aslani, S., Mahdavi-Nasab, H.: Optical flow based moving object detection and tracking for traffic surveillance. *Int. J. Electr. Comput. Energ. Electron. Commun. Eng.* 7(9), 1252–1256 (2013)

[Google Scholar](#)

36. Souhila, K., Karim, A.: Optical flow based robot obstacle avoidance. *Int. J. Adv. Robot. Syst.* 4(1), 2 (2007)

[Article](#) [Google Scholar](#)

37. A. Dosovitskiy, P. Fischer, E. Ilg, P. Hausser, C. Hazirbas, V. Golkov, P. Van Der Smagt, D. Cremers, and T. Brox, "Flownet: Learning optical flow with convolutional networks," in Proceedings of the IEEE international conference on computer vision, pp. 2758–2766, 2015
38. P. Viola and M. Jones, "Rapid object detection using a boosted cascade of simple features," in Proceedings of the 2001 IEEE computer society conference on computer vision and pattern recognition. CVPR 2001, vol. 1, pp. I–I, IEEE, 2001
39. "Dlib python api tutorials link," 2015. Available from: <http://dlib.net/python/index.html>

40. Horn, B.K., Schunck, B.G.: Determining optical flow. *Artif. Intell.* **17**(1–3), 185–203 (1981)
- [Article](#) [MATH](#) [Google Scholar](#)
41. G. Farnebäck, “Two-frame motion estimation based on polynomial expansion,” in *Scandinavian conference on Image analysis*, pp. 363–370, Springer, 2003
42. I. J. Goodfellow, J. Shlens, and C. Szegedy, “Explaining and harnessing adversarial examples,” *arXiv preprint [arXiv:1412.6572](#)*, 2014
43. A. Kurakin, I. Goodfellow, S. Bengio, et al., “Adversarial examples in the physical world,” 2016
44. A. Madry, A. Makelov, L. Schmidt, D. Tsipras, and A. Vladu, “Towards deep learning models resistant to adversarial attacks,” *arXiv preprint [arXiv:1706.06083](#)*, 2017
45. Papernot, N., McDaniel, P., Jha, Somesh, Fredrikson, Matt, Celik, Z. Berkay, Swami, A.: The limitations of deep learning in adversarial settings, In: *2016 IEEE European Symposium on Security and Privacy (EuroS &P)*, pp. 372–387, IEEE, (2016)
46. Carlini, N.: A critique of the deepsec platform for security analysis of deep learning models, *arXiv preprint [arXiv:1905.07112](#)*, (2019)
47. Rössler, A., Cozzolino, D., Verdoliva, L., Riess, C., Thies, J., Nießner, M.: Faceforensics: A large-scale video dataset for forgery detection in human faces, *arXiv preprint [arXiv:1803.09179](#)*, (2018)

Author information

Authors and Affiliations

SCMS School of Engineering and Technology, APJ Abdul Kalam Technological University, Trivandrum, India

S. Asha & Varun G. Menon

Department of Computer Applications, Cochin University of Science and Technology, Cochin, India

P. Vinod

Corresponding author

Correspondence to [S. Asha](#).

Ethics declarations

Conflict of interest

The authors declare that they have no known competing financial interests or personal relationships that could have appeared to influence the work reported in this paper. The authors did not receive support from any organization for the submitted work. This article does not contain any studies with human participants or animals performed by any of the authors. Data openly available in a public repository. The data that support the findings of this study are openly available in FaceForensics [8] at <https://github.com/ondyari/FaceForensics>, Celeb-DF [7] at <https://www.cs.albany.edu/~lsw/celeb-deepfakeforensics.html>.

Additional information

Publisher's Note

Springer Nature remains neutral with regard to jurisdictional claims in published maps and institutional affiliations.

Rights and permissions

Springer Nature or its licensor (e.g. a society or other partner) holds exclusive rights to this article under a publishing agreement with the author(s) or other rightsholder(s); author self-archiving of the accepted manuscript version of this article is solely governed by the terms of such publishing agreement and applicable law.

About this article

Cite this article

Asha, S., Vinod, P. & Menon, V.G. A defensive framework for deepfake detection under adversarial settings using temporal and spatial features. *Int. J. Inf. Secur.* 22, 1371–1382 (2023). <https://doi.org/10.1007/s10207-023-00695-x>

Published

03 May 2023

Issue Date

October 2023

DOI

<https://doi.org/10.1007/s10207-023-00695-x>

Keywords

[Deepfakes](#)

[Attention mechanism](#)

[Optical flow](#)

[Adversarial machine learning](#)

[Cross-dataset generalization](#)